UNIVERSITÄTSKLINIKUM HAMBURG-EPPENDORF

Institut für Molekulare und Zelluläre Kognition

Prof. Dr. Dietmar Kuhl

The role of Arc/Arg3.1 during early development in the wiring of hippocampal networks

Dissertation

zur Erlangung des Doktorgrades Ph.D. an der Medizinischen Fakultät der Universität Hamburg.

vorgelegt von:

Daniela Carolina Ballesteros Cadena aus Bogotá – Kolumbien

Angenommen von der
Medizinischen Fakultät der Universität Hamburg am: 10.10.2024
Veröffentlicht mit Genehmigung der
Medizinischen Fakultät der Universität Hamburg.
Prüfungsausschuss, der/die Vorsitzende: Prof. Dr. Dietmar Kuhl
Prüfungsausschuss, zweite/r Gutachter/in: Prof. Dr. Stefan Kindler

Table of contents

Figures	I
Tables	III
Abbreviati	onsIV
Abstract	VIII
Zusammen	fassungX
Introduction	n1
1.1 T	he hippocampus2
1.1.1	Hippocampal oscillatory activity4
1.2 S	ynaptic transmission6
1.2.1	Excitatory transmission
1.2.2	Inhibitory transmission9
1.3 A	rc/Arg3.111
1.3.1	Arc/Arg3.1 in synaptic plasticity
1.3.2	Arc/Arg3.1 in memory consolidation
1.4 M	lass spectrometry-based proteomics
1.5 H	ippocampal development
1.5.1	Development of the hippocampal structure
1.5.2	Development of hippocampal membrane properties
1.5.3	Development of hippocampal transmission
1.5.4	Development of hippocampal-dependent behavior and hippocampal rhythms. 22
1.6 C	ritical periods
1.7 A	rc/Arg3.1 during development
2 Part 1	. Loss of Arc/Arg3.1 during early postnatal development persistently changes
hippocamp	al synaptic transmission
2.1 In	stroduction 25

2.	.2 Ma	terials and methods
	2.2.1	Mice
	2.2.2	Generation of constitutive and conditional <i>Arc/Arg3.1</i> KO mice
	2.2.3	Patch-clamp recordings
	2.2.4	Extracellular field recordings
	2.2.5	Immunofluorescence staining and confocal imaging
	2.2.6	Western-blot analyses
	2.2.7	Subcellular fractionation
	2.2.8	Experimental design and statistical analyses
2.	.3 Res	ults
	2.3.1	Reduced fEPSP amplitude in germline and early <i>Arc/Arg3.1</i> KOs
	2.3.2	Deletion of Arc/Arg3.1 does not alter the amplitude or frequency of spontaneous
	excitato	ry postsynaptic currents (sEPSCs)
	2.3.3	Deletion of Arc/Arg3.1 before P21 is associated with changes in the kinetics of
	sEPSCs	34
	2.3.4	Germline and Early Arc/Arg3.1 KO mice exhibit a lower density of excitatory
	clusters	in the CA1 region of the hippocampus
	2.3.5	Germline and early Arc/Arg3.1 KOs have decreased levels of PSD-95 protein in
	the hipp	ocampus
	2.3.6	Germline but not early or late Arc/Arg3.1 exhibit reduced TARPy8 in the
	postsyn	aptic density40
	2.3.7	Germline <i>Arc/Arg3.1</i> KO exhibit slower sIPSCs41
	2.3.8	Germline <i>Arc/Arg3.1</i> KO exhibit slower somatic eIPSCs
	2.3.9	Arc/Arg3.1 deletion does not affect paired-pulse modulation of inhibition 43
	2.3.10	Germline Arc/Arg3.1 KO mice exhibited higher intensity of inhibitory clusters in
	the pyra	midal and LM layers of CA144
		C 1' 4 /4 21WO1 1 4' 1 1 C 1 ' 1CADA
	2.3.11	Germline Arc/Arg3.1 KO have normal synaptic levels of gephyrin and GABA _A
		subunits in the hippocampus

3	Part II.	Mass Spectrometry Profiling of Arg3.1 KO Mice in Distinct Hippocampal
Sub	fields	54
3	.1 Intr	oduction
3	.2 Me	thods
	3.2.1	Mice
	3.2.2	Spectral Library55
	3.2.3	Laser Ablation and sample processing
	3.2.4	LC-MS/MS Parameters
	3.2.5	Raw Data Processing
	3.2.6	Gel Samples
	3.2.7	Western-blot analyses
	3.2.8	Statistical Analysis
3	.3 Res	sults61
	3.3.1	Hippocampal Subfields Show Distinct Protein Signatures, with Potentially
	Intrigui	ng Differences within CA361
	3.3.2	Protein expression of DG differs greatly from CA1 and CA3 subfields
	3.3.3	Gene Ontology enrichment analysis revealed significantly over-represented
	function	nal terms in DG, CA1, and CA3-CA1 dominant proteins
	3.3.4	Unveiling Subfield-Specific Protein Signatures in the Hippocampus: A Look at
	Volcan	o Plots
	3.3.5	Comparison of the hippocampal molecular profile using transcriptomics vs
	proteon	nics
	3.3.6	Differences between subfields CA3 and CA1 are highly consistent with other
	proteon	nic studies
	3.3.7	Subtle Changes in the Proteome of Arc/Arg3.1 Knockout Hippocampi under
	Baselin	e Conditions71
	3.3.8	Arc/Arg3.1 regulates a subset of proteins in the hippocampus, in a subfield-
	specific	manner72

3.3.9 <i>Arc/A</i>	Frequency analysis reveals an additional subset of proteins regulated by rg3.1 in hippocampal subfields
3.3.10	
Arc/A	rg3.1-regulated proteins within the hippocampus
3.3.11 mice	Abundances of synaptic protein in the dorsal hippocampus of WT and KO
3.3.12 mice	Them6 is highly upregulated in the dorsal hippocampus of <i>Arc/Arg3.1</i> KO
3.4 D	iscussion81
3.4.1	Proteomic profiles of the hippocampal subfields
3.4.2	Arc/Arg3.1 regulation of the hippocampal protein profiles
	II. Selective Impairment of Excitatory Synapses in the Young Hippocampus Early Arc/Arg3.1 Deletion
4.1 In	troduction87
4.2 M	aterials and methods
4.2.1	Mice
4.2.2	Generation of constitutive and conditional Arc/Arg3.1 KO mice
4.2.3	Patch-clamp recordings
4.2.4	Neuron reconstructions
4.2.5	Fluorescent <i>in situ</i> hybridization: RNAscope
4.2.6	Immunofluorescence staining and confocal imaging
4.2.7	Spine analysis
4.2.8	Experimental design and statistical analyses
4.3 R	esults96
4.3.1	Arc/Arg3.1 deletion has minimal impact on the dendritic morphology of
hippoo	campal CA1 neurons in early postnatal development96
4.3.2	Timeline deletion in conditional <i>Arc/Arg3.1</i> KO mice
4.3.3	Arc/Arg3.1 deletion has minimal impact on input resistance but shapes action
notent	ial waveform 99

	4.3.4	Transient	Effects	of	Arc/Arg3.1	on	Firing	Frequencies	During	Early
	Develop	oment	•••••				•••••		•••••	102
	4.3.5	Early but n	ot germli	ne o	r late <i>Arc/Ar</i>	g3.1 c	deletion	reduces sEPS	C amplitu	de and
	frequen	cy at P28		•••••						103
	4.3.6	Normal de	velopmen	t of	sEPSC kinet	ics in	Arc/Arg	3.1 KO mice.	•••••	105
	4.3.7	Reduced el	EPSC am	plitu	de in early A	rc/Ar	g3.1 KC	mice at P28.		106
	4.3.8	Reduced sp	pine dens	ity ir	n early-cKO	mice	at P28			108
	4.3.9	Early-cKO	mice ex	hibit	ed fewer ex	citato	ry clust	ers in the CA	1 region	of the
	hippoca	mpus		•••••		•••••				111
	4.3.10	Early-cKO	mice ex	hibit	ted fewer in	nibito	ry clust	ers in the CA	1 region	of the
	hippoca	mpus		•••••						114
	4.3.11	Early-cKO	mice exh	nibit	unaltered sII	PSCs.	•••••		•••••	115
	4.3.12	Early Arc/	<i>Arg3.1</i> de	letio	n does not in	npact	eIPSCs	or paired-puls	se modula	tion of
	inhibitio	on								116
4.	4 Dis	cussion								119
5	Conclud	ding Remark	ks and Ou	tlool	k	•••••				124
6	Referen	ces								128
7	Stateme	ent of contril	butions							150
8	Acknov	vledgments.								151
9	Curricu	lum Vitae				•••••	•••••		•••••	153
10	Eides	stattliche Ve	ersicherur	ıg						154

Figures

Figure 1.1. The hippocampal circuit.	3
Figure 1.2. Excitatory and inhibitory synapses.	11
Figure 1.3. Arc/Arg3.1 on synaptic plasticity	15
Figure 2.1. Arc/Arg3.1 genetic deletion before P21 decreases the amplitude of the	e fEPSP
responses	32
Figure 2.2. Normal sEPSC amplitude and frequency in Arc/Arg3.1 KO mice	33
Figure 2.3. Genetic deletion of Arc/Arg3.1 before P21 results in fast kinetics of sEPSC	s35
Figure 2.4. Decreased excitatory synaptic clusters following germline and early Arc	c/Arg3.1
deletion	37
Figure 2.5. Arc/Arg3.1 deletion before P21 reduces hippocampal PSD-95 protein about	undance
	38
Figure 2.6. Germline <i>Arc/Arg3.1</i> KO have lower synaptic TARPγ8	40
Figure 2.7. Normal sIPSC amplitude and frequency but slower kinetics in Arc/Arg3.1 K	O mice.
	41
Figure 2.8. Slower somatic but normal dendritic eIPSCs.	42
Figure 2.9. Unaltered inhibitory paired-pulse depression in Arc/Arg3.1 KO mice	44
Figure 2.10. Unaltered number of inhibitory synaptic clusters in Arc/Arg3.1 KO n	nice but
increased intensity in the pyramidal and LM layers	45
Figure 2.11. Germline Arc/Arg3.1 KO mice exhibit normal synaptic levels of gephy	yrin and
GABA-A receptor subunits in the hippocampus	46
Figure 2.12. Arc/Arg3.1 deficiency permanently alters hippocampal neurotransmiss	ion in a
development-dependent manner.	52
Figure 3.1. Proteins detected in the hippocampus group according to the subfield	61
Figure 3.2. Subfield dominance classification.	62
Figure 3.3. Gene ontology analysis on the proteins in the different regions	64
Figure 3.4. High Abundance Proteins in Hippocampal Subfields.	65
Figure 3.5. Hippocampal profile comparison mRNA and protein	67
Figure 3.6. Positive correlation with previous studies.	70
Figure 3.7. Proteins detected in the hippocampus group according to the genotype	71
Figure 3.8. Arc/Arg3.1 regulates a subset of proteins in hippocampal subfields	72

Figure 3.9. Frequency analysis for protein abundance in WT vs. Arc/Arg3.1 KO Hippocampus
74
Figure 3.10. Gene ontology analysis on the Arc/Arg3.1 regulated proteins in the different
hippocampal subfields
Figure 3.11. Impact of Arc/Arg3.1 deletion on the expression of synaptic proteins evaluated
with WB and Mass-spectrometry in the different hippocampal regions
Figure 3.12. Them6 is highly upregulated in the dorsal hippocampus of Arc/Arg3.1 KO mice
80
Figure 4.1. Unaltered dendritic morphology in Arc/Arg3.1 KO mice
Figure 4.2. Deletion timeline of conditional <i>Arc/Arg3.1</i> KO mice
Figure 4.3. Electrical properties of pyramidal CA1 neurons in Arc/Arg3.1 KO mice99
Figure 4.4. Frequency-current (F-I) curves of CA1 neurons of Arc/Arg3.1 KO mice 102
Figure 4.5. Reduced sEPSC amplitude and frequency in early Arc/Arg3.1 KO mice at P28 104
Figure 4.6. Normal sEPSCs kinetics in <i>Arc/Arg3.1</i> KO cells
Figure 4.7. Smaller eEPSC amplitude in early Arc/Arg3.1 KO mice at P28107
Figure 4.8. Reduced spine density in early Arc/Arg3.1 KO mice at P28
Figure 4.9. Decreased excitatory synaptic clusters in early-cKO
Figure 4.10. Decreased inhibitory synaptic clusters in early-cKO
Figure 4.11. Preserved sIPSC amplitude, frequency, and kinetics in early-cKO mice 115
Figure 4.12. Unaltered eIPSC and paired-pulse ratio in early-cKO mice

Tables

Γable 2.1. Mann-Whitney comparisons of excitatory synaptic proteins in hippocampal sample
For all Arc/Arg3.1 KO lines
Table 2.2. Mann-Whitney comparisons of inhibitory synaptic proteins in hippocampal sample
For Arc/Arg3.1 KO mice4
Table 3.1. Proteins with conflicting classification with respect to the work by Lein et al., 200
6
Table 3.2 Comparison to the study by von Ziegler et al., 20186
Table 3.3 Arc/Arg3.1 effect on an additional subset of synaptic proteins using western blot of
mass spectrometry

Abbreviations

ACN acetonitrile

ACSF artificial cerebrospinal fluid

AMPA α-amino-3-hydroxy-5-methyl-isoxazole-propionic acid

AMPARs AMPA receptors

ANOVA Analysis of variance

AP action potential

BDNF brain-derived neurotrophic factor

BP Biological Process

BSA bovine serum albumin

CA cornu ammonis
CAG glutamine codon

CC Cellular Compartment

CGG arginine codon

Crb cerebellum

DAVID Database for Annotation, Visualization, and Integrated Discovery

DCX doublecortin

DDA data-dependent acquisition mode

DG dentate gyrus**Dsp** Desmoplakin

early-cKO early conditional KO

EC entorhinal cortex

EDTA Ethylenediaminetetraacetic acid

EGTA ethylene glycol-bis(β-aminoethyl ether)-N,N,N',N'-tetraacetic acid

eIPSCs evoked inhibitory postsynaptic currents

EPSC excitatory postsynaptic current

fEPSP field excitatory postsynaptic potential

GABA γ-Aminobutyric acid

GABA_A ionotropic GABA receptor

GABA_B metabotropic GABA receptor

GB gel bandsGephGephyrin

GluK1-5 Glutamatergic Kainate Receptor subunits 1-5

GO Gene Ontology

Grm2 metabotropic glutamate receptor 2

HCD higher energy collisional dissociation

Hippo hippocampus

IEG immediate early genes

IEI interevent interval

IPSC inhibitory postsynaptic current

IPSCs inhibitory postsynaptic currents

ISH in situ hybridization

ISI inter-stimulus interval

late-cKO late conditional KO

LC-MS/MS liquid chromatography-tandem mass spectrometry

IEC lateral entorhinal cortex

LFPs local field potentials

LFS low-frequency stimulation

LM stratum lacunosum-moleculare

LM lacunosum moleculare

LTD long-term depression

LTP Long-term potentiation

MAGUKs membrane-associated guanylate kinases

MD monocular deprivation

mEC medial entorhinal cortex

mEPSCs miniature EPSCs

MF Molecular Function

mGluR metabotropic glutamate receptor

mIPSCs miniature IPSCs

MS mass spectrometry

nano-ESI nano-electrospray ionization

NIRL nanosecond infrared laser

NMDA N-methyl-D-aspartate

ODN oligodeoxynucleotide

OR stratum oriens

ORF open reading frame

P postnatal day

PBS phosphate-buffered saline

PCA Principal Component Analysis

PFA Paraformaldehyde

PNNs perineural nets

PSD postsynaptic density

PTM post-translational modifications

PV parvalbumin

PVDF Polyvinylidene fluoride

PYR stratum pyramidale

R/G arginine to glycine site

RAD stratum radiatum

RBPs RNA-binding proteins

R_m membrane resistivity

ROI regions of interest

Rs series resistance

SDC sodium deoxycholate

SEM standard error of the mean

sEPSC spontaneous excitatory postsynaptic currents

SN extrasynaptic fraction

SPM synaptic plasma membrane

SPW-R Sharp wave-ripple

SPWs sharp waves

SST somatostatin

Sub subiculum

SYN Synaptophysin

TARPs transmembrane AMPA receptor regulatory proteins

TEA tetraethylammonium chloride

TEAB triethylammonium bicarbonate buffer

Tesc Tescalcin

Them6 thioesterase superfamily member 6

Thy thymus

TTX tetrodotoxin

UTR untranslated region

VGAT vesicular GABA transporter

VGLUT vesicular glutamate transporter

 V_m membrane potential

WB western blot

WH Whole hippocampus

Abstract

Critical periods are time windows in early development when genetical programs, and environmental and experiential factors confluence to tune functional properties of brain circuits towards their maturation. Concurrently, neural activity, synaptogenesis, and plasticity complete the wiring of hippocampal circuits giving rise to rhythmic activity. Work from our group has previously identified a critical period for hippocampal learning, wherein spontaneous upregulation of Arc/Arg3.1 in the hippocampus during the first postnatal month, permanently influences adult learning and hippocampal oscillations. Here, I propose that Arc/Arg3.1 shapes hippocampal circuits' wiring and functional maturation during the critical period.

This thesis aimed to delve into the impact of Arc/Arg3.1 on the maturation of synaptic transmission in the hippocampus. My approach was to investigate the molecular, structural, and functional properties of hippocampal circuits in conditional Arc/Arg3.1 knockout (cKO) mice engineered in earlier studies, featuring deletions of the gene at various time points during the first postnatal month. These included a germline KO line, in which the deletion occurs during embryogenesis; an "early-cKO" line, where Arc/Arg3.1 is present during the first postnatal week and the deletion is completed between postnatal days 7-14 (P7-P14); and a "late-cKO" line, where the deletion is completed between P21-P36. I employed a broad range of methods encompassing: in-vitro field recordings, patch-clamp techniques, 3D dendritic reconstructions, immunohistochemistry and quantitative confocal microscopy, electron-microscopy, mass spectrometry-based proteomics, and subcellular fractionation with Western blotting.

The first part of this thesis evaluated the adult KO and cKO mice, at a time point where Arc/Arg3.1 had been fully deleted in the hippocampus and deficits in oscillatory activity and learning had been observed. The findings presented here revealed an essential role of Arc/Arg3.1 in regulating the temporal dynamics of excitatory synapses in a development-dependent manner, with the most pronounced effects observed upon the earliest deletion. These effects were associated with changes in critical components of the postsynaptic density, including the transmembrane AMPA receptor regulatory proteins (TARPs) and PSD-95. Remarkably, my findings also showed alterations in the inhibitory synaptic transmission, hitherto believed to be independent of Arc/Arg3.1 plasticity, providing a first mechanistic understanding of the oscillatory deficits.

Part II of this thesis described the proteomic profile of the hippocampus in adult WT and Arc/Arg3.1 KO mice, focusing on differences between the CA1, CA3, and DG subfields. The results proved the efficacy of a nanosecond infrared laser (NIRL) ablation method to reliably isolate distinct regions of the mouse brain for subsequent proteomic analysis. Furthermore, I demonstrated that Arc/Arg3.1 regulates the proteomic hippocampal profile in a subfield-specific manner and identified novel exciting candidate proteins regulated by Arc/Arg3.1 under low activity levels. Additionally, enrichment analyses highlighted Arc/Arg3.1's role in protein transport.

Finally, part III evaluated the role of *Arc/Arg3.1* in the development of hippocampal function by examining mice of two and four weeks of age. My findings demonstrated that the kinetics of excitatory synaptic transmission are not altered in any of the KO lines at this stage of development, indicating that the alterations seen in the adult hippocampus develop at a later stage. In contrast to its effects in the adult brain, *Arc/Arg3.1*'s effects in the developing brain are more pronounced in response to early postnatal deletion, resulting in the active elimination of functional excitatory synapses and possibly the elimination of non-functional inhibitory synapses.

Collectively, this work provides further evidence of the existence of a critical period for the development of hippocampal function and demonstrates that Arc/Arg3.1 plays a vital role in the modulation of this critical period by shaping the wiring of hippocampal circuitry, not only by modulating excitatory synapses but, notably, also inhibitory transmission. My findings open new directions for investigating Arc/Arg3.1-dependent molecular pathways and cellular processes involved in brain wiring and plasticity.

Zusammenfassung

Kritische Perioden sind Zeitfenster in der frühen Entwicklung, in denen genetische Programme sowie Umwelt- und Erfahrungsfaktoren zusammenkommen, um die funktionellen Eigenschaften der Gehirnschaltungen für ihre Reifung abzustimmen. Gleichzeitig vervollständigen neuronale Aktivität, Synaptogenese und Plastizität die Verdrahtung der Schaltkreise im Hippocampus, die zu rhythmischer Aktivität führen. Arbeiten unserer Gruppe haben bereits einen kritischen Zeitraum für das Lernen im Hippocampus identifiziert, in dem die spontane Hochregulierung von Arc/Arg3.1 im Hippocampus während des ersten postnatalen Monats das Lernen und die Oszillationen im Hippocampus im Erwachsenenalter dauerhaft beeinflusst. Ich schlage vor, dass Arc/Arg3.1 die Verdrahtung und funktionelle Reifung der Hippocampus-Schaltkreise während der kritischen Periode prägt.

Ziel dieser Arbeit war es, die Auswirkungen von *Arc/Arg3.1* auf die Reifung der synaptischen Übertragung im Hippocampus zu erforschen. Mein Ansatz bestand darin, die molekularen, strukturellen und funktionellen Eigenschaften von Schaltkreisen im Hippocampus in konditionalen *Arc/Arg3.1*-Knockout-Mäusen (cKO) zu untersuchen, die in früheren Studien mit Deletionen des Gens zu verschiedenen Zeitpunkten während des ersten postnatalen Monats entwickelt wurden. Dazu gehörten eine Keimbahn-KO-Linie, bei der die Deletion während der Embryogenese auftritt, eine "early-cKO"-Linie, bei der *Arc/Arg3.1* während der ersten postnatalen Woche vorhanden ist und die Deletion zwischen den postnatalen Tagen 7-14 (P7-P14) abgeschlossen ist, und eine "late-cKO"-Linie, bei der die Deletion zwischen P21-P36 abgeschlossen ist. Ich setzte eine breite Palette von Methoden ein: In-vitro-Feldaufnahmen, Patch-Clamp-Techniken, 3D-Rekonstruktionen von Dendriten, Immunhistochemie und quantitative konfokale Mikroskopie, Elektronenmikroskopie, Proteomik auf der Basis von Massenspektrometrie und subzelluläre Fraktionierung mit Western Blotting.

Im ersten Teil dieser Arbeit wurden die erwachsenen KO- und cKO-Mäuse zu einem Zeitpunkt untersucht, an dem Arc/Arg3.1 im Hippocampus vollständig deletiert und Defizite bei der oszillatorischen Aktivität und beim Lernen festgestellt worden waren. Die hier vorgestellten Ergebnisse zeigen, dass Arc/Arg3.1 eine wesentliche Rolle bei der Regulierung der zeitlichen Dynamik exzitatorischer Synapsen in einer entwicklungsabhängigen Weise spielt, wobei die stärksten Auswirkungen bei der frühesten Deletion beobachtet wurden. Diese Effekte waren mit Veränderungen von Schlüsselkomponenten der postsynaptischen Dichte verbunden,

darunter die transmembranen AMPA-Rezeptor-Regulationsproteine (TARPs) und PSD-95. Bemerkenswerterweise zeigten meine Ergebnisse auch Veränderungen in der hemmenden synaptischen Übertragung, von denen bisher angenommen wurde, dass sie unabhängig von der *Arc/Arg3.1*-Plastizität sind, was ein erstes mechanistisches Verständnis der oszillatorischen Defizite ermöglicht.

In Teil II dieser Arbeit wurde das proteomische Profil des Hippocampus von erwachsenen WTund Arc/Arg3.1 KO-Mäusen beschrieben, wobei der Schwerpunkt auf den Unterschieden
zwischen den CA1-, CA3- und DG-Unterfeldern lag. Die Ergebnisse bewiesen die Wirksamkeit
einer Nanosekunden-Infrarot-Laser (NIRL)-Ablationsmethode zur zuverlässigen Isolierung
verschiedener Regionen des Mäusegehirns für die anschließende Proteomanalyse. Darüber
hinaus konnte ich zeigen, dass Arc/Arg3.1 das proteomische Profil des Hippocampus auf
subfeldspezifische Weise reguliert, und ich identifizierte neue, interessante Protein-Kandidaten,
die von Arc/Arg3.1 bei niedriger Aktivität reguliert werden. Zusätzlich wurde durch
Anreicherungsanalysen die Rolle von Arc/Arg3.1 beim Proteintransport hervorgehoben.

Schließlich wurde in Teil III die Rolle von *Arc/Arg3.1* bei der Entwicklung der Hippocampusfunktion durch die Untersuchung von Mäusen im Alter von zwei und vier Wochen untersucht. Die Ergebnisse zeigten, dass die Kinetik der exzitatorischen synaptischen Übertragung in keiner der KO-Linien in diesem Entwicklungsstadium verändert ist, was darauf hindeutet, dass sich die im erwachsenen Hippocampus beobachteten Veränderungen in einem späteren Stadium entwickeln. Im Gegensatz zu den Auswirkungen im erwachsenen Gehirn sind die Auswirkungen von *Arc/Arg3.1* im sich entwickelnden Gehirn als Reaktion auf die frühe postnatale Deletion ausgeprägter, was zur aktiven Eliminierung funktioneller exzitatorischer Synapsen und möglicherweise auch zur Eliminierung nicht-funktioneller inhibitorischer Synapsen führt.

Insgesamt liefert diese Arbeit weitere Beweise für die Existenz einer kritischen Periode für die Entwicklung der Hippocampusfunktion und zeigt, dass Arc/Arg3.1 eine Schlüsselrolle bei der Modulation dieser kritischen Periode spielt, indem es die Verdrahtung des Hippocampus-Schaltkreises formt, und zwar nicht nur durch die Modulation exzitatorischer Synapsen, sondern bemerkenswerter Weise auch der inhibitorischen Übertragung. Meine Ergebnisse eröffnen neue Wege zur Erforschung von Arc/Arg3.1-abhängigen molekularen Pfaden und zellulären Prozessen, die an der Verschaltung und Plastizität des Gehirns beteiligt sind.

Introduction

Learning and memory are two interconnected cognitive functions that allow organisms to process and utilize sensory information and adapt to their environment. Learning is defined as a lasting change in behavior due to experience (Domjan, 2018). Memory, on the other hand, refers to the storage of previously learned information (Squire, 2009).

The understanding of how these processes work comes largely from the famous case of Henry Molaison (H.M.), studied by the neuropsychologist Brenda Milner. H.M. suffered from severe seizures caused by a childhood bicycle accident. To alleviate them, neurosurgeon William Scoville performed an experimental surgery, ablating parts of his medial temporal lobe, including both hippocampi. While the surgery worked successfully in reducing seizures, it resulted in a profound inability to form new memories (Scoville & Milner, 1957).

The studies of Milner on the H.M. patient helped to expose the existence of different types of memory. H.M. could still learn new motor skills, which led to a distinction between declarative memories (consciously accessible information) and non-declarative memories (skills and habits). Furthermore, H.M. had no compromises in short-term memory, maintaining information relevant to the current task for a few seconds to minutes. However, he could not consolidate these short-term memories into long-term storage. The case of H.M. provided strong evidence of the role of the medial temporal lobe in converting new experiences into long-term memories. Following studies using animal models have further pinpointed the hippocampus as the critical structure for long-term memory formation (Deacon et al., 2002; Glick & Greenstein, 1973).

A second major function of the hippocampus is spatial navigation. The theory of the hippocampus as a cognitive map was proposed by O'Keefe and Nadel, after the discovery of a group of hippocampal pyramidal cells that represented specific locations in an environment, they named them "place cells" (O'keefe & Nadel, 1978). Subsequent research led to the discovery of three additional cell types, that further supported the hippocampal role in spatial processing. The first type, "Head direction cells" are found in the dorsal subiculum, and complement the activity of place cells. They are independent of the animal's location and signal the horizontal direction of the animal relative to the environment (O'Keefe, 2006; Taube, 2007; Taube et al., 1990). The second type is "grid cells", they are found in the medial entorhinal cortex. These cells fire in multiple locations in an environment, and these locations form a

triangular matrix covering the regions visited by the animal. Grid cells use information about the head direction to provide information on the Euclidean distance and direction metric for the cognitive map (Bush et al., 2014; O'Keefe, 2006). Finally, "boundary cells" fire at a specific distance and direction from environmental boundaries, and they are found in the subiculum, parasubiculum, and medial entorhinal cortex (Bush et al., 2014; Lever et al., 2009; Solstad et al., 2008).

1.1 The hippocampus

The term "hippocampus" frequently refers to the broader "hippocampal formation," which comprises several interconnected regions. The main structure is the hippocampus proper, containing subfields CA1, CA2, and CA3 (CA stands for *cornu ammonis*). Other key regions include the dentate gyrus (DG) and subiculum. The entorhinal cortex, while technically separate, acts as the main input gateway to the hippocampus and is often considered the starting point of the hippocampal circuit (**Figure 1.1**). The key feature of these regions is their functional link through unidirectional pathways. Generally, research has focused on the "trisynaptic circuit". This circuit includes: 1) neurons in layer II of the EC projecting to the DG and the CA3 subfield via the perforant pathway, 2) the granule cells of the DG projecting to the CA3 subfield via mossy fiber projections and 3) pyramidal cells of CA3 projecting to the CA1 subfield through the Schaffer collaterals. However, additional connections exist. For instance, a separate perforant pathway component connects layer III EC neurons to CA1 (also known as the temporoammonic pathway). Moreover, CA1 pyramidal cells project to the subiculum, and both CA1 and the subiculum project back to layer V of the EC, completing the "hippocampal loop" (**Figure 1.1B**).

CA1 is the principal output region of the hippocampus, it stands out for high evolutionary conservation (Benavides-Piccione et al., 2020) and has an essential role in memory consolidation (Ji & Maren, 2007; Lee & Kesner, 2004). Interestingly, CA1 is also more vulnerable to injury compared to other hippocampal areas (Davolio & Greenamyre, 1995). These, among other factors, have made CA1 a region of particular interest for research, which has resulted in a more comprehensive understanding of its structure and function compared to other subfields. Regarding its structure, CA1 is organized into distinct cell layers called strata. The *stratum oriens* (or) mostly contains the basal dendrites of CA1 pyramidal cells and the bodies of some interneurons, including somatostatin (SST)-positive interneurons (also known as OLM cells). Deeper inside, we find the *stratum pyramidale* (pyr) which contains the cell

bodies of pyramidal neurons, along with some interneurons. Including the largest population of inhibitory parvalbumin (PV)-containing interneurons. Next, we find the *stratum radiatum* (rad), a relatively cell-free layer containing the most proximal section of the apical dendrites of pyramidal neurons. Finally, we find the *stratum lacunosum-moleculare* (LM) which contains the cell bodies of some inhibitory interneurons like neurogliaform cells and the most distal part of the apical dendrites of pyramidal cells (Amaral & Lavenex, 2006).

CA1 neurons integrate signals from both excitatory and inhibitory sources. The principal excitatory input originates from CA3 via Schaffer collaterals (**Figure 1.1B**). While these are often depicted as terminating only in the *stratum radiatum*, CA3 axons innervate both the *stratum radiatum* and *stratum oriens* of CA1 (Hjorth-Simonsen, 1973). A second major excitatory input arrives from layer III of the EC through the temporoammonic pathway. This pathway selectively targets the distal apical dendrites in the LM (Deller et al., 1996). Additional excitatory inputs reach CA1 from the nucleus reuniens of the thalamus and the basolateral amygdala, also especially innervating the distal apical dendrites (Dolleman-Van Der Weel & Witter, 1996; Kemppainen et al., 2002).

Inhibitory interneurons, though only about 10% of the cells in CA1, play a substantial role in closely regulating excitatory connections. They are very diverse and can be classified based on several factors, including their anatomy, developmental origin, molecular expression, intrinsic electric properties, and firing patterns (Pelkey et al., 2017).

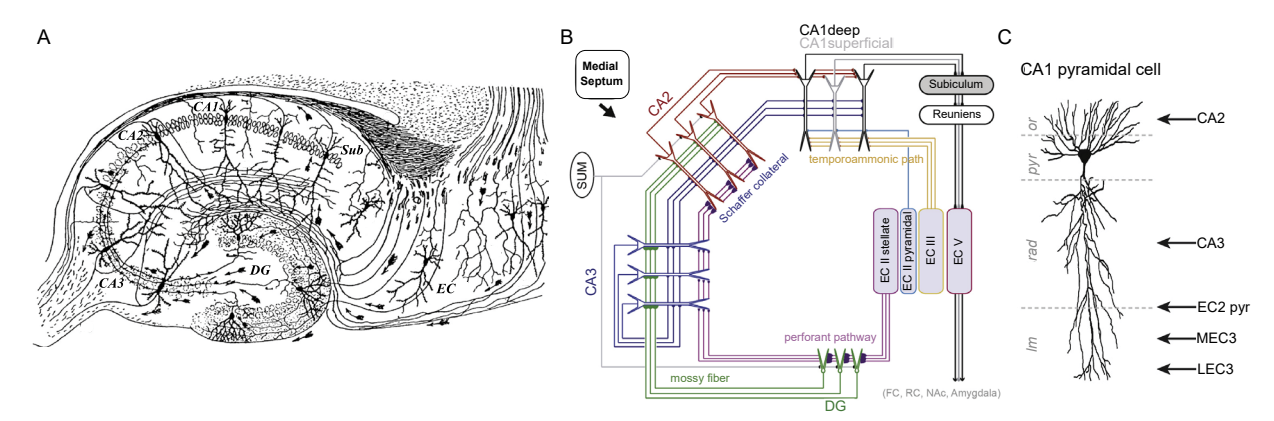


Figure 1.1. The hippocampal circuit. A. Hippocampal formation as originally illustrated by Ramón y Cajal (1911). Horizontal section of a rodent brain with the defined subfields of the hippocampal formation: entorhinal cortex (EC), dentate gyrus (DG), hippocampal CA3, CA2, and CA1, the subiculum (Sub). B. Schematic representation of the hippocampal excitatory circuit. C. Representation of a CA1 pyramidal cell indicating the major excitatory afferents and their location in the axodendritic axis (Adapted with permission from Pignatelli & Rockland, 2020)

One useful way to classify interneurons is by exploring their axonal targets and the specific layers they innervate (Megias et al., 2001). For instance, basket cells, chandelier cells, and axo-axonic cells target either the cell bodies (somata) or the initial segment of the axon of pyramidal

neurons (Somogyi, 1977). This placement grants them strong control over the generation of action potentials in the pyramidal cells (Cobb et al., 1995). On the other hand, OLM cells target the distal dendrites within the stratum lacunosum-moleculare (LM). Their influence is probably focused on regulating local processing within the dendrites, potentially shunting excitatory inputs before they reach the cell body, or modulating the generation and propagation of dendritic spikes (Freund & Buzsaki, 1996).

1.1.1 Hippocampal oscillatory activity

Although GABAergic synapses are a minority in the hippocampus, they play a key role in shaping its rhythmic activity. These rhythms reflect the synchronized firing of large neuronal populations. When these synchronized currents summate, they generate large deflections in electrical recordings, measurable through local field potentials (LFPs). The hippocampus, particularly CA1, is well-suited for the detection of these rhythms due to its densely packed neurons. Here, the parallel alignment of pyramidal cells allows synaptic currents to flow in the same direction and add up, resulting in robust LFP signals. The hippocampus has different forms of brain rhythms including theta rhythms, gamma rhythms, and sharp wave–ripple complexes (Colgin, 2016).

Theta rhythms comprise frequencies that extend between 4 and 12 Hz and are thought to be important for learning, memory, and spatial navigation (Boyce et al., 2016; Buzsaki, 2005; Olvera-Cortes et al., 2002). These theta waves can be detected in all layers of CA1, CA3 and the DG, but have a particularly large amplitude in the LM layer of CA1, indicating their EC origin. Several theta generators have been identified including the medial septum, EC and the hippocampus itself. Theta observed in the stratum LM of CA1 and during awake behavior arise from GABAergic cells of the medial septum which rhythmically disinhibit hippocampal pyramidal cells and thus promote their theta rhythmic firing (Buzsaki, 2002). Cholinergic and glutamatergic inputs from the medial septum also participate in generating and pasting theta oscillations, during attentional tasks and REM-sleep. The critical role of the medial septum in generating theta has been further supported by studies showing that lesions in this area effectively eliminate hippocampal theta activity and rhythmic neuronal firing (Lee et al., 1994; Mitchell et al., 1982).

Gamma rhythms in the hippocampus cover a wide range of frequencies (25-100 Hz). Some researchers propose a further distinction within this range, suggesting the presence of at least two subtypes (Colgin & Moser, 2010).

The first subtype, slow gamma (25-55 Hz), is thought to be driven by interneurons activated by the pyramidal cells in the CA3 subfield and is most prominent within the *stratum radiatum* layer. In contrast, fast gamma (60-100 Hz) seems to be driven by interneurons influenced by the medial entorhinal cortex (MEC). This fast gamma rhythm is specifically dominant in the *stratum lacunosum-moleculare* (Colgin et al., 2009). Supporting this distinction, reports are showing a reduction in fast gamma rhythms when MEC projections to CA1 were blocked in mice performing a spatial memory task (Yamamoto et al., 2014). The specific functions of these gamma subtypes are still under study. Nevertheless, some theories suggest that slow gamma might be involved in retrieving memories, while fast gamma might play a role in encoding sensory information transmitted from the MEC to the hippocampus. Further research is needed to solidify these hypotheses and fully comprehend the functional roles of these different gamma rhythms (Colgin, 2016).

Sharp wave-ripple (SPW-R) complexes consist of very distinct patterns observed in LFP recordings in CA1. These complexes are characterized by large amplitude deflections of negative polarity (~0.01–3 Hz) in the CA1 *stratum radiatum*, known as sharp waves (SPWs), accompanied by a brief, high-frequency (~110–250 Hz) oscillatory pattern of the local field potential (LFP) in the pyramidal layer of CA1, known as "ripples" (Buzsaki, 2015). These phenomena are consistently seen in dissected hippocampal slices, suggesting that they originate within the hippocampus (Maier et al., 2003).

SPWs predominantly reflect excitatory depolarization of the apical dendrites of CA1 resulting from the synchronous bursting of CA3 pyramidal cells (Csicsvari et al., 2000). Studies showing that long-term potentiation of the Schaffer collateral-CA1 synapses leads to an increase in SPW amplitude further supported this fact (Buzsaki, 1984b). In contrast, ripples are the result of local interactions between CA1 pyramidal cells and fast-spiking inhibitory interneurons that target perisomatic regions (Schlingloff et al., 2014; Ylinen et al., 1995). Regarding their function, SPW-R complexes are most common during the slow-wave sleep phase, which led initial studies to focus on their role in "offline" memory functions like consolidation and memory trace elimination (Girardeau et al., 2009; Nadasdy et al., 1999; Nakashiba et al., 2009). However, recent studies suggest a key role for SPW-Rs in "online" functions such as active navigation (Carr et al., 2011; Roumis & Frank, 2015).

1.2 Synaptic transmission

Synapses are contact points between two neurons that allow them to communicate with each other. Synaptic transmission starts with an action potential generated in the presynaptic cell that travels down the axon and finally reaches the presynaptic bouton. Here, via voltage-gated Ca²⁺ channels, it triggers the release of neurotransmitters into the synaptic cleft. These released neurotransmitters then bind to receptors mainly located on the postsynaptic neuron, which leads to the opening of ion channels that ultimately lead to a change in its membrane potential. This change can depolarize the cell, meaning that it brings it closer to its firing threshold and increases the chances of generating an action potential, or hyperpolarize it, in which case it pushes the membrane potential further from the threshold and therefore decreases the probability of firing. Neurotransmitters that depolarize the postsynaptic neuron are considered excitatory, while those that hyperpolarize it are classified as inhibitory.

1.2.1 Excitatory transmission

Glutamate is the primary excitatory neurotransmitter in the brain. Within the presynaptic terminal, glutamate is transferred into vesicles for subsequent release by the vesicular glutamate transporters (VGLUTs). The postsynaptic element on an excitatory synapse is typically located on a dendritic protrusion called a spine (Megias et al., 2001; Uchizono, 1965). Therefore, the number of spines on a dendrite is often used as a proxy for the number of excitatory synapses it has (reviewed in Berry & Nedivi, 2017; Bhatt et al., 2009; Runge et al., 2020). The postsynaptic sites are enriched with scaffold proteins such as PSD-95, which are crucial for the clustering and anchoring of glutamatergic receptors at the membrane (Chen et al., 2015; Niethammer et al., 1996). Other proteins include Shank and Homer which contribute to organizing and holding the postsynaptic structure (Sala et al., 2005).

Glutamate receptors can be ionotropic or metabotropic. However, most excitatory transmission is mediated by the three main ionotropic receptors: kainate, N-methyl-D-aspartate (NMDA), and α-amino-3-hydroxy-5-methyl-isoxazole-propionic acid (AMPA). These receptors are permeable to sodium (Na⁺) ions, and some also to calcium (Ca²⁺) ions, leading to the depolarization of the postsynaptic membrane. This depolarizing current is known as the excitatory postsynaptic current (EPSC) and depends on factors like the membrane potential, the reversal potential of each ion species, its permeability through the receptor, and the mean number of receptor channels opening (Kullmann, 2006). Regarding the structure, each receptor is a tetramer, built from combinations of different subunits arranged around a central pore.

The first type is Kainate receptors. There are five known subunits (GluK1-5) that can form the tetramer and are abundant in the hippocampus; the highest concentration of kainate receptors is found in the CA2 and CA3 subfields, particularly in stratum lucidum, while the lowest density is observed in CA1 (Oermann et al., 2005). Accordingly, recent evidence suggests kainate receptors play a role in hippocampal circuits, particularly the CA2 subfield, but also participate in the regulation of CA1 interneurons (Falcón-Moya et al., 2021; Pressey & Woodin, 2021). The recent development of selective antagonists for Kainate receptors has substantially improved our knowledge, however, they remain poorly understood compared to AMPA and NMDA receptors (Carta et al., 2014; Jane et al., 2009).

NMDA receptors consist of hetero-multimers of NR1 and NR2A-D subunits. Except for the NR3B subtype, all NMDA receptor subtypes are expressed in the hippocampus; the NR2A and NR2B subtypes are the main forms in the hippocampus. NMDA receptors stand out from AMPA and Kainate receptors due to their unique properties. These features aid in their unique role in synaptic function. First, NMDA receptors exhibit slow activation and deactivation kinetics, taking several milliseconds to activate (~7 ms) and hundreds of milliseconds to deactivate (Lester et al., 1990). Second, they have a high permeability for calcium Ca²⁺ ions (Ascher & Nowak, 1988). Finally, a voltage-dependent magnesium (Mg²⁺) blockade resides within the NMDA receptor pore, rendering it inactive at resting membrane potentials (more negative than -50 mV) despite glutamate presence (Nowak et al., 1984). This interplay between high Ca²⁺ permeability and the Mg²⁺ blockade makes NMDA receptors great coincidence detectors at synapses. Calcium influx only occurs when two events overlap: glutamate release from the presynaptic neuron and depolarization of the postsynaptic neuron. This specific scenario takes place only during simultaneous pre- and postsynaptic activity (Wigstrom & Gustafsson, 1986). This coincidence detection is believed to be a crucial element in specific forms of synaptic plasticity, potentially underlying long-term memory storage.

In the hippocampus, AMPA receptors (AMPARs) tend to generate EPSCs much larger than those produced by the other ionotropic receptors. This has led to consider AMPARs as the primary mediators of excitatory transmission. However, the function of excitatory synapses relies not only on the magnitude of depolarizing currents but also on their temporal properties such as rise time, deactivation, and desensitization kinetics of synaptic AMPA receptors. These factors dictate the amount of charge transferred and the timing of synaptic currents, which directly influence synaptic communication (Jacobi & von Engelhardt, 2021).

AMPA receptors (AMPARs) exhibit fast kinetics, with decay time constants of around 5-10 ms (Mosbacher et al., 1994; Schmitz et al., 2017). However, their gating kinetics depend on the subunit composition of the receptors. AMPA receptors are composed of subunits GluA1 to GluA4. AMPAR subunits are subjected to RNA editing at different sites, generating different subunit isoforms. This process allows the swapping of two specific receptor domains. One key region affected by splicing is the "flip/flop" module located near the S2-LBD domain in the extracellular loop (Sommer et al., 1990). Remarkably, in early development, AMPA receptors predominantly contain subunits with the "flip" module. However, as the brain matures, these "flip" subunits are progressively replaced by isoforms containing the "flop" module (Monyer et al., 1991). This shift in subunit composition has an important functional consequence: AMPA receptors with "flip" subunits exhibit slower desensitization compared to those containing "flop" subunits (Koike et al., 2000; Sprengel, 2006).

Of the four subunits, GluA2 probably plays the most important role as it determines crucial ion channel properties: GluA2 has two different editing sites: the arginine to glycine site (R/G), and the Q/R site, where the RNA editing event implies the conversion of a CAG (glutamine) codon to a CGG (arginine) codon, this edition leads to Ca²⁺ impermeability in the entire AMPA channel (Filippini et al., 2017; Osten et al., 2006). In pyramidal cells, the most prevalent receptor assemblies are GluA1/GluA2 heteromers, with a smaller contribution from GluA2/GluA3 combinations and an even smaller proportion (~8%) of GluA1 homomers (Wenthold et al., 1996; Zeng et al., 2019). Importantly, in the mature brain, over 95% of GluA2 transcripts are edited which renders most of the mature AMPA receptors Ca²⁺ impermeable (Seeburg et al., 2001; van der Spek et al., 2022; Wenthold et al., 1996).

AMPA receptors function together with auxiliary subunits, critically influencing their trafficking, localization, and kinetics. A key family of auxiliary subunits is the transmembrane AMPA receptor regulatory proteins (TARPs), with six known isoforms: γ 2, γ 3, γ 4, γ 5, γ 7, and γ 8 (Tomita et al., 2003). The first identified TARP, γ 2 (also known as stargazing), was discovered in a genetic screen of the stargazer mutant mouse, which exhibits a complete loss of surface AMPA receptors on cerebellar granule cells (Chen et al., 2000). Notably, TARP γ 8, with high sequence homology to γ 2, is especially expressed in the hippocampus (Klugbauer et al., 2000).

Excluding γ 5, all TARP family members regulate the synaptic localization of AMPA receptors. Additionally, auxiliary subunits often demonstrate functional redundancy, compensating for each other's absence (Menuz et al., 2008). The amplitude of AMPA receptor-mediated currents

depends not only on the number of postsynaptic receptors but also on their glutamate affinity. And TARP isoforms enhance glutamate affinity (Jacobi & von Engelhardt, 2021; Rouach et al., 2005).

TARPs not only improve synaptic strength by increasing the number of AMPA receptors in synaptic locations but also by anchoring them in nanodomains close to presynaptic vesicle release sites. This is accomplished by strengthening interactions between AMPA receptors and membrane-associated guanylate kinases (MAGUKs) such as PSD-95 (Nair et al., 2013; Zeng et al., 2019).

Importantly, TARPs also regulate the kinetics of synaptic AMPA receptors, particularly deactivation and desensitization rates. Most auxiliary subunits, except for $\gamma 5$, slow down the deactivation rate of AMPA receptors. For instance, heterologously expressed AMPA receptors without auxiliary subunits exhibit deactivation time constants around 0.7 ms (homomeric GluA2) and 1.3 ms (homomeric GluA1), a difference of only 600 μ s. In contrast, incorporating TARP $\gamma 8$ into AMPA receptors significantly increases the deactivation time constant of homomeric GluA1 receptors to around 5 ms and 9 ms, respectively (Jacobi & von Engelhardt, 2021; Kato et al., 2010).

1.2.2 Inhibitory transmission

GABA is the major inhibitory neurotransmitter in the brain, and it is essential for modulating neuronal activity. It is produced from glutamate via the enzyme glutamic acid decarboxylase and then packaged within synaptic vesicles by the vesicular GABA transporter (VGAT) until its release at inhibitory synapses (Gasnier, 2000). Analogous to excitatory synapses, inhibitory synapses are characterized by the presence of specific scaffold proteins. In the case of GABAergic synapses, the key scaffold protein is gephyrin, which serves to anchor GABA receptors at the postsynaptic membrane (Tyagarajan & Fritschy, 2014).

GABA receptors are classified into two main types: ionotropic (GABA_A) and metabotropic (GABA_B). GABA_A receptors, mediate fast transmission and are permeable to chloride (Cl-) ions and, to a lesser extent, bicarbonate (HCO3-) ions (Osten et al., 2006). Since mature neurons have a resting membrane potential more positive than the Cl- reversal potential, the binding of GABA to these receptors triggers an inward flow of Cl- ions, leading to hyperpolarization of the postsynaptic neuron (Bormann et al., 1987; Herbison & Moenter, 2011). This hyperpolarization works against excitatory signals and is called inhibitory postsynaptic current (IPSC).

GABA_A receptors are heteropentameric, implying that they are formed from five different subunits drawn from a large family: α 1-6, β 1-3, γ 1-3, δ , ϵ , π , and θ (Simon et al., 2004). This diversity allows for a wide range of receptor properties, including affinity for GABA and modulators, activation and desensitization rates, channel conductance, and cellular localization. The most common arrangement is two α subunits, two β subunits, and one γ or δ subunit. The two α and β subunits are often the same isoform, but not always. The most abundant subtype in the brain is α 1 β 2 γ 2, estimated to cover 60% of all GABA_A receptors (Osten et al., 2006; Rudolph & Knoflach, 2011).

The expression of GABA_A receptors along the brain strongly influences neuronal activity. Depending on the cell type, their location can vary, they can be found in dendrites, the cell body, or axons. However, they are typically concentrated at postsynaptic sites, mediating inhibitory neurotransmission. Remarkably, some GABA_A receptors are also found extrasynaptically and perisynaptically (Brickley & Mody, 2012). For example, the α 5 subunit is highly enriched in the hippocampus, but it is mostly located in extrasynaptic sites, with only about 25% of these located in the synaptic component (Brunig et al., 2002; Fritschy et al., 1998).

An average pyramidal cell in the CA1 region of the hippocampus receives around 1700 GABAergic synapses, with the highest density concentrated around the cell body (Megias et al., 2001). Inhibitory synapses can target any area of the somatodendritic domain, including the axon initial segment, the critical zone where action potentials are initiated. Inhibiting this region effectively suppresses the activity of the pyramidal cell, controlling its global output (Nathanson et al., 2019; Zhu et al., 2004). Additionally, the apical dendritic trunk has a high density of GABAergic terminals compared to the rest of the dendrite (Papp et al., 2001). Notably, the distribution of GABA_A receptor subunits varies across different synapses of the same pyramidal cell. For example, the α2 subunit is enriched in the axon initial segment but sparsely found at the cell body and dendritic synapses (Nusser et al., 1996). The expression of the α5 subunit is remarkably high on *stratum radiatum*, indicating enrichment in the apical dendrites of hippocampal neurons (Sur et al., 1999).

The location of GABAergic synapses on pyramidal neurons influences the kinetics of IPSCs. CA1 pyramidal cells exhibit at least two distinct IPSC types. A fast component with a decay time constant of around 9 ms, observed on the soma, is mediated by basket cells, and, probably, axo-axonic, bistratified, and horizontal trilaminar cells also contribute. In contrast, a slower dendritic component with a decay time constant of 50 ms, is likely activated by interneurons in the stratum lacunosum moleculare because they project to dendritic regions exclusively (Banks

et al., 1998). While the possibility of distinct receptor subtypes for these two components exists, an alternative explanation lies in electrotonic filtering and the limitations of voltage-clamp recording techniques at distal locations (Maccaferri et al., 2000).

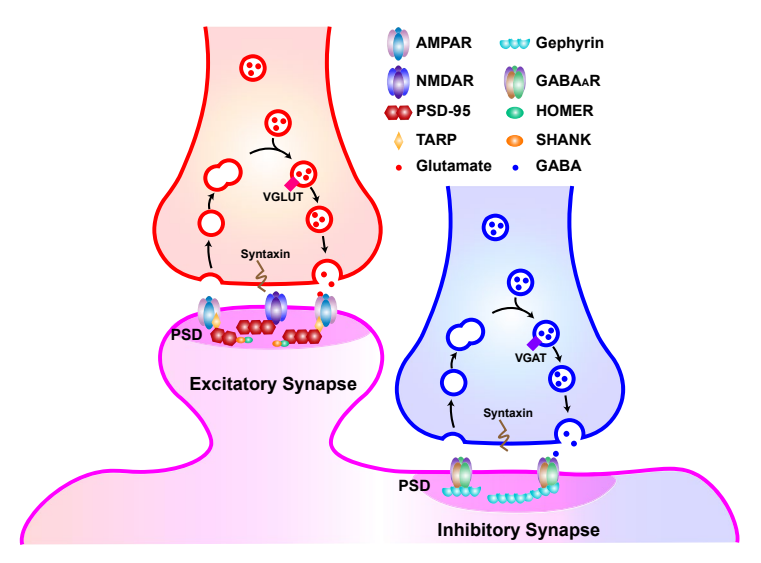


Figure 1.2. Excitatory and inhibitory synapses. Schematic representation depicting some of the main proteins involved in excitatory (left) and inhibitory (right) synapses. The postsynaptic cell is shown in magenta and the presynaptic terminals in red (glutamatergic) and blue (GABAergic).

1.3 *Arc/Arg3.1*

The activity-regulated gene (Arg3.1, also known as Arc) was discovered independently by Paul Worley and Dietmar Kuhl in 1995 (Link et al., 1995; Lyford et al., 1995). This gene has 3.1 kilobases (kb) and encodes a protein of about 45 kilodaltons (kDa). It is highly conserved among mammals, situated on chromosome 8 in humans and chromosome 15 in mice. The Arc/Arg3.1 gene contains a single coding exon and a 3' untranslated region (UTR) with two introns that are spliced to form the mature Arc/Arg3.1 messenger RNA (mRNA), with no known alternative splice variants (Eriksen & Bramham, 2022).

Arc/Arg3.1 is a member of the family of immediate early genes (IEG), and as such it is expressed at very low levels under baseline conditions but is rapidly induced upon robust synaptic activity, including seizures, LTP, and memory-inducing behavioral paradigms (Chawla et al., 2018; Guzowski et al., 1999; Link et al., 1995; Lyford et al., 1995; Plath et al., 2006). What makes Arc/Arg3.1 unique is that its mRNA is induced by patterned synaptic activity and rapidly transported to the dendrites, where it accumulates and undergoes local translation (Steward et al., 1998). Additionally, Arc protein enters the nucleus and there it interacts with histone acetylases, CREB binding protein, and TIP60. Nuclear Arc/Arg3.1 has been shown to contribute to synaptic downscaling by reducing the transcription of AMPA receptor GluA1 subunits and increasing promyelocytic leukemia levels (Korb et al., 2013).

Recent studies also suggest a role for *Arc/Arg3.1* in regulating chromatin state, although the precise mechanism remains unclear (Zhang & Bramham, 2021).

Although *Arc/Arg3.1* is mainly expressed in the brain, *Arc/Arg3.1* mRNA is also found in several peripheral tissues including, the kidney, stomach, liver, spleen, lung, muscle, and heart (Link et al., 1995). Notably, within the brain, *Arc/Arg3.1* expression is restricted to principal neurons expressing CaMKII, mostly corresponding to excitatory neurons and a lesser extent inhibitory GABA-containing ones (Vazdarjanova et al., 2006).

A study using genome-wide analysis made an intriguing discovery showing that Arc/Arg3.1 shares a common ancestor with retroviruses, the Ty3/Gypsy retrotransposon, an ancient genetic element (Campillos et al., 2006). A recent body of evidence suggests that recombinant Arc/Arg3.1 from mammals and Drosophila can self-assemble into virus-like structures containing Arc/Arg3.1 mRNA. These structures can potentially be delivered to neighboring cells upon release in extracellular vesicles (Pastuzyn et al., 2018).

The latest findings reveal that Arc/Arg3.1 can naturally form oligomers in the mammalian brain, dimers are the most abundant form but higher-order oligomers are also present at lower levels. These Arc/Arg3.1 dimers are constitutively expressed throughout the cortex, hippocampus, and dentate gyrus, with the dentate gyrus showing the lowest levels (Mergiya et al., 2023).

1.3.1 Arc/Arg3.1 in synaptic plasticity

Synaptic plasticity is the process that describes how the efficacy of synaptic transmission changes in response to activity and it is considered the mechanism that supports the long-lasting changes in neural circuits underlying learning and memory (Hebb, 2005; Morris et al., 1990). Several forms of plasticity in the glutamatergic synapses have been identified to date. Long-term potentiation (LTP) denotes the strengthening of synapses upon periods of increased activity (Bliss & Collingridge, 1993; Bliss & Lomo, 1973). Conversely, long-term depression (LTD) weakens the synapses in response to decreased activity (Linden & Connor, 1995). More recently, homeostatic scaling has emerged as another key form of plasticity. This process allows neurons to adjust their overall synaptic strength to maintain stable and balanced activity levels in response to fluctuating network activity (Turrigiano & Nelson, 2004). Notably, *Arc/Arg3.1* has been implicated in all three of these distinct forms of synaptic plasticity, suggesting a pivotal and complex role in regulating neural circuit function.

The observation of *Arc/Arg3.1* induction in response to LTP-inducing stimuli suggested a potential role in activity-dependent synaptic plasticity (Link et al., 1995). However, it was not

until the study by Guzowski et al. (2000) that the role of *Arc/Arg3.1* in LTP was first confirmed. Guzowski and colleagues used hippocampal infusions of antisense oligodeoxynucleotides to inhibit *Arc/Arg3.1* expression demonstrating that this inhibition impaired the maintenance phase of LTP in the DG without affecting its induction.

Subsequent studies have confirmed and extended this role (Messaoudi et al., 2007; Plath et al., 2006). For instance, our group used Arc/Arg3.1 knockout (KO) mice to evaluate hippocampal LTP, revealing that Arc/Arg3.1 deletion disrupts LTP not only in the DG but also in the CA1 region. This study also showed an enhanced early LTP phase, in the absence of Arc/Arg3.1, suggesting a biphasic role of Arc/Arg3.1 in LTP. This biphasic role indicates that the absence of Arc/Arg3.1 renders synapses more plastic due to their inability to consolidate previous potentiation (Plath et al., 2006).

Several mechanisms have been proposed to underlie this effect. From the structural standpoint, LTP is often associated with increases in spine density and stabilization. Notably, *Arc/Arg3.1* overexpression has been shown to enhance the density of thin spines and filopodia in the hippocampus, suggesting a role in spine morphology (Donai et al., 2003). Dendritic spines are rich in actin-associated proteins including, CaMKIIβ, drebrin A, and cofilin (Hotulainen & Hoogenraad, 2010). Actin polymerization is crucial for the changes observed in spine volume upon synaptic stimulation, implying that spine growth relies on the assembly of filamentous actin (F-actin). CaMKIIβ itself contributes by bundling and stabilizing F-actin filaments, a process essential for both spine maturation and LTP-induced stabilization (Okamoto et al., 2007). Intriguingly, *Arc/Arg3.1* co-immunoprecipitates with F-actin and directly interacts with drebrin A (Nair et al., 2017), which in turn binds to F-actin (Ishikawa, 2017). Notably, *Arc/Arg3.1* also interacts with CaMKIIβ (Okuno et al., 2012). This intricate network of interactions suggests that *Arc/Arg3.1* might regulate spine morphology by influencing the actin polymerization machinery (Newpher et al., 2018)

Arc/Arg3.1 is crucial for various forms of LTD. A study from our group on Arc/Arg3.1 KO mice demonstrated reduced low-frequency stimulation (LFS)-induced LTD at the Schaffer collateral to CA1 synapse (Plath et al., 2006). Later research, utilizing Arc/Arg3.1 knockdown, revealed that Arc/Arg3.1 is specifically required for metabotropic glutamate receptor (mGluR)-dependent LTD, an effect linked to increased AMPA receptor endocytosis (Waung et al., 2008). The interaction between Arc/Arg3.1 and the endocytic machinery was previously described by Chowdhury et al. (2006). They showed that Arc/Arg3.1 interacts with dynamin and endophilin, proposing that this interaction accelerates AMPA receptor endocytosis. Acute increases in

Arc/Arg3.1 levels led to a downregulation of surface GluA1 and GluA2 receptors. Conversely, neurons lacking *Arc/Arg3.1* exhibited elevated levels of surface GluA1 receptors and reduced endocytosis rates (Chowdhury et al., 2006).

The role of Arc/Arg3.1 on AMPAR endocytosis has been also linked with homeostatic plasticity. Shepherd et al. (2006) investigated this link using cultured neurons. They found that blocking network activity for two days with tetrodotoxin (TTX), a sodium channel blocker, led to a downregulation of Arc/Arg3.1 protein expression. This downregulation, in turn, resulted in an upregulation of surface AMPARs and a subsequent increase in synaptic strength. Conversely, overactivation of the network for two days with bicuculline, a blocker of GABAA receptors, triggered upregulation of Arc/Arg3.1 expression. This increase in Arc/Arg3.1 led to a reduction in surface AMPARs and a decrease in synaptic strength. Notably, these activity-dependent adjustments in synaptic strength via AMPAR trafficking were entirely abolished in cultured Arc/Arg3.1 KO neurons, highlighting the critical role of Arc/Arg3.1 in this homeostatic process (Shepherd et al., 2006).

Okuno et al. (2012) proposed a novel mechanism for LTD termed "inverse tagging". In contrast to the typical scenario where potentiation strengthens active synapses, inverse tagging targets inactive synapses for weakening. Here, newly synthesized *Arc/Arg3.1* interacts with CaMKIIβ under low intracellular calcium concentration. This interaction recruits *Arc/Arg3.1* to these inactive synapses, where it accumulates. The accumulation of *Arc/Arg3.1* then triggers the removal of GluA1 receptors from the postsynaptic density. This reduction in AMPARs ultimately leads to a weakening of the inactive synapses (Okuno et al., 2012).

However, a more recent study challenges the idea that the cellular machinery for endocytosis can directly remove deeply anchored AMPARs from the PSD. Instead, the study by Chen et al. (2022) proposes that Arc/Arg3.1 competes with PSD-95, for binding to transmembrane AMPAR regulatory proteins (TARPs). Since the binding sites for Arc/Arg3.1 and PSD-95 on TARPs overlap, Arc/Arg3.1 could potentially displace AMPARs from the PSD, making them accessible for subsequent endocytosis (Chen et al., 2022).

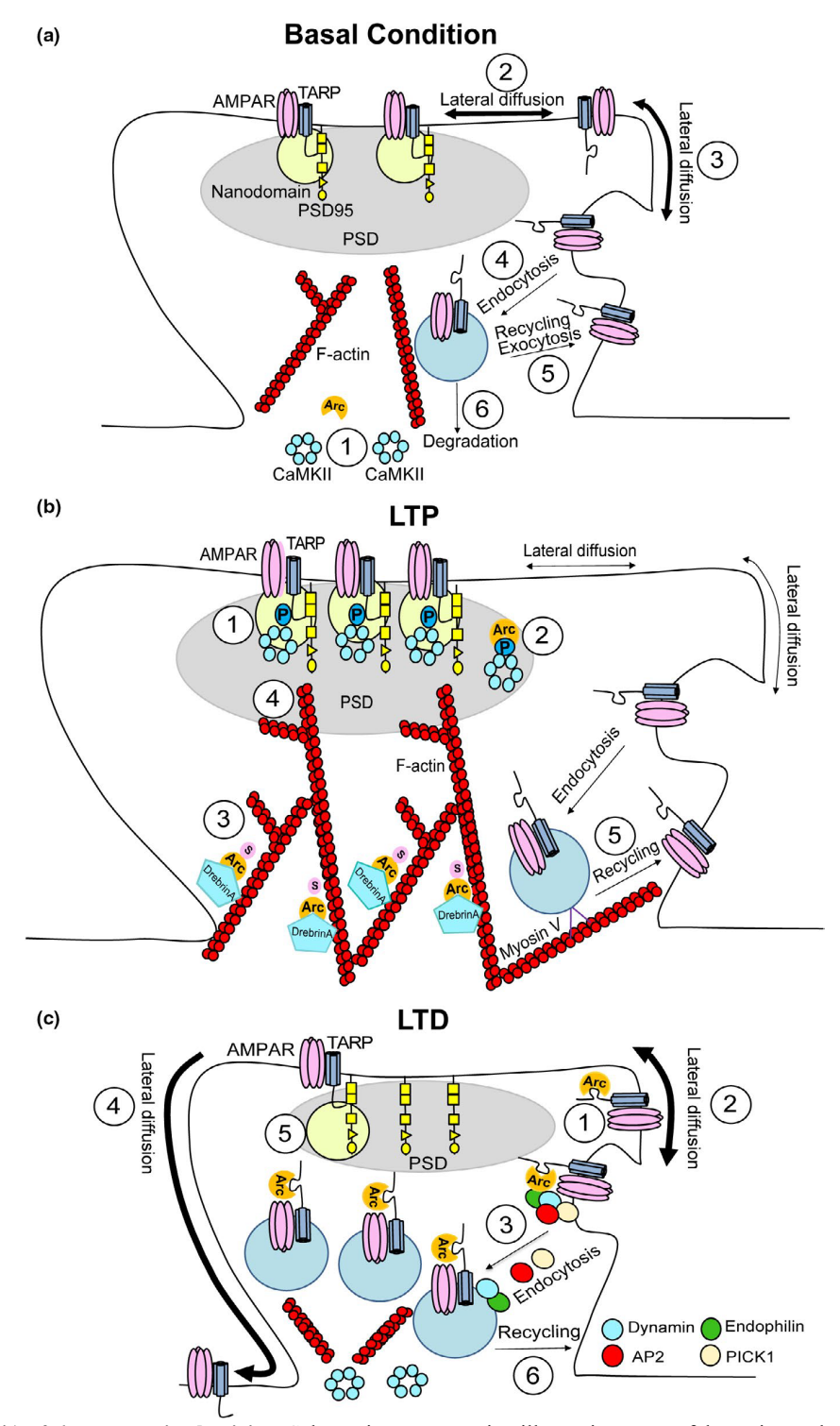


Figure 1.3. *Arc/Arg3.1* **on synaptic plasticity** . Schematic representation illustrating some of the main mechanisms underlying *Arc/Arg3.1* effects on synaptic plasticity (reproduced with permission from Zhang & Bramham, 2021).

1.3.2 Arc/Arg3.1 in memory consolidation

Consolidation is the process by which a new memory trace gradually stabilizes after an initial learning experience (Dudai, 2004). Similar to LTP, memory consolidation depends on *de novo* protein synthesis. Early studies, using different behavioral paradigms, have demonstrated that protein synthesis inhibitors effectively block long-term memory consolidation without affecting

learning or short-term memory (Barondes & Cohen, 1966; Dudai, 1996; Flexner & Flexner, 1966; Nader et al., 2000). The rapid activation of IEGs, including Arc/Arg3.1, in response to synaptic activity made them attractive candidates for regulating memory consolidation. The first report confirming the role of Arc/Arg3.1 in memory consolidation was published in 2000 using hippocampal ODNs. In this study, Guzowski and colleagues demonstrated that blocking Arc/Arg3.1 specifically impairs long-term memory consolidation, with no impact on short-term memory in a spatial memory task in the Morris water maze (Guzowski et al., 2000).

Later on, the study from our group using Arc/Arg3.1 KO mice confirmed and extended these results. They showed that Arc/Arg3.1 KO mice exhibit impaired memory consolidation on the water maze, but also have deficient spatial learning strategies. Furthermore, this study showed that Arc/Arg3.1 is not only required for consolidation in spatial tasks but also for novel-object recognition, contextual, and auditory fear conditioning as well as conditioned taste aversion (Plath et al., 2006). Subsequent studies have demonstrated a role for Arc/Arg3.1 in long-term memory consolidation of an inhibitory avoidance task (Holloway & McIntyre, 2011). And in Pavlovian fear conditioning specifically in the lateral amygdala (Ploski et al., 2008).

1.4 Mass spectrometry-based proteomics

Cells contain thousands of proteins, which are fundamental to every biological process. The proteome refers to the entire set of proteins in an organism, tissue, or cell line (Wilkins, Pasquali, et al., 1996) and proteomics is the study of proteomes. A proteome is the product of a genome, although a proteome is more dynamic, for instance, the number of proteins in the proteome can be higher than the number of genes due to alternative splicing or post-translational modifications (PTM) (Wilkins, Sanchez, et al., 1996). Developments in the field of wholegenome sequencing have allowed the assessment of the complexity of the human proteome. Various techniques have been developed to study the proteome, including two-dimensional electrophoresis, two-hybrid analysis, protein microarrays, and mass spectrometry (MS). MS is the most widely used because it provides the most comprehensive analysis of the complexity of the proteome (Han et al., 2008).

Over the past several years, mass spectrometry-based proteomics has been used to aid in the understanding of the molecular mechanisms in health and disease. An important use is its application in molecular medicine for biomarkers discovery. With a particular focus on the early detection and diagnosis of cancer (Kwon et al., 2021). In the brain, MS-based proteomics has been highly used for the discovery of biomarkers of neurodegenerative diseases including

amyotrophic lateral sclerosis, Alzheimer's, Parkinson's, and Huntington's diseases with a special interest in PTM (Azevedo et al., 2022).

In the healthy brain, MS has been used in a variety of applications. MS has been employed to provide insights into individual cell proteomes of embryonic stem cells, neurons, astrocytes, and oligodendrocytes (Chaerkady et al., 2009; Han et al., 2014; Iwata et al., 2013). Combined with the up-front enrichment of organelles, it has been used to reveal the constituents of synaptic and other subcellular fractions, including excitatory and inhibitory synaptic clefts (Loh et al., 2016; Pandya et al., 2017). Additionally, MS has been used with affinity purification to investigate protein-protein interactions (Pires et al., 2023). Furthermore, MS has been used to resolve the adult mouse brain proteome and identify major brain regions (Sharma et al., 2015).

1.5 Hippocampal development

The mammalian hippocampus is formed prenatally but only matures after birth, with neural migration, dendritic growth, and synaptogenesis, continuing well into infancy. Consequently, hippocampal functions emerge late in postnatal development, after the completion of sensory development (Ohana et al., 2022).

The sequence of maturation of hippocampal circuits underlying memory and spatial representations has been recently described using a targeted pharmacogenetic approach (Donato et al., 2017). The study by Donato and colleagues revealed that stellate cells in the mEC are the first to mature and generate an activity-dependent signal that drives a unidirectional and stage-wise maturation of the other subfields. Three different markers were used as signals of maturation, resulting in slightly different timelines; lack of doublecortin (DCX) expression, parvalbumin (PV) upregulation, and increases in Basson expression. The maturation sequence is: Stellate cells of mEC layer II mature first at P14-17, next pyramidal cells in mEC layer II at P17-20, followed by CA3 at P20, next CA1 at P23-26, followed by a cluster comprising subiculum, layer V mEC, layer V lEC, and DG at P26-P30. Finally, cells in layer II of the lEC lag and develop after P30. These findings suggested that rather than being genetically determined, the maturation of the hippocampal circuit is driven by neural activity (Donato et al., 2017).

1.5.1 Development of the hippocampal structure

In the mouse, pyramidal cells are generated between embryonic (E) days 10 and 18 and the peak generation of CA1 pyramidal cells is from E18 to E19 (Angevine Jr, 1965; Bayer, 1980;

Frotscher & Seress, 2006) while the generation of granule cells in the DG peaks during the first postnatal week (Frotscher & Seress, 2006). *Stratum pyramidale* at birth is thick and composed of 6 to 10 rows of somata, as the hippocampus develops, this layer becomes thinner, with a final composition of 2 to 3 rows of somata in the adult rodent (Frotscher & Seress, 2006). This reorganization process is likely associated with the postnatal generation of glial cells. Another possible contributing factor is the migration of late-born CA1 neurons which is strongly regulated by the glycoprotein Reelin (Ishii et al., 2023). Despite the small percentage of late-born cells that are still migrating, the cell layers of the hippocampus proper and subiculum have already at birth a defined adult-like structure. In striking contrast, over 80% of the granulate cells in DG are generated after birth, the peak generation is around the first postnatal week but some new cells are also formed during adulthood (Frotscher & Seress, 2006). This makes the DG one of the select brain regions where adult neurogenesis takes place. Interestingly, hippocampal interneurons are generated earlier than the excitatory. In CA1 and CA3 they originate at E12-E13 while in DG at E13-14, therefore early development of the hippocampal circuit is disproportionately influenced by GABAergic interneurons (Danglot et al., 2006).

One crucial change during postnatal maturation of the hippocampus is dendrogenesis. While the mature dendritic tree is relatively stable with very low branch turnover, during development the dendritic arbor is very plastic, undergoing high rates of branch additions and retractions (Urbanska et al., 2008). In CA1 neurons, the main branch of the apical dendrite has already reached the hippocampal fissure by postnatal day (P) 5, but they have only a few short branches (Pokorny & Yamamoto, 1981). The apical dendrite undergoes accelerated growth during the first two weeks which then slows down. In mice, apical dendrites typically reach their mature size around P18-P21, however moderate expansion continues until 3.5 - 4 months of age (Sfakianos et al., 2007). In contrast, the basal dendritic tree has already reached its final number of dendrites by P5, albeit, these are still short and unbranched (Pokorny & Yamamoto, 1981). Basal dendrites undergo fast growth between P6 and P12, after which growth slows down but extends up to P30 (Nishimura et al., 2011; Stanke, 2022).

In addition to the gross changes in dendritic structure described above, the first postnatal month is a period characterized by critical changes in fine dendritic structures, namely, dendritic spines. At birth, the number of spines is low and most synapses make contact on dendritic shafts (Fiala et al., 1998; Lohmann & Kessels, 2014). Spinogenesis then increases dramatically reaching its peak around the third postnatal week (Schachtele et al., 2011). It slows down during the fourth week to reach mature levels (Lohmann & Kessels, 2014). It is worth noting that,

although much more stable, compared to the developing brain, the density, shape, and size of spines, remain dynamic in the mature brain (Leuner & Shors, 2004). Mature spines can be regulated by several factors including behavioral training, hormone treatment, environmental enrichment, and sleep (Gould et al., 1990; Greenough et al., 1979; Moser et al., 1994; O'Malley et al., 2000; Rampon et al., 2000; Zhou et al., 2020).

1.5.2 Development of hippocampal membrane properties

The firing of a neuron depends greatly on the number and properties of the synapses it receives. However, three key factors regulate the response of a neuron to synaptic inputs: its dendritic structure and membrane properties; often classified into passive and active properties (Spruston et al., 1994). Passive properties are characterized by their independence from voltage-gated channels and include the resting membrane potential (V_m), membrane resistivity (R_m, input resistance), membrane capacitance, membrane time constant, and intracellular resistivity. Active properties, in contrast, do depend on voltage-gated channels (Spruston & McBain, 2006). Some commonly measured active properties include action potential (AP) features like amplitude, duration, and frequency.

Consistent with the morphological changes, the electric properties of hippocampal cells leave them in a highly excitable state at birth that progressively decreases until the third postnatal week (Pignatelli & Rockland, 2020). In rats, the input resistance and membrane time constant decrease from P2 to P15, whereas the resting membrane potential becomes more hyperpolarized (Spigelman et al., 1992). Regarding the AP waveform, AP amplitude increases dramatically from P2 until P20-P25, whereas AP duration decreases during this period, reaching stable levels by P15 (Spigelman et al., 1992). These changes occur alongside modifications in the currents of Na⁺ channels (Costa, 1996), increases in the number of voltage-dependent K⁺ channels (Sanchez-Aguilera et al., 2020; Spigelman et al., 1992), and changes in the kinetics of K+ currents (Costa et al., 1994; Giglio & Storm, 2014).

1.5.3 Development of hippocampal transmission

As mentioned above, most excitatory synapses generated after the first postnatal week are localized on dendritic spines. Specifically, at P5 over half of the synapses occur on dendritic shafts, by the third week this number decreases to around 20 percent and continues to decrease, while spine synapses proliferate and become dominant in the mature brain (Boyer et al., 1998). Overall, the density of excitatory synapses in the hippocampus is very low at birth and the peak of synaptogenesis is at the end of the fourth postnatal week (Steward & Falk, 1991).

It is worth noting that the composition of excitatory synapses undergoes substantial changes during early development, which results in significant alterations of their function. Regarding NMDARs, GluN2B subunits are predominant during the first two postnatal weeks, later on, their expression decreases whereas GluN2A expression steadily increases during the first postnatal month (Sans et al., 2000). Given than GluN2B-containing NMADRs have higher glutamate affinity (Laurie & Seeburg, 1994), deactivate and desensitize more slowly (Vicini et al., 1998), traffic more rapidly (Groc et al., 2006), and have higher affinity to CaMKII (Leonard et al., 1999); they have a lower threshold for LTP (Clayton et al., 2002). This makes mature NMDARs less likely to undergo synaptic plasticity compared to young NMADRs (reviewed by Lohmann & Kessels, 2014).

Similarly, AMPAR composition changes substantially during the first postnatal weeks. GluA4containing AMPARs in the hippocampus are only observed perinatally, exhibiting almost complete absence by the end of the second week (Zhu et al., 2000). Conversely, the expression levels of GluA1, GluA2, and GluA3 increase dramatically during the second postnatal week and reach adult-like levels around the third postnatal week (Lohmann & Kessels, 2014; Zhu et al., 2000). As mentioned earlier, the expression pattern of "flip" and "flop" versions of the AMPAR subunits is also developmentally regulated (Osten et al., 2006). The flop versions are expressed at low levels during the first postnatal week and increase during the second postnatal week, reaching adult-like levels by P14, whereas the "flip" levels remain stable from birth (Monyer et al., 1991). In addition to the flip/flop variants, GluA2 is prone to alternative splicing in its C-terminal, originating two variants: GluA2 "short" (~50 amino acids) and GluA2 "long" (~70-80 amino acids). The short version, also simply called GluA2, is the most common one. However, the ratio of GluA2 long/GluA2 decreases significantly as the brain develops, from ~0.2 at P7 to ~0.05 at P42 (Kolleker et al., 2003; Osten et al., 2006). One clear functional consequence of the developmental fluctuations in AMPAR composition is a change in their current kinetics. During the first postnatal week, AMPAR-mediated synapses exhibit significantly faster kinetics, which is often attributed to the presence of GluA2-lacking and calcium-permeable exclusively during this time window. In contrast, from P8, AMPARs gradually incorporate more GluA2 subunits, leading to slower synaptic kinetics (Stubblefield & Benke, 2010).

Substantial changes take place also in the presynaptic site of excitatory synapses. VGLUTs are expressed in the glutamatergic neurons and mediate vesicular uptake of glutamate, three different isoforms of VGLUTs are known: VGLUT1-3. However, VGLUT3 has been

associated with other neurotransmitters including acetylcholine, serotonin, and even GABA (Gras et al., 2002). In contrast, in the mature brain, VGLUT1 and VGLUT2 are found exclusively in typical asymmetric excitatory synapses and are therefore considered the classical excitatory vesicular transporters (Fremeau et al., 2002). VGLUT1 and VGLUT2 have a highly complementary expression pattern across the brain and also within specific structures like the hippocampus (Fremeau et al., 2001). Interestingly, the two isoforms show a developmental switch in the hippocampus and cerebellum, with VGLUT2 mRNA expressing transiently in hippocampal pyramidal cells during the first two postnatal weeks and VGLUT1 mRNA expressed in adults (Miyazaki et al., 2003). Subsequent findings further confirmed that VGLUT2 contributes to the high release probability observed in young CA1-CA3 synapses and to the structural maturation of the dendritic tree of CA1 pyramidal cells. (He et al., 2012).

Despite the low number of excitatory synapses during the first postnatal week, substantial spontaneous network activity is observed. This activity results from gap junctions, extrasynaptic transmission, and GABAergic transmission (Blankenship & Feller, 2010). Importantly, until P10, GABA release exerts depolarizing effects on the postsynaptic neuron. The shift to hyperpolarizing actions of GABA is caused by a reduction in the intracellular chloride concentration, which is in turn mediated by the expression of the K^{+/}Cl⁻ cotransporter (Rivera et al., 1999). The early spontaneous activity is crucial for the maturation of early connections and synaptic plasticity.

During the first postnatal week, there is a substantial number of silent synapses (Durand et al., 1996; Gasparini et al., 2000). These are characterized by the presence of functional NMDA receptors and the absence of surface AMPA receptors, at hyperpolarized potentials NMDA receptors are blocked by Mg⁺² and hence remain non-conducting (Kerchner & Nicoll, 2008). GABA-mediated depolarizations, for instance, can remove the Mg⁺² block from NMDA receptors, thereby promoting the insertion of AMPARs into the membrane and unsilencing excitatory synapses (Chancey et al., 2013).

GABAergic synaptogenesis precedes the glutamatergic. Already at birth, over 90 % of the hippocampal interneurons receive postsynaptic currents (PSCs), whereas more than 80 % of CA1 pyramidal cells receive no PSCs (Danglot et al., 2006). Despite the early presence of GABAergic synapses, further dramatic increases in GABAergic synaptogenesis occur until the third postnatal week, as indicated by the increased presence of GABA-positive puncta around the somata of pyramidal cells (Danglot et al., 2006; Seress & Ribak, 1988). Increases in functional inhibitory synapses are also observed within the first postnatal month. The frequency

of GABA_A slow IPSCs increases up to sevenfold from P11 to P35, an effect associated with increased excitability of LM-targeting interneurons with age (Banks et al., 2002).

1.5.4 Development of hippocampal-dependent behavior and hippocampal rhythms

Performance of rodents in hippocampus-dependent tasks is poor before weaning and emerges around P21-P25 in rats (Altman et al., 1973; Stanton et al., 2009). This has been demonstrated using several paradigms, including conditioned eye-blink response (P20-P24; Andrews et al., 1995), passive avoidance (P21; Riccio & Schulenburg, 1969), contextual fear conditioning (P23; Pugh & Rudy, 1996; Rudy & Morledge, 1994) and, spatial learning in the Morris water maze (P21-P23; Rudy et al., 1987).

The maturation of the coordinated activity underlying the complex behaviors mediated by the hippocampus extends over a long postnatal period. Place cells are detectable as early as P14, reach adult numbers by the end of the first month, and continue to develop during the second month (Muessig et al., 2015; Tan et al., 2017). Head direction cell signals are detectable already at P11-P12, however, they do not reach a mature state until P15-P16 (Langston et al., 2010; Tan et al., 2015; Tan et al., 2017). Boundary cells appear at P17, and grid cells can be detected from P16 but do not show mature behavior before P28 (Bjerknes et al., 2014; Langston et al., 2010; Ray & Brecht, 2016; Tan et al., 2017).

At the network level, theta waves are detected from P8, but their power and frequency remain low at P16, reaching adult-like levels by P22 (Wills et al., 2010). Early beta-gamma oscillations (20-30 Hz) are observed as early as P2 (Karlsson et al., 2006). These oscillations subsequently increase in frequency toward the gamma range and are modulated by the emergency of theta waves around P8 (Cossart & Khazipov, 2022; Mohns & Blumberg, 2008). Immature SWPs can be observed as early as P3-P6. In contrast to the mature SPWs, they are not accompanied by ripples in the neonatal brain, which only start to appear around P10 (Leinekugel et al., 2002) and continue developing until P18. This developmental timeline coincides with the switch in GABA signaling from depolarizing to hyperpolarizing (Buhl & Buzsaki, 2005).

1.6 Critical periods

A critical period is a temporal window characterized by heightened plasticity in which experience plays a vital role in the normal development of brain functions. A well-known example of critical periods comes from the work of Konrad Lorenz in the imprinting behavior in hatching birds. His work showed that goslings tend to follow the first large moving object

they see and hear. In nature, this object would be the mother goose, however, in the absence of the mother, goslings will imprint on inappropriate objects. The temporal window for this behavior is around one day, if the exposure to the mother goose does not occur during this period, appropriate parental relationships will never be established (Purves et al., 2013).

Possibly the best-studied example of critical periods for network development is the visual system. The temporal occlusion of one eye during a short time window after birth results in poor vision through that eye, although the eye remains physically healthy, the occlusion exclusively during the critical period deeply alters the structure of the brain (Hensch, 2005). Specifically, research has shown that monocular deprivation causes changes in the structure and function of the primary visual cortex (V1) due to a shift in the ocular dominance of binocular neurons from the occluded eye to the open eye (Hensch, 2018).

One of the effects of monocular deprivation (MD) is a weakening of the synaptic responses upon stimulation of the deprived eye. A possible mechanism mediating this effect is the LTD of intracortical and thalamo-cortical connections. Brief MD alters the spine density of pyramidal neurons while longer MD results in lasting alterations in the length of thalamocortical dendritic trees. An adequate excitation/inhibition balance is considered a signal of the onset of critical periods (Takesian & Hensch, 2013). The parvalbumin (PV) positive inhibitory interneurons have been particularly associated with this process because MD and early auditory deprivation dramatically weaken the connections between PV interneurons and pyramidal cells, whereas connections from other interneurons remain unchanged or even increase in strength (Maffei et al., 2004; Takesian & Hensch, 2013; Takesian et al., 2013). Finally, the duration of critical periods is limited by structural and functional brakes that prevent excessive synaptic plasticity. An example of these brakes is the perineural nets (PNNs), specialized structures of the extracellular matrix that mature by the end of the critical period and surround PV neurons to restrict their function (Carulli et al., 2010; Hensch & Fagiolini, 2005; Takesian & Hensch, 2013). More recent reports support the existence of critical periods in the hippocampus, indicating that, similar to observations in the visual system, early learning experiences are necessary for the functional maturation of the hippocampal system (Bessieres et al., 2020; Sakimoto et al., 2022; Travaglia et al., 2016).

1.7 Arc/Arg3.1 during development

Already in the initial work describing *Arc/Arg3.1*, it was observed that its spontaneous expression in the forebrain is first visible at P8, increases substantially during the second week,

and, reaches its peak around P21. This led to the hypothesis that *Arc/Arg3.1* could have a role in activity-dependent development (Lyford et al., 1995).

The role of Arc/Arg3.1 in the experience-dependent development of the visual system was demonstrated in a study by McCurry and colleagues. Using a KO mouse model, they showed that Arc/Arg3.1 does not disrupt the normal development of V1 organization, visual acuity, or responsiveness. However, Arc/Arg3.1 is necessary for changes in ocular dominance in response to MD during the critical period. These effects were associated with decreased LTD and AMPAR endocytosis in V1 in Arc/Arg3.1 KO mice (McCurry et al., 2010). Furthermore, a following study by Jenks and colleagues found that inducing Arc/Arg3.1 overexpression in adult mice can partially restore juvenile-like ocular plasticity (Jenks et al., 2017).

Recent work from our group used in-situ hybridization to explore the spontaneous expression pattern of Arc/Arg3.1 during the first postnatal month. Confirming previous findings, a semi-quantitative analysis revealed that Arc/Arg3.1 is first detectable in the hippocampus at P7, starting in CA3. Its expression then increases dramatically reaching its peak between the third and fourth weeks. The highest expression is observed in CA1, followed by CA3, whereas DG exhibits only weak levels between P21 and P28 (Castro Gómez, 2016; Gao et al., 2018). The transient spontaneous upregulation of Arc/Arg3.1 when hippocampal-dependent behaviors are just emerging indicated a potential role of Arc/Arg3.1 in the development of the mnemonic network.

Using a conditional deletion approach to ablate Arc/Arg3.1 during distinct developmental stages, the study by Gao and colleagues demonstrated that regardless of the time of deletion, Arc/Arg3.1 is essential for long-term memory consolidation. Additionally, they demonstrated that deleting Arc/Arg3.1 before but not after P21 impairs adult learning in the water maze and alters spatial navigation strategies. Furthermore, deletion before P21 permanently disrupted hippocampal oscillatory activity. Specifically, the results showed that germline deletion (KO) resulted in reduced theta and gamma power and significantly fewer ripples, with the remaining ones showing higher frequency. Arc/Arg3.1 deletion between P7 and P14 (Early-cKO) led to lower theta but normal gamma power. The number of ripples was normal, but the amplitude of the sharp-waves was significantly lower. In strong contrast, deletion after P21 (late-cKO) resulted in an oscillatory activity that was not significantly different from that of WT animals. These findings revealed a role for Arc/Arg3.1 in the regulation of a critical period for spatial learning and hippocampal circuit wiring (Gao et al., 2018).

2 Part I. Loss of Arc/Arg3.1 during early postnatal development persistently changes hippocampal synaptic transmission

2.1 Introduction

The hippocampus is known for its vital role in long-term memory and spatial navigation (Deacon et al., 2002; O'keefe & Nadel, 1978; Scoville & Milner, 1957). The first postnatal month is essential for the structural and functional development of the hippocampus, characterized by massive synaptogenesis, the emergence of oscillatory activity, and complex mnemonic behavior (Lohmann & Kessels, 2014; Nishimura et al., 2011; Pokorny & Yamamoto, 1981; Schachtele et al., 2011; Steward & Falk, 1991; Tan et al., 2017; Urbanska et al., 2008). Recent reports suggest that this temporal window constitutes a critical period for the establishment of learning and memory, mimicking the critical periods observed in sensory structures such as the visual and auditory systems (Bessieres et al., 2020; Ohana et al., 2022; Sakimoto et al., 2022; Travaglia et al., 2016).

Arc/Arg3.1 is an immediate early gene known for its crucial role in memory consolidation and various forms of synaptic plasticity (Plath et al., 2006; Shepherd et al., 2006; Zhang & Bramham, 2021). More recently, reports have shown that *Arc/Arg3.1* expression can regulate the critical period of ocular dominance in the visual cortex (Jenks et al., 2017; McCurry et al., 2010).

Previous work from our group revealed a transient and spontaneous upregulation of Arc/Arg3.1 during the first postnatal month. The study employed three distinct mouse lines lacking the Arc/Arg3.1 gene, each with a precisely controlled deletion timing during development. This approach allowed us to demonstrate that early upregulation of Arc/Arg3.1 in the hippocampus is essential for adult learning and hippocampal oscillations (Gao et al., 2018). The generation of hippocampal oscillatory rhythms is believed to arise from a complex interplay of synaptic connections, including synchronized firing patterns propagating from CA3 to CA1 pyramidal neurons and recurrent inhibition mediated by the connections between pyramidal cells and local interneurons (Buzsaki, 2015; Buzsáki & Wang, 2012; Colgin, 2016). The present study aims to evaluate whether the expression of Arc/Arg3.1 during early postnatal development alters the microarchitecture of excitatory and inhibitory transmission in the hippocampus of adult mice.

2.2 Materials and methods

2.2.1 Mice.

Naïve male and female animals, 3-6 months in age, were housed on an inverted 12 h light/dark cycle (8:00-20:00 dark period) in groups of 3-5 mice per cage under standard conditions (23±1°C, 40-50% humidity; food and water *ad libitum*). All experiments were approved by the city of Hamburg's local authorities and were performed following German and European law for the protection of experimental animals.

2.2.2 Generation of constitutive and conditional Arc/Arg3.1 KO mice.

Three lines of Arc/Arg3.1 deficient mice were generated in which the gene deletion took place at different time points in development as previously described (Gao et al., 2018). Briefly, constitutive Arc/Arg3.1 KO mice were generated as described in Plath et al. (2006) together with floxed Arc/Arg3.1 mutants. To achieve this, vectors were generated of the Arc/Arg3.1 gene in which three LoxP sites were inserted. The vectors were electroporated into embryonic stem cells and subjected to a transient expression of Cre recombinase. The recombination yielded clones in which the open reading frame (ORF) of the gene was deleted (KO) or flanked by two LoxP sites (Arc/Arg3.1 fl/fl). Clones were injected into C57Bl/6J blastocytes and chimeras were bred in the C57Bl/6J background to finally generate the conventional KO and floxed lines. Arc/Arg3.1 fl/fl mice were bred with two different Cre recombinase transgenic mice to produce conditional KO with Arc/Arg3.1 ablated at two different time points. The early conditional KO (early-cKO) mice were generated through breeding with Tg(CaMKIIα-cre)1Gsc mice (Casanova et al., 2001) and Arc/Arg3.1 ablation took place after P7 but before P14. The late conditional KO (late-cKO) mice were generated by breeding to Tg(CaMKIIα-cre)T29-1Stl (Tsien et al., 1996) and Arc/Arg3. I ablation occurred between P21 and P36. Arc/Arg3. I mice were also bred with these respective Cre recombinase transgenic mice to create WT controls for the mutant counterparts.

2.2.3 Patch-clamp recordings

Mice were deeply anesthetized with isoflurane and quickly decapitated. Brains were immediately removed and placed in an ice-cold carbogenated (95% O₂/5% CO₂) dissection artificial cerebrospinal fluid (dACSF) containing (mM): 2.6 KCl, 26 NaHCO₃, 1.23 NaH₂PO₄, 3 MgCl₂, 1 CaCl₂, 212.7 sucrose, and 10 D-glucose. Acute 350 μm horizontal hippocampal slices were prepared with a vibratome (HM 650 V) in dACSF. Slices were placed in warmed

 $(30 \pm 2^{\circ}\text{C})$ dACSF for 30 min followed by recovery for 30 min at $30 \pm 2^{\circ}\text{C}$ in a carbogenated recording ACSF (rACSF) containing (mM): 119 NaCl, 2.5 KCl, 26 NaHCO₃, 1.25 NaH₂PO₄, 1.3 MgSO₄, 2.5 CaCl₂, and 10 D-glucose. Slices were then kept in the rACSF at room temperature until used for whole-cell recordings. Slices were submerged and constantly perfused (4.2 mL/min) with rACSF at 37 ±2°C in a glass bottom recording chamber. A nylon grid was placed over the slices to keep them in place. The slices encompassing the dorsal hippocampus (with bregma coordinates ranging from -2.16 to -2.8) were visualized with an Olympus BX51W1 upright microscope (Olympus, Tokyo, Japan). To locate the Ca1 pyramidal layer, a 4X objective was employed, while a 63X objective was utilized to identify and select cells for patching. For EPSCs: Pipettes (5-7M Ω) were pulled from thin-walled Borosilicate glass and filled with a pipette solution containing (in mM): 107 Cs-gluconate (CsOH + Gluconic acid), 10 tetraethylammonium chloride (TEA), 10 HEPES, 5 QX-314, 4 Mg-ATP, 2.5 CsCl, 0.3 Na₃-GTP and 0.2 EGTA (pH 7.25, 276 mOsm. 0,5% biocytin was added for post hoc morphological visualization. Recordings were performed with a Multiclamp 700B amplifier (Molecular Devices, California, USA), sampled at 10 kHz, and filtered at 3 kHz with a D/A converter (Digidata 1440, Molecular Devices). Spontaneous excitatory (sEPSC) were measured in voltage clamp mode at -70 mV. A square pulse was applied every 20 s to monitor the series resistance (Rs). Recordings with Rs exceeding 30 M Ω or with fluctuations >30% over a period of 1 hr, were excluded from the analysis. Data were collected and analyzed offline using the pCLAMP 10.7 software suit (Molecular Devices). For sEPSC analysis, raw traces were first lowpass filtered at 1 KHz using a Bessel filter in the eighth order and sEPSCs were detected by a threshold-detection algorithm in Clampfit 10.7 set at a threshold of 8 pA and a minimum duration of 1 ms. Events occurring in close succession were considered to be single events if the previous event had decayed to a minimum of 4 pA and remained under 4 pA for at least 1 ms before again crossing the trigger level. Events were visually inspected by the experimenter and the baseline was manually adjusted accordingly. Averages and medians were calculated per cell for the parameters of peak amplitude, decay τ, interevent interval, time to peak, and maximum rise slope. Events with a decay $\tau \ge 50$ ms were excluded from further analysis, as they were deemed biologically unsound. For IPSC: the same conditions were used for the evaluation of inhibitory transmission (Figure 2.7-9) with the following changes: The glutamatergic antagonists CNQX (20µM) and APV (50µM) were applied in the perfusion chamber to isolate inhibitory transmission. The voltage was held at 0 mV to increase the chloride electrochemical drive and consequently the synaptic currents. Detection of sIPSCs was done using the "template search" function in ClampFit. Two types of sIPSCs with distinct

kinetics were observed (with half-widths of 3 and 22 ms, respectively). two templates were created based on traces from 5 WT and 5 KO cells. Final analysis showed that the slow sIPSCs represented ~ 1 % of the total events. Events of the two types are included in the final analysis.

2.2.4 Extracellular field recordings

Slices were prepared following the methodology outlined in the patch-clamp section, with the only difference being that the slicing, recovery, and recordings were performed in the same recording ACSF. Slices were transferred to submerged recording chambers and allowed to equilibrate for an additional 120 minutes before recordings. Extracellular field recordings were made with Synchrobrain (Lohres research, Germany), a system of 4 parallel recording chambers, which allowed the simultaneous recording of 4 brain slices. Recording chambers were continuously perfused with recirculated warmed (37°C) and carbogenated rACSF at a rate of 3 ml/min per chamber. An extracellular electrode (SE-100 concentric bipolar stainless steel) was positioned in the stratum radiatum of CA1, at a distance of approximately 300 µm from the stratum pyramidale. Recordings were conducted without the use of GABA blockers. First, the currents responsible for producing the smallest and largest fEPSP amplitudes were identified. Subsequently, a series of six to ten pulses, randomly generated within this range, were applied. The maximal possible range of stimulation intensities in all experiments was 0-1600 μA. The fEPSP amplitudes were measured online and fitted with a sigmoidal function that was used to generate the input/output curves (IO curves). A mean sigmoidal function per genotype was generated by averaging the individual functions obtained from each slice.

2.2.5 Immunofluorescence staining and confocal imaging

Adult mice were deeply anesthetized with urethane (1-1.5 mg/g body weight) and transcardially perfused with 25 ml 0.1 M PBS followed by 25 ml 4% PFA. The brains were then extracted and postfixed in 4 % PFA for 2-6 days. Cryoprotection was achieved by immersing the brains in a series of 10 %, 20 %, and 30% sucrose/PSB for 3 days. Subsequently, the brains were embedded in Tissue-Tek OCT (Sakura, Finetek) quickly frozen, and then sliced into 20 µm thick sections using a cryostat (Hyrax C60, Microm). For staining of inhibitory clusters, an antigen retrieval step was performed by heating the sections for 60 minutes at 80°C in a citrate buffer at pH 6.0. To prepare the sections for immunostaining, the free-floating sections were first blocked with a solution consisting of 10% horse serum, 0.2% bovine serum albumin (BSA), and 0.3% Triton X in PBS for 1 hour. Following the blocking step, the sections were incubated with the primary antibody solution for 48 hours. The primary antibody solution contained 1% horse serum, 0.2% BSA, and 0.3% Triton X-100 in PBS. To analyze excitatory

synaptic clusters antibodies against the presynaptic marker synaptophysin alongside the postsynaptic scaffolding protein PSD-95 were applied. The primary antibodies in this study were used as follows: rabbit anti-PSD-95 (1:500; Invitrogen, 51-6900), and guinea pig antisynaptophysin 1 (1:1000; Synaptic Systems, 101004). To analyze inhibitory synaptic clusters antibodies against the presynaptic marker VGAT and gephyrin were applied. The primary antibodies in this study were used as follows: Mouse anti-gephyrin (1:300; Synaptic Systems, 147 011), and guinea pig anti-VGAT (1:500; Synaptic Systems, 131004). Following primary antibody incubation, the sections were subjected to incubation with secondary antibodies conjugated with fluorophores at room temperature for 2 h. The secondary antibodies were used as follows: goat anti-mouse DyLight 633 (1:200; ThermoFisher, 35513), goat anti-rabbit AlexaFluor 555 (1:200; ThermoFisher, A-21428), and goat anti-guinea pig AlexaFluor 488 (1:200; ThermoFisher, A-11073). Subsequently, the sections were rinsed with PBS and mounted using ProLong Gold Antifade Mountant with DAPI (Invitrogen, P36931), and stored in the dark. For excitatory clusters: The quantification of synaptic clusters was performed in the strata oriens, pyramidale, and radiatum of the hippocampal CA1 region, a minimum of 3 animals per group was used. Two brain sections per mouse were selected at bregma coordinates -1.94 to -2.06. Non-overlapping image stacks (4 per mouse) were obtained, using a 63X 1.4 NA oil-immersion objective and a 1X digital zoom with the pinhole set to 1 AU. Image stacks consisting of four consecutive images were captured with dimensions of 2272 x 2272 pixels and an increment of 0.25 µm per step. This imaging setup resulted in an imaged region size of $184.52 \times 184.52 \times 0.75 \mu m$, with a voxel size of $0.0813 \times 0.0813 \times 0.25 \mu m$. The laser intensity, detector sensitivity, and line averaging parameters were optimized using sections stained with secondary antibodies only. The same image acquisition parameters were applied to all mice sections to ensure consistency. For analysis, two regions of interest (ROI) were manually selected from each image. Each ROI had dimensions of 800 x 800 x 4 pixels, resulting in an imaged region size of 65.04 x 65.04 x 0.75 µm. The analysis of the selected ROIs was performed using Imaris 9.3 (Bitplane) using the Spot function and the MATLAB R2017 (MathWorks) extension for Spot colocalization. Automatic spot detection was employed, using specific diameter thresholds for each protein marker. Spots with a diameter greater than 0.2 µm for PSD-95 and gephyrin, and greater than 0.3 µm for synaptophysin and VGAT, were considered for further analysis. To assess colocalization, the largest center-to-center distance between either synaptophysin and PSD-95 or VGAT and gephyrin spots was set at 0.7 µm. This criterion ensured that only spots within proximity were considered colocalized. For inhibitory clusters: the same conditions were used with the following changes: Four animals per group were used

and *lacunosum moleculare* was included in the analysis. The image stacks consisted of 5 instead of 4 planes. The digital zoom was set to 2.5 to capture images of 1024 x 1024 pixels. This imaging setup resulted in an imaged region size of 73.81 x 73.81 x 1 μ m, with a voxel size of 0.072 x 0.072 x 0.25 μ m. The entire image was used as a ROI except for pictures of the pyramidal layer. In this case, a ROI of 1024 x 814 x 5 pixels was selected to avoid the inclusion of small segments of strata *oriens* and *radiatum*.

2.2.6 Western-blot analyses

Mice were deeply anesthetized with isoflurane, quickly decapitated and brains were immediately dissected on ice to obtain the hippocampus. The tissue was frozen in dry ice and stored at -80°C for further processing. Samples were homogenized in ice-cold Triton-X lysis buffer with protease and phosphatase inhibitors (containing 1x PBS, 1mM EDTA, 1mM EGTA, 1% Triton-X100, and 1x cOmplete protease inhibitor cocktail). Protein concentrations were determined using the PierceTM BCA Protein Assay Kit following the manufacturer's instructions (Thermo-Fisher Scientific, Waltham, USA). Equal amounts of protein were separated on 10% SDS-PAGE and transferred to Polyvinylidene fluoride (PVDF) membranes (Merck Millipore, Darmstadt, Germany) for 2 h at 4°C with 110V using Mini-PROTEAN TransBlot system (Bio-Rad, Hercules, USA) and blotting buffer (25 mM Tris-Base, 192 mM glycine and 10% methanol). Membranes were blocked in PBS containing 5% non-fat milk with 0,01% tween-20 for 1 h at room temperature. Membranes were then incubated with primary antibody overnight at 4°C in the buffer recommended by the manufacturer. The following antibodies were used at the indicated dilutions: Mouse anti- β-Actin (1:1000, Sigma, 5441), mouse anti-PSD95 (1:2000, Dianova, MA1-046), mouse anti-SAP102 (1:5000, Biozol, ANI-75-058), rabbit anti-GAPDH (1:1000, Cell Signaling, #2118), rabbit anti-GluA1 (1:1000, Millipore, AB 1504), rabbit anti-GluA2 (1:1000, Millipore, AB1768), mouse anti-GluA3 (1:200, Millipore, MAB5416), rabbit anti-Stargazin TARPy2/8 (1:1000, Millipore, 07-577), mouse anti-VGlut1 (1:2000, Synaptic systems, 135011), guinea pig anti-VGlut2 (1:5000, Synaptic systems, 135404), mouse anti-gephyrin (1:250, DB Bioscience, 610585), rabbit, anti-GABA-A receptor γ2 (1:1000, Synaptic Systems, 224003), rabbit anti-GABA-A receptor α2 (1:1000, ThermoFisher Scientific, 224103), guinea pig, anti-GABA-A receptor β3 (1:2000, Synaptic Systems, 224004). The membranes were then washed and incubated with fluorescently conjugated secondary antibodies according to the species for 1 h at room temperature as follows: goat anti-mouse (1:5000, Cell Signaling, #7076), goat anti-rabbit (1:5000, Cell Signaling, #7074) and, goat anti-guinea pig (1:2000, Invitrogen, 614620).

Membranes were washed again and visualized using the Super Signal chemiluminescence reagent (ThermoFisher Scientific) and the signals were detected by ImageQuant LAS4000 (Fujifilm, GE Healthcare Europe). B-Actin and GAPDH were used as loading controls.

2.2.7 Subcellular fractionation

Subcellular fractions of hippocampal samples were prepared by differential centrifugation as described previously (Henson et al., 2012). Hippocampi were homogenized in a buffer containing 320 mM sucrose and 4 mM HEPES, pH 7.4, 2 mM EDTA pH 8.0, and PhosStop. The homogenate was centrifuged at 4°C for 10 min at 1400 g to produce a pellet (P0), the supernatant (S0) was stored for later and the pellet was resuspended and spun again at 700g for 10 min at 4 °C. The pellet P1 was discarded, while the supernatant was collected, combined with the previous one, and centrifuged at 13,800 g for 10 min to produce a pellet (P2) and supernatant (S2). The pellet was resuspended in the original volume of homogenization buffer and centrifuged for 10 min at 13,800 g. The pellet was resuspended in a buffer containing 2 mM EDTA pH 8.0, and PhosStop and hypotonically lysed by the addition of ice-cold water and homogenized in a glass Teflon homogenizer (five strokes). The lysate was adjusted to 4 mM HEPES by the addition of 1 M HEPES, pH 7.4, and centrifuged for 20 min at 25,000 g. The synaptosomal fraction was layered on a discontinuous gradient consisting of 0.85, 1.0, and 1.2 M sucrose in 4 mM HEPES, pH 7.4, and subjected to density centrifugation at 4°C for 2 h at 82,500 g. The synaptic plasma membrane (SPM) fraction was collected, resuspended in 0.5% Triton X-100-containing buffer, and centrifuged for 30 min at 22,000 g to obtain the postsynaptic density (PSD) and extrasynaptic (SN) fractions.

2.2.8 Experimental design and statistical analyses

Data were analyzed with Prism 8 (GraphPad Software Inc.). No statistical method was used to predetermine sample size, but our sample sizes are comparable to those reported in previous studies. Statistical tests used were as follows: Mann–Whitney U test, Kolmogorov–Smirnov test, and mixed-design analysis of variance with Sidak's post hoc test. The type of test is indicated in the main text. A p-value below 0.05 was considered significant. All graphs were generated with Prism 8, Origin-Pro 2017, Igor Pro 6.3 (WaveMetrics), Adobe Illustrator CS5.5, and MATLAB R2021a/R2022b (MathWorks). Experimenters were blind to the genotype until the conclusion of the experiments and analysis. Values presented in the figures are mean ± SEM or median with 25th and 75th percentile, as indicated.

2.3 Results

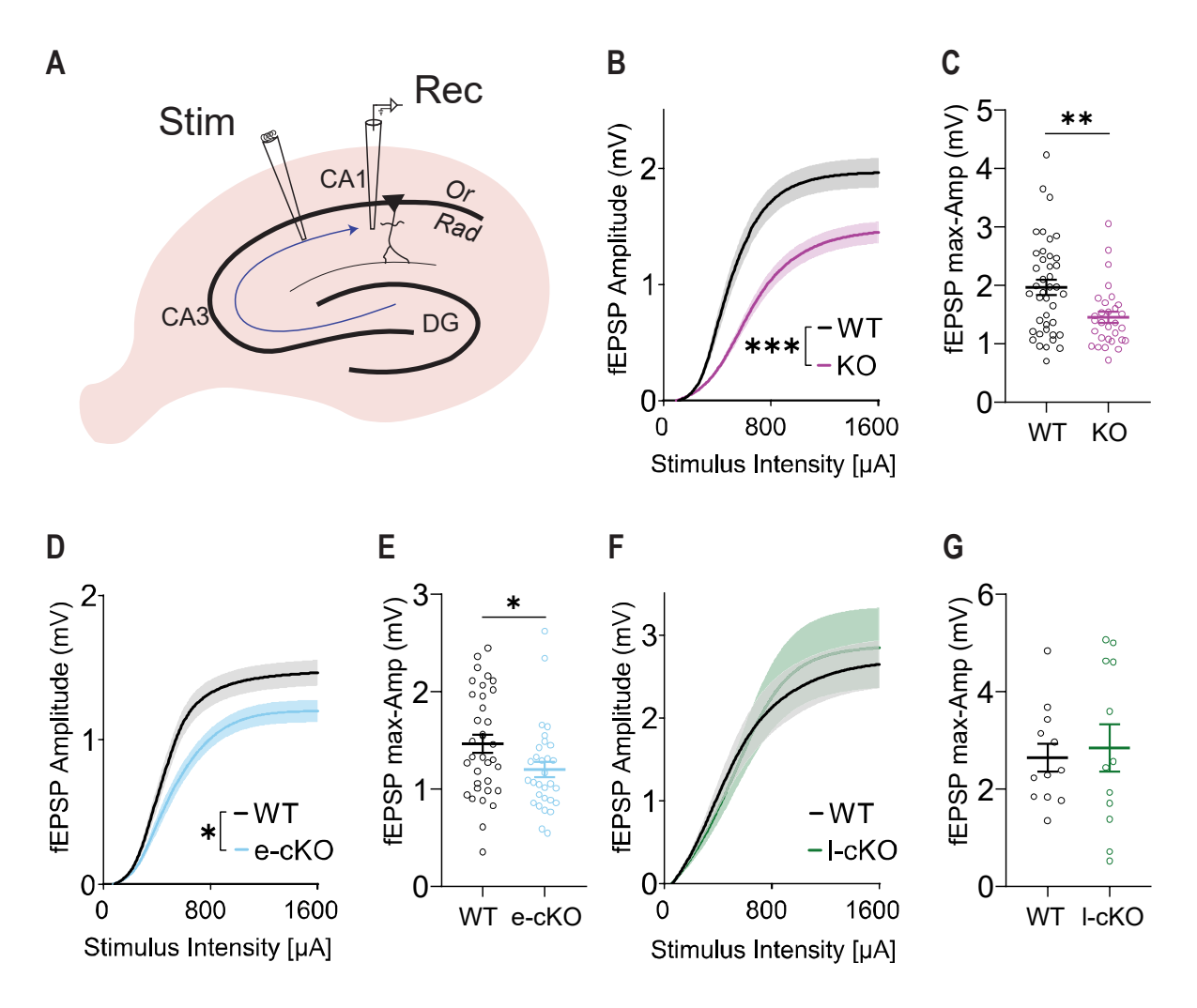


Figure 2.1. Arc/Arg3.1 genetic deletion before P21 decreases the amplitude of the fEPSP responses . A. Schematic representation of the recording protocol. B, D, F: IO curves of the different KO lines compared to their respective WT controls. Continuous lines represent mean values and shadows \pm SEM. (Mixed-effects ANOVA, genotype effect marked *p<0.05, **p<0.01). C, E, G: Scatter plots, mean \pm SEM of the response amplitude at the maximal intensity (1600 μ A). (Mann-Whitney U test *p<0.05, **p<0.01).

2.3.1 Reduced fEPSP amplitude in germline and early Arc/Arg3.1 KOs

To investigate the role of Arc/Arg3.1 in the establishment of the network architecture during early postnatal development, the three KO lines developed by Gao and colleagues will be used. The first line, a germline knockout (KO), has the gene deleted in its germline, meaning all offspring are either wildtype (WT) or KO already at embryogenesis (Plath et al., 2006). Conditional KO (cKO) lines were generated by breeding $Arc/Arg3.1^{\text{fl/fl}}$ with Cre-carrying transgenic mice. In the early conditional knockout (early-cKO) line, Arc/Arg3.1 is selectively deleted between postnatal days 7-14 (P7-P14). Whereas, in the late conditional knockout (late-cKO) line, the Cre recombinase triggers deletion later, between P21-P36 (Gao et al., 2018). To investigate baseline synaptic transmission in WT and Arc/Arg3.1 KO mice, fEPSP amplitudes

were recorded at CA3-CA1 synapses (**Figure 2.1A**). Late-cKO mice showed similar fEPSP amplitudes to WT controls. However, both germline and early-cKO mice exhibited significantly reduced fEPSP amplitudes (**Figure 2.1B**. WT vs KO, F_(1,69)=14.62, p=0.0003, WT: n=41, KO: n=30; **Figure 2.1D**. WT-control vs early-cKO, F_(1,65) = 6.412, p=0.0138, WT-control: n=35, early-cKO: n=32; **Figure 2.1F**. WT-control vs late-cKO, F_(1,22)= 0.04113, p=0.841, WT-control: n=12, late-cKO: n=12). Our findings demonstrate that eliminating *Arc/Arg3.1* in early postnatal development (before P21) leads to suppressed hippocampal synaptic responses in adulthood. This effect is evident in the scatter plots, which illustrate a reduced fEPSP amplitude in response to the maximal stimulus intensity compared to control mice (**Figure 2.1C**. WT vs KO, U=379, p=0.005, WT: n=41, KO: n=30; **Figure 2.1E**. WT-control vs early-cKO, U=387, p=0.029, WT-control: n=35, early-cKO: n=32; **Figure 2.1G**. WT-control vs late-cKO, U=68, p=0.843 WT-control: n=12, late-cKO: n=12).

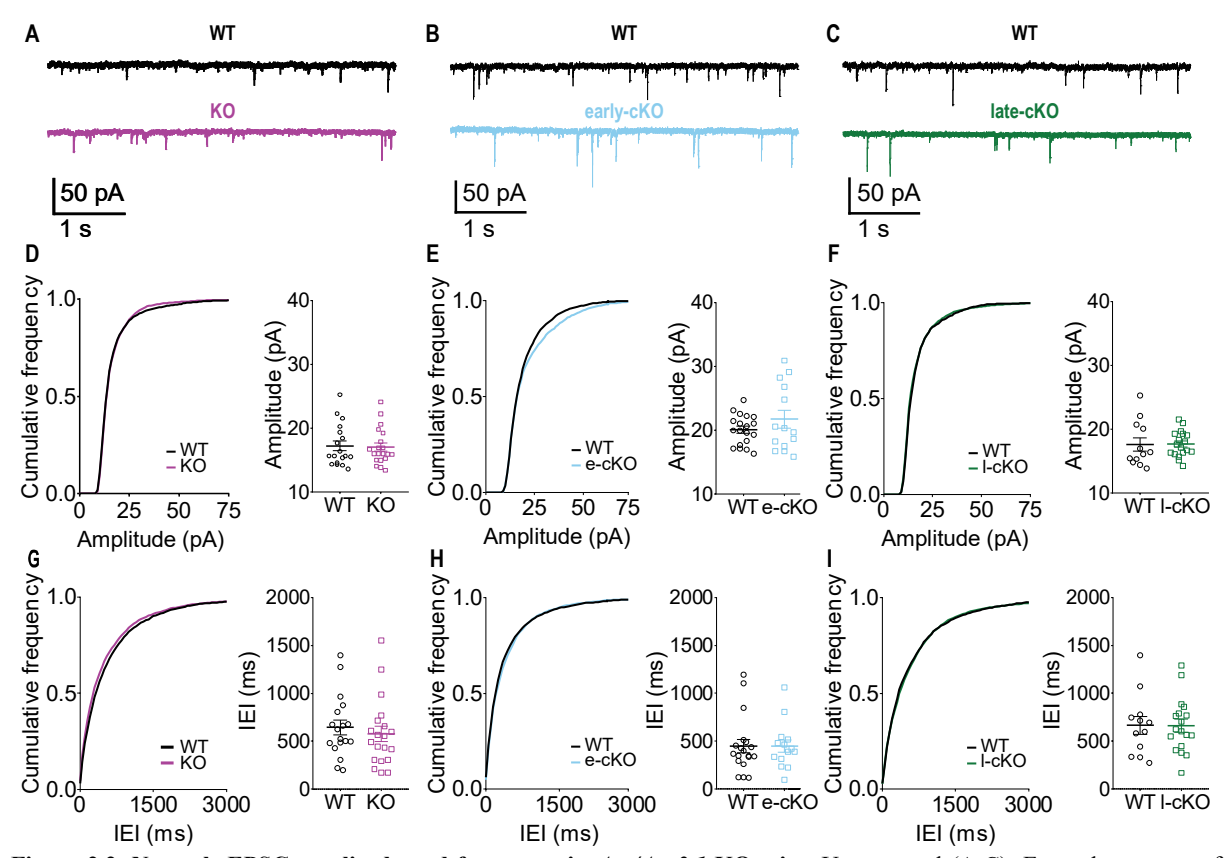


Figure 2.2. Normal sEPSC amplitude and frequency in *Arc/Arg3.1* **KO mice**. Upper panel (A-C): Exemplary traces of sEPSCs recorded at -70 mV in WT (black), KO (magenta), early-cKO (blue; e-cKO), and late-cKO (green; l-cKO) mice. D-I Left: Cumulative frequency histograms of sEPSC amplitude (D-F) and interevent interval (IEI) (G-I) for WT, KO, early-cKO, and late-cKO mice. D-I Right: Scatter plots showing the mean ± SEM of each parameter for each group. Each point represents the mean value from one cell. No significant differences were observed between the groups (Mann-Whitney U test p>0.05). The recordings presented in this figure were performed by Alexa Sliby as part of her master's thesis.

2.3.2 Deletion of *Arc/Arg3.1* does not alter the amplitude or frequency of spontaneous excitatory postsynaptic currents (sEPSCs)

The diminished fEPSP amplitude suggests a reduction in overall CA3-CA1 network output following Arc/Arg3.1 deletion before P21. However, since the recordings were performed without GABAergic blockers, the influence of inhibitory transmission on the fEPSP responses cannot be completely ruled out. Furthermore, fEPSPs reflect the combined response of multiple synapses, to reveal whether the total number of synapses is reduced or whether the properties of unitary synapses are altered; we employed patch-clamp recordings to measure spontaneous excitatory postsynaptic currents (sEPSCs). By holding the cells at -70mV, we reduced the driving force for GABAergic transmission, thereby minimizing its contribution to the recordings. The peak amplitude and frequency of sEPSCs were measured to evaluate excitatory synapse strength and number. Representative traces revealed comparable amplitude and frequency patterns across KO lines relative to their WT counterparts (Figure 2.2A-C). Cumulative histograms failed to indicate obvious differences between groups, although earlycKO mice exhibited a slight deviation in the right tail of the distribution, suggesting the presence of more sEPSCs with larger amplitudes compared to WT controls (Figure 2.2D-F). Quantitative analysis of mean peak amplitudes yielded no statistically significant differences between WT and KO mice across all lines (Figure 2.2D. WT vs KO, U=173, p=0.85, WT: n=18, KO: n=20; **Figure 2.2E.** WT-control vs early-cKO, U=126, p=0.82, WT-control: n=19, early-cKO: n=14; Figure 2.2F. WT-control vs late-cKO, U=91, p=0.49, WT-control: n=12, late-cKO: n= 18). The frequency of sEPSCs, as determined by inter-event intervals, did not show significant differences between WT and KO mice across all lines (Figure 2.2G. WT vs KO, U=147, p=0.34, WT: n=18, KO: n=20; **Figure 2.2H**. WT-control vs early-cKO, U=126, p=0.82, WT-control: n=19, early-cKO: n=14; **Figure 2.2I**. WT-control vs late-cKO, U=102, p=0.82, WT-control: n=12, late-cKO: n= 18). Small shifts in the upper 30% of the cumulative frequency histograms were detected in KO mice, which did not affect the medians and further indicated the absence of overt effects on sEPSC frequency.

2.3.3 Deletion of *Arc/Arg3.1* before P21 is associated with changes in the kinetics of sEPSCs

The persistent alteration of hippocampal oscillations following early *Arc/Arg3.1* deletion adds to the ongoing debate about the underlying mechanisms of these oscillations. One prominent model, proposed by Brunel and Wang (2003), suggests that network synchrony hinges on synaptic time constants. To examine the kinetics of sEPSCs, we measured their rise and decay

components, namely the time to peak, and decay time constant (decay τ). Germline KO mice exhibited a significant decrease in the time to peak compared to WT controls (**Figure 2.3D**. U=93, p=0.0094, WT: n=18, KO: n=20). Early-cKO mice, although not significantly different, showed a tendency towards a shorter rise time (**Figure 2.3E**. U=87, p=0.098, WT-control: n=19, early-cKO: n=14). In contrast, late-cKO mice had no significant differences in time to peak compared to WT controls (**Figure 2.3F**, U=82, p=0.29, WT-control: n=12, late-cKO: n=18). These data suggest that deletion of Arc/Arg3.1 before P21 but not after reduces the rise kinetics of sEPSCs. The shift in the cumulative histograms of both germline and early-cKO further supports this finding (**Figure 2.3D-E**). In contrast, the late-cKOs exhibited a slight shift in the right end of the histogram, suggesting that only a small subset of events with longer rise times are absent in late-cKO mice compared to their corresponding WT controls (**Figure 2.3F**).

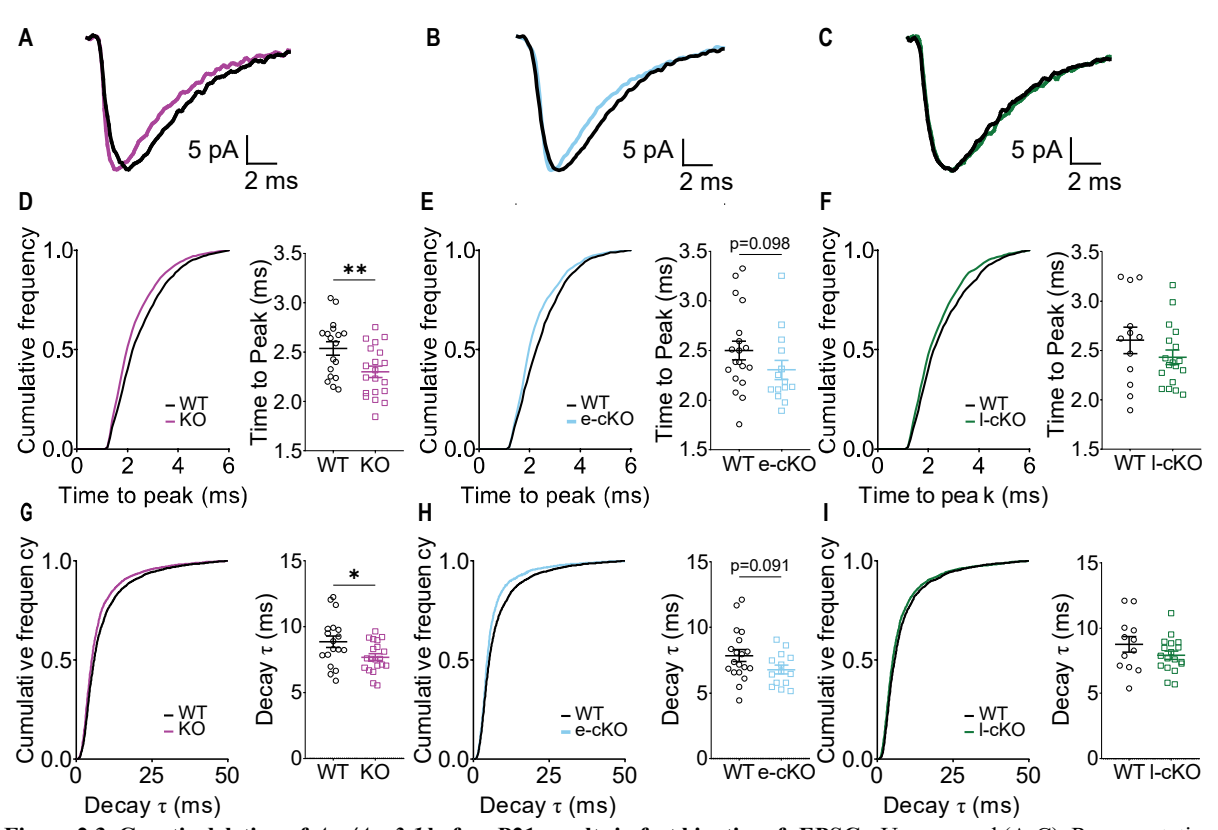


Figure 2.3. Genetic deletion of Arc/Arg3.1 before P21 results in fast kinetics of sEPSCs. Upper panel (A-C): Representative averaged sEPSC traces recorded from WT, KO, and conditional KO mice (30-50 events per trace). Left panels (D-I): Cumulative frequency histograms of sEPSC time to peak (D-F) and decay τ (G-I) for each group. Right panels: Scatter plots showing mean \pm SEM values for each parameter, with each point representing the mean value from a single cell. Statistical significance was determined using Mann-Whitney U tests, with *p<0.05 and **p<0.01 indicating significant differences between groups. e-cKO= early-cKO; l-cKO= Late-cKO. The recordings presented in this figure were performed by Alexa Sliby as part of her master's thesis.

Similarly, the decay time constant of sEPSCs was shortened when *Arc/Arg3.1* deletion occurred before P21 but not after. Germline KO mice exhibited a significant decrease in decay time constant (**Figure 2.3G**. U=111, p=0.044, WT: n=18, KO: n=20). Early-cKO mice again showed a tendency towards a reduced decay time (**Figure 2.3H**. U=86, p=0.091, WT-control: n=19,

early-cKO: n=14). Conversely, late-cKO mice showed no significant differences compared to their WT controls (**Figure 2.3I**. U=83, p=0.3, WT-control: n=12, late-cKO: n= 18). The cumulative histograms further corroborated this effect, demonstrating a shift in the distribution for both germline and early-cKO mice, but not for late-cKO mice (**Figure 2.3G-I**). These findings collectively indicate that *Arc/Arg3.1* deletion before P21 significantly reduces the rise and decay kinetics of sEPSCs, while deletion after P21 does not. This suggests that synaptic kinetics can be established during early development and continue into adulthood, with *Arc/Arg3.1* playing a crucial role in regulating this ongoing process.

2.3.4 Germline and Early *Arc/Arg3.1* KO mice exhibit a lower density of excitatory clusters in the CA1 region of the hippocampus.

Our electrophysiological studies revealed that deletion of *Arc/Arg3.1*, especially when occurring before the third postnatal week, significantly impacts excitatory hippocampal synaptic function. To assess synaptic organization from a structural perspective, we used immunostaining to visualize and quantify synapses across the various layers of CA1, labeling presynaptic sites with synaptophysin and excitatory postsynaptic sites with PSD-95, colocalization of these two markers was considered an indicative of excitatory synapses. In both germline and early-cKO mice, we observed a significant decrease in the total number of PSD-95 clusters and a reduction in colocalized PSD-95 with Synaptophysin clusters. (Germline: Total. **Figure 2.4**B. WT: n=12, KO: n=12; OR: U=12, p<0.001; PYR: U=8, p<0.001; RAD: U=23, p=0.004, Colocalized. **Figure 2.4**C. WT: n=12, KO: n=12; OR: U=4, p<0.001; PYR: U=7, p<0.001; RAD: U=12, p<0.001; early-cKO: Total. **Figure 2.4**

Figure 2.4E. WT-control: n=12, early-cKO: n=12; OR: U=32, p=0.021; PYR: U=36, p=0.039; RAD: U=41, p=0.078, Colocalized. **Figure 2.4Figure 2.4**F. WT-control: n=12, early-cKO: n=12; OR: U=32, p=0.021; PYR: U=33, p=0.024; RAD: U=38, p=0.052). In contrast, late-cKO mice exhibited remarkable preservation of total and colocalized PSD-95 clusters, except for a slight increase in colocalized clusters in the pyramidal layer (Total. **Figure 2.4**H. WT-control: n=12, late-cKO: n=12; OR: U=69, p=0.89; PYR: U=51, p=0.24; RAD: U=54, p=0.32, Colocalized. **Figure 2.4Figure 2.4**I. WT: n=12, late-cKO: n=12; OR: U=70, p=0.93; PYR: U=35, p=0.033; RAD: U=55, p=0.35). This indicates that late deletion of *Arc/Arg3.1* does not significantly alter synaptic clustering patterns. Therefore, our data indicate that *Arc/Arg3.1* deletion before P21 disrupts excitatory synaptic clustering in CA1, while late deletion does not have a significant impact on this process. These findings highlight the crucial role of *Arc/Arg3.1*

in regulating synaptic development and function during early postnatal hippocampal maturation.

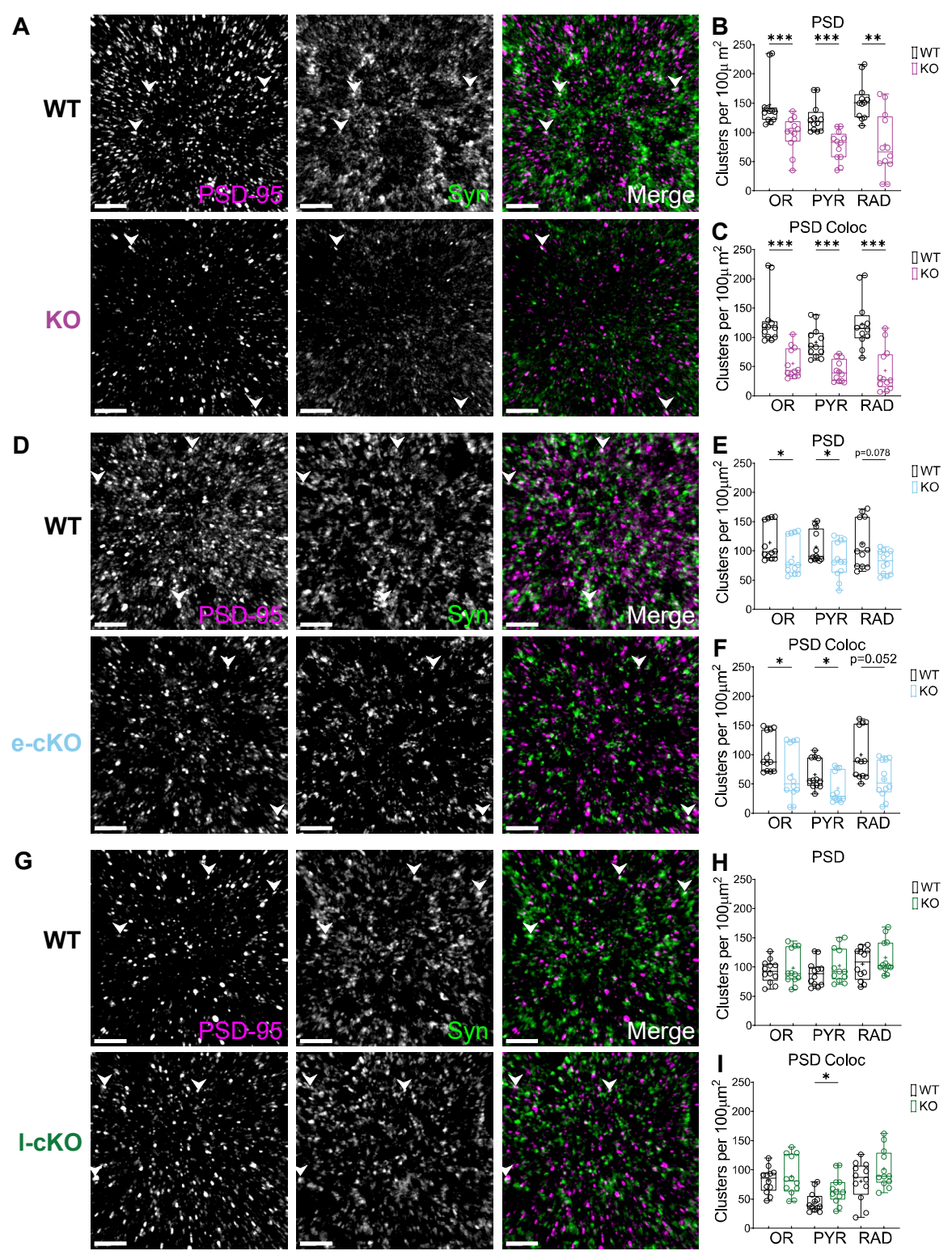


Figure 2.4. Decreased excitatory synaptic clusters following germline and early Arc/Arg3.1 deletion . Representative images (A, D, G) from CA1 st. oriens region show immunostaining for PSD-95 and Synaptophysin (SYN). Scale bars, 4 μ m. White arrows indicate puncta exhibiting colocalization of PSD-95 and SYN. Summary box plots depict the number of total PSD-95 clusters (B, E, H), and those that colocalized with SYN (C, F, I). Median \pm interquartile range, + represents the mean, and each point represents the value from one confocal scan. e-cKO= early-cKO; l-cKO= Late-cKO. Statistical analysis using Mann-Whitney U test revealed significant differences (*p<0.05, **p<0.01, ***p<0.01).

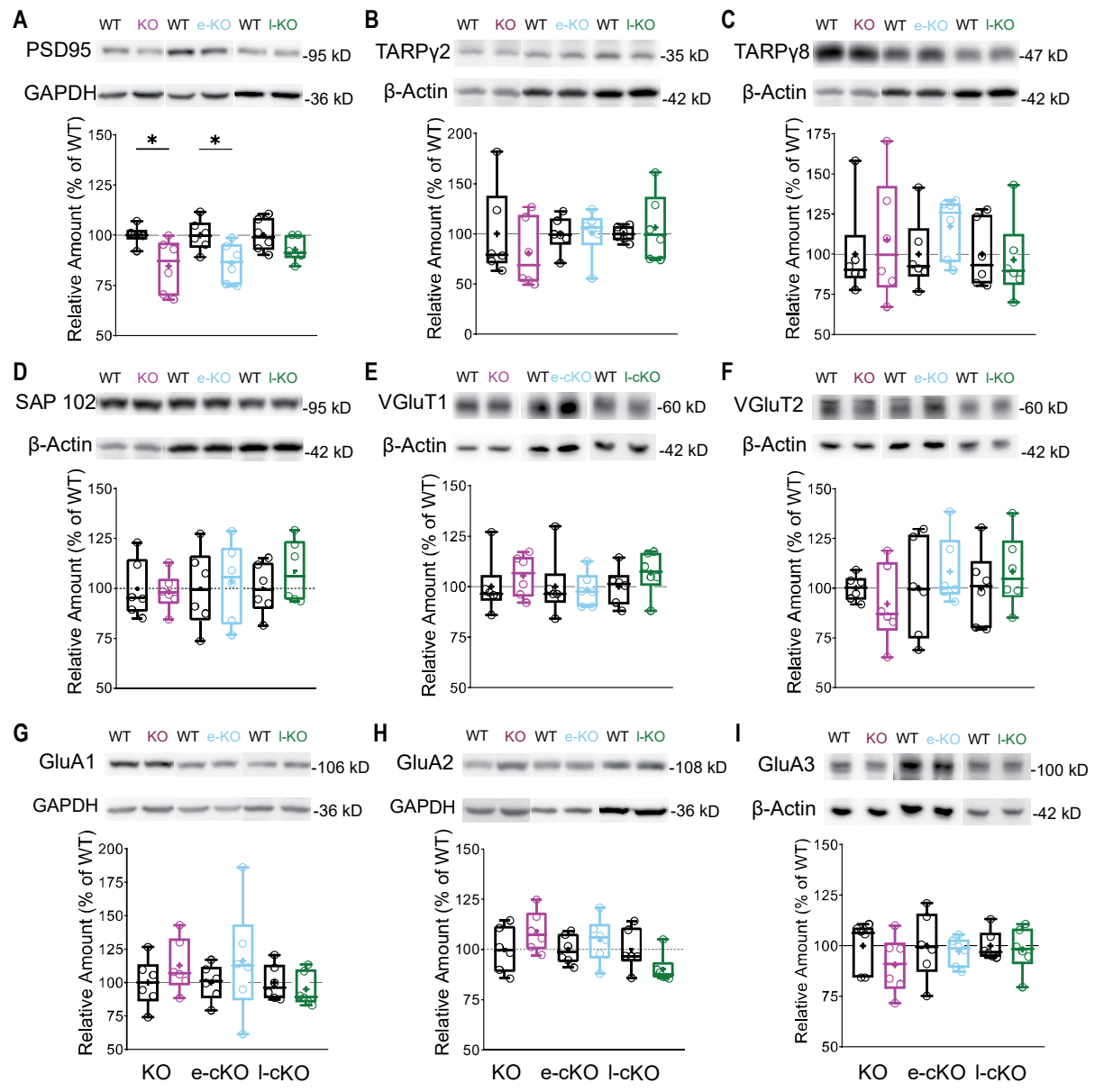


Figure 2.5. *Arc/Arg3.1* **deletion before P21 reduces hippocampal PSD-95 protein abundance**. Examples and densitometric western blot analysis of the hippocampus of WT, KO, and conditional KO mice. e-cKO= early-cKO; l-cKO= Late-cKO. Box plots show the median, 25th, and 75th percentiles and crosses represent the mean values (Mann-Whitney U test *p<0.05).

2.3.5 Germline and early *Arc/Arg3.1* KOs have decreased levels of PSD-95 protein in the hippocampus

Next, we employed western blotting to quantify the total protein levels of a subset of proteins involved in excitatory synaptic function in the hippocampus, including PSD-95 and the AMPA receptor subunits. Consistent with the observed reduction in PSD-95 clusters, we found a significant decrease in PSD-95 protein levels in both germline and early-cKO mice. In contrast, late-cKO mice exhibited no significant alterations in PSD-95 levels (**Figure 2.5A**. WT vs KO: U=4, p=0.026, WT: n=6, KO: n=6; WT-control vs early-cKO: U=5, p=0.041, WT-control: n=6, early-cKO: n=6; WT-control vs late-cKO: U=8, p=0.13, WT-control: n=6, late-cKO: n=6).

When analyzing the AMPA receptor subunits, we found no differences in GluA2 protein levels, in any of the KO lines (**Figure 2.5H**. WT vs KO, U=10, p=0.240, WT: n=6, KO: n=6; WT-control vs early-cKO, U=13, p=0.485, WT-control: n=6, early-cKO: n=6; WT-control vs late-cKO, U=8, p=0.132, WT-control: n=6, late-cKO: n=6). The other AMPA receptor subunits and all other excitatory proteins examined did not exhibit significant differences in any of the KO lines. A comprehensive summary of the findings can be found in Table 2.1.

Table 2.1. Mann-Whitney comparisons of excitatory synaptic proteins in hippocampal samples for all *Arc/Arg3.1* KO lines

Protein	ко				Early-cKO				Late-cKO			
	p- value	U	Median WT	Median KO	p- value	U	Median WT	Median KO	p- value	U	Median WT	Median KO
PSD-95	0.026*	4	100.1, n=6	87.11, n=6	0.041*	5	99.69, n=6	86.54, n=6	0.132	8	98.93, n=6	91.16, n=6
TARPy2	0.485	13	79.25, n=6	68.88, n=6	0.699	15	99.28, n=6	106.4, n=6	0.937	17	99.57, n=6	99.36, n=6
TARPy8	0.819	16	90.17, n=6	99.60, n=6	0.240	10	92.43, n=6	125.8, n=6	>0.99	18	93.12, n=6	89.63, n=6
SAP102	0.937	17	95.29, n=6	97.78, n=6	0.818	16	99.27, n=6	105.9, n=6	0.310	11	99.28, n=6	106.1, n=6
VGlut1	0.394	12	96.44, n=6	106.7, n=6	0.818	16	96.34, n=6	97.54, n=6	0.132	8	101.3, n=6	107.3, n=6
VGlut2	0.394	12	100.2, n=6	87.01, n=6	0.699	15	99.45, n=6	100.4, n=6	0.394	12	101.0, n=6	104.7, n=6
GluA1	0.394	12	100.0, n=6	107.1, n=6	0.394	12	101.3, n=6	112.6, n=6	0.394	12	96.26, n=6	89.22, n=6
GluA2	0.240	10	99.71, n=6	107.5, n=6	0.485	13	98.85, n=6	105.8, n=6	0.132	8	96.76, n=6	87.47, n=6
GluA3	0.180	9	106.3, n=6	91.06, n=6	0.699	15	99.28, n=6	98.66, n=6	>0.99	18	96.88, n=6	98.33, n=6

^{*}p<0.05

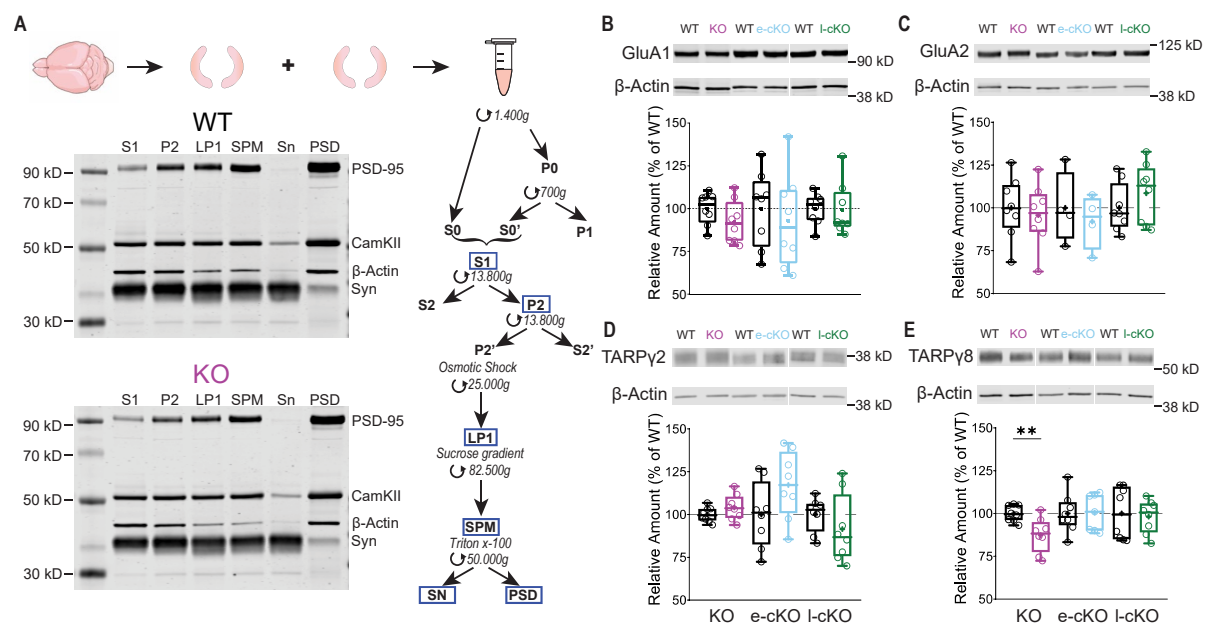


Figure 2.6. Germline *Arc/Arg3.1* KO have lower synaptic TARPγ8. A. Scheme exhibiting the workflow for PSD fractionations. The hippocampi from two animals were pooled together to collect enough tissue for the subcellular fractionation process. Exemplary gels are shown for WT and KO samples depicting the amount of several relevant proteins in the different subcellular fractions. Fractions quantified are highlighted with a blue square. B-E. Examples and densitometric western blot analysis of PSD fractions of the hippocampus of WT, KO, and conditional KO mice. e-cKO= early-cKO; l-cKO= Late-cKO. Box plots show the median, 25th, and 75th percentiles and crosses represent the mean values (Mann-Whitney U test *p<0.05, **p<0.01).

2.3.6 Germline but not early or late *Arc/Arg3.1* exhibit reduced TARPγ8 in the postsynaptic density

Changes in the kinetics of glutamatergic currents have been linked to modifications in the composition of AMPA receptor subunits and the expression of transmembrane AMPA receptorassociated proteins (TARPs). TARPy8 is the predominant isoform in the hippocampus while TARPy2 is less abundant but has been established as a direct Arc/Arg3.1 interaction partner. We, therefore, employed subcellular fractionations to evaluate the presence of AMPA receptor subunits and TARPs in the postsynaptic density using western blot techniques. An initial evaluation proved comparable enrichment of the different fractions for both WT and KO mice (Figure 2.6A). We, therefore, employed subcellular fractionations to evaluate the presence of AMPA receptor subunits and TARPs in the postsynaptic density using western blot techniques. The GluA subunits remained unaltered across all KO mice (Figure 2.6B. GluA1 WT vs KO: U=18, p=0.161, WT: n=8, KO: n=8; WT-control vs early-cKO: U=27, p=0.645, WT-control: n=8, early-cKO: n=8; WT-control vs late-cKO, U=24, p=0.442, WT-control: n=8, late-cKO: n=8; **Figure 2.6C**. GluA2 WT vs KO: U=26, p=0.574, WT: n=8, KO: n=8; WT-control vs early-cKO, U=7, p=0.886, WT-control: n=4, early-cKO: n=4; WT-control vs early-cKO, U=25, p=0.505, WT-control: n=8, late-cKO: n=8). Arc/Arg3.1 deletion did not impact the synaptic expression of TARPy2 in any of the lines investigated (Figure 2.6D. WT vs KO: U=26, p=0.574, WT: n=8, KO: n=8; WT-control vs early-cKO: U=7, p=0.886, WT-control: n=4,

early-cKO: n=4; WT-control vs late-cKO, U=25, p=0.505, WT-control: n=8, late-cKO: n=8). However, TARPγ8 exhibited a lower expression in the germline KO line while remaining unchanged in the two conditional KO lines (**Figure 2.6E**. WT vs KO: U=7, p=0.007, WT: n=8, KO: n=8; WT-control vs early-cKO: U=27, p=0.645, WT-control: n=8, early-cKO: n=8; WT-control vs late-cKO: U=28, p=0.721, WT-control: n=8, late-cKO: n=8). Taken together, our findings on excitatory transmission suggest that deletion of *Arc/Arg3.1* before P21 leads to accelerated synaptic kinetics and reduced PSD-95 protein levels. The most pronounced effects were observed in germline KO mice, highlighting a critical role for *Arc/Arg3.1* during early development, particularly before P7. Consistent with this, reductions in synaptic TARPγ8 were only detected in germline KO mice. These findings underscore the profound impact of germline deletion, and consequently, this mouse line was chosen for subsequent analysis.

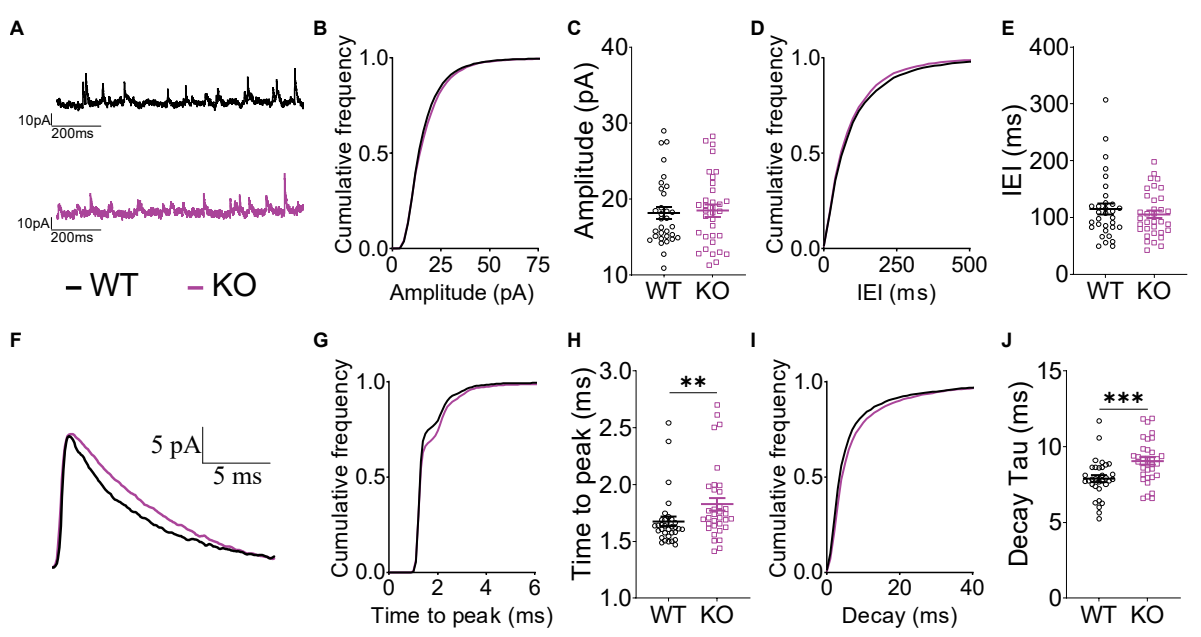


Figure 2.7. Normal sIPSC amplitude and frequency but slower kinetics in Arc/Arg3.1 KO mice. A. Exemplary traces of sIPSC recorded at 0mV. The upper panel (B-E) shows indistinguishable amplitude and IEI for WT (in black) and KO (in magenta). F. Representative single traces. G-J. Scatter plots show the mean \pm SEM of the respective parameter, every point represents the mean value from one cell. (Mann-Whitney U test **:p>0.01, ***: p>0.001).

2.3.7 Germline Arc/Arg3.1 KO exhibit slower sIPSCs

The characteristic hippocampal phenomena of sharp wave ripples are thought to arise from finely tuned synaptic connectivity within the hippocampus. The sharp wave component is believed to be triggered by synchronized excitatory input from CA3 to CA1, while ripples are generated through the interplay of fast-spiking interneurons and pyramidal cells (Buzsaki, 2015). Inhibitory neurons and synapses are also responsible for fast oscillations in the gamma band frequency (γ -oscillations) (Buzsáki & Wang, 2012). Previous research from our group revealed that germline Arc/Arg3.1 deletion, differing from early deletion, predominantly affected γ -oscillations, and ripple frequency while preserving the sharp wave amplitude (Gao

et al., 2018). Intrigued by the observed effects on sharp wave ripples, we examined the inhibitory transmission of germline *Arc/arg3.1* KO mice. Using patch-clamp recordings, we measured spontaneous inhibitory postsynaptic currents (sIPSCs) while holding cells at 0 mV and in the presence of AMPA and NMDA receptor antagonists to isolate inhibitory currents. The peak amplitude and frequency of sIPSCs were determined to assess inhibitory synapse strength and number. Representative traces revealed no significant differences in amplitude or frequency patterns between KO and WT mice (**Figure 2.7A**). Cumulative histograms and quantitative analysis of mean peak amplitudes and frequency as determined by IEI also failed to reveal any statistically significant differences between the groups (**Figure 2.7B**. Amplitude: U= 509, p=0. 0.66, WT: n=32, KO: n=34; **Figure 2.7C**. IEI: U=510, p=0.67, WT: n=32, KO: n=34).

Since the type of oscillation generated in the hippocampus is influenced by the relative timing of excitatory and inhibitory synaptic currents and the interplay between excitation-inhibition and inhibition-inhibition loops, we also investigated the kinetics of sIPSCs by analyzing their rise and decay components, expressed by the time to peak and decay τ parameters. *Arc/Arg3.1* KO mice displayed a significant increase in the time to peak compared to WT controls (**Figure 2.7G-H**. U=317, p=0.0032, WT: n=32, KO: n=34), also observed in the cumulative IEI histogram. In addition, germline KO mice exhibited significantly prolonged decay τ constants (**Figure 2.7I-J**. U=268, p=<0.001, WT: n=32, KO: n=34). The cumulative histograms corroborated this effect, demonstrating a right shift in the distribution in KO mice. These findings collectively indicate that *Arc/Arg3.1* deletion significantly slows the rise and decay kinetics of sIPSCs, highlighting its crucial role in regulating the temporal dynamics of inhibitory synaptic transmission in the hippocampus during early development.

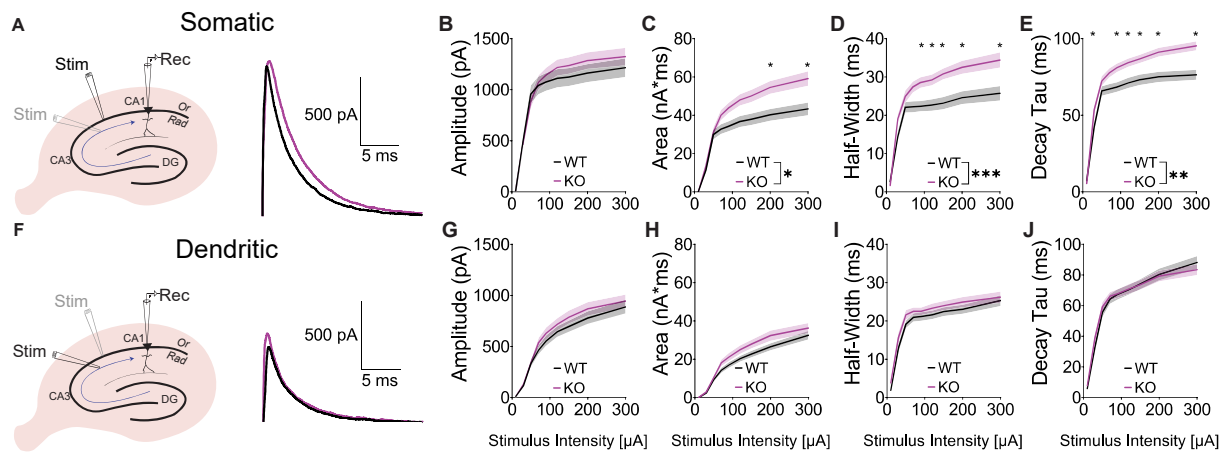


Figure 2.8. Slower somatic but normal dendritic eIPSCs. A. Recording protocol sketch and exemplary traces of somatic and dendritic eIPSCs, respectively. B-E. Averaged curves of the somatic uIPSCs displayed against stimulus intensity in *st. pyramidale.* G-E Averaged curves of the dendritic uIPSCs displayed against stimulus intensity in *st. radiatum.* In B-J continuous lines represent mean values and shadows mark ±SEM. Legend asterisks indicate the effects of the factor "Genotype"

within a Mixed-effects ANOVA. Individual asterisks indicate "Genotype x Intensity" interaction effects and subsequent significant post-hoc comparisons, *p<0.05, **p<0.01, **p<0.001

2.3.8 Germline Arc/Arg3.1 KO exhibit slower somatic eIPSCs

Different subtypes of inhibitory neurons provide synaptic inputs to CA1 pyramidal neurons that are preferentially located on distinct somatic or dendritic compartments (Milstein et al., 2015). Synchronous activation of each input type affects CA1 firing differentially and contributes to different aspects of neural oscillations and hippocampal function (Cutsuridis & Taxidis, 2013; Schonberger et al., 2014). To investigate the source of the faster sIPSCs recorded in KO CA1 pyramids; we placed extracellular electrodes in both the pyramidal and radiatum CA1 layers and examined the effects of stimuli of varying intensity on evoked inhibitory postsynaptic currents (eIPSCs).

Although somatic recordings in KO mice revealed no difference in the peak amplitude of eIPSCs compared to WT animals (**Figure 2.8B**. $F_{(1,74)}$ =0.273, p=0.6029, WT: n=38, KO: n=38), the KO group exhibited significantly larger eIPSC areas (**Figure 2.8C**. $F_{(1,74)}$ =6.25, p=0.015, WT: n=38, KO: n=38). The latter was primarily attributed to slower eIPSCs kinetics in KO neurons, as indicated by significantly wider half-widths and prolonged decay constants (**Figure 2.8D**. Half-Width: $F_{(1,76)}$ =12.88, p=0.0006, WT: n=38, KO: n=38; **Figure 2.8E**. Decay τ : $F_{(1,74)}$ =9.685, p=0.0026, WT: n=38, KO: n=38). Notably, this effect was specific to somatic stimulation as dendritic eIPSCs showed no differences between genotypes, suggesting a compartment-specific modulation of inhibitory transmission in KO animals (**Figure 2.8G**. Amplitude: $F_{(1,74)}$ =0.743, p=0.392; **Figure 2.8H**. Area: $F_{(1,74)}$ =2.686, p=0,106; **Figure 2.8I**. Half-width: $F_{(1,74)}$ =1.548, p=0.217; **Figure 2.8J**. Decay τ : $F_{(1,74)}$ =0.035, p=0.852). These findings highlight the potential role of Arc/Arg3.1 in shaping the temporal dynamics of inhibitory signaling in specific subcellular compartments.

2.3.9 Arc/Arg3.1 deletion does not affect paired-pulse modulation of inhibition

To assess whether Arc/Arg3.1 deletion impacts presynaptic mechanisms of inhibitory transmission, we employed a paired-pulse stimulation protocol with a 100 ms inter-stimulus interval (ISI). Representative traces display inhibitory paired-pulse depression, suggesting a relatively high release probability at these synapses. As predicted from their longer electrotonic distance, dendritic stimulation elicited smaller responses in CA1 somata, confirmed by the quantitative analysis in **Figure 2.9B**. Crucially, no significant differences were observed between WT and KO animals in either amplitude or the rate of depression, indicating that Arc/Arg3.1 deletion does not appear to alter presynaptic release probability at inhibitory

synapses (**Figure 2.9**. Somatic: U=688, p=0.729, WT: n=38, KO: n=38; Dendritic U=646, p=0.987, WT: n=36, KO: n=36). These findings suggest that the previously observed changes in inhibitory postsynaptic currents are not likely the result of presynaptic alterations but rather involve postsynaptic modulations in GABAergic synapses.

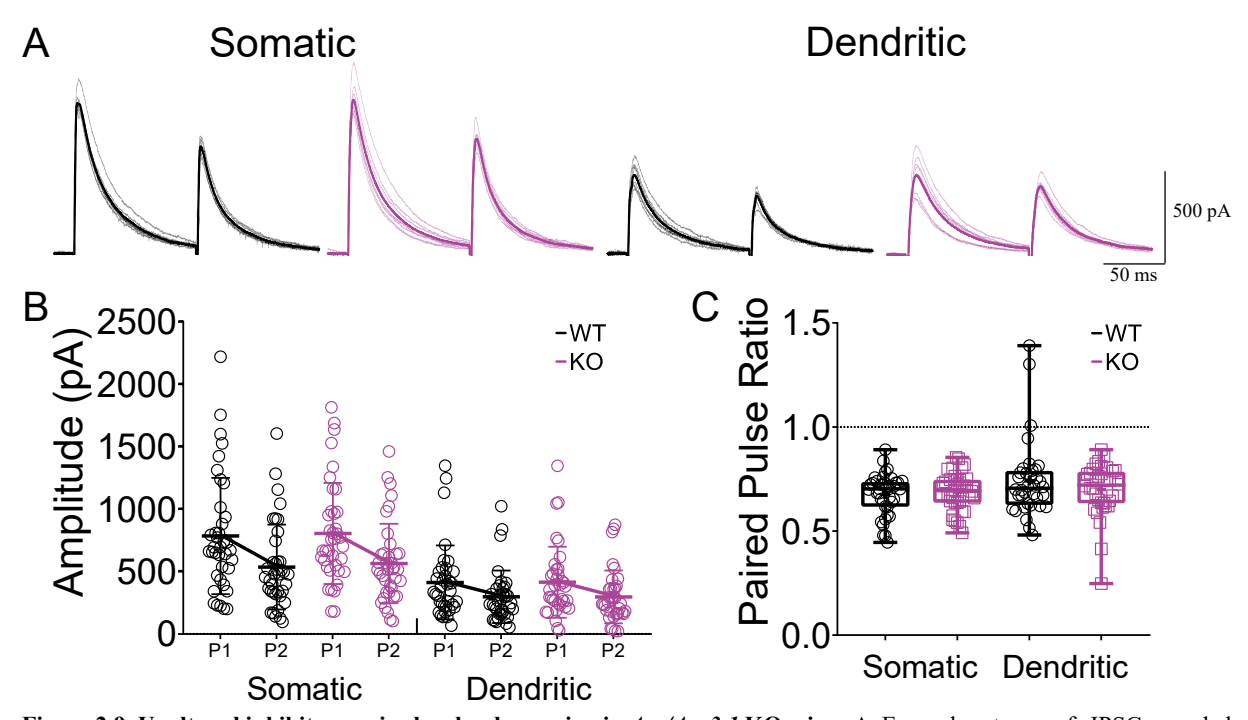


Figure 2.9. Unaltered inhibitory paired-pulse depression in Arc/Arg3.1 KO mice . A. Exemplary traces of eIPSC recorded at 0mV. B shows indistinguishable paired pulse amplitude in WT and KO mice in response to both, somatic and dendritic stimulation. C. Paired pulse ratio of somatic and dendritic stimulation. Scatter plots show the mean \pm SEM of the respective parameter, every point represents the mean value from one cell. Paired pulse ISI=100ms.

2.3.10 Germline *Arc/Arg3.1* KO mice exhibited higher intensity of inhibitory clusters in the pyramidal and LM layers of CA1

Collectively, our functional results unveiled a new role for *Arc/Arg3.1* in sculpting hippocampal inhibitory function. While the number and strength of inhibitory connections (measured by sIPSC frequency and amplitude, respectively) remain unchanged, *Arc/Arg3.1* deletion significantly slows inhibitory transmission. This is evident in both spontaneous and evoked activity, as demonstrated by increased rise and decay times of inhibitory currents. Notably, this effect seems specific to the perisomatic region, suggesting targeted modulation within this critical subcellular domain. To evaluate inhibitory synaptic dynamics at the structural level, we performed immunostaining in the CA1 region. We targeted presynaptic sites with the GABA vesicular transporter (VGAT) and postsynaptic sites with the inhibitory scaffolding protein gephyrin. Co-localization of these markers served as a measure of functional inhibitory synapses. Our results revealed a normal number and distribution of both total gephyrin and VGAT clusters, as well as an intact co-localization of these markers across all CA1 layers. (WT:

n=23, KO: n=24; **Figure 2.10B**. Gephyrin, OR: U=237, p=0.413; PYR: U=259, p=0.728; RAD: U=199, p=0.103; LM: U=213, p=0.185; **Figure 2.10C**. VGAT, OR: U=254, p=0.65; PYR: U=209, p=0.157; RAD: U=254, p=0.65; LM: U=197, p=0.092, **Figure 2.10D**. Colocalized: OR: U=259, p=0.728; PYR: U=222, p=0.25; RAD: U=233, p=0.366; LM: U=239, p=432).

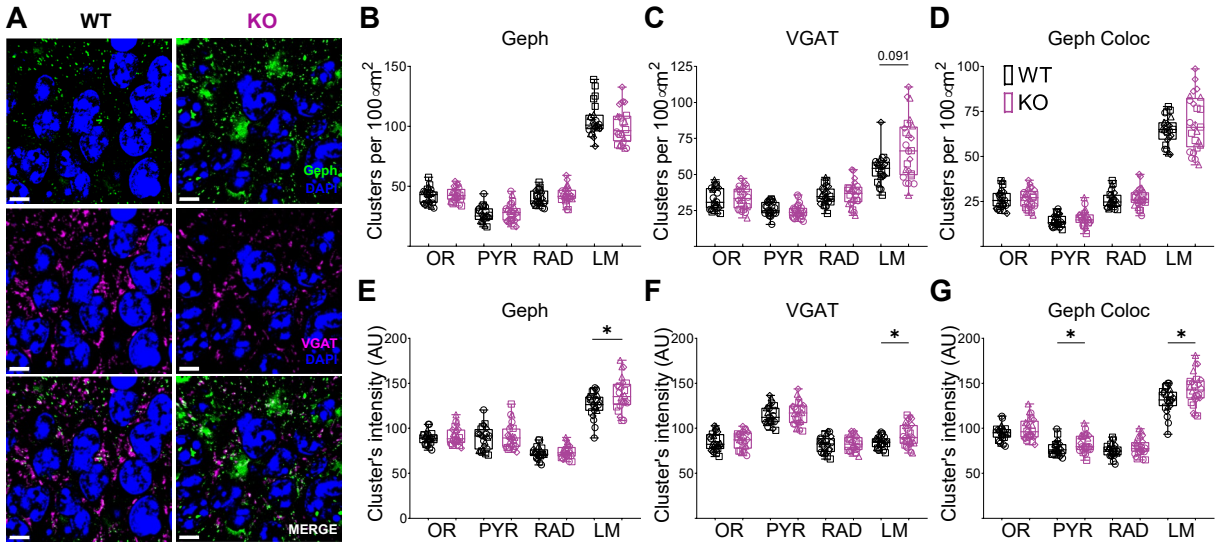


Figure 2.10. Unaltered number of inhibitory synaptic clusters in *Arc/Arg3.1* KO mice but increased intensity in the *pyramidal* and *LM* layers. A. Exemplary images from the CA1 Oriens region show immunostaining for Gephyrin (Geph) and GABA vesicular transporter (VGAT). Scale bars, 5μm. Summary box plots depict the number of total Gephyrin (B), VGAT (C) clusters, and the colocalized ones (D). Summary box plots depict the intensity of total Gephyrin (E), VGAT (F) clusters, and the colocalized ones (G). Median ± interquartile range, + represents the mean, and each point represents the value from one confocal scan. Statistical analysis using *the Mann-Whitney* U test revealed significant differences (*p<0.05, **p<0.01, ****p<0.01).

Next, we assessed individual cluster intensity as an indirect measure of the relative amount of protein within the postsynaptic density. In the dendritic layers, oriens, and radiatum, where functional experiments showed normal evoked responses, the intensity remained unchanged (WT: n=23, KO: n=24; **Figure 2.10E**. Gephyrin, OR: U=257, p=0.697; RAD: U=241, p=0.466; Figure 2.10F. VGAT, OR: U=255, p=0.666; RAD: U=257, p=0.697, Figure 2.10G. Colocalized: OR: U=228, p=0.315; RAD: U=212, p=0.178). In contrast, cluster quantification in the pyramidal layer showed distinct differences between WT and KO mice. Here, the intensity of gephyrin clusters colocalized with VGAT, representing perisomatic synapses, was significantly higher in KO mice compared to WT controls (WT: n=23, KO: n=24; Figure **2.10**E. Gephyrin, U=262, p=0.776; Figure 2.10F. VGAT, U=262, p=0.776; Figure 2.10G. Colocalized: U=176, p=0.033). Since the absolute number of molecules of a protein in the postsynaptic density can be not resolved using confocal imaging, the intensity can only be used as a good insight into the packing of synaptic proteins (Curran et al., 2021). We can conclude that Arc/Arg3.1 deletion specifically targets and alters the structure of perisomatic inhibitory synapses. An even more pronounced effect was observed in the lacunosum moleculare (LM) layer. KO mice exhibited increased intensity in gephyrin, VGAT, and their colocalized clusters,

suggesting synapses in this layer are the most affected by the deletion (WT: n=23, KO: n=24; Figure 2.10E, Gephyrin, U=180, p=0.041; Figure 2.10F, VGAT, U=180, p=0.041; Figure 2.10G, Colocalized: U=169, p=0.022). As we did not record from isolated LM synapses, their physiological properties could not be directly linked to cluster intensity. However, we suspect that a few slow sIPSCs measured in KO neurons may reflect LM synapses. In essence, although *Arc/Arg3.1* deletion does not alter the overall number of inhibitory synapses, it seems to significantly impact their clustering, particularly in perisomatic and potentially *lacunosum moleculare* regions. Further investigation focusing on LM function is crucial to fully understand the implications of these changes for overall inhibitory transmission.

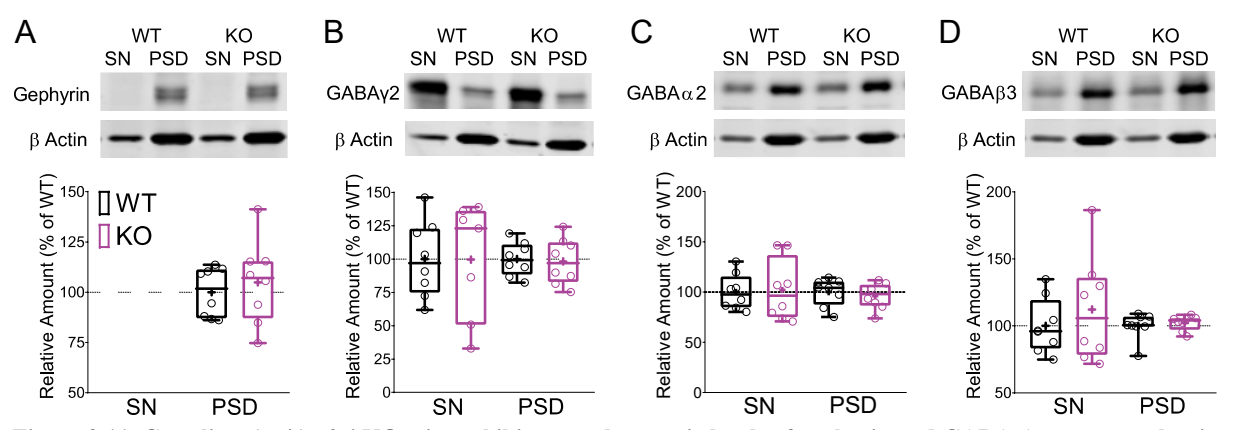


Figure 2.11. Germline *Arc/Arg3.1* KO mice exhibit normal synaptic levels of gephyrin and GABA-A receptor subunits in the hippocampus. Examples and densitometric western blot analysis of SN and PSD fractions of the hippocampus of WT, KO mice. Box plots show the median, 25th, and 75th percentiles and crosses represent the mean values (Mann-Whitney U test).

2.3.11 Germline *Arc/Arg3.1* KO have normal synaptic levels of gephyrin and GABAA receptor subunits in the hippocampus

Like with glutamatergic synapses, changes in the speed of GABAergic currents, or kinetics, have been linked to alterations in the composition of GABA receptor subunits. Since our fast sIPSCs disappeared with the GABA_A receptor blocker gabazine, we can confidently exclude GABA_B receptors from contributing to the recorded currents. This leaves GABA_A receptor subunits as the main candidates responsible for the slower kinetics in the KO IPSCs. To investigate this possibility, we prepared subcellular fractions and analyzed the protein content in the postsynaptic density (PSD) and in the extrasynaptic membrane (SN) fraction, where GABA_A receptors reside. We quantified the most abundant GABA_A receptor subunits and their scaffolding protein gephyrin. However, our Western blot analysis revealed no significant differences between WT and KO mice, in either the PSD or the SN fractions (Figure 2.11). A detailed summary of these results is provided in Table 2.2.

Table 2.2. Mann-Whitney comparisons of inhibitory synaptic proteins in hippocampal samples for Arc/Arg3.1 KO mice.

Protein			SN fraction		PSD fraction			
	p-value	U	Median WT	Median KO	p-value	U	Median WT	Median KO
Gephyrin					0.7984	29	101.8, n=8	107.1, n=8
GABAy2	0.8665	26	96.96, n=8	123.0, n=7	0.867	26	96.96, n=8	123.0, n=7
GABAα2	0.1304	17	99.51, n=8	107.1, n=8	0.3282	22	94.55, n=8	121.2, n=8
GABAβ3	0.8665	26	96.96, n=8	123.0, n=7	0.8785	30	100.4, n=8	104.1, n=8

2.4 Discussion

Previous results showed that the first postnatal month constitutes a critical period for the development of hippocampal functions and that the upregulation of *Arc/Arg3.1* is necessary for the proper maturation of hippocampal network activity. Early-life *Arc/Arg3.1* deficiency results in permanent impairments in spatial navigation and oscillatory rhythms (Gao et al., 2018). Consistent with these impairments, our findings show that *Arc/Arg3.1* deletion before, but not after, P21 results in reduced amplitude of synaptic responses in CA1 cells in extracellular recordings. These reductions suggest a decreased excitatory drive in the Schaffer collateral synapses. However, although changes in the fEPSP mainly reflect changes in excitatory synapses, changes in inhibitory transmission could also impact fEPSPs, either via increases in feed-forward and feed-back inhibition, or through changes in shunting inhibition (Buzsaki, 1984a; Isaacson & Scanziani, 2011).

Furthermore, even in the absence of inhibitory contributions to fEPSPs, the decreases observed in germline and early-cKO mice could be due to reductions in the total number of excitatory synapses or changes in the properties of individual synapses. To evaluate these possibilities, we used patch-clamp to assess single excitatory synapses. The results indicated that, regardless of the time of deletion, neither the frequency nor the amplitude of sEPSCs differed significantly between WT and Arc/Arg3.1 KO mice. These results align with our previous findings using hippocampal acute slices, where miniature EPSCs (mEPSCs) were recorded instead of spontaneous EPSCs (Plath et al., 2006). Given that mEPSCs are recorded in the presence of TTX to isolate action potential (AP)-independent release, our current findings complement the previous study by demonstrating that Arc/Arg3.1 does not affect AP-dependent release either. The lack of differences in amplitude and frequency of sEPSCs implies that these parameters were not dictated by early-life or life-long constitutive expression of Arc/Arg3.1.

In contrast, we found an acceleration of the kinetics of sEPSCs, affecting both their rise time and decay components, which only occurred when Arc/Arg3.1 was deleted before P21. One factor known to affect the kinetics of excitatory synaptic inputs in the hippocampus is the electrotonic distance, with distally generated EPSPs being significantly slower than those generated proximally to the soma (Andreasen & Lambert, 1998; Turner, 1988). The accelerated kinetics in germline KO and the tendency in early-cKO would suggest a shift toward more proximal synapses in these animals. Therefore, we would expect to observe more synaptic clusters in the stratum pyramidale or the most proximal regions of *radiatum* and *oriens* and

fewer in the most distal regions. However, our evaluation of synaptic clusters showed reductions in both KO lines across all the CA1 strata evaluated, indicating lower intrahippocampal excitatory synaptic input not only from CA3 but likely also from CA2. One limitation of our study is that we did not evaluate the most distal dendrites forming *stratum lacunosum moleculare*. Therefore, whether *Arc/Arg3.1* differentially modulates the synaptic inputs from the entorhinal cortex, remains to be tested in future studies.

The reductions in the number of clusters were accompanied by decreases in hippocampal PSD-95 protein levels. Given that PSD-95 is a protein of the membrane-associated guanylate kinases (MAGUK) family, known to influence the trafficking of AMPARs, an interaction of Arc/Arg3.1 with PSD-95 has long been suggested. Some evidence supporting this includes the finding that Arc/Arg3.1 is found in the postsynaptic density (Steward & Worley, 2001), it copurifies with the NMDAR complex (Husi et al., 2000), and it is present in protein complexes where PSD-95 is the most abundant protein (Fernandez et al., 2017). However, whether this interaction is direct or indirect is not entirely clear. Some studies suggest the interaction might be indirect, with Arc/Arg3.1 associating with PSD-95 through other proteins like GKAP, NR2B, and Stargazin, which act as intermediaries in the multiprotein complexes formed by PSD-95 (Hallin et al., 2018; reviewed by Zhang & Bramham, 2021; Zhang et al., 2015). The absence of changes in the late-cKO indicates that these changes are developmentally modulated. Similar to Arc/Arg3.1, PSD-95 is also highly upregulated during the first postnatal month, with the highest increases taking place between the second and fourth postnatal weeks (Sans et al., 2000). Whereas during the first postnatal week another protein of the MAGUK family, SAP-102, is responsible for most of AMPAR trafficking (Nagura et al., 2012). It is thus conceivable that alterations in these proteins during this critical period profoundly shape hippocampal maturation. Our findings indicate that such alterations (in PSD-95) do not come to be compensated and persist into adulthood.

Another important factor regulating the kinetics of excitatory transmission is the subunit composition of glutamatergic receptors. Under our recording conditions (-70 mV), the expected contribution of NMDAR to the detected sEPSCs is very low due to the Mg⁺² ion blocking the pore; therefore, we focus solely on AMPARs. Given the association of *Arc/Arg3.1* with the endocytosis of GluA1 and GluA2 subunits, we anticipated that their composition could be altered. Intriguingly, our analysis revealed no changes in either the overall protein levels of AMPAR subunits or their synaptic localization in any of the KO lines. This contrasts with the findings of Shepherd et al. (2006), who reported a 2-fold increase in surface AMPA receptor

expression in cultured hippocampal neurons from *Arc/Arg3.1* knockout mice, accompanied by larger mEPSC amplitude. However, this effect was not observed under conditions of reduced activity (TTX treatment). Since primary cultures exhibit higher activity levels compared to acute slices (Szczot et al., 2010), this difference in activity levels may explain the discrepancy between the two studies. Alternatively, the non-physiological biochemical, structural, and cellular conditions of neural growth in primary cultures, may affect synaptogenesis in ways different to natural development.

Despite a strong association of PSD-95 and AMPAR, a direct interaction has not been identified. Instead, transmembrane AMPAR regulatory proteins (TARPs) mediated this interaction (Bats et al., 2007; Zeng et al., 2019). Furthermore, TARPs are known to play a crucial role in stabilizing AMPAR in the postsynaptic density. Among TARPs, Stargazing (TARPγ2) is the best studied, and its phosphorylation by CaMKII has been reported to immobilize AMPARs in the synapses (Opazo et al., 2010). TARPγ8 is predominantly expressed in the hippocampus and is critical for AMPAR expression and synaptic transmission (Rouach et al., 2005). *Arc/Arg3.1* binds with high affinity to both of these TARPs, with the association being stronger with TARP γ8 (Chen et al., 2022; Zhang et al., 2015). Notably, TARPs slow AMPAR deactivation and desensitization and the slowing is greatest with γ4 and γ8 (Cho et al., 2007; Milstein et al., 2007). The decrease of synaptic TARP γ8 content observed in the germline KO could explain the acceleration of sEPCS observed in this group.

The role of Arc/Arg3.1 in shaping inhibitory transmission is largely unknown. To date, there are very few studies evaluating Arc/Arg3.1 effects on inhibitory synapses in the hippocampus. The study by Rial Verde et al. (2006), used hippocampal organotypic slice cultures and found no changes in IPSC amplitude, frequency, or kinetics between cells expressing recombinant Arc/Arg3.1 and neighboring control cells. An important difference that could explain the contrasting results is that levels of spontaneous activity are higher in slice cultures compared to acute slices (Okamoto et al., 2014). As suggested earlier for excitatory synapses the differences in activity levels seem to highly regulate the effects of Arc/Arg3.1. Moreover, these recordings were performed at 1 week in culture, a period during which spontaneous Arc/Arg3.1 expression is expected to be higher than in the adult hippocampus. This developmental difference could also contribute to the discrepancies observed.

On the other hand, the study by Gao et al. (2010) used acute slices from the visual cortex in juvenile animals (P23) and found increased IPSCs amplitude in *Arc/Arg3.1* KO mice, with no changes in frequency or kinetics. This study serves as a precedent for the potential role of

Arc/Arg3.1 in inhibitory synaptic transmission. The authors linked the upregulation of mIPSCs to the increases they observed in Grip1, a protein mainly associated with glutamate receptors but also found at inhibitory synapses associated with GABA_A receptors.

Our findings revealed slower kinetics of inhibitory synapses in Arc/Arg3.1 KO mice. The kinetics of IPSCs are highly regulated by GABAAR subunit composition. For instance, subunits α1 and α2 are highly expressed in CA1 pyramidal cells, and the decay time of IPSCs mediated by α2 subunit-containing GABA_ARs is several folds slower compared to that of IPSCs mediated by all subunit-containing GABAARs (Kerti-Szigeti & Nusser, 2016). Although our results showed no changes in the evaluated GABAA receptor subunits, it is still possible that some other subunits, including a1, are regulated by Arc/Arg3.1, explaining the observed differences in kinetics. Furthermore, although we did not find changes in the GABA γ2 subunit, it is worth noting that two splice variants of this subunit exist: $\gamma 2$ long and $\gamma 2$ short, which grant the receptors different kinetic properties (Sallard et al., 2021). Additionally, posttranslational modifications are crucial for the modulation of GABAAR properties. Specifically, phosphorylation of β3 subunit-containing GABA_AR by CaMKII results in increased IPSC decay times (Houston et al., 2009). Although evidence for differential posttranslational modulations of GABAAR was not obtained in the current study, given the well-established association of Arc/Arg3.1 and CaMKII, we speculate that these mechanisms might contribute to the modulation of inhibitory transmission.

Previous reports show that two different types of inhibitory synapses contacting CA1 pyramidal cells can be distinguished based on their kinetics: a fast type with decay time constants of 9 ms and a slow type with constants of 50 ms. The fast type is likely mediated by basket cells, axo-axonic, bistratified, and horizontal trilaminar cells, whereas the slow synapses are likely activated by interneurons that project exclusively to dendritic regions (Banks et al., 1998). The sIPSCs recorded in our study also seemed to split into two types based on their kinetics, with half-widths of 3 ms and 22 ms. However, approximately 99 % of them belonged to the fast type. This, along with the observed slower kinetics in Arc/Arg3.1 KO upon somatic but not dendritic stimulation, indicates that Arc/Arg3.1 preferentially modulates perisomatic inhibitory synapses. However, since we did not stimulate in the LM region, we cannot rule out modifications of these synapses as well. Furthermore, the enhanced clustering of VGAT in the KO mice suggests that Arc/Arg3.1 might modulate these synapses too. Further studies are needed to establish the precise type of inhibitory synapses regulated by Arc/Arg3.1.

Overall, our current findings reveal that Arc/Arg3.1 upregulation during the first postnatal month is crucial for the wiring of the hippocampal circuitry. Its deletion before P21 significantly and permanently disrupts excitatory transmission. Notably, Arc/Arg3.1 deficiency from the germline also impacts inhibitory transmission. These results could potentially explain the alterations observed in the oscillatory activity of these animals in our previous study. Specifically, the reduced theta and gamma power, fewer sharp-wave ripple complexes, and the higher frequency of the remaining ones observed upon germline KOs, suggest that not only excitatory but also inhibitory transmission is altered in these animals. The precise mechanisms on how the changes in kinetics of excitatory and inhibitory transmission translate into the precise oscillatory patterns observed need to be examined in future studies, computational studies on synaptic integration would substantially help us to comprehend these phenomena.

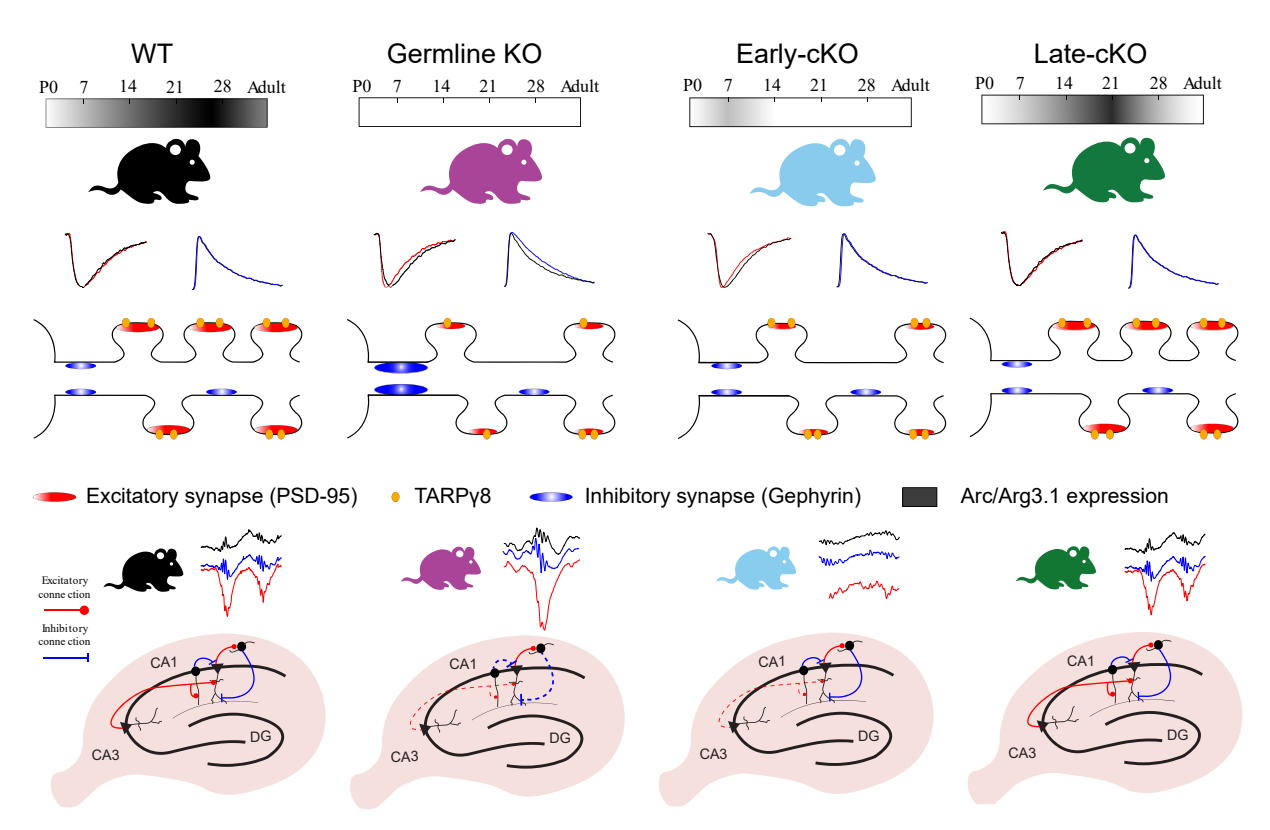


Figure 2.12. Arc/Arg3.1 deficiency permanently alters hippocampal neurotransmission in a development-dependent manner. Our findings show that germline Arc/Arg3.1 deletion results in altered excitatory transmission in CA1. This is reflected by a reduced excitatory drive from CA3, accompanied by fewer excitatory synaptic clusters across dendritic and somatic layers, and reductions in PSD-95 total protein levels. Functionally, excitatory transmission in germline Arc/Arg3.1 KO exhibits accelerated kinetics accompanied by lower levels of TARPγ8 in synaptic fractions. Regarding inhibitory transmission, germline deletion seems to spare the number and strength of inhibitory synapses but prolongs inhibitory events. This effect is specific to perisomatic synapses and is accompanied by enhanced clustering of inhibitory synaptic proteins. Similar to germline Arc/Arg3.1 deletion, early postnatal deletion results in a reduced number of excitatory clusters and PSD-95 levels, and a trend toward faster kinetics. However, changes in TARPγ8 levels were not observed in this mouse line. In stark contrast, late Arc/Arg3.1 deletion did not alter excitatory transmission. These results align with the observed alterations in oscillatory activity observed in our previous study. And although inhibitory transmission was not assessed in the conditional KO lines, given the preserved oscillatory rhythms reflecting inhibitory activity observed in our previous study, we anticipate minor or no changes.

Moreover, early *Arc/Arg3.1* deletion led to lower theta but normal gamma power, a normal number of ripples but the amplitude of the sharp-waves was significantly lower. This is highly

consistent with our observations of lower excitatory drive from CA3 and reduced excitatory clusters and PSD-95 levels. In strong contrast, the late deletion resulted in oscillatory activity comparable to that of WT animals, which is consistent with the lack of effects in this mouse line observed in the current study. We did not evaluate the inhibitory transmission of early and late-cKO mice, therefore we cannot rule out possible changes, however, based on the unaltered power in the gamma frequency band observed in these lines we speculate that inhibitory transmission would be well-preserved in these animals.

3 Part II. Mass Spectrometry Profiling of Arg3.1 KO Mice in Distinct Hippocampal Subfields

3.1 Introduction

The protein Arc/Arg3.1 has been linked to learning and memory consolidation, primarily through its effects on the hippocampus. Studies, including ours, have demonstrated its involvement in hippocampal physiology, showing disruptions in both oscillatory activity and synaptic plasticity in Arc/Arg3.1 knockout (KO) mice (Beique et al., 2011; Gao et al., 2018; Malkki et al., 2016; Plath et al., 2006). On the molecular level, Arc/Arg3.1 interacts with numerous synaptic (Cao et al., 2013; Chowdhury et al., 2006; Zhang et al., 2015) and several nuclear proteins (Greer et al., 2010; Irie et al., 2000; Korb et al., 2013) to promote activitydependent receptor trafficking, gene expression, and inter-cellular communication. The functional outcome of Arc/Arg3.1 protein-protein interactions depends on the availability of interaction partners and may result in opposing effects, such as LTP and LTD (Plath et al., 2006; Zhang & Bramham, 2021). The hippocampus is composed of 3 main subfields: CA1, CA3, and DG, each containing unique cell types, synapses, and forms of plasticity. Moreover, each of the hippocampal subfields contributes differentially to intra- and inter-regional circuitry, and oscillatory activity and carries specific functions in learning and memory (Chinnakkaruppan et al., 2014; Hainmueller et al., 2024; Ji & Maren, 2008; Oliva et al., 2016). The developmental trajectories of these subfields show unique patterns in synaptogenesis and circuit maturation (Donato et al., 2017) as well as Arc/Arg3.1 expression dynamics (Gao et al., 2018). It is thus conceivable that the proteomic landscape supporting these regional specializations will be unique to each subfield. While some evidence has accumulated that supports this hypothesis (Gerber et al., 2019; Smith et al., 2020; von Ziegler et al., 2018), it remains lacking, partly due to the technical difficulty of separating the hippocampal tissue into distinct subfields. We further hypothesize that Arc/Arg3.1 might exert different effects on circuit development and plasticity, in each subfield, depending on their unique proteome.

To address this hypothesis, we set out to investigate the molecular profiles of different hippocampal subfields in the hippocampi of WT and *Arc/Arg3.1* KO mice. We employed a tunable nanosecond infrared laser (NIRL) ablation method (Hahn et al., 2021) to dissect tissue form specific areas (CA1, CA3, and DG) and processed each subfield for liquid chromatography-tandem mass spectrometry (LC-MS/MS). This approach served two purposes:

1) To demonstrate the efficacy of NIRL ablation for isolating specific mouse brain subfields for proteomic analysis and, 2) To compare the proteomic profiles of *Arc/Arg3.1* KO hippocampi with WT controls under baseline conditions, focusing on potential regional differences. We deliberately focused on investigating non-stimulated brains (i.e. from home cage, not exposed to behavioral, chemical, or electrical stimuli), in order to reveal salient differences in the natural hippocampal circuitry.

3.2 Methods

3.2.1 Mice

Naïve male and female animals, 3-6 months in age, were housed on an inverted 12 h light/dark cycle (8:00-20:00 dark period) in groups of 3-5 mice per cage under standard conditions (23±1°C, 40-50% humidity; food and water *ad libitum*). Germline *Arc/Arg3.1* KO mice were generated as described in Plath et al. (2006). Briefly, vectors were generated of the *Arc/Arg3.1* gene in which three LoxP sites were inserted. The vectors were electroporated into embryonic stem cells and subjected to a transient expression of Cre recombinase. The recombination yielded clones in which the open reading frame (ORF) of the gene was deleted (*Arc/Arg3.1* ^{-/-}, KO) or flanked by two LoxP sites (*Arc/Arg3.1* ^{fl/fl}). Clones were injected into C57Bl/6J blastocytes and chimeras were bred in the C57Bl/6J background to finally generate the germline KO. All experiments were approved by the city of Hamburg's local authorities and were performed following German and European law for the protection of experimental animals.

3.2.2 Spectral Library

To create a spectral library, and ensure the detection of *Arc/Arg3.1* by maximizing it expression one adult WT mouse was subjected to a Kainate-induced seizure. The animal was injected with Kainic acid (Abcam) intraperitoneally (14.8 mg/kg body weight) prepared in PBS. Seizures were scored as generalized if the mouse exhibited bilateral forelimb tonic and clonic activity; with loss of postural tone. 90-120 min after the onset of generalized seizures, the animal was deeply anesthetized with isoflurane, quickly decapitated and the whole hippocampus was immediately dissected on ice. The hippocampus was first dissolved in 100 μL 1 % w/v sodium deoxycholate (SDC) in 0.1 M triethylammonium bicarbonate buffer (TEAB) and shredded using a bead mill (TissueLyser LT, Qiagen N.V., Venlo, Netherlands). It was then incubated for 10 minutes at a temperature of 95 °C to induce cell lysis. To destroy interfering DNA the samples were sonicated (Electronic Sonicator UW2200, Bandelin, Berlin, Germany) for 5 seconds at an energy of 30 %.

A bicinchoninic acid assay (Pierce BCA Protein Assay Kit, Thermo Fisher Scientific, Waltham, MA, catalog-no. 23225) was subsequently performed according to the manufacturer's instruction to determine the protein concentration. Tryptic digestion was performed with 50 µg of protein using the single-pot, solid-phase-enhanced sample preparation (SP3) protocol, as described by Hughes et al. (2019). The eluted peptides were dried in a Savant SpeedVac vacuum concentrator (Thermo Fisher Scientific, Waltham, MA) and were stored at -20 °C. Pierce High pH Reversed-Phase Peptide Fractionation Kit (Catalog number 84868, Thermo Fisher Scientific, Waltham, MA) was then used according to the manufacturer's instructions to reduce sample complexity by dividing the sample into 8 fractions. Immediately prior to MS measurement, the dried peptides were dissolved in 0.1 % FA.

3.2.3 Laser Ablation and sample processing

Naïve, adult WT, and *Arc/Arg3.1* KO mice underwent deep anesthesia with isoflurane and were subsequently euthanized by decapitation. Following decapitation, the brains were rapidly dissected and frozen using dry ice, with special attention given to preventing contamination. The frozen brains were then stored at -80°C until further processing. Using a cryostat (Hyrax C60, Microm), 100μm-thick coronal sections encompassing AP coordinates -1.82 to -2.30 bregma, were sliced and placed on Superfrost Plus slides.

A nanosecond infrared laser (NIRL) system was used for tissue ablation. The general laser system build-up has been published (Voss et al., 2022). The laser with a pulse width of 7 ns was set to a wavelength of 2940 nm s, pulsing with the maximum repetition rate of 20 Hz, when triggered during the ablation sequence. The beam was focussed with a scan lens (focal length of 100 mm). At the sample position, a pulse energy of 650 μ J was measured. The glass slide with the tissue section was placed on a cooling stage, which was set to -1° C. The cooling stage is mounted onto a translation stage composed of two motorized linear stages (MLT25, Newport, CA), which were driven by a motor controller (XPS-RLD4 with two XPS-DRV11 cards, Newport, CA). A PTFE-coated glass slide with 12 wells (Epredia X5XER202WAD1, catalogno. 17342650) was placed at a short distance (<1 mm) over the sample with the region of interest (ROI; 400 μ m \times 400 μ m) centered in a well. The ablation sequence consisted of a meander scan pattern for the sample stage covering the ROI, resulting in 5 x 5 triggered laser shots with 100 μ m spacing for each of the four runs. The plume material of each sequence with 100 laser shots in total, was collected in a single well.

Three hippocampal regions (DG, CA1, and CA3) were sampled from five *Arc/Arg3.1*-KO mice and five WT mice, resulting in 30 samples in total. The location of the specific hippocampus

area was targeted with a camera prior to laser ablation, which was also used to monitor the ablation sequence. One sample from a KO animal in the CA3 subfield was deemed an outlier based on the protein amount and was removed from the analysis.

Further sample processing was performed following a protocol published by (Tsai et al., 2021), 20 μ L of 0.01% DDM (n-dodecyl β -D-maltoside) were used to collect the condensed sample aerosol and transferred from the well into a protein low binding tube (Protein LoBind Tubes, Eppendorf SE, catalog-no. 0030108116). All other sample preparation steps were adapted from the mentioned protocol, except for using 20 ng trypsin for tryptic digestion. The samples were dried in a vacuum centrifuge and stored at -20 °C. Prior to mass spectrometric measurement, tryptic peptides were resuspended in 10 μ L of 0.1% formic acid (FA).

3.2.4 LC-MS/MS Parameters

Liquid chromatography-tandem mass spectrometry (LC-MS/MS) measurements were performed on an Orbitrap Fusion Tribrid mass spectrometer (Thermo Fisher Scientific, Waltham, MA) coupled to a nano-UPLC (Dionex Ultimate 3000 UPLC system, Thermo Fisher Scientific, Waltham, MA). A two-buffer system was used for chromatographic separation of peptides, with buffer A containing 0.1% FA in H₂O (MS grade) and buffer B containing 0.1 % FA in acetonitrile (ACN, MS grade). For desalting and purification, the samples were loaded onto a trap column (100 μm x 20 mm, 100 Å pore size, 5 μm particle size, Acclaim PepMap 100), followed by C18 reversed-phase column (75 μm x 250 mm, 130 Å pore size, 1.7 μm particle size, nanoEase M/Z Peptide BEH C18, Waters). An 80-minute method with trapping for 5 minutes at a flow rate of 5 µL/min followed by a linearly increasing concentration of B from 2% to 30% over 65 minutes at a flow rate of 0.3 µL/min was used for peptide separation. Eluting peptides were ionized with a nano-electrospray ionization (nano-ESI) source with a spray voltage of 1,800 V, transferred into the MS, and analyzed in data-dependent acquisition mode (DDA). Ions were accumulated for a maximum of 120 ms or until a charge density of 2 x 10⁵ ions (AGC Target) was reached. A mass range of m/z 400 – 1,300 was covered with a resolution of 120,000 at m/z 200. Charges of the peptides with a state between +2 - +5 and an intensity threshold of 1,000 or above were isolated within a window of m/z 1.6 in Top Speed mode for 3 s from each precursor scan. For fragmentation, a normalized collision energy of 30 % using higher energy collisional dissociation (HCD) was used. An ion trap mass analyzer with the first mass set to m/z 120 at a rapid scan rate was used. Fragments were accumulated for 60 ms or to an AGC target of 1 x 10⁴ for MS2 scanning. Already fragmented peptides were excluded for 30 s.

3.2.5 Raw Data Processing

LC-MS/MS data were searched with the Chimerys algorithm integrated into the Proteome Discoverer software (v3.0.0.757, Thermo Fisher Scientific) against a reviewed mouse **SwissProt** database, obtained in January 2023, containing 17013 entries. Carbamidomethylation was set as a fixed modification for cysteine residues. The oxidation of methionine was allowed as a variable modification as well as acetylation of the N-terminus and methionine loss. A maximum number of two missing tryptic cleavages was set. Peptides between six and 144 amino acids were considered. A strict cutoff (FDR < 0.01) was set for peptide and protein identification. The laser-ablated samples were searched together with the fractions from the spectral library to boost protein identification by matching between runs. For matching fragment peaks, the mass tolerance was set to 0.6 Da. For chromatographic alignment, the maximum RT shift was set to 10 min with a mass tolerance of 10 ppm. Both unique and razor peptides were considered for quantification. Normalization was done on the peptide level in Proteome Discoverer.

3.2.6 Gel Samples

Sample Preparation:

5 WT and 5 *Arc/Arg3.1* KO mice were deeply anesthetized with isoflurane, quickly decapitated and the brains were immediately dissected on ice to obtain only the dorsal hippocampus. Samples were homogenized in ice-cold Triton-X lysis buffer with protease and phosphatase inhibitors (containing 50mM Tris HCl, 150 mM NaCl, 1 % Triton-X100, 0.5 % sodium deoxylcholate, 0.1 % SDS, 1 mM EDTA, 10 mM NaF, 1 mM PMSF, 1x cOmplete protease inhibitor cocktail, and PhosStop). Protein concentrations were determined using the PierceTM BCA Protein Assay Kit following the manufacturer's instructions (Thermo-Fisher Scientific, Waltham, USA). Samples of 20 μg protein per mouse were separated on 4-12 % Nu-PAGE gels and visualized using a quick Commassie blue staining (SERVA, Heidelberg, Germany). Gel bands between 20 and 28 kDa were excised for subsequent in-gel digestion and LC-MS/MS analysis.

In-gel digestion was done following Shevchenko et al. (2006). Shrinking and swelling were performed with 100 % ACN and 100 mM NH₄HCO₃. In-gel reduction was achieved with 10 mM dithiothreitol (dissolved in 100 mM NH₄HCO₃). Alkylation was performed with 55 mM iodoacetamide (dissolved in 100 mM NH₄HCO₃). Proteins in the gel pieces were digested by covering them with a trypsin solution (8 ng/μL sequencing-grade trypsin, dissolved in 50 mM

NH₄HCO₃) and incubating the mixture at 37°C overnight. Tryptic peptides were yielded by extraction with 2 % FA, and 80 % ACN. The extract was evaporated. For LC-MS/MS analysis, samples were dissolved in 20 μ L 0.1% FA.

LC-MS/MS Parameters:

Chromatographic separation of peptides was done as described in "3.2.4 LC-MS/MS Parameters". MS/MS measurements were performed on a quadrupole-orbitrap hybrid mass spectrometer (QExactive, Thermo Fisher Scientific). Eluting peptides were ionized using a nano-electrospray ionization source (nano-ESI) with a spray voltage of 1,800 and analyzed in data-dependent acquisition (DDA) mode. For each MS1 scan, ions were accumulated for a maximum of 240 milliseconds or until a charge density of 1 x 10^6 ions (AGC Target) was reached. Fourier-transformation-based mass analysis of the data from the orbitrap mass analyzer was performed covering a mass range of m/z 400 - 1,200 with a resolution of 70,000 at m/z = 200. Peptides being responsible for the 15 highest signal intensities per precursor scan with a minimum AGC target of 5 x 10^3 and charge state from +2 to +5 were isolated within a m/z 2 isolation window and fragmented with a normalized collision energy of 25% using higher energy collisional dissociation (HCD). MS2 scanning was performed, covering a mass range starting at m/z 100 and accumulated for 50 ms or to an AGC target of 1 x 10^5 at a resolution of 17,500 at m/z = 200. Already fragmented peptides were excluded for 20 s.

Raw Data Processing:

LC-MS/MS data were processed as described for the laser-ablated samples "3.2.5Raw Data Processing", with the exception of the algorithm used. Data from in-gel digest samples were searched using the well-established Sequest algorithm integrated into the Proteome Discoverer software (v.3.1.0.638, Thermo Fisher Scientific) against the reviewed mouse SwissProt database. Due to its robustness and high compatibility with various preparation methods, including in-gel digestion, the Sequest algorithm was chosen over Chimerys.

3.2.7 Western-blot analyses.

Mice were deeply anesthetized with isoflurane, quickly decapitated and the brains were immediately dissected on ice to obtain only the dorsal hippocampus. The tissue was frozen in dry ice and stored at -80°C for further processing. Samples were homogenized in ice-cold Triton-X lysis buffer with protease and phosphatase inhibitors (containing 50mM Tris HCl, 150 mM NaCl, 1 % Triton-X100, 0.5 % sodium deoxylcholate, 0.1 % SDS, 1 mM EDTA, 10 mM NaF, 1 mM PMSF, 1x cOmplete protease inhibitor cocktail, and PhosStop). Protein

concentrations were determined using the PierceTM BCA Protein Assay Kit following the manufacturer's instructions (Thermo-Fisher Scientific, Waltham, USA). Equal amounts of protein were separated on 4-12 % Nu-PAGE and transferred to Polyvinylidene fluoride (PVDF) membranes (Merck Millipore, Darmstadt, Germany) for 2 h at 4°C with 110V using Mini-PROTEAN TransBlot system (Bio-Rad, Hercules, USA) and blotting buffer (25 mM Tris-Base, 192 mM glycine and 10% methanol). Membranes were blocked in PBS containing 5% non-fat milk with 0,01% tween-20 for 1 h at room temperature. Membranes were then incubated with primary antibody overnight at 4°C in the buffer recommended by the manufacturer. The following antibodies were used at the indicated dilutions: mouse anti-PSD95 (1:2000, Dianova, MA1-046), rabbit anti-Arc/Arg3.1 (1:1000, Synaptic systems, 156003), rabbit anti-GluA2 (1:1000, Millipore, AB1768), mouse anti-GluA3 (1:200, Millipore, MAB5416), mouse anti-VGlut1 (1:2000, Synaptic systems, 135011), guinea pig anti-GABA-A receptor β3 (1:2000, Synaptic Systems, 224004), mouse anti-gephyrin (1:250, DB Bioscience, 610585), rabbit anti-Shisa7 (1:2000, Biozol, ORB186120), rabbit anti-somatostatin (1:500, MyBiosource, MBS2005557), rabbit anti-them6 (1:500, Invitrogen, PA5-69461), rabbit anti-them6 (1:500, Bioss, BS-15296R) and, mouse anti-β-Actin (1:2000, Sigma Aldrich, a5441). The membranes were then washed and incubated with fluorescently conjugated secondary antibodies according to the species for 1 h at room temperature as follows: IRDye 680RD donkey anti-mouse (1:20000, Li-Cor, 926-68072), IRDye 680RD donkey anti-Guinea pig (1:20000, Li-Cor, 926-68077) and, IRDye 800CW donkey anti-rabbit (1:20000, Li-Cor, 926-32213). Membranes were washed again and visualized using the LI-COR's Odyssey Infrared Imaging System (LI-COR Biotechnology, Lincoln, NE). Revert total protein staining was used as a loading control.

3.2.8 Statistical Analysis

Statistical analysis was performed in Perseus Version 2.0.10.0 (The Perseus computational platform for comprehensive analysis of (prote)omics data (Tyanova et al., 2016) GraphPad Prism10 and, MatLabR2020a. The proteome data was log2-transformed. For all mean differences analyses a threshold of minimum three valid values in each group was set. For Genotype comparisons Student t-tests were conducted between WT and KO samples. Proteins with a p-value below 0.05 and a fold change > 1.25 were considered significantly up- or downregulated. A total of 196 proteins were identified as differentially regulated by Arc/Agr3.1 in either the whole hippocampus or specific regions. For these proteins, only the samples from

WT mice were considered for the subfield comparisons. For subfield comparisons, a one-way ANOVA test was conducted for those proteins fulfilling the requirement of a minimum of 3 samples per group. Post-Hoc all pairwise Tukey-HSD were used to compare the different regions. Proteins with a p-value below 0.05 and a fold change > 1.25 were considered significantly up - or downregulated. For proteins with missing data (below 3 samples per region), a frequency-based approach was employed. If a protein was found in a minimum of 5 samples within one subfield but in fewer than 2 samples in the other two, it was classified as "dominant" in that region. For frequency-based genotype comparisons, we created 2 x 2 contingency tables to test whether the detection of a protein was associated with the genotype. Fisher's exact test was used to determine the significance of the association. For western blot analysis, normality was confirmed using Kolmogorov-Smirnov tests, subsequently Student t-tests were conducted between 7 WT and 7 KO animals. P-values <0.05 were considered statistically significant in all cases.

3.3 Results

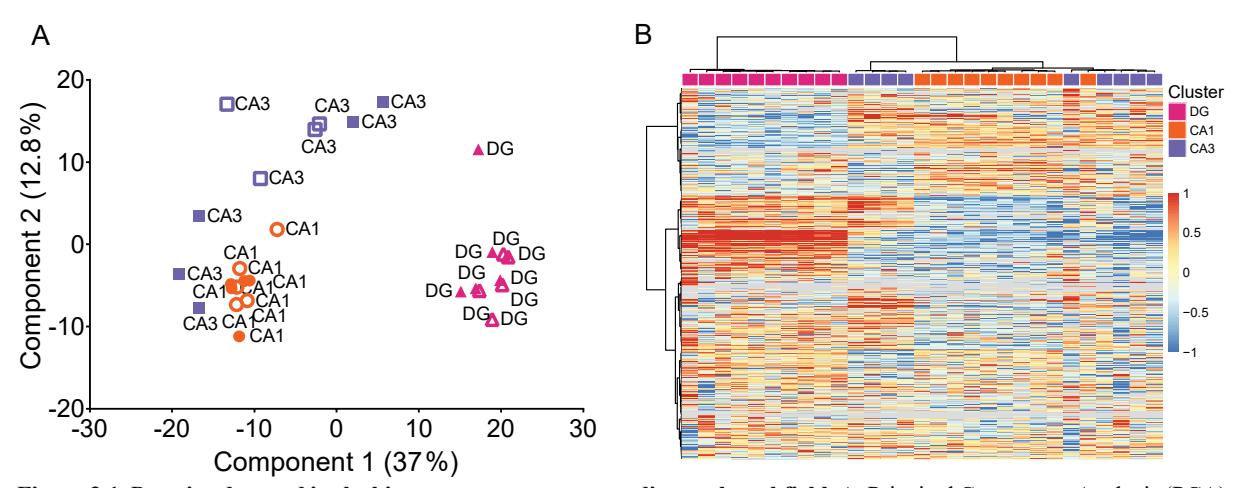


Figure 3.1. Proteins detected in the hippocampus group according to the subfield. A. Principal Component Analysis (PCA) on laser-ablated samples from the hippocampus (Filled symbols represent samples from WT animals). Empty symbols represent samples from KO animals). B. Unsupervised hierarchical clustering of hippocampal proteins associated with the subfields.

3.3.1 Hippocampal Subfields Show Distinct Protein Signatures, with Potentially Intriguing Differences within CA3

We first focused on identifying potential regional differences within the hippocampus, regardless of the mouse genotype (WT or Arc/Arg3.1 KO). We combined protein profiles from both groups and employed principal component analysis (PCA) to search for potential clusters. The PCA revealed two distinct clusters separating the DG and CA1 subfields (**Figure 3.1A**). CA3 samples formed a less distinct third cluster, with some partial overlap towards CA1 but not DG. This pattern of regional variation was further confirmed by unsupervised hierarchical

clustering (**Figure 3.1B**). Interestingly, while CA1 and DG displayed consistent clustering, CA3 samples seemed to split into two distinct sub-clusters in both PCA and hierarchical analyses. This suggests unique protein profiles for each hippocampal subfield, with CA3 potentially exhibiting additional internal diversity. It is worth noting that the samples overlapping with CA1 in the PCA (**Figure 3.1A**, filled squares) originated solely from WT animals.

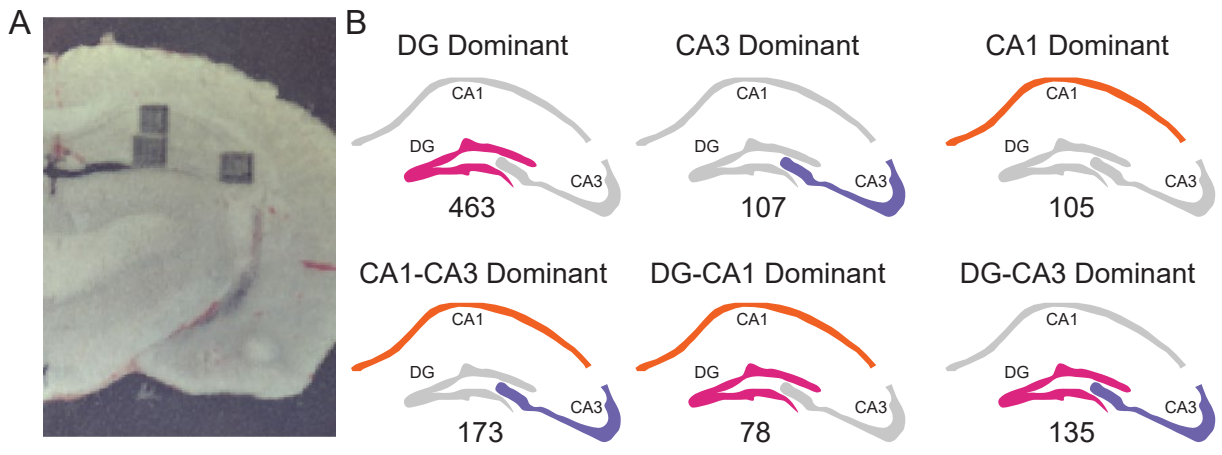


Figure 3.2. Subfield dominance classification. A. Exemplary images of the laser ablation for the different hippocampal subfields. B. Schematic representation of the classification of the proteins based on their abundance profiles, including the number of proteins per class. Dominance classification included selection based on ANOVA and post-hoc analysis as well as frequency analysis for those proteins with a sample size smaller than 3.

3.3.2 Protein expression of DG differs greatly from CA1 and CA3 subfields

Out of the 3464 proteins detected, only 2972 had sufficient data (at least 3 samples per subfield) for a robust statistical analysis using ANOVA. This analysis revealed significant differences in the average abundance of 1590 proteins across the three subfields: DG, CA3, and CA1 (ANOVA main effect: p<0.05). To compare protein abundance between subfields, we employed Tukey's HSD pairwise comparison tests. A minimum fold change of 1.25 was set as a threshold and p-values < 0.05 were used for significance. Using these criteria, proteins were classified into dominance categories based on their abundance patterns across subfields. Proteins significantly higher in one subfield compared to the other two were categorized as dominant in that specific subfield (e.g., DG dominant). Conversely, proteins significantly higher in two subfields compared to the third but not different between the higher ones were classified as dominant in those two subfields (e.g., CA1-CA3 dominant). This classification yielded a distribution with the following protein counts: 430 proteins displayed higher abundance in DG compared to CA1 and CA3 (DG dominant), 105 proteins displayed higher abundance in CA3 compared to CA1 and DG (CA3 dominant), 103 proteins displayed higher abundance in CA1 compared to CA3 and DG (CA1 dominant), 171 proteins displayed higher abundance in CA1 and CA3 compared to DG (CA1-CA3 dominant), 65 proteins displayed higher abundance in DG and CA1 compared to CA3 (DG-CA1 dominant), 119 proteins displayed higher abundance in DG and CA3 compared to CA1 (DG-CA3 dominant). The remaining 529 proteins did not meet the criteria for clear subfield dominance and remained unclassified.

The previous analysis focused on proteins with sufficient data (at least 3 samples per subfield) for conventional statistical comparisons. However, this approach might exclude proteins with subfield-specific expression that fall below the detection threshold in other regions.

To address this limitation, we employed a frequency-based approach. We counted the number of samples in which each protein was detected across subfields. Proteins were then classified as dominant in specific subfields based on the following criteria: A protein found in at least 5 samples within one subfield, but in less than 2 samples in each of the other two subfields, was classified as "dominant" in that subfield. For example, Desmoplakin (Dsp) was detected in 7 DG samples, 1 CA3 sample, and 6 CA1 samples. This pattern led to its classification as a DG-CA1 dominant protein. This approach allows us to identify potential subfield-specific proteins even if their overall abundance is low. It complements the previous analysis by providing insights into potentially rare but functionally important proteins within specific hippocampal subfields. This classification yielded a distribution with the following protein counts: 33 DG dominant, 2 CA3 dominant, 2 CA1 dominant, 2 CA1-CA3 dominant, and 13 DG-CA3 dominant.

Taking the two analyses together, the dominance classification shows that with 463, DG is the subfield with the highest amount of proteins enriched, followed by CA3 and CA1. The second most-abundant group of proteins was shared between the CA3-CA1 subfields (173), indicating that indeed the difference between the DG and the CA subfields is the most pronounced. A schematic representation of this classification and the number of proteins assigned to each category can be seen in **Figure 3.2B** (a complete list of the proteins and their classification can be provided upon request).

3.3.3 Gene Ontology enrichment analysis revealed significantly over-represented functional terms in DG, CA1, and CA3-CA1 dominant proteins

To investigate the functional characteristics linked to proteins dominating individual hippocampal subfields, we employed the Database for Annotation, Visualization, and Integrated Discovery (DAVID). This allowed us to identify statistically significant Gene Ontology (GO) terms. Using the Functional Annotation Chart tool, we selected the top 5 terms

for each GO domain, including Biological Process (BP), Cellular Compartment (CC), and Molecular Function (MF).

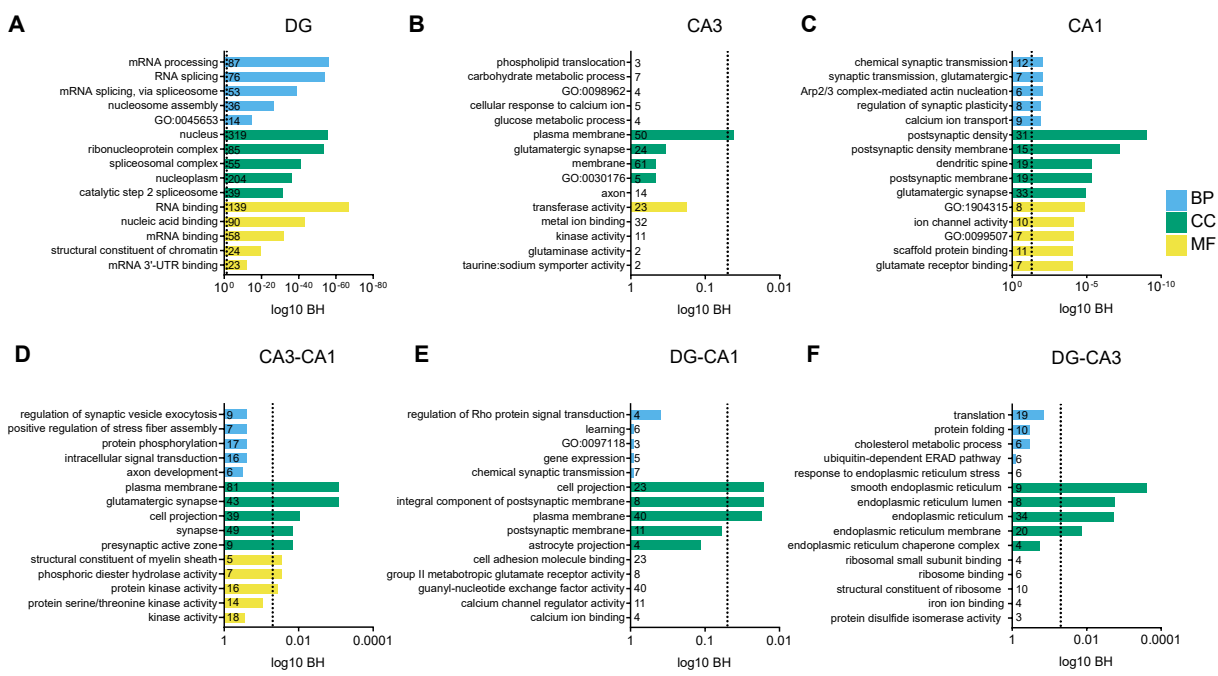


Figure 3.3. Gene ontology analysis on the proteins in the different regions . Discontinued lines show the 0.05 threshold for significance on the Benjamini-Hochberg adjusted p-value. Colors represent the three aspects of the gene ontology (GO) domains; Blue; BP: Biological Process; Green; CC: Cellular Component and Yellow; MF: Molecular Function. Numbers show the amount of proteins found enriched in each term. In **A**, GO:0045653= negative regulation of megakaryocyte differentiation. In **B**, GO:0098962 = regulation of postsynaptic neurotransmitter receptor activity, GO:0030176=integral component of endoplasmic reticulum membrane. In **C**, GO:1904315= transmitter-gated ion channel activity involved in the regulation of postsynaptic membrane potential, GO:0099507= ligand-gated ion channel activity involved in the regulation of presynaptic membrane potential. In **E**, GO:0097118= neuroligin clustering involved in postsynaptic membrane assembly.

DG: The dominant proteins in this subfield displayed enriched GO terms across all three domains, each containing at least 14 proteins. Notably, the BP terms were mostly related to RNA processing, the CC terms highlighted "nucleus" and "ribonucleoprotein complex," and the MF terms pointed to RNA binding (**Figure 3.3A**). This suggests that RNA-binding proteins (RBPs) play a unique role in DG. Possibly as mediators of neurogenesis (Chan et al., 2022), a process that occurs almost exclusively in the DG of adult mice (Kempermann, 2022). These findings may reflect the increased adult neurogenesis taking place primarily in DG.

CA3: Surprisingly, the analysis of the dominant proteins in CA3 (107 proteins) found no significant enrichment in BP or MF categories. Only the CC domain showed enrichment, of the term "plasma membrane" with 50 genes (**Figure 3.3B**).

CA1: In contrast, the dominant proteins in CA1 (105 proteins) had enriched GO terms in all three categories. The BP terms, include proteins strongly linked to the regulation of synaptic transmission and synaptic plasticity. Similarly, the CC terms pointed to various synaptic locations, particularly postsynaptic compartments. Notably, the MF terms indicated ion channel

activity at both pre- and postsynaptic sites. Overall, dominant proteins in CA1 seem heavily involved in synaptic transmission (**Figure 3.3C**).

CA3-CA1: Proteins dominant in both CA3 and CA1 (low in DG), lacked enrichment in BP terms. However, CC terms suggested potential roles in synaptic locations like "plasma membrane" and "glutamatergic synapse". Only 3 MF terms were significant for CA3-CA1, but interpreting their meaning was challenging, two of the terms focused on enzymatic activity while the most enriched term was "structural constituent of myelin sheath" (Figure 3.3D).

Finally, both DG-CA1 and DG-CA3 dominant proteins lacked significant enrichments in BP and MF categories. However, CC terms for DG-CA1 pointed to synaptic structures and cell projections, while DG-CA3 terms exclusively highlighted the endoplasmic reticulum (**Figure 3.3E-F**).

Taken together, the distinct proteome profiles of hippocampal subfields underscore local specializations in molecular and cellular processes serving unique biological functions.

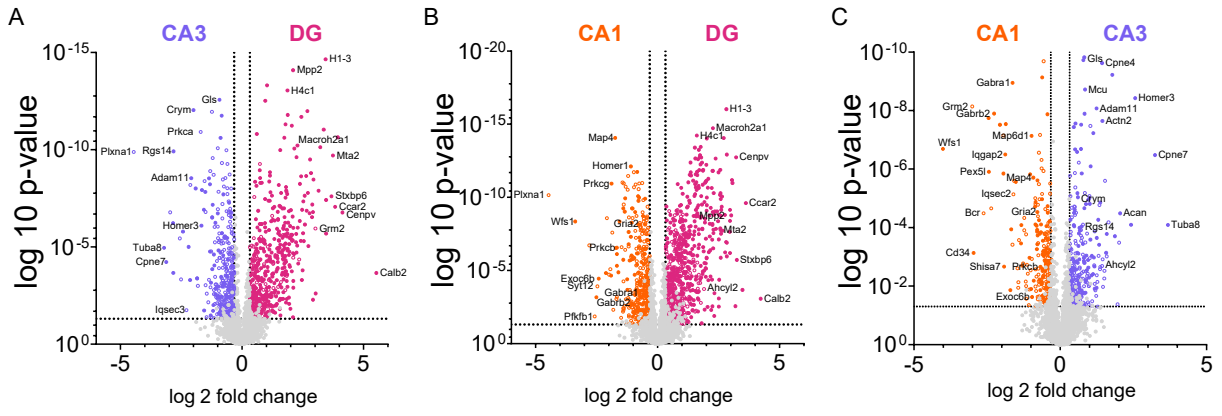


Figure 3.4. High Abundance Proteins in Hippocampal Subfields. Volcano plots reveal significant differences in protein abundance between the three hippocampal subfields: DG, CA3, and CA1. Each plot compares two subfields, with proteins significantly more abundant in each subfield highlighted in their respective colors: pink for DG, purple for CA3, and orange for CA1. Filled circles represent proteins significantly higher in the specific subfield compared with the two others (e.g., protein X is more abundant in both DG vs. CA3 and DG vs. CA1). Empty circles depict proteins showing significant differences only within the compared pair (e.g., protein Y is more abundant in DG vs. CA3 but not in DG vs. CA1). Significance was determined using a Tukey HSD post hoc test with a fold change threshold of >1.25 and a p-value of <0.05.

3.3.4 Unveiling Subfield-Specific Protein Signatures in the Hippocampus: A Look at Volcano Plots

Examining the proteins differentially expressed in the various subfields may uncover potential candidates for a detailed analysis of the hippocampus at the molecular level. In the CA3 subfield, the most notable differences were observed in tubulin α-8 (Tuba8), Copine7 (Cpne7), and Homer3 (**Figure 3.4A and C**). Approximately half of these proteins were linked to the cellular component "plasma membrane" based on GO analysis. However, establishing a clear functional association among the dominant proteins in CA3 proved challenging due to the lack of significantly enriched GO terms, suggesting their involvement in independent processes. In

the DG subfield, Calretinin (Calb2) emerged as the most dominant protein, known for its high enrichment in the hilar region (Figure 3.4A-B). Surprisingly, it was not associated with the most significant GO terms, except for being part of the "nucleus" cellular component. Conversely, other highly dominant proteins in DG, such as Histones 1.3 (H1-3), 2a (Macroh2a1), and 4 (H4c1), were closely associated with enriched molecular function terms, particularly in the "structural constituent of chromatin" category. In CA1, Wolframin (Wfs1) stood out as the most dominant protein, primarily linked to cellular calcium homeostasis (Figure 3.4B-C). Despite not being included in the most enriched GO terms for CA1, the majority of dominant CA1 proteins were associated with terms in the "biological process" domain like "chemical synaptic transmission" or "regulation of postsynaptic membrane potential". This included proteins like the GluA2 receptor (Gria2), the α1 subunit of the GABA-A receptor (Gabra1), the β2 subunit of the GABA-B receptor (Gabrb2), protein kinase C γ (Prkcg), Ras GTPase-activating-like protein (Iggap2), and protein kinase C β (Prkcb). In the cellular component domain, these proteins were part of the terms "postsynaptic density" and "postsynaptic membrane". In the molecular function domain, Gria2, Gabra1, and Gabrb2 were components of the top three terms, including "transmitter-gated ion channel activity involved in the regulation of postsynaptic membrane potential," "ion channel activity," and "ligand-gated ion channel activity involved in the regulation of presynaptic membrane potential". In the CA3-CA1 subfields, the standout protein was Plexin-A1 (Plxna1), primarily associated with the cellular component (CC) term "plasma membrane" (Figure 3.4A-B). Moving to the DG-CA1 subfields, the predominant protein was the metabotropic glutamate receptor 2 (Grm2), featured in all significantly enriched CC terms, including "cell projection," "integral component of postsynaptic membrane," and "plasma membrane" (Figure 3.4A and C). Finally, in DG-CA3 subfields, the most influential protein was the putative adenosylhomocysteinase 3 (Ahcyl2), exclusively associated with the CC term "endoplasmic reticulum" (Figure 3.4B-C).

3.3.5 Comparison of the hippocampal molecular profile using transcriptomics vs proteomics.

In a seminal study by Lein et al. (2004), the molecular distinctions among various subfields of the hippocampus were thoroughly investigated using DNA microarrays and in situ hybridization. The researchers identified 109 candidate genes and categorized them based on their enrichment in specific hippocampal subfields. Notably, the study of Lein and colleagues encompassed the CA2 subfield, which, for simplicity and comparison with our dataset, was not presented here.

The results of Lein et al. (2004) indicated that a majority of genes were enriched in CA3 (33.03%), followed by DG (21.10%), CA3-CA1 (12.84%), DG-CA3 (11.93%), DG-CA1 (11.93%), and CA1 (9.17%). In our study, utilizing proteomics, a different pattern emerged. We identified a total of 1061 differentially expressed proteins, with the highest dominance observed in DG (43.64%), followed by CA3-CA1 (16.31%), DG-CA3 (12.72%), CA3 (10.08%), CA1 (9.9%), and DG-CA1 (7.35%) (**Figure 3.5**).

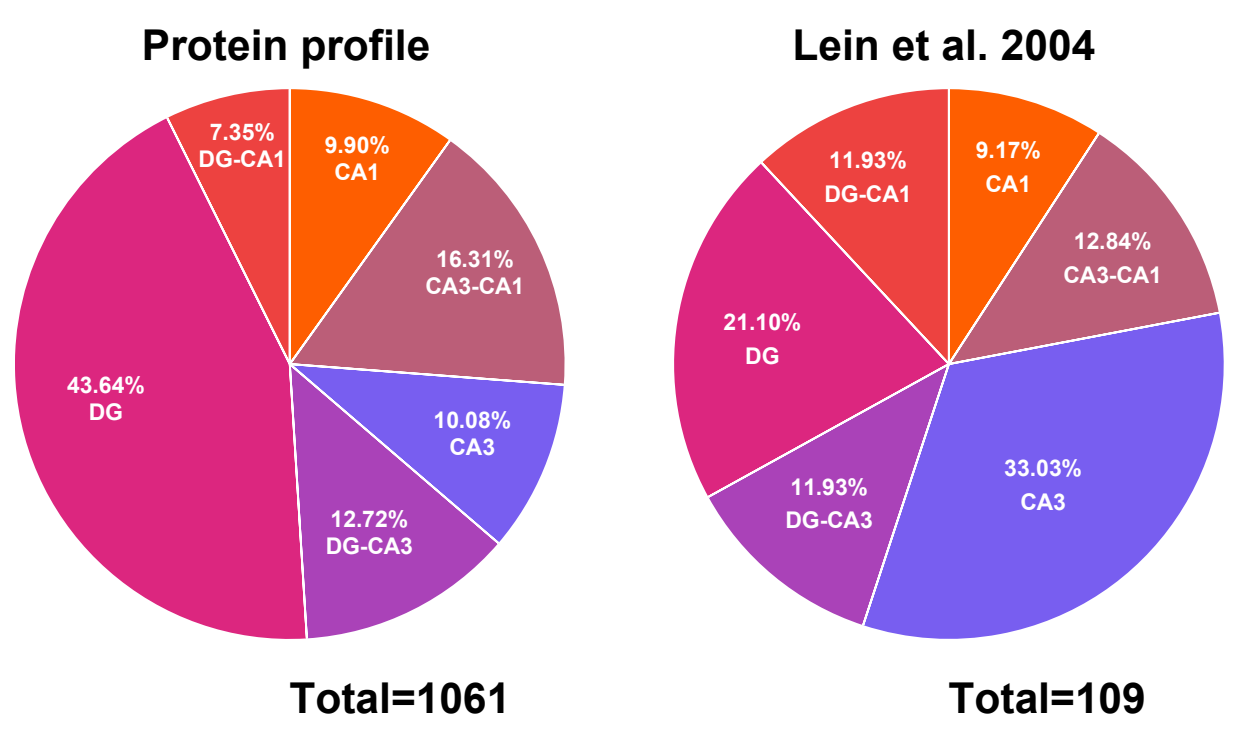


Figure 3.5. Hippocampal profile comparison mRNA and protein . The left panel depicts the protein profile found in the current study. The right panel shows an adapted version of the profile found in Lein et al. (2004) using the same hippocampal division.

While both studies identified subfield-specific enrichment, discrepancies in the results were evident. The gene expression study by Lein and colleagues primarily found enrichment in CA3, followed by DG. Conversely, our proteomics data showed the highest dominance in DG, followed by CA3-CA1 and other subfields. To better understand these differences, a comprehensive comparison of the two studies was conducted. Using fold change calculations for proteins with a minimum of 3 samples per subfield, along with frequency analysis for samples with missing data, we identified 50 out of the 104 candidate genes from the study by Lein et al. in our samples. A detailed comparison of these genes is provided in supplementary table 2, revealing a coherence of 72% in the classification between the two studies.

Of the 14 proteins with conflicting classification, 8 were classified as CA3-enriched by Lein et al., while in our study, they were either CA3-CA1 dominant or showed no differences across the subfields. This discrepancy underscores the importance of considering both gene and protein expression for a comprehensive understanding of regional specialization within the

hippocampus. **Table 3.1.** summarizes the information for the 14 proteins with conflicting classifications.

Table 3.1. Proteins with conflicting classification with respect to the work by Lein et al., 2004

Protein ID	Protein Name	Gene Name	Mean Values Lein et at., 2004 DG CA3	Fold change Lein et at., 2004 DG/CA3 DG/CA1 CA3/CA1	Final Hippocampal Classification	Sample number DG CA3 CA1	_ ANOVA p- _ value	Log2 Mean Abundances DG CA1 CA3	Fold change DG/CA3 DG/CA1 CA3/CA1	Final Hippocampal Classification
E9Q557	Desmoplakin [OS=Mus musculus]	Dsp	2854 906 678	3.34 5.58 1.48	DG	7 1 6	-	CAS	CAS/CAI	DG+CA1
Q9WVK4	EH domain-containing protein 1 [OS=Mus musculus]	Ehd1	9370 5424 4229	1.89 2.47 1.11	DG	10 9 10	0.0769269	23.601 23.301 22.690	-0.81 1.88 1.53	No differences
P17427	AP-2 complex subunit alpha-2 [OS=Mus musculus]	Ap2a2	1724 2529 1404	-1.37 1.32 1.69	CA2+CA3	10 9 10	1.48552E-09	27.846 28.397 28.295	-1.47 -1.37 1.07	CA3+CA1
Q64444	Carbonic anhydrase 4 [OS=Mus musculus]	Ca4	3187 4231 2867	-1.21 1.37 1.70	CA1+CA3	5 5 5	0.000129794	22.945 24.172 23.223	-2.34 -1.21 1.93	CA3
P50396	Rab GDP dissociation inhibitor alpha [OS=Mus musculus]	Gdi1	7736 11191 7897	-1.38 -1.16 1.48	CA2+CA3	10 9 10	0.0878922	28.016 28.296 28.167	-1.215 -1.110 1.094	No differences
Q9QZF2	Glypican-1 [OS=Mus musculus]	Gpc1	10334 16902 8839	-1.5 1.29 1.77	CA2+CA3	10 9 10	9.8483E-15	23.999 25.312 25.439	-2.479 -2.713 -1.092	CA3+CA1
P06801	NADP- dependent malic enzyme [OS=Mus musculus]	Me1	2499 4257 2511	-1.89 1.13 1.66	CA2+CA3	10 9 10	6.24063E-14	24.085 25.085 24.988	-2.000 -1.870 1.069	CA3+CA1
P08551	Neurofilament light polypeptide [OS=Mus musculus]	Nefl	6051 9468 4949	-1.38 1.01 2.20	CA2+CA3	10 9 10	0.00748443	27.938 29.000 28.402	-2.085 -1.379 1.514	CA3>DG
Q9WUA3	ATP-dependent 6 -phosphofructokinase. platelet type [OS=Mus musculus]	Pfkp	2391 3506 2282	-1.54 1.08 1.52	CA3	10 9 10	0.146665	26.246 26.443 26.380	-1.147 -1.098 1.045	No differences
P20444	Protein kinase C alpha type [OS=Mus musculus]	Prkca	275 894 270	-2.93 1.16 2.83	CA2+CA3	10 9 10	5.02854E-16	24.558 26.258 25.944	-3.249 -2.621 1.244	CA3+CA1
Q62420	Endophilin-A1 [OS=Mus musculus]	Sh3gl2	5266 8690 5422	-1.74 -1.05 1.67	CA3	10 9 10	2.51156E-14	27.685 28.369 28.465	-1.608 -1.717 -1.069	CA3+CA1
P07309	Transthyretin [OS=Mus musculus]	Ttr	3477 9703 6564	-2.19 -1.88 1.25	Not expressed in hippocampus	2 5 6				CA1+CA3
Q9CZT8	Ras-related protein Rab-3B [OS=Mus musculus]	Rab3b	1640 1613 3017	1.19 -1.91 -2.00	Uniform expression in primary excitatory hippocampal neurons	9 9 10	0.0324924	22.237 21.281 21.210	1.940 2.042 1.051	DG
Q99K46	Ubiquitin carboxyl-terminal hydrolase 11 [OS=Mus musculus]	Usp11	1040 1136 340	-1.13 3.17 2.32	Uniform expression in primary excitatory hippocampal neurons	1 0 0				Low expression

We describe each identified protein using its protein accession number and standardized nomenclature from Mouse Genome Informatics (MGI). The leftmost columns present the original data and classification from the study by Lein et al., with their mean values representing average expression based on microarray results. The rightmost columns show the results of our current study, including data and classification. Additionally, we include a column indicating the number of samples where each protein was detected. Proteins lacking data in the ANOVA and mean abundances correspond to those with not meeting the minimum threshold of 3 samples per subfield. These proteins were classified using the frequency-based approach detailed in the Results section.

Table 3.2 Comparison to the study by von Ziegler et al., 2018

33 genes with significant differences on both protein and mRNA level	Short name	Log2 FC mRNA CA3/CA1 Newrzella et	Log2 FC protein CA3/CA1 von	Log2 FC protein CA3/CA1 current
		al.	Ziegler et al.	study
Copine-4	Cpne4	3.98	0.67	1.43
Neurocalcin-delta	Neald	3.33	0.4	0.84
Synaptoporin	Synpr	2.69	0.63	0.616
Hippocalcin-like protein 1	Hpcal1	1.89	0.5	ns
Rabphilin-3A	Rph3a	1.85	-0.25	-0.377
Protein piccolo	Pclo	1.6	-0.28	-0.224
Hexokinase-2	Hk2	1.49	0.29	nd
Stathmin-2	Stmn2	1.35	-0.38	nd
Dihydrolipoyllysine-residue acetyltransferase component of pyruvate dehydrogenase complex, mitochondrial	Dlat	1	0.27	0.464
CD200 antigen	Cd200	0.84	-0.29	-0.394
Mammalian ependymin-related protein 1	Epdr1	0.79	0.23	ns
Annexin A6	Anxa6	0.78	0.26	0.292
Kinesin light chain 1	Klc1	0.76	-0.21	0.204
Glutathione S-transferase A4	Gsta4	0.68	-0.24	-0.426
Mitochondrial glutamate carrier 1	Slc25a22	0.63	0.42	0.71
Importin subunit alpha-7	Kpna6	-0.42	0.24	ns
EF-hand domain-containing protein D2	Efhd2	-0.62	-0.61	ns
L-lactate dehydrogenase B chain	Ldhb	-0.67	-0.41	ns
Protein IMPACT	Impact	-0.71	-0.2	ns
Serine/threonine-protein phosphatase 2A 55 kDa regulatory subunit B beta isoform	Ppp2r2b	-0.76	-0.25	nd
Septin-9	Septin9	-0.76	-0.26	-0.268
Catenin delta-2	Ctnnd2	-0.79	-0.2	-0.565
Thioredoxin-dependent peroxide reductase, mitochondrial	Prdx3	-0.79	-0.23	-0.334
Neuromodulin	Gap43	-0.81	-0.7	-0.568
Protein FAM49B	Fam49b	-0.86	-0.34	nd
OCIA domain-containing protein 2	Ociad2	-0.97	0.34	ns
Protein FAM49A	Fam49a	-1	-0.35	nd
Aldehyde dehydrogenase, mitochondrial	Aldh2	-1.15	-0.4	-0.407
RasGAP-activating-like protein 1	Rasal1	-1.15	-0.43	-0.394
N-terminal EF-hand calcium-binding protein 2	Necab2	-2	0.26	1.78
Neurotrimin	Ntm	-2.12	-0.61	-0.618
Alpha globin 1	Hba-a2	-2.18	-0.37	nd
Inositol-trisphosphate 3-kinase A	Itpka	-2.74	-0.9	-2.45

In the color-coded scheme, green denotes consistent findings across studies, while grey indicates conflicting results between Newrzella et al. and von Ziegler et al., as well as between von Ziegler et al. and the present study. Positive and negative values within the color code indicate higher expression in CA3 and CA1, respectively. "nd" represents proteins not detected, and "ns" denotes no significant differences.

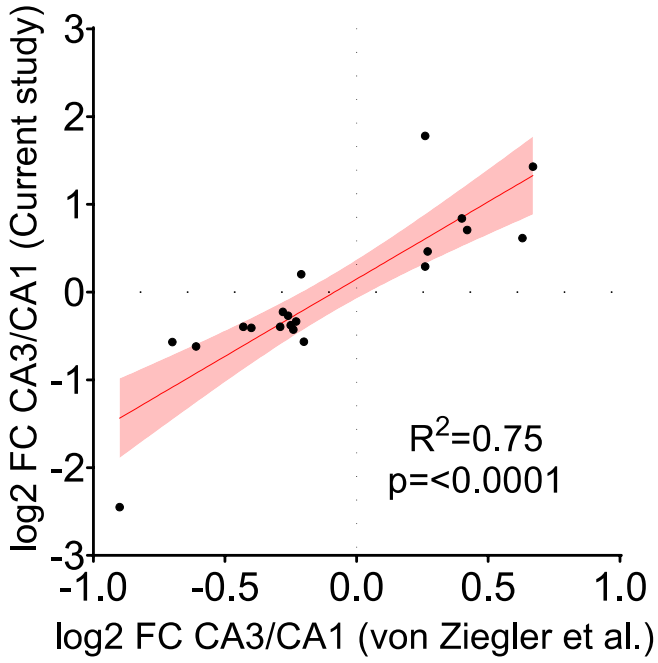


Figure 3.6. Positive correlation with previous studies. Linear correlation between the data in von Ziegler et al., 2018 and the current study (Pearson; $r_{(18)}$ =0,8667; R^2 =0,75; p<0,0001).

3.3.6 Differences between subfields CA3 and CA1 are highly consistent with other proteomic studies

Several studies have emphasized that relying solely on mRNA profiling offers an incomplete understanding of molecular processes. Examining changes in proteins becomes crucial to grasping elements not transcriptionally regulated. In a study by von Ziegler et al. (2018), a comparison of differences in CA3 and CA1 areas was conducted, quantifying 33 genes with significant variations at both mRNA and protein levels. In our analysis, 27 of these genes were detected, and among them, 20 exhibited significant differences between CA3 and CA1 subfields. Notably, our results confirmed the identified protein-level distinctions for 19 out of those 20 genes, indicating a validation rate of 95%. Additionally, a correlation analysis was performed between the log 2-fold changes in our study and those in von Ziegler's study, revealing a robust and statistically significant positive correlation of 0.75 (**Figure 3.6**, Pearson; R²=0,75, p<0,0001). This further supports the high comparability of our findings with those from studies utilizing similar techniques.

3.3.7 Subtle Changes in the Proteome of *Arc/Arg3.1* Knockout Hippocampi under Baseline Conditions

The results discussed above demonstrate the efficiency of NIRL ablation as a method for precisely isolating distinct mouse brain regions for proteomic analysis. Specifically, our findings reveal unique protein profiles in the hippocampal subfields CA1, CA3, and DG. The GO analysis further indicates that these hippocampal subfields possess distinct protein profiles, allowing for specialized cellular functions. For instance, DG shows enrichment in proteins associated with RNA processing, potentially linked to neurogenesis, while CA1 is enriched in proteins involved in synaptic transmission.

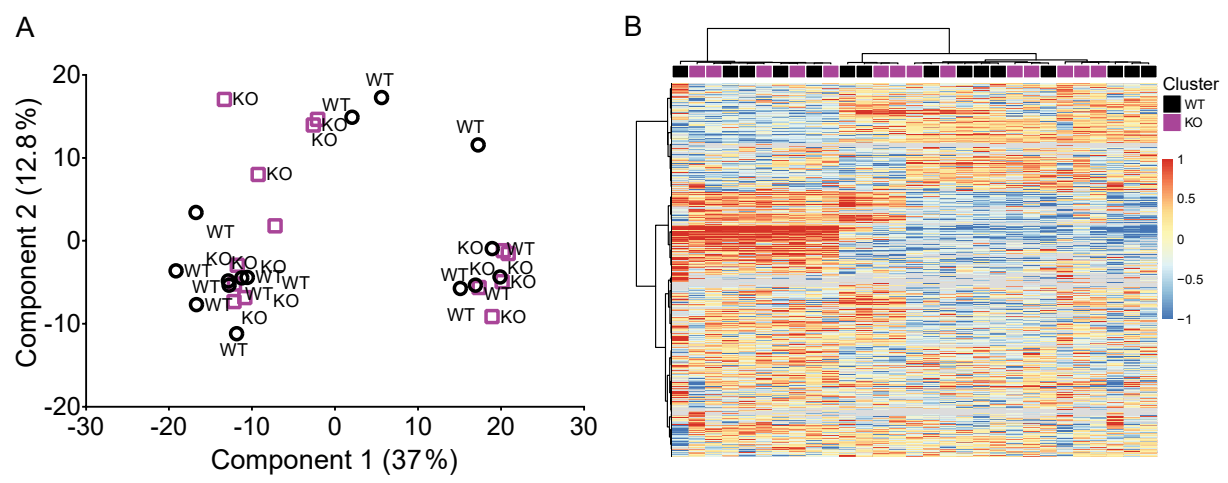


Figure 3.7. Proteins detected in the hippocampus group according to the genotype. A. Principal Component Analysis (PCA) on samples ablated from the hippocampus. B. Unsupervised hierarchical clustering of hippocampal proteins associated with the genotype.

Moreover, a comparison of our proteomics data with a previous transcriptomics study revealed a significant overlap in the identified regionally enriched genes. However, discrepancies were also noted, underscoring the importance of considering both gene and protein expression for a comprehensive understanding. Lastly, in comparison to other proteomic studies, our results demonstrated even higher similarity, thereby validating the efficacy of NIRL for the targeted sampling of specific regions in the mouse brain.

To address the second purpose, we analyzed protein profiles in the subfields of the hippocampi of WT and KO mice lacking the *Arc/Arg3.1* gene. Initial exploration using principal component analysis showed no clear separation between the two groups (**Figure 3.7A**). Similarly, unsupervised hierarchical clustering failed to distinguish between genotypes, with WT and KO samples intermixing randomly (**Figure 3.7B**). These findings collectively indicate that the absence of *Arc/Arg3.1* has minimal impact on the overall proteomic profile of the hippocampus under baseline conditions.

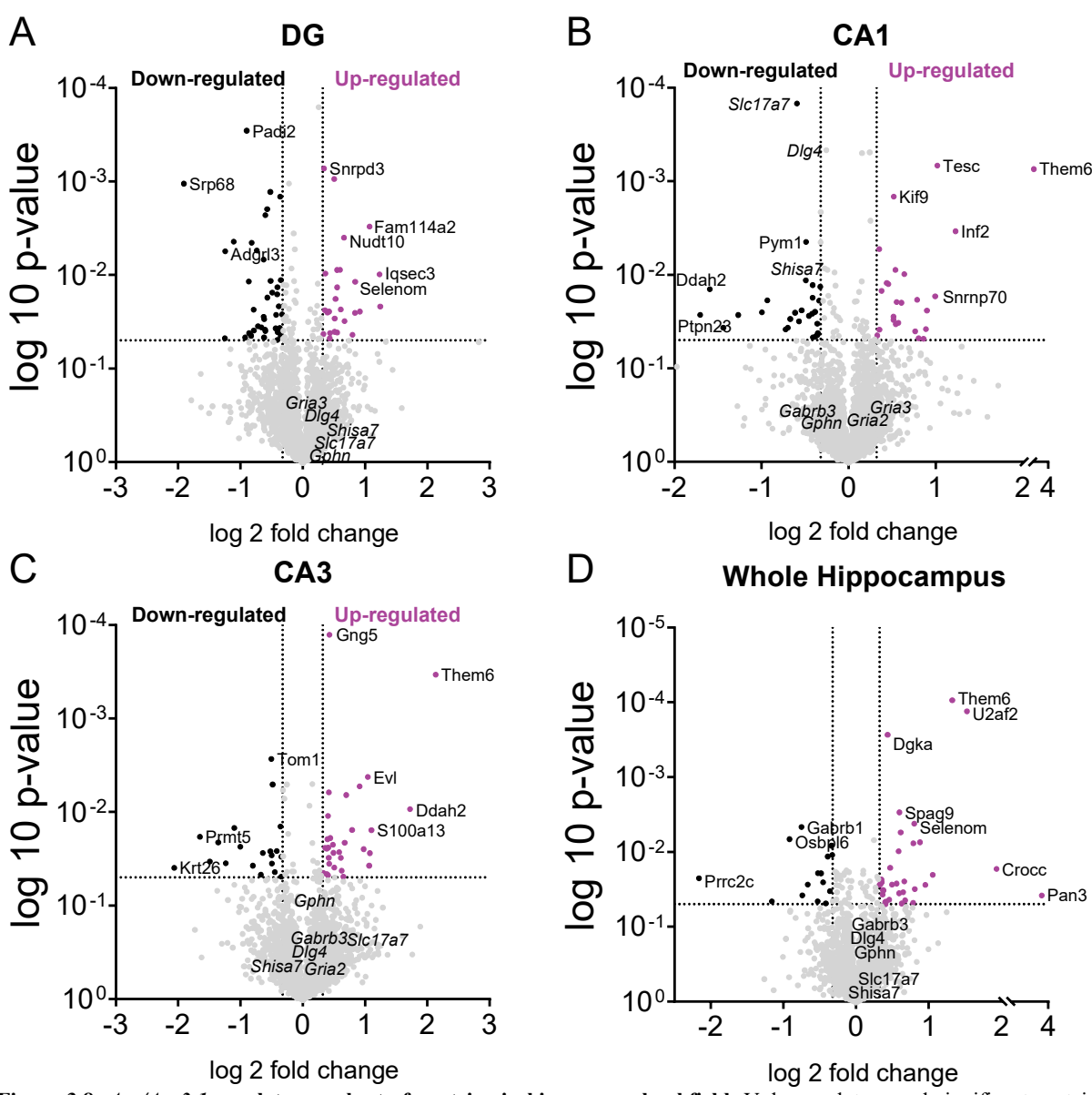


Figure 3.8. Arc/Arg3.1 regulates a subset of proteins in hippocampal subfields. Volcano plots reveal significant protein abundance differences between WT and KO mice in the different hippocampal subfields: Whole hippocampus (WH), DG, CA3, and CA1. In each plot, proteins significantly down-regulated are represented by black spots, while magenta spots indicate up-regulated proteins in Arc/Arg3.1 KO mice. The names of some highly regulated proteins as well as some relevant synaptic proteins are depicted in each plot. Significance was determined using double-tailed T-tests with a fold change threshold of >1.25 and a p-value of <0.05.

3.3.8 Arc/Arg3.1 regulates a subset of proteins in the hippocampus, in a subfield-specific manner.

The overall protein profile of WT and *Arc/Arg3.1* KO mice appears very similar. Yet, the effects of *Arc/Arg3.1* deletion on specific proteins may still exist. To address this possibility, we compared the protein abundance of WT and *Arc/Arg3.1* KO samples in each subfield (CA1, CA3, and DG). Additionally, we assessed potential global hippocampal effects by averaging protein abundance across all three subfields for each animal (whole hippocampus, WH). We employed double-tailed T-tests to compare WT and KO groups, focusing only on proteins detected in at least 3 samples per group. Out of the 3464 proteins detected, roughly 5% (193)

proteins) displayed significant differences in abundance between WT and KO samples. In CA1, out of 2786 proteins detected in at least 3 samples per group, 25 were upregulated and 27 were downregulated in the KO group (**Figure 3.8A**). The most strongly upregulated proteins were calcium-binding protein Tescalcin (Tesc) and Them6, while the most strongly downregulated were vesicular glutamate transporter 1 (VGLUT1, also known as Slc17a7) and Tyrosine-protein phosphatase non-receptor type 23 (Ptpn23).

For CA3, out of 2673 proteins detected in at least 3 samples per group, 31 were upregulated and 20 were downregulated in the KO (**Figure 3.8B**). The most strongly upregulated proteins were Guanine nucleotide-binding protein subunit gamma-5 (Gng5) and Them6, while the most strongly downregulated were Target of Myb1 membrane trafficking protein (Tom1) and Keratin, type I cytoskeletal 26 (Krt26).

In DG, out of 2893 proteins detected in at least 3 samples per group, 26 were upregulated and 40 were downregulated in the KO (**Figure 3.8C**). The most strongly upregulated proteins were Small nuclear ribonucleoprotein Sm D3 (Snrpd3) and IQ motif and SEC7 domain-containing protein 3 (Iqsec3), while the most strongly downregulated were calcium-binding Protein-arginine deiminase type-2 (Padi2) and Signal recognition particle subunit SRP68 (Srp68).

Finally, in the whole hippocampus, among 3194 proteins detected in at least 3 animals per group; 34 were upregulated and 15 were downregulated (**Figure 3.8D**). The most strongly upregulated proteins in the Arc/Arg3.1 KO mice were thioesterase superfamily member 6 (Them6) and Poly(A)-nuclease deadenylation complex subunit 3 (Pan3), while the most strongly downregulated were GABA-A receptor subunit $\beta1$ (Gabrb1) and Proline-rich and coiled-coil-containing protein (Prrc2c).

3.3.9 Frequency analysis reveals an additional subset of proteins regulated by Arc/Arg3.1 in hippocampal subfields

The failure to detect proteins in certain samples could indicate subthreshold abundance, absence of the protein in the sample, or modifications in the proteins precluding their identification (Hamid et al., 2022; Kim et al., 2016; Lai et al., 2013). To address missing protein data (below 3 samples per group), we applied a frequency-based approach. We constructed 2x2 contingency tables to assess any association between protein detection and its membership in either the WT or KO group. The categories included in the table were: WT with protein detected, WT with protein not detected, KO with protein detected, and KO with protein not detected. Fisher's exact

test was applied to these tables to determine if a significant association existed between the "protein detection" and "genotype" variables.

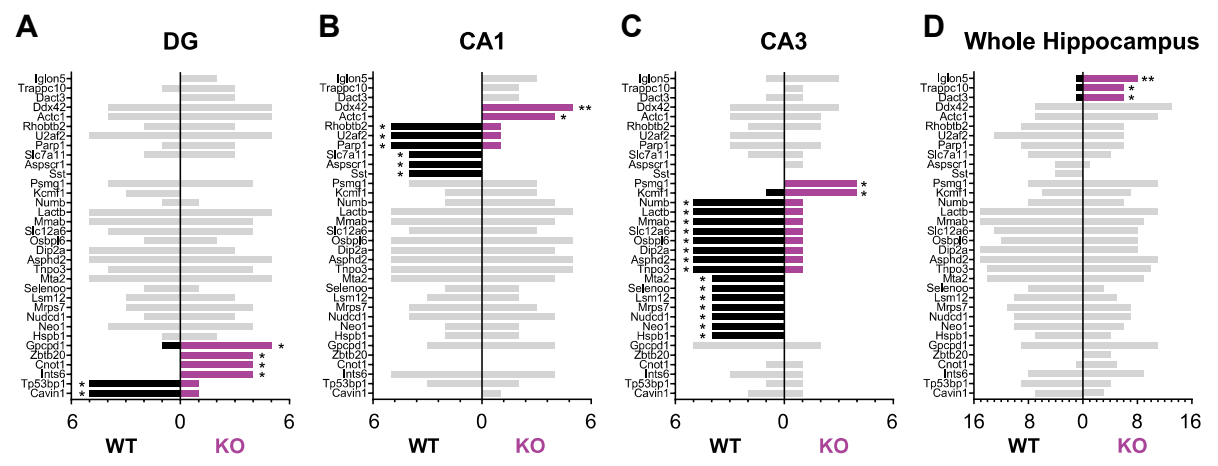


Figure 3.9. Frequency analysis for protein abundance in WT vs. *Arc/Arg3.1* KO Hippocampus. Bar plots present the number of samples in which a protein was detected for WT and KO groups (left and right, respectively). The focus is on a subset of 34 proteins identified with differential detection in the whole hippocampus, CA1, CA3, or DG. Colored bars (black and magenta) indicate associations between the genotype and protein detection in the samples, revealing non-random distributions. Significance was determined through a double-tailed Fisher's exact test. *:p<0.05, **:p<0.01.

In DG, four proteins were notably identified in a significantly higher number of samples within the KO group, among which Zinc finger and BTB domain-containing protein 20 (Zbtb20), CCR4-NOT transcription complex subunit 1 (Cnot1), and Integrator complex subunit 6 (Ints6) were exclusively detected in KO samples. Conversely, two proteins were primarily found in WT samples (**Figure 3.9A**).

In CA1, two proteins were exclusively identified in KO samples: ATP-dependent RNA helicase DDX42 (Ddx42) and Alpha-cardiac actin (Actc1). Conversely, a total of six proteins exhibited a notably higher occurrence in the WT group, suggesting downregulation in KO CA1. These proteins include Cystine/glutamate transporter (Slc7a11), Tether containing UBX domain for GLUT4 (Aspscr1), and Somatostatin (Sst), all of which were exclusively found in WT samples (**Figure 3.9B**).

In CA3, two proteins were notably identified in a significantly higher number of samples within the KO group, and Proteasome assembly chaperone 1 (Psmg1) was exclusively detected in KO samples. Conversely, a total of 15 proteins exhibited a significantly higher occurrence in the WT group. Among them, Metastasis-associated protein 2 (Mta2), Protein adenylyltransferase SelO, mitochondrial (Selenoo), Protein LSM12 (Lsm12), Small ribosomal subunit protein uS7m (Mrps7), NudC domain-containing protein 1 (Nucdc1), Neogenin (Neo1), and Heat shock protein beta-1 (Hspb1) were exclusively found in WT samples (**Figure 3.9C**).

Finally, in the average of the three subfields (whole hippocampus), we identified three proteins with significantly higher frequency in the KO group: IgLON family member 5 (Iglon5), Trafficking protein particle complex subunit 10 (Trappc10), and Dapper homolog 3 (Dact3) (**Figure 3.9D**).

3.3.10 Exploratory functional annotation analysis reveals subfield-specific roles for *Arc/Arg3.1*-regulated proteins within the hippocampus.

The combination of t-tests for comparing protein abundance and frequency analysis enabled us to effectively identify proteins that were either up- or down-regulated in Arc/Arg3.1 KO mice (Supplementary table 5). Interestingly, these results showed that most of the proteins regulated by Arc/Arg3.1 were specific to each subfield, meaning that these proteins were not found to be up- or down-regulated in the other subfields. Of the 60 proteins in CA1, 42 were unique to this subfield; of the 68 proteins in CA3, 57 were unique; and of the 72 proteins in DG, 61 were unique. The remaining proteins identified in each subfield showed a broader pattern of regulation, as some were found regulated in other subfields, while others exhibited changes in the average of the whole hippocampus.

Next, we performed GO analysis on these differentially detected proteins, in an attempt to reveal distinct biological processes regulated by Arc/Arg3.1. However, none of the identified terms reached statistical significance. It is important to note that even in the absence of significant enrichment, common themes or patterns within the dataset can still be discerned by examining frequently occurring terms.

To explore these potential themes or patterns further, we utilized the functional annotation table tool in DAVID. Rather than focusing on the significance of enrichment, we identified terms with the highest number of associated proteins across various subfields. This approach allowed us to uncover the most prevalent GO terms, providing valuable insights into the biological functions regulated by Arc/Arg3.1 in different hippocampal subfields.

Surprisingly, the proteins regulated by *Arc/Arg3.1* in the DG did not seem to align with the enriched terms in the DG (**Figure 3.3A**) or those identified in the proteins regulated in the whole hippocampus (**Figure 3.10D**). The prevalent terms suggested a diverse range of functions, including metabolic processes, protein phosphorylation, and immune responses. Cytoplasmic locations were dominant in the Cellular Component domain, and the mitochondrion also played a notable role. The Molecular Function domain highlighted protein binding as a primary term, followed by enzymatic activity (**Figure 3.10A**).

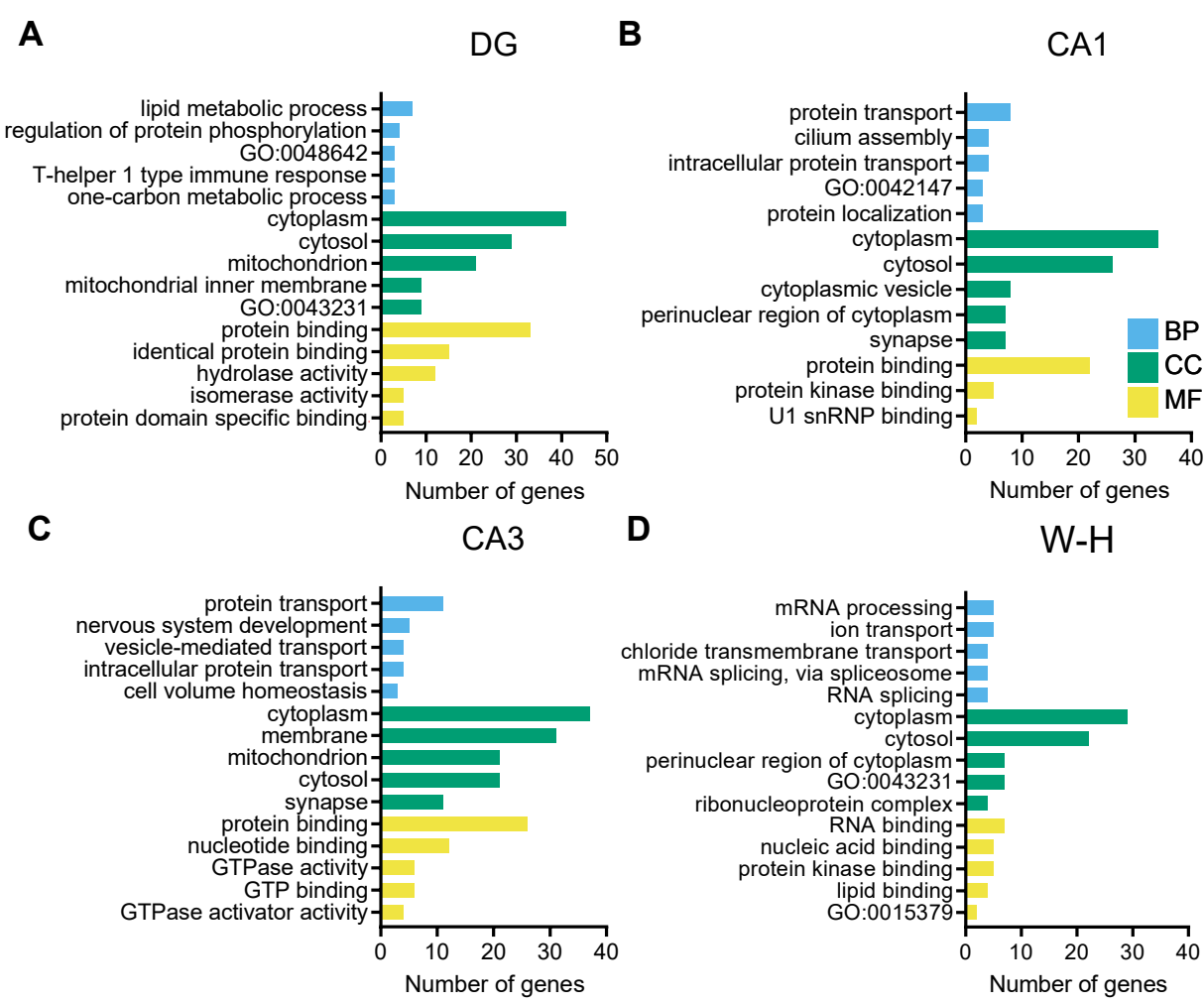


Figure 3.10. Gene ontology analysis on the *Arc/Arg3.1* regulated proteins in the different hippocampal subfields. The bar plots illustrate the top five terms most frequently encountered in the whole hippocampus (A), CA1 (B), CA3 (C), or DG (D) across each Gene Ontology (GO) domain, along with the number of proteins associated with each term. Colors correspond to the three aspects of the gene ontology domains: Blue for Biological Process (BP), Green for Cellular Component (CC), and Yellow for Molecular Function (MF). In A, GO:0043231= intracellular membrane-bounded organelle, and GO:0015379 = potassium: chloride symporter activity. In B, GO:0042147 = retrograde transport, endosome to Golgi. In D, GO:0048642 = negative regulation of skeletal muscle tissue development, GO:0043231 = intracellular membrane-bounded organelle.

In CA1, the regional profile analysis revealed a significant engagement of this hippocampal subfield in regulating synaptic function (**Figure 3.3C**). Given the established role of *Arc/Arg3.1* in synaptic plasticity, we expected a strong association of differentially regulated proteins with synaptic terms. Surprisingly, the most prevalent terms were linked to protein transport in the Biological Process (BP) domain and protein binding in the Molecular Function (MF) domain. In terms of the Cellular Component domain, the majority of terms indicated cytoplasmic locations, and the term "synapse" appeared in association with seven of the proteins (**Figure 3.10B**).

The proteins influenced by *Arc/Arg3.1* in CA3 exhibited a pattern akin to those in CA1, primarily linked to protein transport in the Biological Process domain. In terms of Cellular Component, they were mainly associated with cytoplasmic locations and the synapse, with a

notable presence in the membrane and mitochondrion. Additionally, in the Molecular Function domain, terms such as protein binding and GTPase activity were prevalent (**Figure 3.10C**).

In the whole hippocampus, proteins regulated by *Arc/Arg3.1* were often associated with biological processes related to RNA processing and ion transport. Interestingly, three of these commonly associated terms were also found to be significantly enriched in the DG, as detailed in the profile description of the different subfields (**Figure 3.3A**).

Regarding the Cellular Component domain, most terms suggest a cytoplasmic location and the ribonucleoprotein complex, which again showed high enrichment in the DG (**Figure 3.3A**). Similarly, in the Molecular Function domain, terms related to RNA and nucleic acid binding were prevalent, mirroring the enrichment observed in the DG (**Figure 3.10D**).

Overall, our findings suggest subfield-specific roles for *Arc/Arg3.1*-regulated proteins within the hippocampus. While some terms such as cytoplasmic localization and protein binding, were consistent across hippocampal subfields, there were also notable differences. For example, while the whole hippocampus showed enrichment in RNA processing and ion transport, CA1 and CA3 were primarily associated with protein transport and showed involvement in synaptic functions. The proteins regulated by *Arc/Arg3.1* in the DG exhibited a diverse range of functions, including metabolic processes and immune responses, suggesting a complex regulatory landscape in this region. The observed patterns of protein regulation suggest that, under baseline conditions, *Arc/Arg3.1* may play a role in coordinating various cellular processes within the hippocampus, including RNA processing, ion transport, protein transport, synaptic function, and possibly other functions yet to be fully characterized.

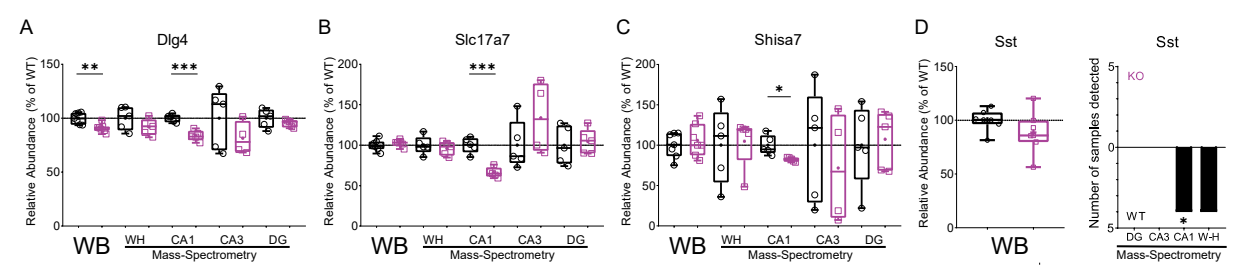


Figure 3.11. Impact of *Arc/Arg3.1* deletion on the expression of synaptic proteins evaluated with WB and Mass-spectrometry in the different hippocampal regions. A-C. Box plots illustrate the relative protein abundance as a percentage of the WT group, assessed with WB or mass-spectrometry in the different hippocampal subfields. H. Somatostatin (Sst) protein levels: The left panel shows its abundance as a percentage of the WT group, measured by WB. The right panel shows the number of samples in which Sst was detected, with WT on the lower end and KO on the upper part. Significance was determined using double-tailed T-tests and double-tailed Fisher's exact test for Sst. *:p<0.05, **:p<0.01, ***:p<0.001.

3.3.11 Abundances of synaptic protein in the dorsal hippocampus of WT and KO mice

Our previous investigation of synaptic transmission in the hippocampus, indicated a substantial influence of *Arc/Arg3.1* on the density, microarchitecture and physiology of synapses (Chapter

I). Our current mass-spectrometry results reveal a number of differentially abundant proteins in the KO hippocampus with a predicted synaptic localization and function. To verify these differential abundances with a second method, we used Western Blot analysis. We obtained fresh samples of dorsal hippocampus from WT and KO mice, separated them on Nu-PAGE gels, and blotted and immunostained them against the specific protein. The absence of Arc/Arg3.1 protein in the KO samples was confirmed via western blot (data not shown). KO samples were compared to the WT samples average. We assessed the protein levels of PSD-95 and a select group of relevant proteins involved in synaptic transmission. Additionally, we constructed box plots illustrating the protein levels across different subfields to gain a better understanding of the distributions and the impact of Arc/Arg3.1 deletion (Figure 3.11).

The Western Blot analysis reaffirmed a small yet significant (around 10%) decrease in PSD-95 abundance in the KO group within the dorsal hippocampus (WT: n=7, KO: n=7; Fig. 11A. t_(df)= 3.716₁₂, p=0.0029). In the mass-spectrometry results, lower abundances were apparent across all hippocampal subfields, with significant differences observed only in CA1 (Fig. 11A. WH: WT: n=5, KO: n=5, $t_{(df)}$ = 1.369₈, p=0.2081; CA1: WT: n=5, KO: n=5, $t_{(df)}$ = 5.848₈, p=0.0004; CA3: WT: n=5, KO: n=4, $t_{(df)}$ = 1.190₇, p=0.2727; DG: WT: n=5, KO: n=5, $t_{(df)}$ = 1.133₈, p=0.2899). For VGLUT1 (Slc17a7), the Western Blot analysis showed no significant differences (WT: n=7, KO: n=7; Fig. 11B. $t_{(df)}$ = 0.8279₁₂, p=0.4239), despite a significantly lower abundance in KO mice in CA1, observed with mass spectrometry (CA1: WT: n=5, KO: n=5, $t_{(df)}$ = 6.528₈, p=0.0002). The discrepancy might reflect the lack of VGLUT1 modulations in the CA3 and DG subfields or whole hippocampus (Fig. 11B. WH: WT: n=5, KO: n=5, $t_{(df)}=0.63138$, p=0.5455; CA3: WT: n=5, KO: n=4, $t_{(df)}=1.3557$, p=0.2176; DG: WT: n=5, KO: n=5, t_(df)= 0.354₈, p=0.7325). Shisa7 displayed a similar pattern to VGLUT1; no significant differences were observed in the Western Blot analysis (Fig. 11G: WT: n=7, KO: n=7; t(df)= 0.6087, p=0.5541), while the mass-spectrometry results indicated differences only in CA1, with no notable variations in other subfields (Fig. 11G. WH: WT: n=5, KO: n=5, t_(df)=0.1905₈, p=0.8537; CA1: WT: n=5, KO: n=5, $t_{(df)}$ = 3.2088, p=0.0125; CA3: WT: n=5, KO: n=4, $t_{(df)}$ = 0.60777, p=0.5625; DG: WT: n=5, KO: n=5, $t_{(df)}$ = 0.26448, p=0.7982).

We further investigated the abundance of somatostatin (Sst) due to its role in modulating synaptic activity, particularly at inhibitory synapses. However, as depicted in Figure 9, Sst exhibited very low abundance and was only identified in CA1 samples, exclusively in WT mice (Fig. 11H-Right). Consequently, the impact of *Arc/Arg3.1* on somatostatin expression in other hippocampal subfields could not be evaluated. Utilizing frequency analysis, we confirmed a

significant association between genotype and Sst detection in CA1 (Fisher's exact test, p= 0.0476), but not in the whole hippocampus (Fisher's exact test, p= 0.0996). Consistently, Western Blot results also failed to demonstrate significant differences between the groups (Fig. 11H-Left: WT: n=7, KO: n=7, $t_{(df)}=1.368_{12}$, p=0.1964).

We previously evaluated the expression of a subset of relevant synaptic proteins in the entire hippocampus and found no alteration associated with Arc/Arg3.1 deletion. To investigate whether that Arc/Arg3.1 specifically affects a sub-region, we re-analyzed these proteins in the dorsal hippocampus using both mass spectrometry and western blot techniques. Consistent with the findings from the whole hippocampus, the results from the dorsal region showed no significant differences between WT and Arc/Arg3.1 KO mice. A comprehensive summary of the proteins evaluated is provided in Table 3.3.

Table 3.3 Arc/Arg3.1 effect on an additional subset of synaptic proteins using western blot or mass spectrometry

Protein	Method	Subfield	P-value	t	Degrees of freedom	Mean WT (%WT)	Mean KO (%WT)	N WT	N KO
GABAβ3	WB	WH	0.5948	0.5464	12	100	95.86	7	7
	M-S	WH	0.1021	1.846	8	100	90.49	5	5
		CA1	0.3194	1.062	8	100	90.7	5	5
		CA3	0.2069	1.391	7	100	80.79	5	4
		DG	0.4518	0.7909	8	100	91.37	5	5
Gephyrin	WB	WH	0.9302	0.08949	12	100	99.57	7	7
	M-S	WH	0.2932	1.125	8	100	94.16	5	5
		CA1	0.3307	1.036	8	100	91.42	5	5
		CA3	0.09	1.967	7	100	84.06	5	4
		DG	0.9825	0.02259	8	100	100.2	5	5
	WB	WH	0.8899	0.1414	12	100	99.42	7	7
	M-S	WH	0.8852	0.149	8	100	101.3	5	5
GluA2		CA1	0.3292	1.039	8	100	93.98	5	5
		CA3	0.3182	1.075	7	100	80.54	5	4
		DG	0.349	0.9948	8	100	108.4	5	5
	WB	WH	0.8361	0.2114	12	100	97.55	7	7
GluA3	M-S	WH	0.3246	1.05	8	100	89.13	5	5
		CA1	0.2369	1.278	8	100	114.3	5	5
		CA3	0.6937	0.4105	7	100	100	5	4
		DG	0.2512	1.237	8	100	80.11	5	5

3.3.12 Them6 is highly upregulated in the dorsal hippocampus of Arc/Arg3.1 KO mice

As observed in **Figure 3.8**, Them6 is the most upregulated protein in Arc/Arg3.1 KO, in CA1, CA3, and the average of the whole hippocampus. Despite the comparable levels of Them6 in the DG of WT and KO mice, the significant differences in the whole hippocampus suggested that this upregulation would be detectable using homogenates from the dorsal hippocampus. Intrigued by the strong differences, we set to confirm these findings using western blotting. We used one of the few available Them6 antibodies with specific mouse reactivity (PA5-69461), but our initial analyses failed to show a band at the expected 23.8 kDa. To account for possible low protein abundance, we increased the protein concentration from 5 to 10 µg. Additionally, Them6 expression was predicted to be high in the mouse thymus, and had been detected in the cerebellum by antibody manufacturers, we then included homogenates from these tissues. However, we did not detect Them6 in any of the tissues or protein concentrations we used (Figure 3.12A). We then tested a second antibody with reactivity for both mouse and human (BS-15296R), but this one also failed to show bands at the expected height (Figure 3.12B). Given the lack of specific antibodies against this protein, we decided to use mass-spectrometry again. We prepared new homogenates of the dorsal hippocampus from 5 WT and 5 Arc/Arg3.1 KO mice, separated them using gel electrophoresis, and visualized them using Coomassie blue staining. Gel bands within a range of 20-25 kDa were excised and processed for LC-MS/MS analysis following an in-gel digestion protocol (Figure 3.12C).

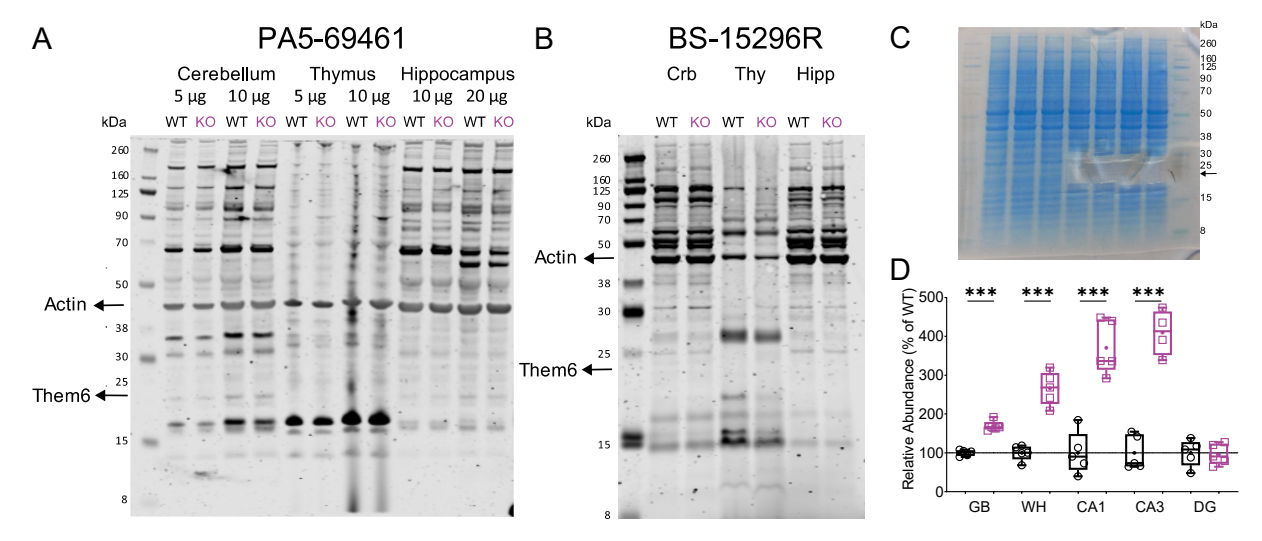


Figure 3.12. Them6 is highly upregulated in the dorsal hippocampus of Arc/Arg3.1 KO mice. A-B: Western blot analysis illustrating the absence of the Them6 band at the expected 23.8 kDa in samples from the cerebellum, thymus, and dorsal hippocampus. In panel A, the antibody rabbit anti-Them6 PA5-69461 was used with protein concentrations of 5 μg, 10 μg and, 20 μg, as indicated. β-Actin was used as a loading control. In panel B, the antibody rabbit anti-Them6 BS-15296R was used with 10 μg of protein for all samples. Abbreviations: Crb (cerebellum), Thy (thymus), Hippo (hippocampus). C: Nu-PAGE gel stained with Coomassie blue showing the bands extracted for mass spectrometry analysis. D: Box plots showing the relative abundance of Them6 protein as a percentage of the WT group, assessed using mass spectrometry in the different hippocampal samples. Abbreviation: GB (gel bands), WH (Whole hippocampus).

Consistent with the results from the laser-ablated samples, we found a significant upregulation of Them6 in *Arc/Arg3.1* KO mice **Figure 3.12D**. It is worth noting that Them6 did not show subfield specificity, indicating that the contributions of the three different hippocampal subfields to the whole hippocampus would be similar. However, while the upregulation of Them6 in *Arc/Arg3.1* KO mice is detectable on a dorsal hippocampus-level, it occurs specifically in the CA1 and CA3 subfields region.

3.4 Discussion

3.4.1 Proteomic profiles of the hippocampal subfields

The presented comparisons revealed a high consistency of our results with previous studies using similar techniques. However, the comparisons to the study by Lein et al. (2004), showed a small number of genes with contrasting hippocampal classifications. One potential explanation for this discrepancy lies in the method used to dissect the different hippocampal subfields. Lein and colleagues isolated the tissue for microarray assay by grossly dissecting the different subregions from fresh hippocampi. They acknowledged that some boundaries could not be easily discerned, resulting in the inclusion of some parts of subiculum in CA1 samples, and parts of fimbria and choroid plexus in the CA3 samples.

In contrast, our laser ablations on previously sliced coronal sections allowed us to target each subfield with high precision. Despite the potential influence of the dissection method on the observed differences between the two studies, Lein and colleagues confirmed their findings using *in situ* hybridization on coronal slices. This approach helped to overcome limitations in spatial resolution, reducing the likelihood that the dissection method alone is responsible for the discrepancies.

Another possible explanation involves differences in the expression of these genes along the dorsoventral axis of the hippocampus. The study by Lein et al. used the entire hippocampus, while our study focused exclusively on the dorsal hippocampus. This is significant because the dorsal and ventral hippocampus differ in their function, response to stress, connectivity, and, importantly, molecular profiles (Czeh et al., 2015; Lee et al., 2017; Leonardo et al., 2006; McHugh et al., 2011; Witter, 1986).

Yet another possibility is the differing approaches used by the two studies. Lein et al. assessed gene expression profiling using microarrays and *in situ* hybridization, while we employed mass spectrometry to analyze the proteomic profile. Although both of these methods offer insights

into gene function, their results can differ due to factors such as alternative splicing, and posttranslational modifications (Wilkins, Sanchez, et al., 1996). Thus, a specific transcript product might not correlate with its protein expression level (Ludvigsen & Honoré, 2018).

Supporting this premise, the study by von Ziegler and colleagues, used proteomics to compare CA1 and CA3 subfields. They contrasted their findings with a previous study doing the same comparison but using mRNA levels. The comparison revealed that most proteins showed consistent expression patterns on the mRNA and protein levels, but some of them exhibited conflicting results. Notably, when we compared our findings to those of von Ziegler's, a high degree of consistency (95%) was observed in protein expression patterns. This suggests that studies analyzing protein levels might yield more consistent results.

Our findings on the dominance classification of different subfields revealed that the dentate gyrus (DG) has the highest amount of highly expressed proteins compared to the other subfields. This is followed by a combination of CA1 and CA3, which have higher protein abundance than DG but are not significantly different between themselves, highlighting the notable difference between DG and the CA regions. These results align with studies using transcriptomics (Masser et al., 2014), and essentially, with the anatomical classification of the hippocampus. DG, CA3, and CA1 form the trisynaptic circuit with unidirectional connectivity, and therefore these regions are often referred to as parts of the hippocampus. However, a distinction exists between the DG and the hippocampus proper or cornu ammonis (CA), which includes CA1, CA2, and CA3. For precision, anatomists refer to the "hippocampal formation" when including the DG (Amaral & Lavenex, 2006). The hippocampus proper differs from DG in several features starting with the type of principal cells that form them: pyramidal and granule cells, respectively. These cells differ in their morphology, precursors, the connections they form, their electrical properties, and their sensitivity to neuromodulators (Becq et al., 2005; Claiborne et al., 1986; Ferguson & Skinner, 2022; Lynch & Bliss, 1986; Penttonen et al., 1997; Spruston & Johnston, 1992; Wu et al., 2015). One key difference between CA and DG lies in their developmental patterns, while pyramidal cells are generated entirely before birth, granule cells reach their peak generation during the first postnatal week and extends into adulthood (Frotscher & Seress, 2006). Additionally, although the generation of interneurons in CA and DG subfields occurs almost simultaneously (Danglot et al., 2006); they have differential responses to novelty and carry distinct information to support spatial navigation (Hainmueller et al., 2024). Considering the aforementioned differences between CA and DG it was highly expected that these differences would translate into distinct proteome profiles.

The results of the enrichment analysis revealed distinct functional characteristics for the different subfields, further highlighting major differences in the DG. The terms enriched in this subfield were mainly related to RNA processing, and RNA binding, and indicated primarily nuclear localizations. RNA binding proteins (RBPs), mediate gene expression by affecting several processes, including splicing, cleavage, RNA stabilization, editing, and translation. These functions give them a significant ability to regulate cell function, and recently several studies have focused on their role in regulating neurodevelopment, and particularly, neurogenesis (Chan et al., 2022; Parra & Johnston, 2022), it is therefore likely that the distinct molecular profile of DG is supporting the unique ability that its cells have of adult neurogenesis.

Our observations on the specific proteins differentially expressed in the various subfields are highly consistent with results obtained using other techniques, such as immunohistochemistry. For instance, Homer3 is primarily expressed in CA3 (Iwano et al., 2012), calretinin is wellknown for its high expression in the DG (Brandt et al., 2003; Gurden et al., 1998; Liu et al., 1996; Mata et al., 2018; Walton et al., 2012), and Wfs1 is often used as a marker for CA1 neurons (Cid et al., 2021; Delpech et al., 2021; Dong et al., 2009). Similarly, proteins showing higher abundance in two subfields compared to the third one, are also consistent with other studies. This includes the increased expression of Grm2 in the DG and CA1 compared to CA3 (Hetzenauer et al., 2008). For Plxn-A1, we did not find other studies reporting differences in its expression across the different subfields. However, consistent with our results, the mRNA data provided by the Allen Brain Institute indicates a clearly enhanced expression in the CA1 and CA3 regions compared to the DG (Allen Mouse Brain Atlas, mouse.brainmap.org/experiment/show/69289721). Similarly, in our study, Ahcyl2 was found to have increased expression in the DG and CA3 compared to CA1. In this case, the mRNA data suggests increased expression in the CA2 and DG subfields (Allen Mouse Brain Atlas, mouse.brain-map.org/experiment/show/70205340). Given that our laser ablation was not precise enough to target CA3 exclusively, it is possible that we included parts of CA2, and the enhanced expression in CA2 is driving the observed results.

3.4.2 *Arc/Arg3.1* regulation of the hippocampal protein profiles

Regarding the molecular profile of *Arc/Arg3.1*KO in the different hippocampal subfields, we found no major differences compared to WT controls. In this study, we focused on brains under baseline conditions to reveal potential differences in the natural hippocampal circuitry mediating baseline synaptic transmission. *Arc/Arg3.1* is an immediate early gene with relatively low baseline expression in the adult hippocampus. Consistent with this, we did not detect

Arc/Arg3.1 protein in our samples. Similarly, other immediate early genes like c-Fos, c-Jun, and Egr1 were not detected. However, upon inducing strong activity through seizures, we detected Arc/Arg3.1 in hippocampal samples, confirming that the failure to detect these proteins initially was due to low baseline expression rather than issues with the detection method. This aligns with the study by Leung et al. (2022) which used a pharmacological model of LTP to induce synaptic activity. They evaluated the expression profile of cortical neurons with RNA sequencing analysis 8 h after LTP induction. Their results revealed regulation of around 1900 by Arc/Arg3.1, including many transcription factors and immediate early genes implicated in memory formation and plasticity. Given the activity-dependent nature of Arc/Arg3.1, we anticipate observing more pronounced differences in the hippocampal proteomic profiles of WT and KO animals under high activity conditions.

Our results demonstrated that under baseline conditions only a small fraction of the total proteins detected (~5 %) are differentially expressed in the hippocampal subfields of Arc/Arg3.1 KO mice. In line with the clear differences observed in the molecular profile of the different subfields we found that most of the proteins regulated by Arc/Arg.31 were unique to every subfield, underscoring that although Arc/Arg3.1 regulates some proteins in a global hippocampal way, most of its effects are specific to the different subfields.

The functional annotation analysis revealed several biological processes potentially regulated by Arc/Arg3.1. The common GO terms found across the different subfields, suggest that most Arc/Arg3.1 regulated proteins shared a cytoplasmic localization and had molecular functions associated with "protein binding". Surprisingly, the terms related to synapses were not found in the analysis, it is worth noting, however, that the most commonly co-occurring term to "protein binding" is "glutamatergic synapse", suggesting a potential although indirect association.

Regarding the subfield-specific terms, consistent with the clear difference between DG and the hippocampus proper, Arc/Arg3.1 regulated proteins in the DG showed the most varied functions. The GO terms suggested associations with terms as varied as metabolic processes, immune responses, and enzymatic activity, and indicated a potential regulation of Arc/Arg3.1 on mitochondrial proteins. These results suggest that the role of Arc/Arg3.1 in the DG might extend beyond the synaptic function, further studies are needed to fully characterize how Arc/Arg3.1 might regulate these processes.

On the other hand, the proteins regulated by Arc/Arg3.1 in the CA subfields seem to be generally associated with synaptic function. Surprisingly, except for PSD-95, we did not find

alterations in many of the synaptic proteins often associated with Arc/Arg3.1 function. This could be linked to the fact that most of Arc/Arg3.1's effects have been evaluated under conditions of robust synaptic activity. It is therefore likely that stronger changes in the molecular profiles of Arc/Arg3.1 KO mice would only be detectable under conditions of high activity.

Importantly, the term "protein transport" was the most frequently observed. *Arc/Arg3.1* interacts with the endocytic machinery to regulate the endocytosis of AMPA receptors and interacts with actin-binding proteins to regulate structural changes in dendritic spines (Chowdhury et al., 2006; Newpher et al., 2018).

In the current study, we did not find differences in many of those proteins, including cofilin, endophilin, dynamin-2, or Drebrin1. However, the *Arc/Arg3.1*-regulated proteins in CA1 and CA3 encompassed in the term "protein transport" included many other proteins associated with endocytic trafficking, such as Rab11 family-interacting protein Rab11fip5 (Machesky, 2019), protein tyrosine phosphatase non-receptor type 23 Ptnp23 (Budzinska et al., 2020), Ras-related protein Rab-23 (Guo et al., 2006), Ras-related protein Rab9 (Kucera et al., 2016), Vamp7 (Advani et al., 1999), and ADP-ribosylation factor ARF1 (Kumari & Mayor, 2008).

Additionally, we identified Arc/Arg3.1 regulated proteins involved in actin polymerization like Formin2 (Stortz et al., 2019), and the ADP-Ribosylation Factor 6 (Boshans et al., 2000), as well as proteins linking endocytic membrane traffic with actin assembly machinery, such as Intersectin-1 Isn1 (Sengar et al., 1999). Collectively, our current findings on the proteins modulated by Arc/Arg3.1 in the hippocampus proper, align well with the functions in trafficking and actin remodeling attributed to Arc/Arg3.1 in the literature, however the specific proteins involved in these functions seem to differ from the ones reported previously. Further understanding of the potential interaction of Arc/Arg3.1 with these proteins would help elucidate the molecular mechanisms allowing its regulation of protein transport.

Overall, our findings demonstrate that the NIRL ablation method successfully allows for the dissection of very specific brain regions for subsequent proteomic analysis. We also confirmed that the functional differences reported in the different hippocampal subfields are accompanied by clearly distinct molecular profiles. In agreement with these differences, we report that the effects of Arc/Arg3.1 deletion on the molecular profile of the hippocampus are specific to each subfield, with marked differences between the DG and the hippocampus proper. These findings are in agreement with previously observed differences in the maintenance of Arc/Arg3.1 mRNA levels upon behavioral induction, with the period extending for several hours in the DG while

decaying within a couple of hours in the hippocampus proper (French et al., 2001; Ramirez-Amaya et al., 2013; reviewed in Zhang & Bramham, 2021). The distinct proteins regulated by Arc/Arg3.1 in the two subfields could mediate its mRNA maintenance differentially in the two subfields. Another possibility is that the differences in the molecular regulation of Arc/Arg3.1 between CA and DG subfields are linked to the role of Arc/Arg3.1 in neurogenesis. Such a role was proposed by Kuipers and colleagues, who suggested that spontaneous Arc/Arg3.1 expression in a subpopulation of newly born cells in the DG could increase the likelihood of these cells surviving and incorporating into the previously established hippocampal circuit (Kuipers et al., 2009).

All things considered, the current study identifies exciting new candidate molecules that may modulate the function of *Arc/Arg3.1* in the hippocampus. However, some of these candidates, like them6, remain poorly understood. Further research is necessary to elucidate these interactions and their significance.

4 Part III. Selective Impairment of Excitatory Synapses in the Young Hippocampus Following Early Arc/Arg3.1 Deletion

4.1 Introduction

The first postnatal month of mice is a critical period marked by a confluence of dramatic changes across behavioral, structural, and molecular levels in the hippocampus. From a behavioral standpoint, this period witnesses the acquisition of crucial milestones. Pups born blind, deaf, and with limited mobility, experience a rapid development of somatosensory capabilities within the first postnatal weeks. This short window encompasses the emergence of quadrupedal walking, hearing onset, eye-opening, olfactory discrimination, and the initiation of spontaneous exploration (Stanton, 2000; Tan et al., 2017).

Concurrently, the hippocampus undergoes significant structural remodeling. This includes a rapid expansion and branching of dendrites and axons, accompanied by changes in finer structures like spines. At the molecular level, this period is characterized by dynamic shifts in the composition of AMPA and NMDA receptors, alongside alterations in the expression of kinases and phosphatases (Lohmann & Kessels, 2014). These molecular changes translate into functional maturation, including the refinement of passive and active electrophysiological properties like intrinsic excitability and action potential waveforms (Dougherty, 2020; Sanchez-Aguilera et al., 2020). Ultimately, these combined phenomena have a profound impact on synaptic transmission and plasticity, shaping the establishment and maturation of cognitive abilities and hippocampal networks.

The high spontaneous expression of *Arc/Arg3.1* during the first postnatal month partially overlaps with a period of strong dendritic elongation, and branching and synapse formation. This overlap suggests a potential role for *Arc/Arg3.1* in regulating dendritic development. This hypothesis is further supported by the established function of BDNF, a known upstream regulator of *Arc/Arg3.1*. BDNF deficiency impairs dendritic arborization, while its augmentation leads to excessive branching (Colucci-D'Amato et al., 2020; Kim & Cho, 2014).

Arc/Arg3.1 expression during the first postnatal month mediates a critical period for spatial learning. Its removal before P21 results in persistent deficits in spatial navigation and learning, alongside alterations in hippocampal oscillatory activity (Gao et al., 2018). Furthermore, the findings described in part I, demonstrated that these alterations are accompanied by changes in

the micro-architecture of excitatory as well as inhibitory connectivity. While the aforementioned studies explored adult cognition and brain function, the current work focuses on the structural and functional changes taking place during early postnatal development.

To investigate the role of *Arc/Arg3.1* in the maturation of the hippocampal circuit during the first postnatal month, we employed the three previously introduced *Arc/Arg3.1* deficient mouse lines: germline knockout (KO), early conditional knockout (early-cKO), and late conditional knockout (late-cKO). We specifically focused on postnatal days 14 (P14) and 28 (P28) as developmental time points of interest since dramatic changes in activity-dependent synaptic plasticity occur after P14, while synaptic circuitry is mainly mature by P28.

4.2 Materials and methods

4.2.1 Mice.

Naïve male and female animals, 14 ± 1 and 28 ± 1 days of age, were housed on a 12 h light/dark cycle (6:00-18:00 light period) under standard conditions ($23\pm1^{\circ}$ C, 40-50% humidity; food and water *ad libitum*). Pups were weaned at postnatal day 21. All experiments were approved by the city of Hamburg's local authorities and were performed following German and European law for the protection of experimental animals.

4.2.2 Generation of constitutive and conditional *Arc/Arg3.1* KO mice.

Three lines of *Arc/Arg3.1* deficient mice were generated in which the gene deletion took place at different time points in development as previously described (Gao et al., 2018). Briefly, constitutive *Arc/Arg3.1* KO mice were generated as described in Plath et al. (2006) together with floxed *Arc/Arg3.1* mutants. To achieve this, vectors were generated of the *Arc/Arg3.1* gene in which three LoxP sites were inserted. The vectors were electroporated into embryonic stem cells and subjected to a transient expression of Cre recombinase. The recombination yielded clones in which the open reading frame (ORF) of the gene was deleted (KO) or flanked by two LoxP sites (*Arc/Arg3.1* ^{fl/fl}). Clones were injected into C57Bl/6J blastocytes and chimeras were bred in the C57Bl/6J background to finally generate the conventional KO and floxed lines. *Arc/Arg3.1* ^{+/fl} mice were bred with two different Cre recombinase transgenic mice to produce conditional KO with *Arc/Arg3.1* ablated at two different time points (*Arc/Arg3.1* fl/fl, Cre+) and WT control littermates (*Arc/Arg3.1* ^{+/fl}, Cre+). The early conditional KO (early-cKO) mice were generated through breeding with Tg(CaMKIIα-cre)1Gsc mice (Casanova et al., 2001) and *Arc/Arg3.1* ablation took place after P7 but before P14. The late conditional KO (late-cKO)

mice were generated by breeding to Tg(CaMKIIα-cre)T29-1Stl (Tsien et al., 1996) and *Arc/Arg3.1* ablation occurred between P21 and P36.

4.2.3 Patch-clamp recordings

Mice were deeply anesthetized with isoflurane and quickly decapitated. Brains were immediately removed and placed in an ice-cold carbogenated (95% O₂/5% CO₂) dissection artificial cerebrospinal fluid (dACSF) containing (mM): 2.6 KCl, 26 NaHCO₃, 1.23 NaH₂PO₄, 7 MgSO₄, 1 CaCl₂, 212.7 sucrose, and 10 D-glucose. Acute 350 μm horizontal hippocampal slices were prepared with a vibratome (HM 650 V) in dACSF. Slices were placed in warmed $(30 \pm 2^{\circ}\text{C})$ dACSF for 30 min followed by recovery for 30 min at $30 \pm 2^{\circ}\text{C}$ in a carbogenated recording ACSF (rACSF) containing (mM): 119 NaCl, 2.5 KCl, 26 NaHCO₃, 1.25 NaH₂PO₄, 1.3 MgSO₄, 2.5 CaCl₂, and 10 D-glucose. Slices were then kept in the rACSF at room temperature until used for whole-cell recordings. Slices were submerged and constantly perfused (4.2 mL/min) with rACSF at 37 ±2°C in a glass bottom recording chamber. A nylon grid was placed over the slices to keep them in place. The slices encompassing the dorsal hippocampus (with coordinates equivalent to adult bregma -2.16 to -2.8) were visualized with an Olympus BX51W1 upright microscope (Olympus, Tokyo, Japan). To locate the Ca1 pyramidal layer, a 4X objective was employed, while a 63X objective was utilized to identify and select cells for patching. For EPSCs and membrane properties: Pipettes (5-7M Ω) were pulled from thin-walled Borosilicate glass and filled with a pipette solution containing (in mM): 130 potassium gluconate, 4 KCl, 10 Hepes, 10 phosphocreatine-Na, 4 ATP-Mg, and 0.3 guanosine triphosphate, osmolarity was adjusted to 270-290 mOsm. Biocytin (2.5 mg/mL, Sigma, Munich, Germany) was added for post hoc morphological visualization. The pipette solution was thoroughly mixed after the addition of biocytin and then filtered. Recordings were performed with a Multiclamp 700B amplifier (Molecular Devices, California, USA), sampled at 10 kHz, and filtered at 3 kHz with a D/A converter (Digidata 1440, Molecular Devices). Recordings were performed either at voltage clamp modus with a gain of 50 or at current clamp mode with a gain of 1-10.

Input resistance was determined as the slope of the voltage-current plot, constructed from the steady-state voltage responses to 500 ms current pulses ranging from -50 to 40 pA in 10 pA increments (only the linear region of these plots was used). To elicit action potentials, current injections of increasing intensities (40 pA increments) were applied for 500 ms. For the action potential waveform, the amplitude and half-width of the first elicited action potential were measured. The number of action potentials fired was recorded to create frequency/current (FI)

curves. Data collected was subsequently analyzed offline using the pCLAMP 10.7 software suit (Molecular Devices).

Spontaneous excitatory (sEPSCs) were measured in voltage clamp mode at -70 mV. A square pulse was applied every 20 s to monitor the series resistance (Rs). Recordings with Rs exceeding $30 \text{ M}\Omega$ or with fluctuations >30% over a period of 1 hr, were excluded from the analysis. Data were collected and analyzed offline using MiniAnalysis software (Synaptosoft). Raw traces were first lowpass filtered at 1 KHz using a Bessel filter in the eighth order. sEPSCs were detected using a threshold of 5 pA. Traces of 2 s at a time, were analyzed semi-automatically, and detected sEPSCs were manually curated by the experimenter, correcting for peak detection and discarding artifacts to improve the accuracy of the analysis. Averages were calculated per cell for the parameters of peak amplitude, decay τ , interevent interval, and, time to peak. For IPSC: the same conditions were used for the evaluation of inhibitory transmission (Fig. 4.2.10-11) with the following changes: The intrapipette solution contained in mM: 107 Cs-gluconate (CsOH + Gluconic acid), 10 tetraethylammonium chloride (TEA), 10 HEPES, 5 QX-314, 4 Mg-ATP, 2.5 CsCl, 0.3 Na₃-GTP and 0.2 EGTA (pH 7.25, 276 mOsm). The voltage was held at 0 mV to increase the chloride electrochemical drive and consequently the synaptic currents. The glutamatergic antagonists CNQX (20μM) and APV (50μM) were applied in the perfusion chamber to isolate inhibitory transmission. Detection of sIPSCs was done using the "template search" function in ClampFit. Two types of sIPSCs with distinct kinetics were observed (with mean half-widths of 3,95 and 13,66 ms, respectively). Two templates were created based on traces from 5 WT and 5 KO cells. The final analysis showed that the slow sIPSCs represented around 11% of the total events. Events of the two types were included in the final analysis. The GABAA receptor antagonist Gabazine (5 µM) was applied at the end of the recordings to investigate the GABA_A-R component.

4.2.4 Neuron reconstructions

Following the recordings, patch pipettes were retracted carefully and the slices were transferred to 4 % paraformaldehyde for fixation. Biocytin-filled neurons were recovered using the 3,3'-diaminobenzidine (DAB) tetra hydrochloride avidin-biotin-peroxidase method. Briefly, free-floating fixed hippocampal sections were rinsed in 0.1 M PBS (4 x 10 min), then blocked for the endogenous peroxidase with 1 % H₂O₂ for 10 min. The sections were then rinsed again in PBS (4 x 10 min), permeabilized with 1 % triton/PBS for 90 min, and incubated in an avidin-biotin coupled horse-radish peroxidase (ABC Elite kit, Vector) in a concentration of 1:200 diluted in 0.5 % triton/PBS for 2 h at room temperature. After incubation, the sections were

rinsed in PBS again (3 x 10 min, 1 x 1 h), sections were then exposed to the DAB solution for 10 min, followed by another rinse in PBS (3 X 10 min).

DAB-stained cells were morphologically reconstructed in three dimensions using the Neurolucida 7.50.2 system (MicroBrightfield, Colchester, VT, USA). Contours of the hippocampal tissue (alveus, lower border of CA1 pyramidal cell layer, and hippocampal fissure) were traced with 10x magnification (0.3 NA). Next, the whole neuron was reconstructed with a 60x oil objective (1.25 NA). Poorly stained cells as well as clearly cut cells were not considered for reconstruction. In some cases, only the apical dendrite was well-stained and reconstructed. Reconstructions were analyzed using the software Neurolucida Explorer 4.50.4. Sholl analysis was used to explore dendritic branching structures as a function of the distance from the soma, with circles of increasing radius (in 10 µm steps) drawn around the soma. The number of intersections crossing each circle and their length were analyzed.

4.2.5 Fluorescent in situ hybridization: RNAscope

Mice (3-4 per group) were deeply anesthetized with urethane (1-1.5 mg/g body weight) and transcardially perfused with 25 ml 0.1 M PBS followed by 25 ml 4% PFA. The brains were then extracted and postfixed in 4 % PFA for 2 days. Cryoprotection was achieved by immersing the brains in a series of 10 %, 20 %, and 30 % sucrose/PSB for 2 days. Subsequently, the brains were embedded in Tissue-Tek OCT (Sakura, Finetek) quickly frozen, and then sliced into 20 µm thick coronal sections using a cryostat (Hyrax C60, Microm). The sections were selected at bregma coordinates -1.94 to -2.06. One section per condition was placed on Superfrost Plus slides (Thermo scientific), to control for possible slide effects. The RNAscope assay was performed using the manufacturer's instructions (ACD (RNAscope® Multiplex Fluorescent Reagent Kit v2 Assay).

For pretreatment, the slides were washed with PBS and baked at 60 °C in the HybEZTM II oven for 30 minutes. For post-fixation, the sections were incubated in cold PFA on ice. After repeated washing with PBS, the sections were dehydrated in several steps with increasing concentrations (50%, 70%, 100%) of ethanol solution at room temperature. To block endogenous peroxidase activity, hydrogen peroxide (H₂O₂) was applied to the dried slides for 10 minutes at room temperature. After fully removing the H₂O₂ and washing the slides, they were incubated for 5 minutes in a target retrieval buffer, in a 99 °C water bath. Next, the slides were washed with PBS and incubated in 100% ethanol. Before continuing, the slides were left to dry at room temperature, and a hydrophobic barrier was created around the sections on the slide using the ImmEdgeTM hydrophobic barrier pen.

For protease treatment, drops of protease III were applied directly on the sections, which were then placed on the oven tray and baked for 30 minutes at 40 °C. Afterward, protease III was removed, and the slides were washed with PBS.

The sections were then incubated with 200 μ l of the mRNA conjugated hybridization probe for Arc/Arg3.1 (Cat. 838921-C1, custom-designed, 1× solution). For the negative control, the same amount of probe dilution solution was applied to the control slide instead of the probe solution. The slides were baked for 2 hours at 40 °C in the oven. The slides were washed with the washing buffer provided in the kit and stored in 5x saline sodium citrate buffer at room temperature in darkness overnight.

For amplification, the slides were placed on the oven tray, covered with drops of amplifier solution (AMP1, provided in the kit) baked for 30 minutes at 40 °C in the oven, and then washed with PBS. For labeling, the probe was combined with a horse-radish peroxidase (HRP) and a corresponding fluorescence dye. The sections were covered with the first HRP and baked at 40 °C for 15 minutes. After washing, the sections were covered with 250 µl of Opal 570 dye and baked at 40 °C for 30 minutes. The sections were washed again and covered with an HRP blocker to stop the binding of dyes to HRP for 15 minutes at 40 °C. After labeling the target mRNA, the slides were covered with DAPI solution and incubated for 15 min in the dark. Afterward, the DAPI solution was removed, and 200 µl of ProLong Gold was used to mount the slides.

The two hippocampi of every mouse section were imaged using the inverted microscope Axio Observer.Z1 / 7 (Zeiss) with a 20 X 0.8 NA air objective. Images of variable dimensions were captured with a voxel size of 0.173 x 0.173 μ m. The laser intensity and time exposure parameters were optimized using the negative control. The same image acquisition parameters were applied to all sections to ensure consistency. For analysis, a region of interest (ROI) of 1824 x 1248 pixels, with an actual area of 314.17 x 215.9 μ m centered around the somatic layer of CA1 was selected. The analysis of the selected ROIs was performed using the mean intensity measure in Fiji (Schindelin et al., 2012).

4.2.6 Immunofluorescence staining and confocal imaging

Male and female mice aged P14 and P28 were deeply anesthetized with urethane (1-1.5 mg/g body weight) and transcardially perfused with 25 ml 0.1 M PBS followed by 25 ml 4% PFA. The brains were then extracted and postfixed in 4% PFA for 2 days. Cryoprotection was achieved by immersing the brains in a series of 10 %, 20 %, and 30 % sucrose/PSB for 2 days.

Subsequently, the brains were embedded in Tissue-Tek OCT (Sakura, Finetek) quickly frozen, and then sliced into 20 µm thick coronal sections using a cryostat (Hyrax C60, Microm). An antigen retrieval step was performed by heating the sections for 60 minutes at 80°C in a citrate buffer at pH 6.0. To prepare the sections for immunostaining, the free-floating sections were first blocked with a solution consisting of 10% horse serum, 0.2% bovine serum albumin (BSA), and 0.3% Triton X in PBS for 1 hour. Following the blocking step, the sections were incubated with the primary antibody solution for 48 hours. The primary antibody solution contained 1% horse serum, 0.2% BSA, and 0.3% Triton X-100 in PBS. To analyze excitatory synaptic clusters antibodies against VGLUT1 and VGLUT2, as presynaptic markers, alongside the postsynaptic scaffolding protein PSD-95 were applied. The primary antibodies in this study were used as follows: rabbit anti-PSD-95 (1:500; Invitrogen, 51-6900), mouse anti-VGLUT1 (1:1000; Synaptic Systems, 135011), and, guinea pig anti-VGAT (1:500, Synaptic Systems, 135404). To analyze inhibitory synaptic clusters antibodies against the presynaptic marker VGAT and gephyrin and, the γ5 subunit of the GABA_A receptor, were applied. The primary antibodies in this study were used as follows: Mouse anti-gephyrin (1:300; Synaptic Systems, 147 011), rabbit anti-GABA γ5 (1:1000, Synaptic Systems, 224003), and guinea pig anti-VGAT (1:500; Synaptic Systems, 131004). Following primary antibody incubation, the sections were subjected to incubation with secondary antibodies conjugated with fluorophores at room temperature for 2 h. The secondary antibodies were used as follows: goat anti-mouse DyLight 633 (1:200; ThermoFisher, 35513), goat anti-rabbit AlexaFluor 555 (1:200; ThermoFisher, A-21428), and goat anti-guinea pig AlexaFluor 488 (1:200; ThermoFisher, A-11073). Subsequently, the sections were rinsed with PBS and mounted using ProLong Gold Antifade Mountant with DAPI (Invitrogen, P36931), and stored in the dark. The quantification of synaptic clusters was performed across the four strata of the hippocampal CA1 region, 4 animals per group were used. Three brain sections per mouse were selected at coordinates equivalent to bregma -1.94 to -2.06 in adult mice. Non-overlapping image stacks (6 per mouse) were obtained, using a 63X 1.4 NA oil-immersion objective and a 2.5 X digital zoom with the pinhole set to 1 AU. Image stacks consisting of five consecutive images were captured with dimensions of 1024 x 1024 pixels and an increment of 0.25 µm per step. This imaging setup resulted in an imaged region size of 73.81 x 73.81 x 1 µm, with a voxel size of 0.072 x 0.072 x 0.25 µm. The laser intensity, detector sensitivity, and line averaging parameters were optimized using sections stained with secondary antibodies only. The same image acquisition parameters were applied to all mice sections to ensure consistency. For analysis, the entire image was used as a ROI except for pictures of the pyramidal layer. In this case, a ROI of 1024 x 814 x 5 pixels

was selected to avoid the inclusion of small segments of strata *oriens* and *radiatum*. The analysis of the selected ROIs was performed using Imaris 9.3 (Bitplane) using the Spot function and the MATLAB R2017 (MathWorks) extension for Spot colocalization. Automatic spot detection was employed, using specific diameter thresholds for each protein marker. Spots with a diameter greater than 0.2 μm for PSD-95, VGLUT2, gephyrin, and GABAγ5, and greater than 0.3 μm for VGLUT1 and VGAT, were considered for further analysis. To assess colocalization, the largest center-to-center distance between either PSD-95 and VGLUT1/VGLUT2 or VGAT and gephyrin/GABAγ2 spots was set at 0.7 μm. This criterion ensured that only spots within close proximity were considered colocalized.

4.2.7 Spine analysis

For spine analysis we employed the Golgi staining technique, using the FD Rapid Golgi Staining Kit (FD Neurotechnologies, Columbia, MD, USA), as described by Du (2019). Briefly, four naïve early-cKO and four of their respective WT-control mice, age P28 were deeply anesthetized with isoflurane and quickly decapitated. The brain was rapidly dissected and rinsed with double-distilled water. Subsequently, the brains were submerged in an impregnation solution containing equal volumes of solutions A and B (provided in the kit) protected from light at room temperature for two weeks. The solution was replaced after 24 h. Next, the brains were transferred to solution C for three days, once again, the solution was replaced after the first 24 h. Next, the brains were frozen by slowly submerging them in isopentane at -70° C. After freezing, 100 µm thick coronal sections were cut using a cryostat (Hyrax C60, Microm). Sections were mounted on gelatin coated-slides and, allowed to dry protected from light for subsequent staining. The staining process began with an initial wash in double-distilled water, followed by immersion of the slides in a solution consisting of one-part solution D, one-part solution E, and two-parts double-distilled water for 10 minutes. Next, the slides were rinsed with double-distilled water and then underwent a series of dehydration steps (4 minutes each) in 50 %, 75 %, 95 %, and 100% ethanol, followed by clearing in xylene (3 x 4 minutes). Finally, the slides were covered with a quick-hardening mounting medium (Eukitt®) and stored at room temperature, protected from light.

CA1 pyramidal neurons from sections with bregma AP coordinates -1.82 to -2.30 were selected for analysis. Imaging was performed using the Confocal Reflection Super-Resolution technique, described by Sivaguru et al. (2019). Briefly, apical oblique and basal dendrites were selected, focusing on secondary or tertiary branches. A minimum of 17 dendritic segments per mouse were imaged and processed. The length of the dendritic branches ranged from 10 to 60

 μ m, with a preference for dendrites extending parallel to the surface to ensure optimal imaging. Images were obtained, using a 63X 1.4 NA oil-immersion objective and a 3X digital zoom with the pinhole set to 0.21 AU, allowing a resolution under 220 μ m (Sivaguru et al., 2019). Image stacks were captured with pixel dimensions of 30.05 x 30.05 nm at 0.16 μ m increments.

Images were analyzed semi-automatically using Imaris 9.3 (Bitplane). Pre-processing included baseline subtraction and the application of a Gaussian filter (0.180 μ m width) that allowed the software to uniformly recognize the signal instead of single Golgi granules (0.150 μ m). The "filament tracer" module was used to manually reconstruct the dendritic segments, and spines were detected using the automatic spine detection tool. Manual curation of the detected spines was done by the experimenter, assuring that only clear spines were included in the analysis. The spine density was calculated by dividing the total spine number by the dendritic branch length.

4.2.8 Experimental design and statistical analyses

Data were analyzed with Prism 8 (GraphPad Software Inc.). No statistical method was used to predetermine sample size, but our sample sizes are comparable to those reported in previous studies. Statistical tests used were as follows: Mann–Whitney U test, Kolmogorov–Smirnov test, and mixed-design analysis of variance with Sidak's post hoc test. The type of test is indicated in the main text. A p-value below 0.05 was considered significant. All graphs were generated with Prism 8, Igor Pro 6.3 (WaveMetrics), Adobe Illustrator CS5.5, and MATLAB R2021a/R2022b (MathWorks). Experimenters were blind to the genotype until the conclusion of the experiments and analysis. Values presented in the figures are mean \pm SEM or median with 25th and 75th percentile, as indicated.

4.3 Results

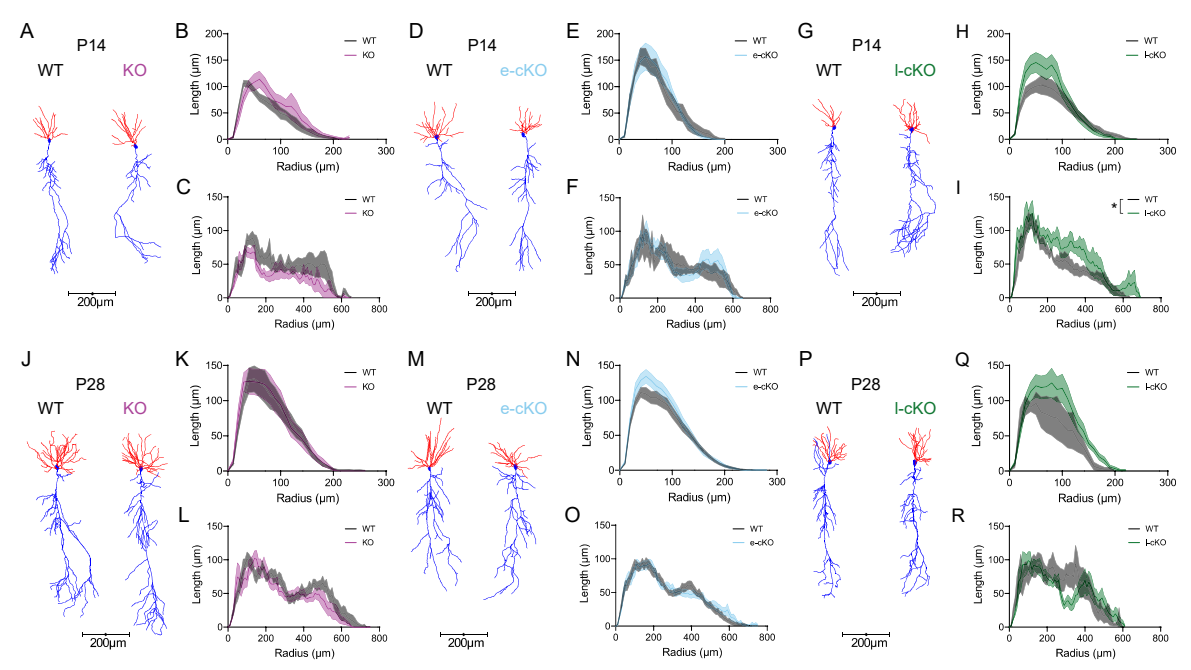


Figure 4.1. Unaltered dendritic morphology in *Arc/Arg3.1* **KO mice**. The top panel displays findings at postnatal day 14 (A-I), while the bottom panel shows results at postnatal day 28 (J-R). Reconstructions of CA1 pyramidal neurons are presented, with basal dendrites drawn in red and apical dendrites in blue (A, D, G, J, M, and P). Quantification of dendritic length using Sholl analysis for basal (B, E, H, K, N, and Q) and apical dendrites (C, F, I, L, O, and R) of the different KO lines compared to their respective WT-controls. The solid lines indicate average values, with shadows indicating ±SEM. (Mixed-effects ANOVA, genotype effect marked *p<0.05). The reconstructions in this figure were performed by Christina Stanke and Tobias Grellrich and were partially presented in their Master's and Bachelor's theses, respectively.

4.3.1 Arc/Arg3.1 deletion has minimal impact on the dendritic morphology of hippocampal CA1 neurons in early postnatal development

To analyze dendritic trees, biocytin-filled CA1 pyramidal cells were reconstructed and their dendritic branch distribution and length relative to the cell body were evaluated by Sholl analysis. The results showed no differences in the length of the basal dendrites at P14 in any of the KO lines compared to their WT-controls (Germline KO: **Figure 4.1A-B**, $F_{(1,15)}$ =1.429, p=0.2505; early-cKO: **Figure 4.1D-E**, $F_{(1,15)}$ =0.0033, p=0.9549; late-cKO: **Figure 4.1G-H**, $F_{(1,22)}$ =1.052, p=0.3163). Consistent with the lack of change in basal dendrites, analysis of apical dendrites in germline KO and early-cKO lines revealed no significant differences compared to WT controls at P14. However, late-cKO mice displayed a distinct pattern. Here, apical dendrites were significantly longer than WT specifically between a radius of 160 and 440 μ m (Germline KO: **Figure 4.1A and C**, $F_{(1,15)}$ =4.439, p=0.0524; early-cKO: **Figure 4.1D and F**, $F_{(1,17)}$ =0.0064, p=0.9372; late-cKO: **Figure 4.1G and I**, $F_{(1,23)}$ =5.303, p=0.0307).

Consistent with the findings at P14, analysis of both basal and apical dendrites in all three Arc/Arg3.1 knockout lines revealed no significant differences compared to their wild-type controls at P28. (Basal: Germline KO: **Figure 4.1J-K**, $F_{(1,25)}$ =0.0059, p=0.9393; early-cKO: **Figure 4.1M-N**, $F_{(1,68)}$ =1.493, p=0.226; late-cKO: **Figure 4.1P-Q**, $F_{(1,13)}$ =1.688, p=0.2164; Apical: Germline KO: **Figure 4.1J-L**, $F_{(1,27)}$ =1.747, p=0.1973; early-cKO: **Figure 4.1M-O**, $F_{(1,68)}$ =0.051, p=0.8221; late-cKO: **Figure 4.1P-R**, $F_{(1,15)}$ =0.6570, p=0.4303). Similar to the analysis of dendritic length, Sholl analysis of the number of intersections yielded comparable results (Supplementary Table 4.1). Collectively, these findings suggest that Arc/Arg3.1 deletion before postnatal day 21 (P21) exerts minimal influence on dendritic morphology.

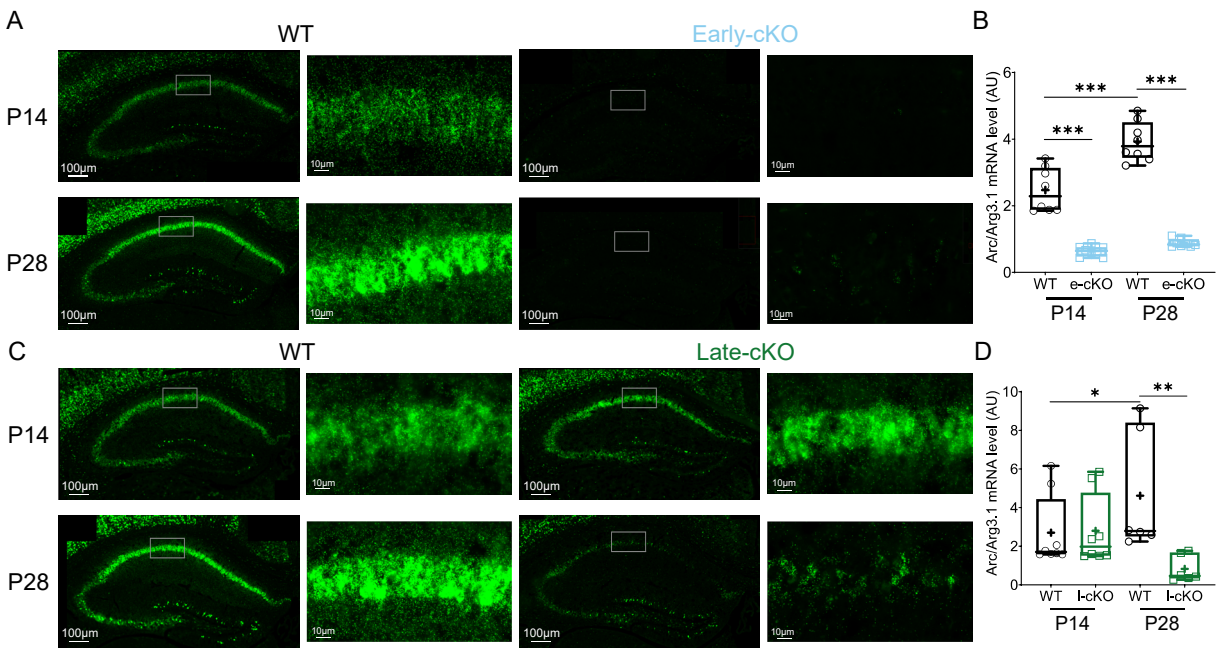


Figure 4.2. Deletion timeline of conditional Arc/Arg3.1 KO mice. A, C. Representative images illustrating Arc/Arg3.1 mRNA level in WT controls and early-cKO (A) and late-cKO (C) mice. Insets depict magnification in the CA1 region. B, D. Box plots show the quantification of mRNA level CA1 for early (B) and late (D) cKO lines. Box plots show the median \pm interquartile range, + represents the mean, and each point represents the mean value from one cell. Statistical analysis using Mann-Whitney U test revealed significant differences (*p<0.05, **p<0.01, ***p<0.01).

4.3.2 Timeline deletion in conditional Arc/Arg3.1 KO mice

Interestingly, late-cKO mice, where Arc/Arg3.1 deletion begins after P21, displayed unexpectedly longer apical dendrites at P14 but not at P28, and no changes in basal dendrites at any time point. We believe this effect is unlikely to result from Arc/Arg3.1 deletion itself, as the other KO lines did not show it, nor can it be caused by the Cre transgene, as it is present in both late-cKO and their WT-control littermates.

A possible explanation for the effects observed in the late-cKO line at P14 is that *Arc/Arg3.1* deletion might take place earlier than P21. Our previous study used radioactive *in situ* hybridization (ISH) followed by a semi-quantitative analysis to track the timeline of *Arc/Arg3.1*

deletion in the cKO mice (Castro Gómez, 2016; Gao et al., 2018). It is conceivable that some differences in mRNA transcripts at P14 had been overlooked due to the limited resolution of the technique. Therefore, we set out to evaluate the timing of the deletion using RNAscope, a very sensitive and specific assay for fluorescent ISH that allows visualization of single molecules while preserving tissue morphology (Wang et al., 2012).

We measured mRNA levels in the conditional *Arc/Arg3.1* KO mice and their respective WT-controls at the developmental times used in this study, P14 and P28. Our results confirmed the natural upregulation in the WT-controls by showing significant increases from P14 to P28 in both, the early and late-cKO lines (**Figure 4.2B**, early WT-control: P14 vs P28, U=2, p<0.001, P14: n=8, P28: n=8; **Figure 4.2D**, late WT-control: P14 vs P28, U=8, p=0.0426, P14: n=8, P28: n=6). Moreover, we also confirmed an effective *Arc/Arg3.1* deletion in the early-cKO by P14 that remains at P28 (**Figure 4.2B** P14: U=0, p<0.001, WT: n=8, KO: n=8; P28: U=0, p<0.001, WT: n=8, KO: n=8). Most importantly, we confirmed the delayed start of the deletion in the late-cKO line, as we observed no differences between WT and KO mice at P14 (**Figure 4.2B** U=28, p=0.7209, WT: n=8, KO: n=8). By P28, the deletion had already started, but it was not completed as some *Arc/Arg3.1* transcripts were still visible (**Figure 4.2D** U=0, p=0.0022, WT: n=6, KO: n=6). These results, rule out the possibility of an earlier deletion in the late-cKO line as an explanation for the longer apical dendrites observed at P14. Alternatively, this effect may reflect a subtle bias in the sampling of the CA1 neurons in this specific group. Further investigation using larger sample sizes might be necessary to clarify this observation.

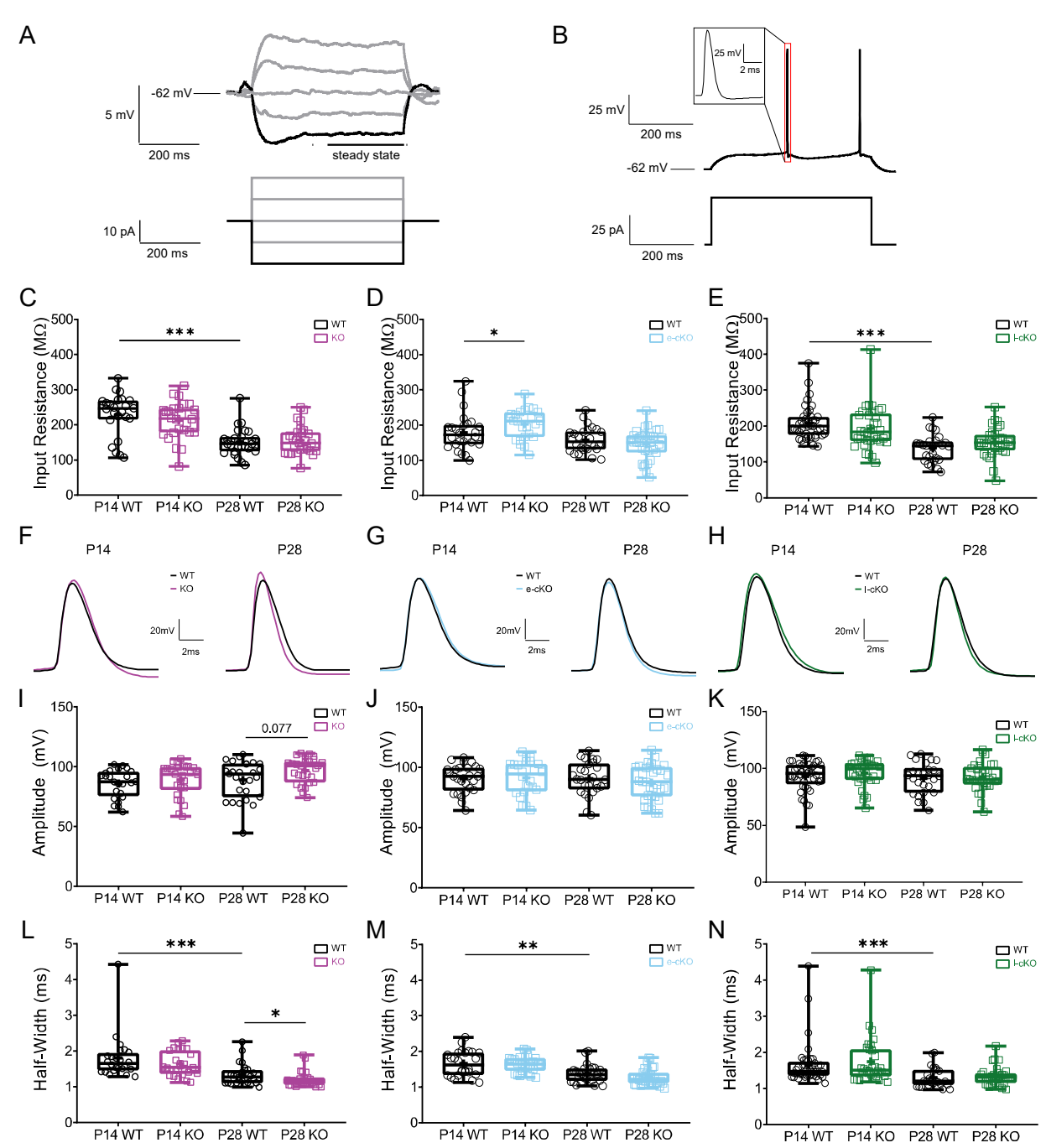


Figure 4.3. Electrical properties of pyramidal CA1 neurons in *Arc/Arg3.1* **KO mice.** Panels A-B, Scheme of the protocol followed: Input resistance was measured in current-clamp mode by quantifying the change in voltage at steady-state in response to small current pulses (**A**). Action potentials (AP) were elicited by threshold depolarizing pulses of 500 ms duration (**B**). The waveform of the first AP fired was analyzed (inset). Panels **C-E**, present box plots showing the input resistance of WT and the different KO lines. Panels **F-H** display exemplary traces of the first action potential recorded from WT (black), KO (magenta), early-cKO (blue), and late-cKO (green) cells. Quantification of action potential amplitude and half-width are presented in panels **I-K** and **L-N**, respectively. Box plots show the median ± interquartile range, + represents the mean, and each point represents the mean value from one cell. Statistical analysis using *Mann-Whitney* U test revealed significant differences (*p<0.05, **p<0.01, ***p<0.01).

4.3.3 Arc/Arg3.1 deletion has minimal impact on input resistance but shapes action potential waveform

Neurons utilize electrical signals for communication. They possess both passive and active properties. Passive properties, such as input resistance, enable neurons to conduct electrical

impulses without the involvement of voltage-gated ion channels. In contrast, active properties rely on voltage-gated ion channels to maintain membrane potential and generate action potentials. This combination of passive and active properties is essential for neurons to effectively receive, process, and transmit information. Similar to dendritic morphology, the electrical properties of neurons significantly impact information processing, synaptic integration, and ultimately, network function. These properties are plastic, adapting to synaptic inputs, neuronal activity, and the surrounding environment (Turrigiano & Nelson, 2004). Importantly, many synaptic receptors are themselves ionic channels, directly influencing the flow of ions across the membrane and thus electrical properties. Since Arc/Arg3.1 is known to regulate the trafficking of these ionic channels, we hypothesized a potential role for Arc/Arg3.1 in the maturation of CA1 cell electrical properties. We investigated this, using patch-clamp whole-cell recordings with native (without ion channel blockers) pipette solution and aCSF. We injected a series of incremental current pulses to measure input resistance and action potential waveforms in wild-type and Arc/Arg3.1 KO mice at postnatal days 14 and 28.

To understand the typical development of these parameters, we compared them in WT controls from each KO line at P14 and P28. Our results revealed a significant decrease in input resistance across this period for both the conventional WT group and the WT controls from the late-cKO line (**Figure 4.3A**, Germline WT: P14 vs P28, U=118, p<0.001, P14: n=24, P28: n=27; **Figure 4.3C**, late WT-control: P14 vs P28, U=113, p<0.001, P14: n=41, P28: n=26). Interestingly, the WT controls from the Early-cKO line displayed noticeably lower input resistance specifically at P14, with no further reduction at P28 (**Figure 4.3B**, Early WT-control: P14 vs P28, U=249, p<0.1057, P14: n=26, P28: n=26). This suggests an accelerated maturation of input resistance in these WT controls compared to the other lines.

When evaluating the effects of *Arc/Arg3.1* deletion on input resistance, we found no significant differences in the germline or late-cKO cells compared to their WT controls at P14 or P28 (**Figure 4.3A**, Germline P14: U=238, p=0.1547, WT: n=24, KO: n=26; Germline P28: U=352, p=0.8369, WT: n=27, KO: n=27; **Figure 4.3C**, Late-cKO P14: U=548, p=0.1649, WT: n=41, KO: n=33; Late-cKO P28: U=308, p=0.0655, WT: n=26, KO: n=33). In contrast, the Early-cKO displayed significantly higher input resistance at P14, but no changes at P28 (**Figure 4.3B**, Early-cKO P14: U=200, p=0.0295, WT: n=26, KO: n=24; Early-cKO P28: U=363, p=0.4146, WT: n=26, KO: n=32). The lower input resistance observed in the WT controls of the Early-cKO line at P14, compared to other WT groups, is intriguing. However, the Early-cKO mice themselves displayed input resistance similar to the other lines at P14. This suggests that the

observed difference is likely due to an accelerated maturation of input resistance in the WT controls of this line, rather than an abnormally high resistance in the Early-cKO group.

Overall, input resistance was similar between KO/cKO and their WT-controls, indicating that *Arc/Arg3.1* does not significantly impact the maturation of cell excitability in CA1 neurons.

Regarding the maturation of the active properties taking place during the first postnatal month, several studies have described changes in action potential waveform, specifically, a reduction of its duration and an increase in its amplitude (Dougherty, 2020; Spigelman et al., 1992). Our evaluation of these parameters failed to show differences in the action potential amplitude between P14 and P28 for any of the KO lines (Figure 4.3G, Germline WT: P14 vs P28, U=257, p=0.2115, P14: n=24, P28: n=27; **Figure 4.3H**, early WT-control: P14 vs P28, U=3343, p=0.9494, P14: n=26, P28: n=26; **Figure 4.3I**, late WT-control: P14 vs P28, U=482, p=0.5185, P14: n=41, P28: n=26). However, a significant reduction of its half-width was observed in WT controls of all KO lines during this period (Figure 4.3J, Germline WT: P14 vs P28, U=98, p<0.0001, P14: n=24, P28: n=27; Figure 4.3K, early WT-control: P14 vs P28, U=190, p=0.0062, P14: n=26, P28: n=26; **Figure 4.3K,** late WT-control: P14 vs P28, U=247, p=0.0002, P14: n=41, P28: n=26). While no significant differences in action potential amplitude were observed between KO lines and their WT controls at either P14 or P28, a slight trend towards larger amplitude emerged in the germline KO group specifically at P28 (Figure 4.3G, Germline P14: U=250, p=0.2347, WT: n=24, KO: n=26; Germline P28: U=262, p=0.0775, WT: n=27, KO: n=27; **Figure 4.3H**, Early-cKO P14: U=294, p=0.7362, WT: n=26, KO: n=24; Early-cKO P28: U=359, p=0.3799, WT: n=26, KO: n=32; Figure 4.3I Late-cKO P14: U=597, p=0.3925, WT: n=41, KO: n=31; Late-cKO P28: U=420, p=0.8975, :WT: n=26, KO: n=33). Interestingly, the germline KO group was the only one to exhibit a significant reduction in action potential half-width compared to its WT control. This effect was specific to P28, as no changes were observed at P14 or in any other KO lines (Figure 4.3J, Germline P14: U=271.5, p=0.4379, WT: n=24, KO: n=26; Germline P28: U=236, p=0.026, WT: n=27, KO: n=27; Figure 4.3K, Early-cKO P14: U=309, p=0.9616, WT: n=26, KO: n=24; Early-cKO P28: U=315, p=0.1166, WT: n=26, KO: n=32; **Figure 4.3L**, Late-cKO P14: U=582, p=0.549, WT: n=41, KO: n=31; Late-cKO P28: U=367, p=0.3504, :WT: n=26, KO: n=33). These findings suggest that Arc/Arg3.1 deletion might influence action potential waveform, but this effect appears delayed and limited to the germline deletion.

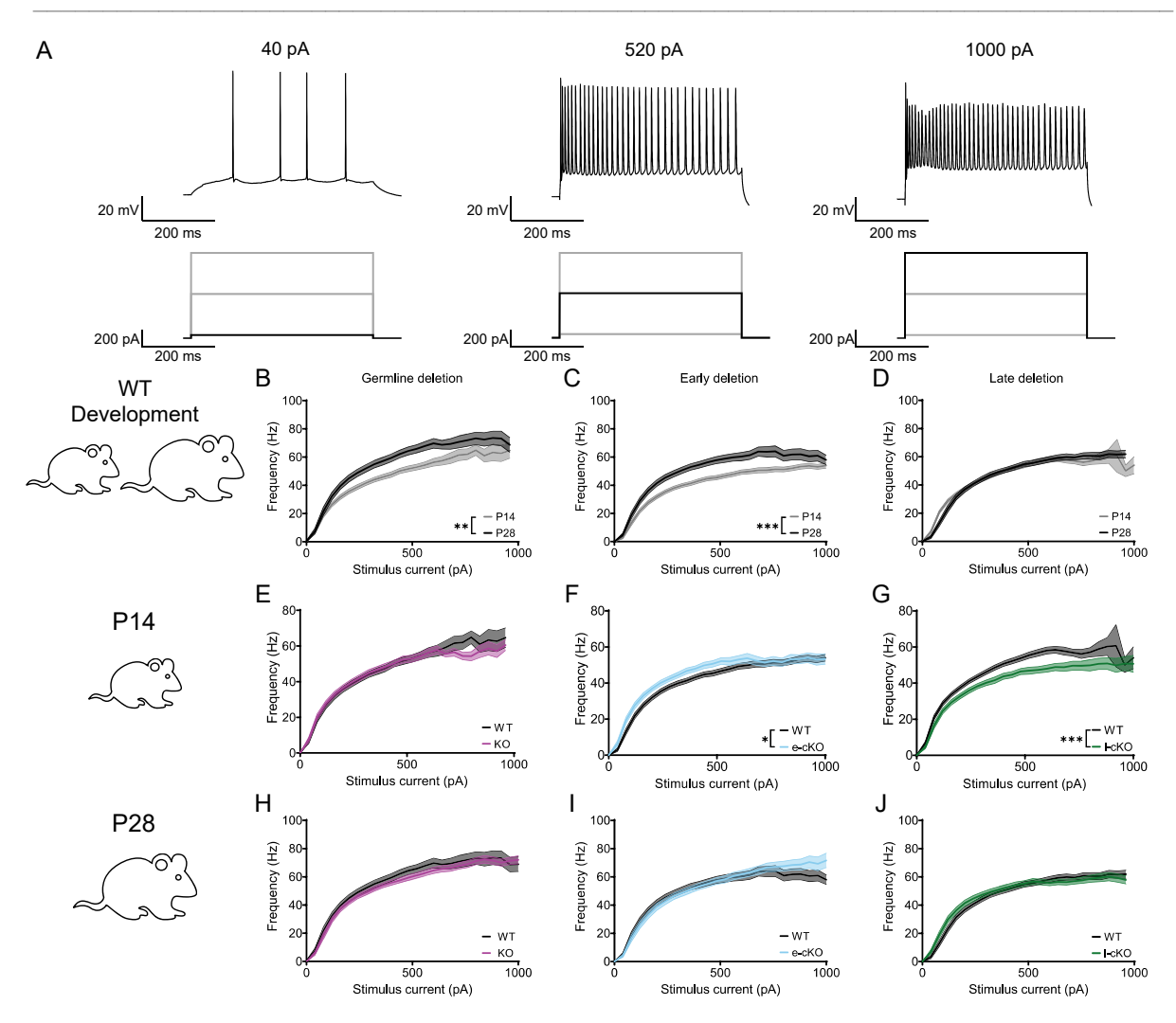


Figure 4.4. Frequency-current (F-I) curves of CA1 neurons of *Arc/Arg3.1* **KO mice. A.** Representative traces of cell firing frequency in response to increasing current injection steps. The left panel shows frequency upon threshold current injection (40pA), and the middle and right panels depict frequencies upon 520 and 1000 pA, respectively. **B–J.** Line plots show quantifications of CA1 cell firing frequency. Comparisons are made between WT controls of each line at two developmental stages; P14 and P28 (**B-D**). The middle and bottom panels (**E-G** and **H-J**) present comparisons between WT and KO cells at P14 and P28, respectively. Solid lines represent average values, with shadows indicating ±SEM. Asterisks in the legend denote the effects of the "Genotype" factor within a Mixed-effects ANOVA (*p<0.05, **p<0.01, ***p<0.001).

4.3.4 Transient Effects of Arc/Arg3.1 on Firing Frequencies During Early Development

In addition to membrane resistance and action potential waveform, the intrinsic excitability of a neuron is also reflected by its firing frequency. We assessed this by applying current injections of increasing intensities (40 pA increments) for 500 ms and measuring the number of action potentials fired (frequency-current curves) (**Figure 4.4A**). Prior research suggests that firing frequency undergoes significant changes during the first postnatal month, highlighting its critical role in maturation (Dougherty, 2020; Sanchez-Aguilera et al., 2020).

To understand the typical development of firing frequency, we compared WT controls from each KO line at P14 and P28 (**Figure 4.4B-D**). Our results revealed a significant increase in firing frequency across this period for the WT controls in both the germline and Early-cKO lines (Germline KO: **Figure 4.4B**, $F_{(1.49)}$ =11.13, p=0.0016; Early-cKO: **Figure 4.4C**,

 $F_{(1,54)}$ =14.71, p=0.0003). Interestingly, the WT controls from the late-cKO line displayed no change in firing frequency between P14 and P28 (late-cKO: **Figure 4.4D**, $F_{(1,65)}$ =0.01135, p=0.9155).

Next, we investigated the effects of Arc/Arg3.1 deletion on firing frequency. The germline KO mice exhibited firing frequencies comparable to their WT controls at both P14 and P28 (Germline KO P14: **Figure 4.4E**, $F_{(1,48)}$ =0.02323, p=0.8795; Germline KO P28: **Figure 4.4H**, $F_{(1,52)}$ =1.409, p=0.2407). However, the Early-cKO line displayed a significantly higher firing frequency than their WT controls at P14, with no difference observed at P28 (Early-cKO P14: **Figure 4.4F**, $F_{(1,48)}$ =5.416, p=0.0242; Early-cKO P28: **Figure 4.4I**, $F_{(1,56)}$ =0.0097, p=0.922). Conversely, the late-cKO mice showed a significantly lower firing frequency than their WT controls at P14, but no change at P28 (Late-cKO P14: **Figure 4.4G**, $F_{(1,72)}$ =10.60, p<0.0001; Late-cKO P28: **Figure 4.4J**, $F_{(1,57)}$ =0.4815, p=0.4906).

Overall, our findings indicate that firing frequency typically increases from the second to the fourth postnatal week (P14 to P28) in WT controls from the germline and Early-cKO lines. However, unlike the other groups, WT controls in the late-cKO line do not exhibit the typical increase in firing frequency between P14 and P28. In fact, upon a comparison of the WT controls from the different lines, we discovered that the firing frequency of WT mice in the late-cKO line at P28 is notably lower compared to the germline WT controls (Mixed-effects ANOVA Line effect: $F_{(2,80)}$ =4.618, p=0.0127, Sidak's multiple comparisons germline-WT vs late-WT: p=0.0113).

Importantly, the effects of *Arc/Arg3.1* deletion on firing frequency appear transient. Both the early and late-cKO lines show deviations from the typical WT maturation at P14, but these differences normalize by P28. This suggests a potential window of influence for *Arc/Arg3.1* on firing frequency regulation, between P7 and P28.

4.3.5 Early but not germline or late *Arc/Arg3.1* deletion reduces sEPSC amplitude and frequency at P28

To assess excitatory synaptic strength and number during this critical period, we measured spontaneous excitatory postsynaptic currents (sEPSCs) at -70 mV in WT controls from each KO line at P14 and P28. The peak amplitude of the sEPSC reflects synaptic strength, while the frequency was taken as a proxy for the number of active synapses.

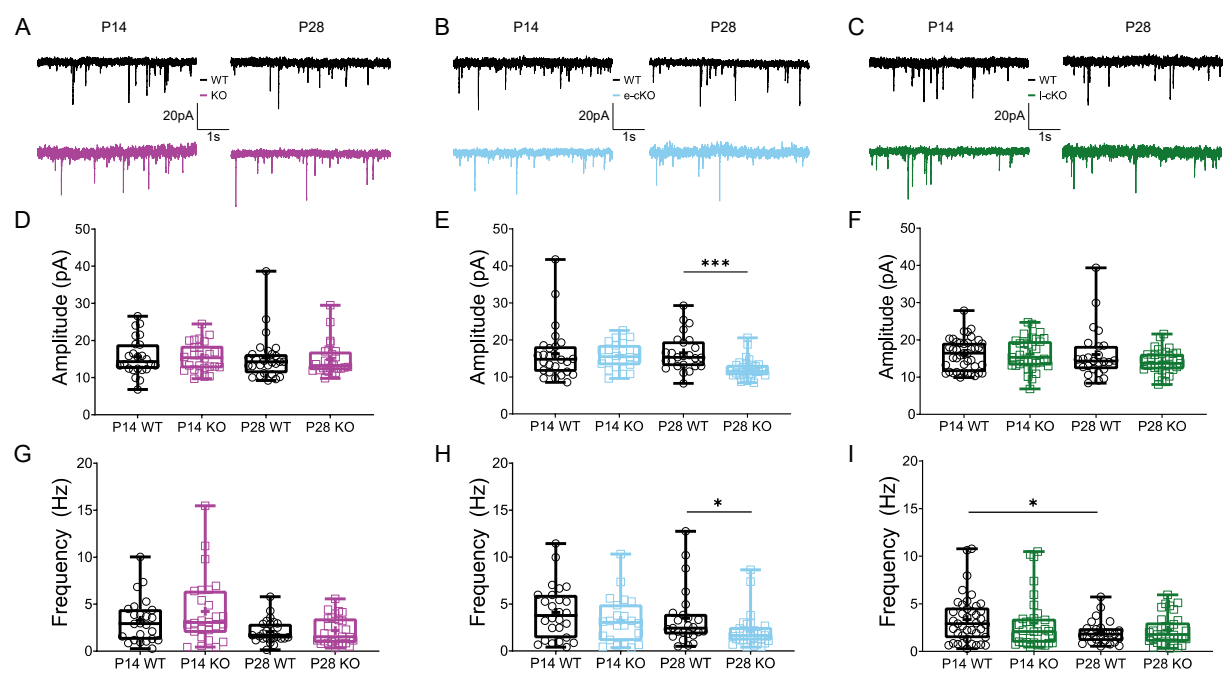


Figure 4.5. Reduced sEPSC amplitude and frequency in early Arc/Arg3.1 KO mice at P28. In the upper panel (A-C), exemplary traces of sEPSCs recorded at -70 mV are depicted for WT (black), KO (magenta), Early-cKO (blue), and late-cKO (green) mice. Boxplots representing sEPSC amplitude (**D-F**) and frequency (**G-I**) for WT, KO, Early-cKO, and late-cKO mice are shown. The box plots display the median \pm interquartile range, with the mean indicated by +, and each point representing the mean value from one cell. Statistical analysis using the Mann-Whitney U test revealed significant differences (*p<0.05, ****p<0.01).

Our analysis revealed no significant changes in sEPSC amplitude across development (P14 to P28) for any WT control group (**Figure 4.5D**, Germline WT: P14 vs P28, U=305, p=0.7293, P14: n=24, P28: n=27; **Figure 4.5E**, early WT-control: P14 vs P28, U=280, p=0.405, P14: n=26, P28: n=25; **Figure 4.5F**, late WT-control: P14 vs P28, U=452, p=0.4304, P14: n=41, P28: n=25). Interestingly, sEPSC frequency appeared to decrease with development in all WT controls, but this decrease only reached statistical significance in the late-cKO line (**Figure 4.5G**, Germline WT: P14 vs P28, U=237, p=0.103, P14: n=24, P28: n=27; **Figure 4.5H**, early WT-control: P14 vs P28, U=264, p=0.2567, P14: n=26, P28: n=25; **Figure 4.5I**, late WT-control: P14 vs P28, U=350, p=0.0315, P14: n=41, P28: n=25).

Next, we investigated the effects of *Arc/Arg3.1* deletion on sEPSC parameters. The germline and late-cKO mice displayed no differences in sEPSC amplitude or frequency compared to their respective WT controls at either P14 or P28 (Amplitude: **Figure 4.5D**, Germline P14: U=312, p>0.999, WT: n=24, KO: n=26; Germline P28: U=347, p=0.7705, WT: n=27, KO: n=27; **Figure 4.5F** Late-cKO P14: U=657, p=0.8373, WT: n=41, KO: n=33; Late-cKO P28: U=372, p=0.53295, WT: n=25, KO: n=33; Frequency: **Figure 4.5G**, Germline P14: U=281, p=0.5569, WT: n=24, KO: n=26; Germline P28: U=346, p=0.7574, WT: n=27, KO: n=27; **Figure 4.5I**, Late-cKO P14: U=570, p=0.2507, WT: n=41, KO: n=33; Late-cKO P28: U=399, p=0.8395, WT: n=25, KO: n=33). In contrast, early deletion of *Arc/Arg3.1* resulted in significantly lower

sEPSC amplitude and frequency at P28, but not at P14, compared to their WT controls (Amplitude: **Figure 4.5E**, Early-cKO P14: U=257, p=0.5587, WT: n=26, KO: n=22; Early-cKO P28: U=139, p<0.0001, WT: n=25, KO: n=29; Frequency: **Figure 4.5H**, Early-cKO P14: U=231, p=0.2621, WT: n=26, KO: n=22; Early-cKO P28: U=227, p=0.0183, WT: n=25, KO: n=29).

Our findings suggest that Arc/Arg3.1 deletion disrupts excitatory synaptic transmission during the first postnatal month. However, this effect was specific to the Early-cKO group, where deletion starts at P7 and is complete by P14. This implies that Arc/Arg3.1 expression during the second postnatal week is critical for the proper function and maintenance of excitatory synapses. Interestingly, the impairment in the Early-cKO line was not observed immediately after deletion (P14), but only by P28. This suggests that the effect might not be due to a failure to form synapses. Instead, it could be a consequence of an active elimination process occurring between the second and fourth postnatal weeks, where synapses lacking sufficient Arc/Arg3.1 are selectively removed.

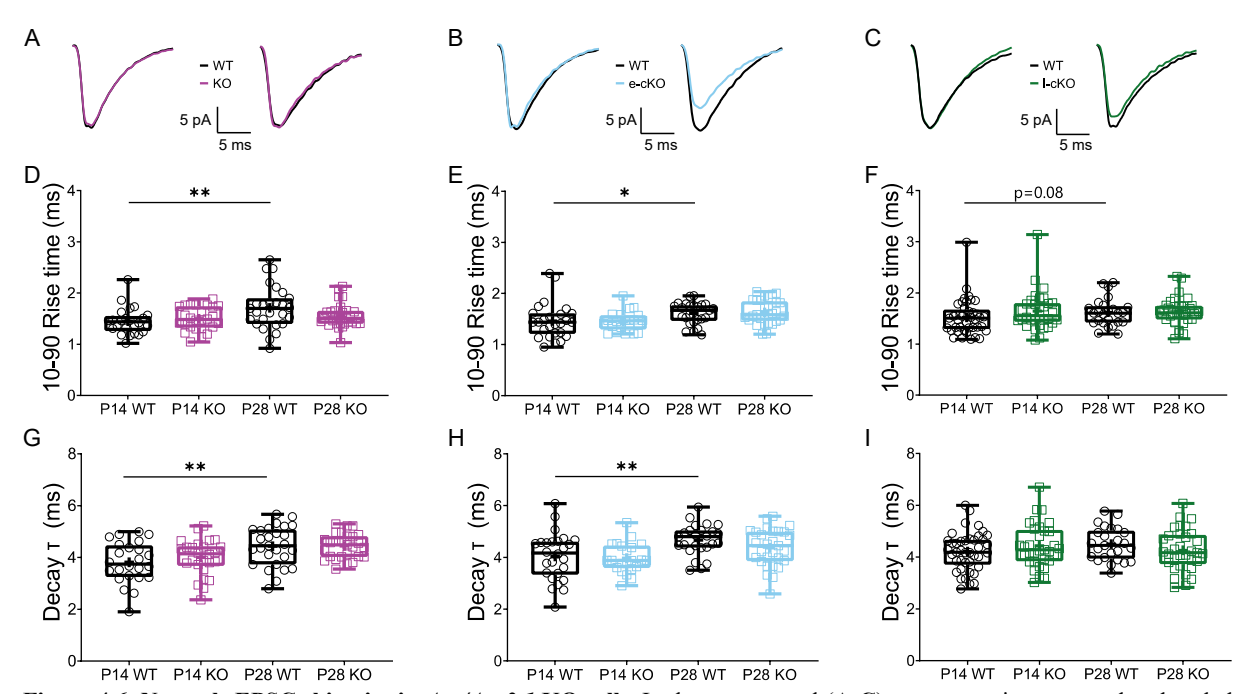


Figure 4.6. Normal sEPSCs kinetics in *Arc/Arg3.1* KO cells. In the upper panel (A-C), representative averaged and scaled (to peak amplitude) sEPSC traces are shown, recorded from WT, KO, Early-cKO, and late-cKO mice. Boxplots depicting sEPSC rise time (**D-F**) and decay time (**G-I**) for these groups are presented. The box plots display the median ± interquartile range, with the mean indicated by +, and each point representing the mean value from one cell. Statistical analysis using the Mann-Whitney U test revealed significant differences (*p<0.05, **p<0.01).

4.3.6 Normal development of sEPSC kinetics in Arc/Arg3.1 KO mice

In Part I of the thesis, we observed changes in the kinetics of sEPSC in the adult hippocampi of germline and early *Arc/Arg3.1* KO mice (**Figure 2.3**). To explore whether this accelerated sEPSC response begins during early developmental stages, we measured sEPSC rise and decay

time constants at P14 and P28. Previous research indicates that sEPSC kinetics tend to slow down during the initial postnatal month, a phenomenon associated with changes in the composition of AMPA receptors (Pickard et al., 2000; Stubblefield & Benke, 2010).

Initially, we examined this typical developmental pattern in our WT controls. Our findings suggested a tendency toward a slower sEPSC rise time at P28 compared to P14 in WT controls from all lines. However, this effect did not reach statistical significance in the late-cKO line (Figure 4.6D, Germline WT: P14 vs P28, U=182, p=0.0068, P14: n=24, P28: n=27; Figure 4.6E, early WT control: P14 vs P28, U=192, p=0.0117, P14: n=26, P28: n=25; Figure 4.6F, late WT control: P14 vs P28, U=380, p=0.081, P14: n=41, P28: n=25). Similarly, the decay time constant also tended to increase with development in the WT controls of the germline and early KO lines (Figure 4.6G, Germline WT: P14 vs P28, U=185, p=0.0081, P14: n=24, P28: n=27; Figure 4.6H, early WT control: P14 vs P28, U=188, p=0.0093, P14: n=26, P28: n=25; Figure 4.6I, late WT control: P14 vs P28, U=408, p=0.1704, P14: n=41, P28: n=25). These results align with the anticipated developmental alterations in sEPSC kinetics.

Next, we explored how *Arc/Arg3.1* deletion affects sEPSC kinetics by comparing *Arc/Arg3.1* KO animals to their corresponding WT controls. Our results showed no significant differences in the rise or decay time in any of the KO lines, at either P14 or P28 (Rise time: Figure 4.6D, Germline P14: U=254, p=0.2668, WT: n=24, KO: n=26; Germline P28: U=282, p=0.1572, WT: n=27, KO: n=27; Figure 4.6E, Early-cKO P14: U=272, p=782, WT: n=26, KO: n=22; Early-cKO P28: U=343, p=0.7437, WT: n=25, KO: n=29; Figure 4.6F, Late-cKO P14: U=530, p=0.1127, WT: n=41, KO: n=33; Late-cKO P28: U=387, p=0.6969, WT: n=25, KO: n=33; Frequency: Figure 4.6G, Germline P14: U=266, p=0.3802, WT: n=24, KO: n=26; Germline P28: U=357, p=0.9044, WT: n=27, KO: n=27; Figure 4.6H, Early-cKO P14: U=261, p=0.6153, WT: n=26, KO: n=22; Early-cKO P28: U=283, p=0.1719, WT: n=25, KO: n=29; Figure 4.6I, Late-cKO P14: U=596, p=0.3865, WT: n=41, KO: n=33; Late-cKO P28: U=336, p=0.2348, WT: n=25, KO: n=33). This suggests that while the first postnatal month is indeed a period of substantial changes in the duration of excitatory currents, *Arc/Arg3.1* does not seem to regulate sEPSC kinetics during this early developmental stage. Instead, the alterations observed in the adult brain begin at later stages of development.

4.3.7 Reduced eEPSC amplitude in early Arc/Arg3.1 KO mice at P28

CA1 pyramidal cells receive a major source of excitatory input from CA3 pyramids via Schaffer collaterals (Megias et al., 2001) terminating on CA1 apical dendrites within the *stratum* radiatum. The number of synapses formed between the CA3 and CA1, as well as their

individual currents, determine the excitatory drive for CA1 and its ability to generate activity patterns essential for learning and memory. To specifically assess the excitatory drive from CA3 to CA1, we employed an extracellular electrode placed in the *stratum radiatum* (main CA1 layer receiving Schaffer collateral input). We then examined the effects of stimuli with varying intensities on evoked excitatory postsynaptic currents (eEPSCs).

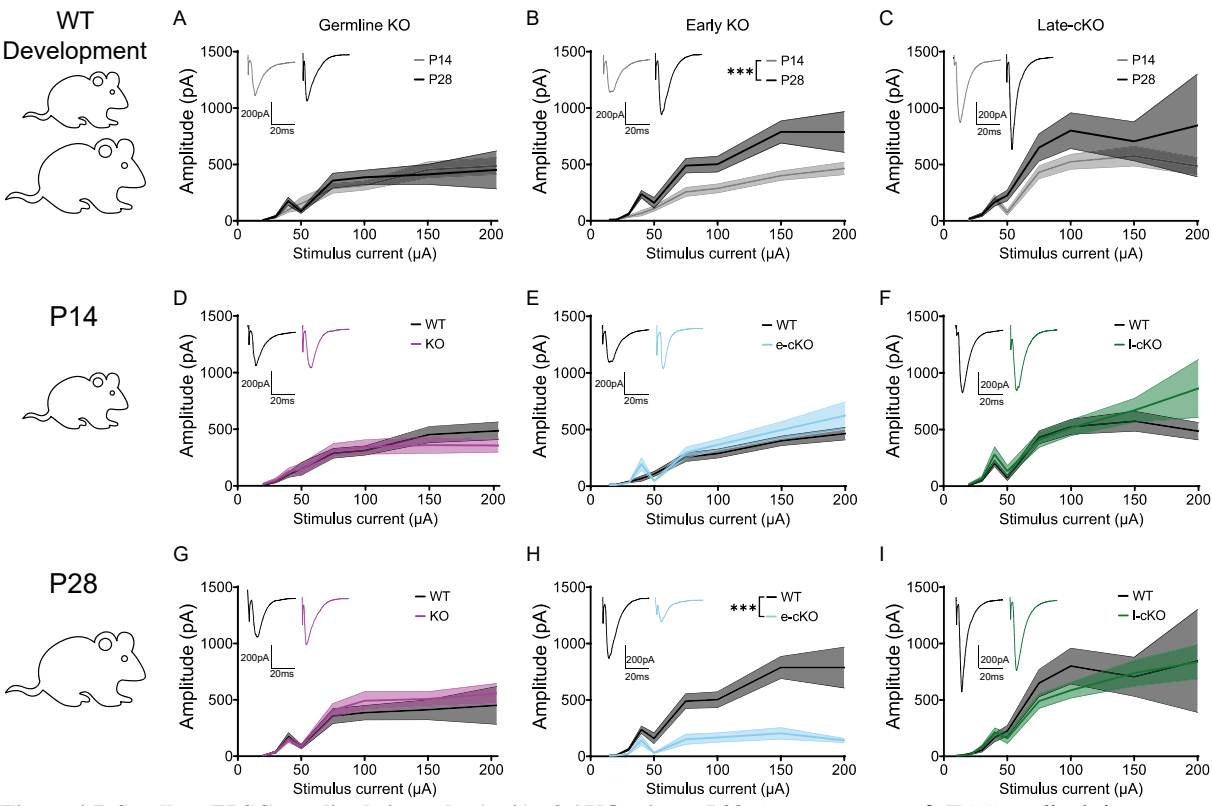


Figure 4.7. Smaller eEPSC amplitude in early *Arc/Arg3.1* KO mice at P28. Average curves of eIPSC amplitude in response to increasing intensity stimuli are presented. The top panel (A-C) compares WT controls of each line at P14 versus P28, while the middle and bottom panels (D-F and G-I) display comparisons of WT versus KO cells at P14 and P28, respectively. Solid lines indicate average values, with shadows indicating ±SEM. Legend asterisks indicate the effects of the factor "Genotype" within a Mixed-effects ANOVA, **p<0.001. Insets display representative traces evoked by 100μA stimulation.

Prior studies suggest that the synaptic strength of Schaffer collaterals projection to CA1 increases beyond the third postnatal week (Bekenstein & Lothman, 1991; Dumas & Foster, 1995). To understand the natural development of these CA3-CA1 synapses, we compared the eEPSC amplitudes in WT controls from each KO line at P14 and P28.

In the germline KO, the WT group exhibited no significant change in eEPSC amplitude between P14 and P28 (**Figure 4.7A**, $F_{(1,43)}$ =0.1768, p=0.6762). However, the WT controls of the early-cKO line displayed a significant increase in eEPSC amplitude from P14 to P28, suggesting a potential strengthening of synaptic connections during this developmental phase (**Figure 4.7B**, $F_{(1,43)}$ =28.09, p<0.0001). Although less pronounced, WT controls of the late-cKO line also showed a tendency toward larger eEPSC amplitude at P28, though this increase did not reach statistical significance (**Figure 4.7C**, $F_{(1.59)}$ =3.884, p=0.0534). These findings partially

corroborate previously reported enhancements in CA3-CA1 synaptic strength between the third and fourth postnatal weeks (Dumas & Foster, 1995).

Next, we evaluated the impact of Arc/Arg3.1 deletion at different developmental stages on eEPSC amplitude. At P14, we observed no differences in any of the Arc/Arg3.1 KO lines compared to their respective WT controls (Germline KO: **Figure 4.7D**, $F_{(1,44)}$ =0.0448, p=0.8333; Early-cKO: **Figure 4.7E**, $F_{(1,37)}$ =1.843, p=0.1828; Late-cKO: **Figure 4.7F**, $F_{(1,65)}$ =0.3368, p=0.7369). However, congruent with decreases in sEPSC amplitude and frequency, our results revealed significantly smaller eEPSC amplitudes in early-cKO neurons at P28 (**Figure 4.7H**, $F_{(1,44)}$ =63.54, p<0.0001). No alterations were detected in the germline or late-cKO cells (Germline KO: **Figure 4.7G**, $F_{(1,48)}$ =0.7173, p=0.4012; Late-cKO: **Figure 4.7I**, $F_{(1,51)}$ =0.1142, p=0.7369). Importantly, eEPSC amplitudes in early-cKO strongly decreased from P14 to P28 (See blue lines in **Figure 4.7E and H**, $F_{(1,38)}$ =8.925, p<0.0049), suggesting that the underlying mechanism involved an active removal of synapses as opposed to stagnating synaptogenesis.

4.3.8 Reduced spine density in early-cKO mice at P28

During the first postnatal week, most excitatory synapses form directly on dendritic shafts (Fiala et al., 1998). By the third postnatal week, a dramatic increase occurs in the number of synapses, with the majority transitioning to dendritic spines (Harris et al., 1992). We investigated whether the reduced synaptic transmission observed in early-cKO mice at P28 is reflected in changes to dendritic spine density and morphology.

To address this question, we employed the Golgi-Cox method to stain neurons in the brains of early-cKO mice and their WT controls. This technique offers high-resolution visualization of neuronal morphology, including dendritic spines. To further enhance image clarity and minimize out-of-focus blur, we utilized Confocal Reflection Super Resolution microscopy (Sivaguru et al., 2019), providing a superior resolution in the z-plane (**Figure 4.8A**). Following image acquisition, we processed the image stacks using a maximum projection function, generating a two-dimensional representation of the dendritic arbor. We then employed the filament tracer module of Imaris software (Bitplane AG) to reconstruct dendritic segments from both the basal and apical trees. Finally, these automated reconstructions were manually curated to eliminate any artificial spines introduced during processing.

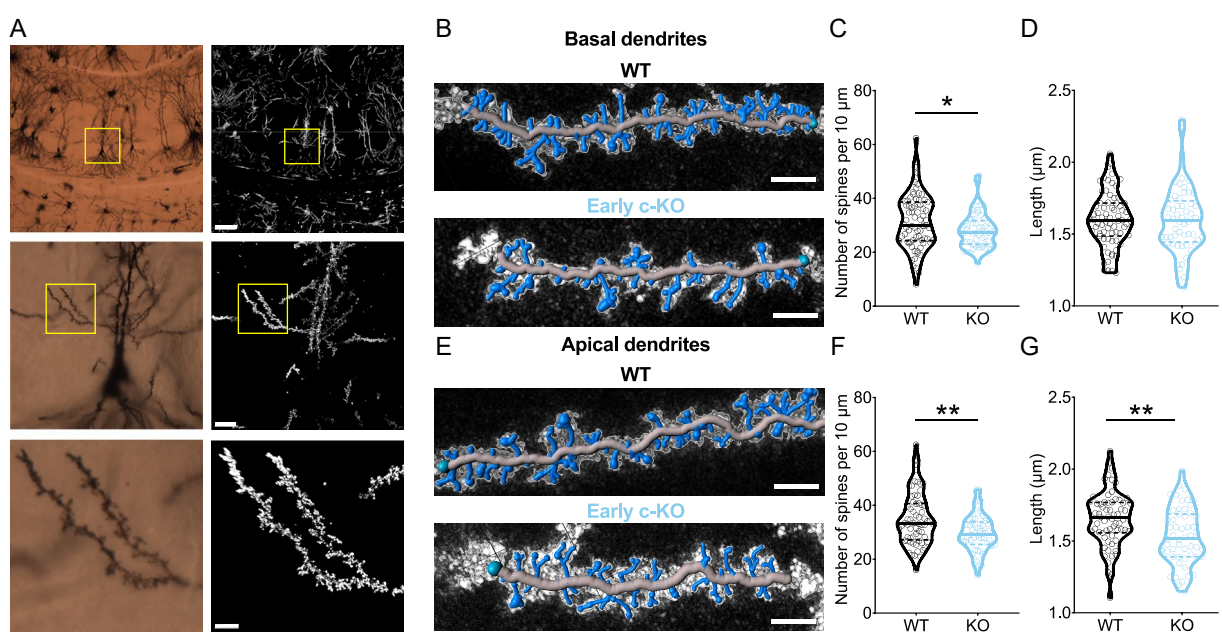


Figure 4.8. Reduced spine density in early *Arc/Arg3.1* KO mice at P28. Panel A presents Golgi-stained hippocampal tissue images at increasing magnifications (10x top, 63x middle, and 100x bottom panels). Images on the left were captured using bright-field microscopy, while those on the right utilized the confocal reflection super-resolution technique. The boxed regions depict the soma and dendrites of two CA1 pyramids. Scale bars are 100μm for the top, 15μm for the middle, and 5μm for the bottom images. Panel B displays representative segments of basal dendrites of both WT and early-cKO mice, with scale bars of 3μm. Spine density and length quantifications are shown in panels C and D, respectively. Panel E shows representative segments of apical dendrites of WT and early-cKO mice, with scale bars of 3μm, and spine density and length quantifications in panels F and G, respectively. Violin plots depict the median ± interquartile range, with each point representing the mean value from one dendritic segment. Statistical analysis using the Mann-Whitney U test revealed significant differences (*p<0.05, **p<0.01). Images in panel A were acquired by Cristina Stanke and were presented as part of her master's thesis (Stanke, 2022).

Our findings aligned with the observed decrease in synaptic function, revealing a significantly lower spine density in both the basal and apical dendrites of early-cKO mice compared to their WT controls (Basal: **Figure 4.8C**, U=1570, p=0.0423, WT: n=71, early-cKO: n=56; Apical: **Figure 4.8F**, U=1194, p=0.0037, WT: n=64, early-cKO: n=54). Additionally, the length of dendritic spines was significantly reduced in the early-cKO group, but this effect was specific to the apical dendrites. No change in spine length was observed in the basal dendrites (Basal: **Figure 4.8D**, U=1908, p=0.7005, WT: n=71, early-cKO: n=56; Apical: **Figure 4.8G**, U=1144, p=0.0015, WT: n=64, early-cKO: n=54).

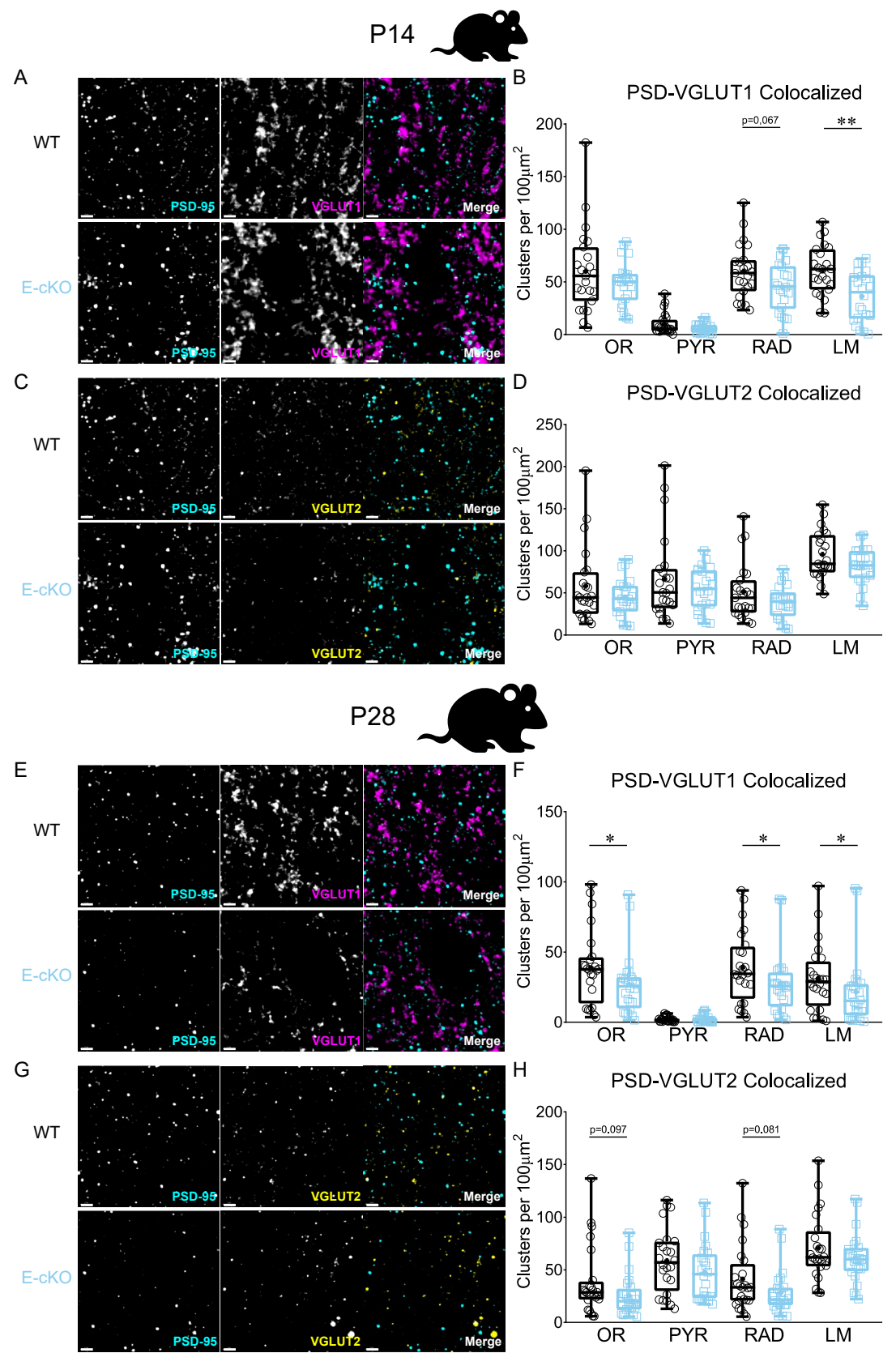


Figure 4.9. Decreased excitatory synaptic clusters in early-cKO. The representative images in panels A and C depict immunostaining for PSD-95 with VGLUT1 and VGLUT2, respectively, in the CA1 stratum radiatum at postnatal day 14 (P14). Panels B and D display the quantification of PSD-95 colocalized clusters with either VGLUT1 or VGLUT2, respectively. Similarly, panels E and G show representative images of immunostaining for PSD-95 with VGLUT1 and VGLUT2, respectively, from the CA1 stratum radiatum at postnatal day 28 (P28). Panels F and H present the corresponding quantification of PSD-95 colocalized clusters with either VGLUT1 or VGLUT2, respectively. Boxplots show the median ± interquartile range, + represents the mean, and each point represents the value from one confocal scan. Statistical analysis using the Mann-Whitney U test revealed significant differences (*p<0.05, **p<0.01). Scale bars, 2μm.

4.3.9 Early-cKO mice exhibited fewer excitatory clusters in the CA1 region of the hippocampus.

We employed immunostaining to visualize and quantify synaptic clusters. We labeled postsynaptic sites with PSD-95, a protein concentrated at excitatory postsynaptic densities, and presynaptic sites with antibodies against VGLUT1 and VGLUT2. This approach allowed us to capture a broad spectrum of potential excitatory synapses, with colocalization of PSD-95 with VGLUTs considered indicative of excitatory synapses.

Vesicular glutamate transporters (VGLUTs) are proteins located in presynaptic terminals that package the neurotransmitter glutamate into synaptic vesicles (Bellocchio et al., 2000). Because of this role, they serve as reliable markers for identifying excitatory nerve terminals throughout the brain. Previous studies have demonstrated distinct and complementary expression patterns of VGLUT1 and VGLUT2 across various brain regions and within specific brain regions, suggesting their potential role in segregating excitatory inputs from different areas (Fremeau et al., 2001). Notably, the expression patterns of VGLUTs undergo significant changes during the first postnatal month, likely reflecting ongoing development and plasticity within excitatory circuits (Nakamura et al., 2005).

Our previous studies using electrophysiological and structural analyses revealed that deleting *Arc/Arg3.1*, particularly during the second postnatal week, disrupts excitatory synaptic function in the hippocampus. To further investigate potential alterations in synaptic organization, we examined the distribution of synapses across different layers of the CA1 region in both WT and early-cKO mice at P14 and P28.

Our findings on VGLUT distribution corroborated previous studies, revealing a distinct pattern across hippocampal layers. PSD-95 clusters colocalized with VGLUT1 (indicating VGLUT1 synapses) were scarce in the *pyramidal* layer but abundant in the stratum oriens and radiatum of CA1. In contrast, PSD-95 clusters colocalized with VGLUT2 (indicating VGLUT2 synapses) were more abundant in the *stratum lacunosum moleculare* but showed a relatively homogeneous distribution across the other layers.

Our comparison of WT and early-cKO mice at P14 revealed a reduction in VGLUT1 synapses specifically within the *lacunosum moleculare* layer. Additionally, there was a trend towards fewer VGLUT1 synapses in the *stratum radiatum*, with no significant changes in *strata oriens* or *pyramidale* (**Figure 4.9A-B**, WT: n=23, early-cKO: n=22, *st. oriens*: U=220, p=0.4643, *st. pyramidale*: U=204, p=0.2737, *st. radiatum*: U=172, p=0.0672, *st. lacunosum moleculare*:

U=126, p=0.0034). Interestingly, the distribution of VGLUT2 synapses remained unchanged in early-cKO mice compared to their WT controls (**Figure 4.9C-D**, WT: n=23, early-cKO: n=22, *st. oriens:* U=227, p=0.5661, *st. pyramidale:* U=245.5, p=0.8709, *st. radiatum:* U=219, p=0.4471, *st. lacunosum moleculare:* U=190, p=0.1573).

At P28, when the most significant deficits in excitatory transmission and reductions in spine density were observed, we found a markedly lower number of VGLUT1 synapses in all dendritic layers of early-cKO mice compared to WT controls. Notably, VGLUT1 synapses in the *stratum pyramidale* were not affected (**Figure 4.9E-F**, WT: n=24, early-cKO: n=24, *st. oriens*: U=182, p=0.0287, *st. pyramidale*: U=262.5, p=0.6057, *st. radiatum*: U=187, p=0.0374, *st. lacunosum moleculare*: U=189, p=0.0415). VGLUT2 results showed a trend towards fewer synapses in the *stratum oriens* and *radiatum* of the early cKO group, although this effect was not statistically significant. Similar to P14, VGLUT2 synapses in *strata pyramidale* and *lacunosum moleculare* remained unchanged compared to WT controls (**Figure 4.9G-H**, WT: n=24, early-cKO: n=24, *st. oriens*: U=207, p=0.0972, *st. pyramidale*: U=233.5, p=0.266, *st. radiatum*: U=203, p=0.0814, *st. lacunosum moleculare*: U=238, p=0.3104).

Taken together, our immunostaining results revealed that deletion of *Arc/Arg3.1* during the early postnatal period (early-cKO) primarily reduced the density of VGLUT1 synapses in CA1 without an overt effect on VGLUT2 synapses. The loss of VGLUT1 synapses in the early-cKO emerged at P14, and early-cKO in the *lacunosum moleculare* layer and spread to all dendritic layers by P28.

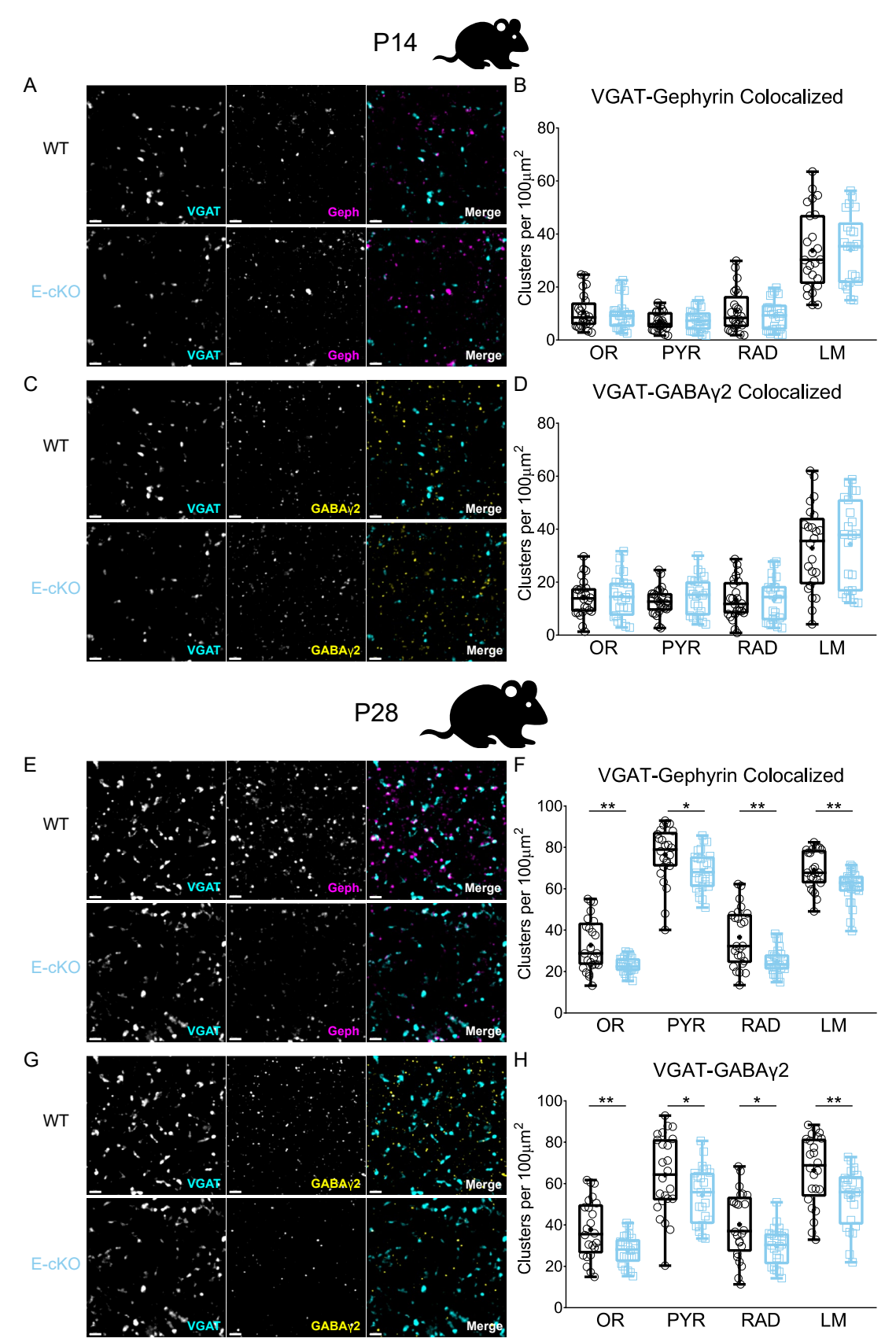


Figure 4.10. Decreased inhibitory synaptic clusters in early-cKO. The representative images in panels A and C depict immunostaining for VGAT with Gephyrin and GABAγ2, respectively, in the CA1 stratum radiatum at postnatal day 14 (P14). Panels B and D display the quantification of VGAT colocalized clusters with either Gephyrin or GABAγ2, respectively. Similarly, panels E and G show representative images of immunostaining for VGAT with Gephyrin and GABAγ2, respectively, from the CA1 stratum radiatum at postnatal day 28 (P28). Panels F and H present the corresponding quantification of VGAT colocalized clusters with either Gephyrin or GABAγ2, respectively. Boxplots show the median ± interquartile range, +

represents the mean, and each point represents the value from one confocal scan. Statistical analysis using the Mann-Whitney U test revealed significant differences (*p<0.05, **p<0.01). Scale bars, $2\mu m$.

4.3.10 Early-cKO mice exhibited fewer inhibitory clusters in the CA1 region of the hippocampus.

The inhibitory transmission also matures during the first postnatal month in an activity-dependent manner (Banks et al., 2002; Chattopadhyaya et al., 2004; Danglot et al., 2006; Huang, 2009). The alterations observed in excitatory transmission in the early-cKO may thus impact inhibition by altering activity levels and synaptic plasticity. To address this possibility, we investigated inhibitory synaptic transmission in CA1 of early-cKO mice.

We labeled presynaptic sites with the vesicular GABA transporter (VGAT), a marker for inhibitory axonic terminals, and postsynaptic sites with antibodies against gephyrin (a key scaffolding protein for inhibitory synapses) and the GABA- γ 2 subunit of GABA-A receptors. Some studies suggest that GABA-A receptors containing the γ 2 subunit can cluster independently from gephyrin (Danglot et al., 2003), so we included this measure to explore a broader range of potential inhibitory synapses. Colocalization of VGAT with either gephyrin or GABA- γ 2 served as an indicator of inhibitory synapses.

At P14, our immunostaining analysis revealed no significant differences in the number of inhibitory synapses between WT and early-cKO mice. This was true for synapses labeled by colocalization of VGAT with either gephyrin or GABA-γ2 across all layers of the CA1 region (VGAT-Gephyrin colocalized: **Figure 4.10A-B**, WT: n=24, early-cKO: n=22, *st. oriens*: U=251, p=0.7855, *st. pyramidale*: U=258, p=0.9047, *st. radiatum*: U=242, p=0.6355, *st. lacunosum moleculare*: U=256, p=0.8703; VGAT- GABA-γ2 colocalized: **Figure 4.10C-D**, WT: n=24, early-cKO: n=22, *st. oriens*: U=260, p=0.9393, *st. pyramidale*: U=230, p=0.465, *st. radiatum*: U=254, p=0.8361, *st. lacunosum moleculare*: U=257, p=0.8875).

However, a striking change emerged at P28. Early-cKO mice displayed a significantly lower number of VGAT clusters colocalized with both gephyrin and GABA-γ2 in all CA1 layers compared to their WT counterparts (VGAT-Gephyrin colocalized: **Figure 4.10E-F**, WT: n=24, early-cKO: n=24, *st. oriens:* U=161, p=0.0082, *st. pyramidale:* U=167, p=0.012, *st. radiatum:* U=147, p=0.0032, *st. lacunosum moleculare:* U=162, p=0.0088; VGAT- GABA-γ2 colocalized: **Figure 4.10G-H**, WT: n=24, early-cKO: n=24, *st. oriens:* U=163.5, p=0.0095, *st. pyramidale:* U=192 p=0.0483, *st. radiatum:* U=179, p=0.0243, *st. lacunosum moleculare:* U=158, p=0.0068). Overall, these findings suggest that early postnatal *Arc/Arg3.1* deletion leads to alterations in inhibitory synaptic clustering across the entire axodendritic axis of CA1.

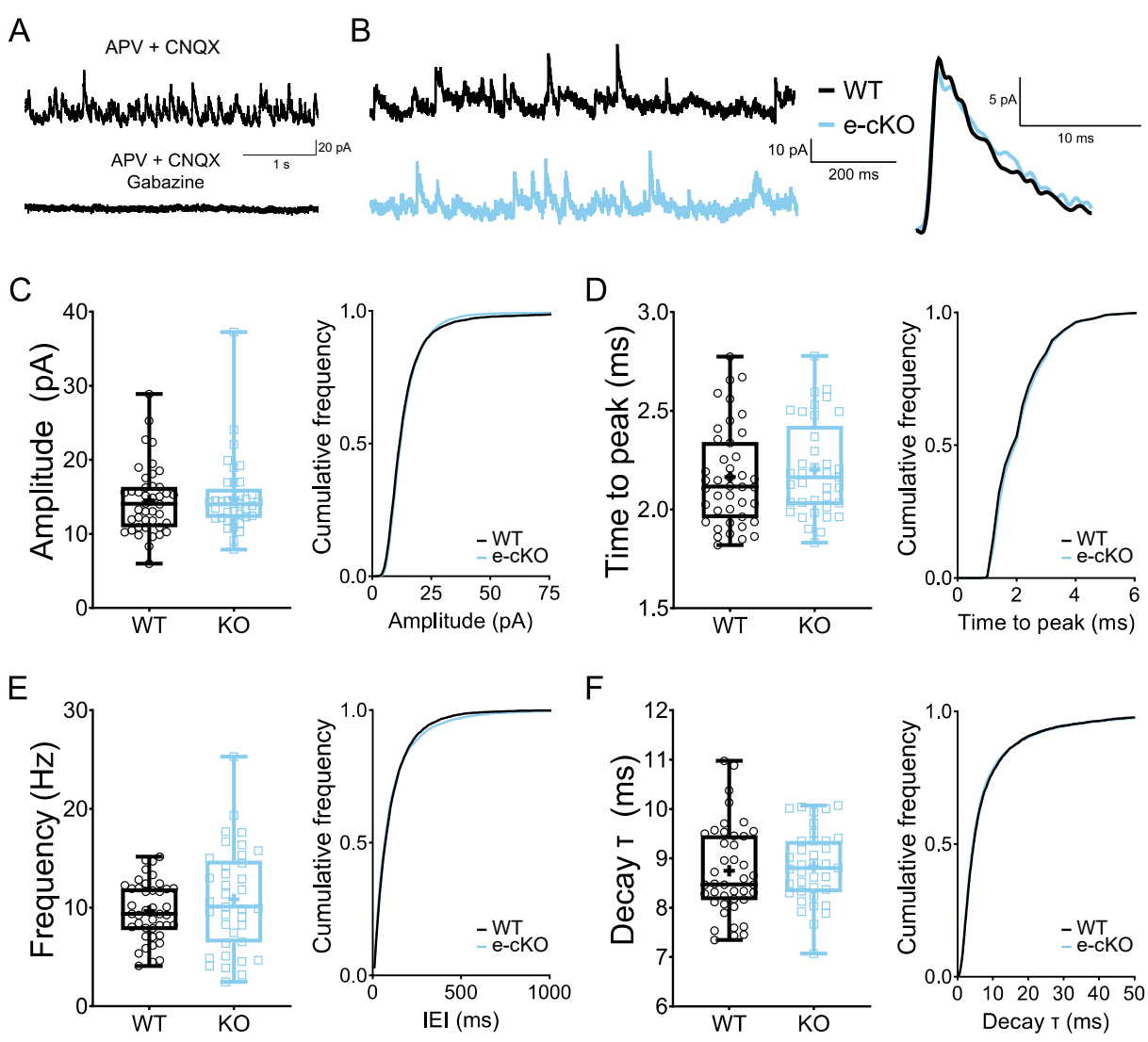


Figure 4.11. Preserved sIPSC amplitude, frequency, and kinetics in early-cKO mice. Panel A displays sample traces of sIPSCs recorded at 0 mV in the presence of glutamatergic blockers (APV and CNQX), followed by traces from the same cell after gabazine was added to the recording solution. Panel B illustrates sIPSC traces with CNQX and APV in WT cells (in black) and early-cKO cells (in blue). Panels C and E show similar amplitude and frequency of sIPSCs between WT and early-cKO cells. Panels D and F demonstrate an unaltered time to peak and decay τ in early-cKO cells. Box plots show the median \pm interquartile range of the respective parameter, + represents the mean, every point represents the mean value from one cell. (Mann-Whitney U test **:p>0.01, ***: p>0.001). Line plots depict cumulative frequency histograms for each parameter.

4.3.11 Early-cKO mice exhibit unaltered sIPSCs

The reduced number of inhibitory clusters observed at P28 in early *Arc/Arg3.1* KO mice suggested a decrease in the number of inhibitory synapses. Subsequently, we investigated whether these reductions translated into functional modifications in inhibitory transmission. To address this, we conducted patch-clamp recordings to measure spontaneous inhibitory postsynaptic currents (sIPSCs) while holding cells at 0 mV and in the presence of AMPA and NMDA receptor antagonists to isolate inhibitory currents. Since sIPSCs disappeared with the GABA-A receptor blocker gabazine, we can confidently exclude GABA-B receptors from contributing to the recorded currents (**Figure 4.11A**). We assessed the inhibitory synapse strength and frequency of sIPSCs.

Representative traces revealed no significant differences in amplitude or frequency patterns between KO and WT mice (**Figure 4.11B**). Cumulative histograms and quantitative analysis of mean peak amplitudes and frequency (determined by IEI) also failed to reveal any statistically significant differences between the groups (Amplitude: **Figure 4.11C**, U= 795, p>0.999, WT: n=43, early-cKO: n=37; Frequency: **Figure 4.11E**, U=706, p=0.3925, WT: n=43, early-cKO: n=37). Considering the importance of synaptic time constants for network synchrony and the previously observed changes in sIPSCs kinetics in germline *Arc/Arg3.1* KO, we then evaluated the rise and decay components of sIPSCs. Our results showed no differences in these parameters in the early-cKO group compared to their WT controls, across the entire parameter distribution, as indicated by the completely overlapping cumulative histograms (Time to peak: **Figure 4.11D**, U= 691, p=0.3174, WT: n=43, early-cKO: n=37; Decay τ: **Figure 4.11F**, U=729, p=0.5263, WT: n=43, early-cKO: n= 37). Together, these findings suggest that despite structural deficits, functional changes in the spontaneous inhibitory synaptic transmission were not detected in early c-KO mice at P28.

4.3.12 Early *Arc/Arg3.1* deletion does not impact eIPSCs or paired-pulse modulation of inhibition

While our staining revealed fewer inhibitory clusters (VGAT colocalized with gephyrin or GABA-γ2) in early-cKO mice at P28, we did not observe changes in sIPSC. This suggests a potential mismatch between the number of inhibitory clusters and the number of functional synapses.

Recent studies indicate a partial segregation between spontaneous and evoked inhibitory neurotransmission, with up to 40% of the evoked responses mediated by GABA_ARs exclusively activated by evoked neurotransmission (Horvath et al., 2020). Therefore, we investigated evoked inhibitory postsynaptic currents (eIPSCs) in early-cKO mice at P28. We applied stimuli of increasing intensity in the CA1 *radiatum* layer and measured eIPSC amplitude and area.

Similar to sIPSCs, no differences in eIPSC parameters were observed between early-cKO and WT mice (Mixed-effects ANOVA Genotype effect; Amplitude: **Figure 4.12B**, $F_{(1,77)}$ =0.062, p=0.804, WT: n=43, KO: n=36; Area: **Figure 4.12C**, $F_{(1,77)}$ =0.8456, p=0.3607, WT: n=43, KO: n=36). This suggests that neither spontaneous nor evoked inhibitory transmission is altered by early Arc/Arg3.1 deletion at P28.

Since our assessment of inhibitory synaptic clusters relied on counting VGAT clusters colocalized with either gephyrin or GABA γ 2 clusters, where VGAT indicates presynaptic sites

of inhibitory synapses, we explored whether alterations in inhibitory synaptic transmission corresponded to changes in presynaptic mechanisms. To do this, we investigated potential modifications in inhibitory presynaptic transmission by measuring the paired-pulse ratio during stimulation protocols with varying inter-pulse intervals (1000, 100, and 50 ms).

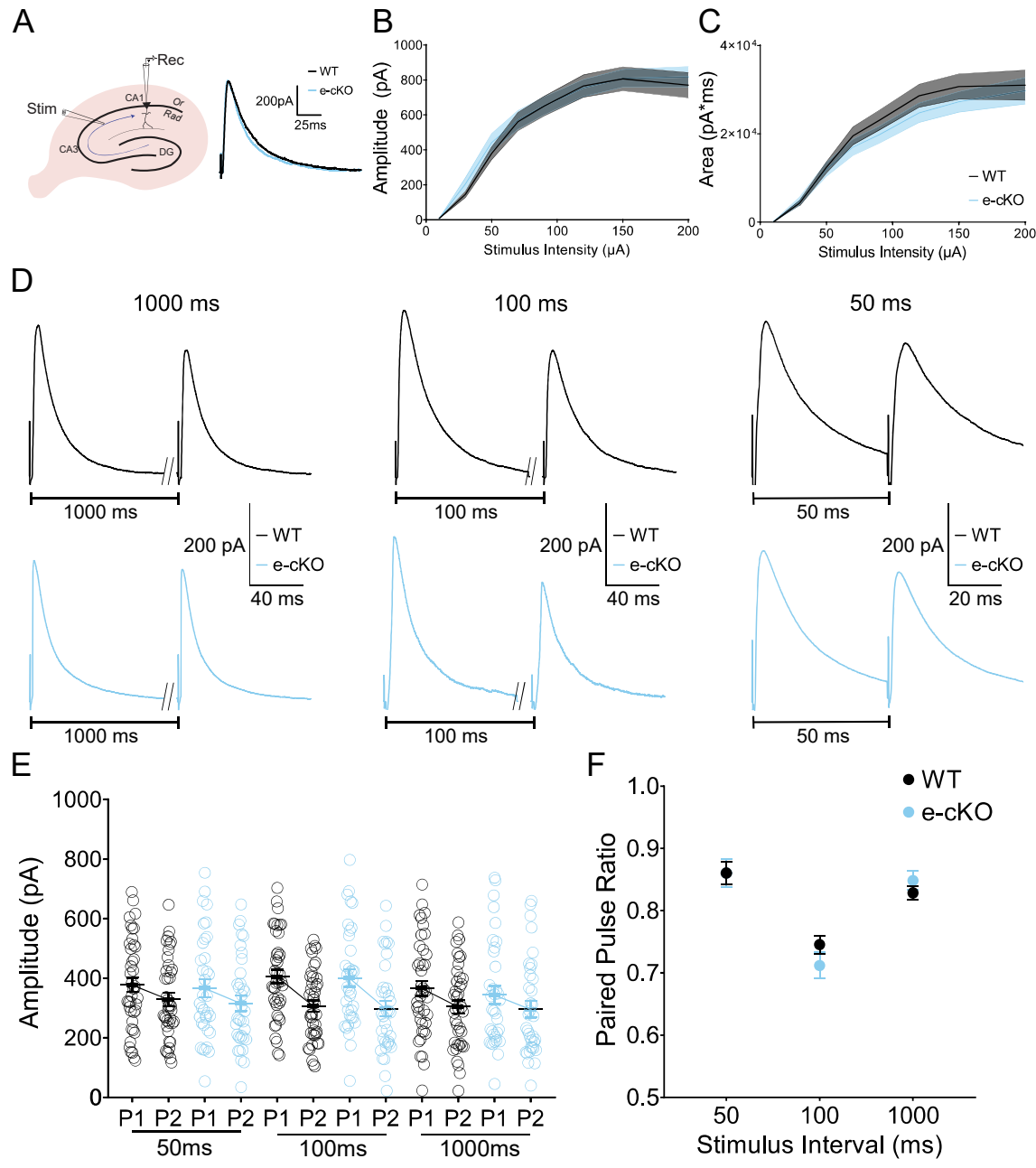


Figure 4.12. Unaltered eIPSC and paired-pulse ratio in early-cKO mice. A Shows the recording protocol sketch on the left indicating the positions of stimulating and recording electrodes, while scaled representative traces of eIPSCs evoked by 90μ A stimulation are shown on the right. Panels B and C display averaged curves of eIPSCs amplitude and area, respectively. Panel D presents exemplary traces of eIPSCs in response to paired pulses with different inter-stimulus intervals (ISI). E demonstrates indistinguishable paired-pulse amplitudes in WT and early Arc/Arg3.1 KO mice in response to stimulation, regardless of the ISI, and F illustrates preserved paired-pulse ratios for all ISIs in early Arc/Arg3.1 KO mice. Scatter plots depict the mean \pm standard error of the mean (SEM) of the respective parameter, with each point representing the mean value from one cell.

Interestingly, both groups displayed paired-pulse depression, suggesting a high release probability regardless of inter-pulse interval (Figure 4.12D-E). However, no significant

differences were found between early-cKO and WT mice (**Figure 4.12F**; 1000 ms: U= 603, p=0.2363, WT: n=41, early-cKO: n=35; 100 ms: U= 587, p=0.1765, WT: n=41, early-cKO: n=35; 50 ms: U= 661, p=0.6844, WT: n=40, early-cKO: n=35), indicating that early *Arc/Arg3.1* deletion does not alter the presynaptic mechanisms of inhibitory transmission.

Taken together, our functional analysis suggests that early *Arc/Arg3.1* deletion at P28 does not impact spontaneous or evoked inhibitory transmission, despite a decrease in the number of inhibitory clusters observed through staining. How could this discrepancy be explained? One possibility is that the colocalization of pre- and postsynaptic markers does not necessarily reflect functional synapses, but rather silent or immature ones.

4.4 Discussion

The natural upregulation of *Arc/Arg3.1* during the first postnatal month substantially overlaps with the period of dendritic growth in the hippocampus. Given its association with the actin cytoskeleton, *Arc/Arg3.1* could potentially modulate this dendritic growth. Previous work from our group compared the gross dendritic morphology of a small number of cells in the adult hippocampus and found no clear alterations (Plath et al., 2006). However, the role of *Arc/Arg3.1* in the development of dendritic morphology has not been evaluated. Some studies have shown that one of its closest associated molecules, the brain-derived neurotrophic factor (BDNF) (Bramham et al., 2010; Messaoudi et al., 2007; Yin et al., 2002), regulates dendritic outgrowth and arborization (Colucci-D'Amato et al., 2020; Gorski et al., 2003; Kim & Cho, 2014). However, there is conflicting evidence suggesting that BDNF is necessary for dendritic growth in regions like the striatum but is dispensable for this process in the hippocampus (Rauskolb et al., 2010). Our results showed normal dendritic morphology in *Arc/Arg3.1* KO mice at the end of both the second and fourth weeks, indicating that *Arc/Arg3.1* does not play a role in gross dendritic morphology in the hippocampus.

Regarding membrane properties, we observed no major effects of *Arc/Arg3.1* deletion in membrane resistance regardless of the time of deletion, except for a tendency towards higher membrane resistance in the early-cKO mice at P14. However, upon closer examination, we found that the input resistance of this group was comparable to that of the KO mice from the other two KO lines and their WT controls. In contrast, the WT controls of the early-cKO line exhibited significantly lower input resistance compared to the WT controls of the other two KO lines. Consistently, the expected reduction in input resistance from the second to the fourth week, observed in the other two lines, did not occur in the WT controls of the early-cKO line.

The only difference between the WT controls in the different lines is their expression of Cre recombinase. Thus, the observed differences could be attributed to the off-target effects of Cre recombinase, which is a known limitation of the Cre-loxP system (McLellan et al., 2017). However, it is important to note that while we cannot entirely exclude such off-target effects, they are likely minor. As suggested by the lack of differences between the WT controls in other physiological parameters evaluated in this study. Further research is necessary to assess these potential effects on input resistance and clarify the impact of these observations.

Our findings showed an age-related reduction in action potential duration, a maturational change previously shown by other studies and dependent on the expression of sodium and

potassium channels (Costa et al., 1994; Isagai et al., 1999; Sanchez-Alonso et al., 2010; Spigelman et al., 1992). Furthermore, we found that germline deletion sharpens the action potential waveform at P28, while postnatal deletions have no effect. This suggests that this property is particularly sensitive to Arc/Arg3.1 presence during the first 2 postnatal weeks. In line with this, action potential duration in immature neurons (P3-5) is especially sensitive to changes in membrane potential and K⁺ blockers (Spigelman et al., 1992). Therefore, it is possible that the absence of Arc/Arg3.1 during this very early period alters development by regulating the expression of K⁺ channels, and this could explain why this AP sharpening is not observed in the early and late-cKOs.

Neurons with shorter action potential duration often reach higher firing frequencies. Consistent with this, our FI curves revealed a significant age-related increase in the frequency of action potentials. However, despite the shorter AP duration in the germline KO cells, we did not observe further increases in firing frequency P28 in this line. Instead, we observed an acceleration of this maturation in the early-cKO cells, reflected by higher firing frequencies at P14. This effect, in the absence of clear differences in AP half-width, might reflect an increase in the bursting probability of these cells. This possibility needs to be addressed in future studies, as we did not evaluate this parameter in this study. Collectively, our findings show that Arc/Arg3.1 during early development modulates the maturation of active, but not passive, properties, possibly by regulating the expression of Na⁺ and K⁺, channels.

Studies using electron microscopy show that the number of excitatory synapses increases dramatically during the first postnatal month, with the sharpest increases observed between weeks one and three, followed by a slowdown into the fourth week (Steward Falk 1991). In comparison, our findings on sEPSC frequency showed no increases from the second to the fourth week and even a tendency towards lower frequency. These findings align well with a recent report that measured mEPSCs, their results showed no increases in amplitude and also a tendency toward a decrease in frequency from the second to the fourth week (Sakimoto et al., 2022). A possible explanation for the reduction in sEPSCs frequency lies in synaptic pruning. The development of diverse circuits in the central nervous system relies on neural activity to drive this maturation not only by promoting the addition of a large number of synapses but also by the elimination of synapses present within inappropriate regions (Katz & Shatz, 1996).

Our findings on sEPSCs in the different KO lines revealed no differences at P14 in any of the lines, but a significant reduction in the strength and number of excitatory synapses in the early-cKO line at P28. Consistent with this, we also observed reductions in spine density. Deficits

that are likely the result of an active synapse elimination rather than a failure to develop new ones. A role of *Arc/Arg3.1* in activity-dependent synapse elimination in the cerebellum during the third and fourth postnatal weeks was already shown in the study by Mikuni et al. (2013). However, while Mikuni et al. suggest that *Arc/Arg3.1* presence is necessary for this elimination to occur, our results suggest that *Arc/Arg3.1* presence would actually prevent this elimination. This discrepancy adds to the previously observed dual and opposite roles of *Arc/Arg3.1* in synaptic function, such as its involvement in both LTP and LTD processes. This highlights the view of *Arc/Arg3.1* as a hub protein whose functions change depending on its interaction partners and their different effector mechanisms (Zhang & Bramham, 2021). One candidate partner of *Arc/Arg3.1* that might explain the differences in synapse elimination in the hippocampus and the cerebellum is the differential expression of CaMKII subunits. While the hippocampus is preferentially rich in CaMKIIα, the cerebellum expresses almost exclusively CaMKIIβ (Burgin et al., 1990). Future studies need to address the precise mechanisms of these interactions in the two brain regions and their potential impact on synapse elimination.

On a circuit level, the reductions upon extracellular stimulations in the *stratum radiatum* indicated impaired synaptic excitatory drive from CA3, although reductions of synaptic input from extrahippocampal sources were not ruled out. As a matter of fact, our quantification of synaptic clusters reveals a consistent decrease in stratum LM beginning already at P14, indicating that excitatory drive from the entorhinal cortex is also altered after *Arc/Arg3.1* deletion. Previous research indicates a distinct developmental timeline for hippocampal connections. The temporoammonic pathway, projecting from the entorhinal cortex to the LM layer of CA1, matures earlier than the perforant pathway (innervating the DG and CA3) (Deng et al., 2007; Gomez-Di Cesare et al., 1997; Marty et al., 2002; Super & Soriano, 1994) and the Schaffer collaterals (connecting CA3 to CA1 in stratum radiatum and oriens) (reviewed in Cossart & Khazipov, 2022). This indicates that the effects of early *Arc/Arg3.1* deletion on excitatory transmission are activity and development-dependent, with earlier developing synapses being regulated by *Arc/Arg3.1* sooner.

Interestingly, despite the higher abundance of VGLUT2 positive synapses in the LM layer, and the preferential expression of VGLUT2 during development, these synapses were not altered by *Arc/Arg3.1* deletion. One key difference between VGLUT1 and VGLUT2 synapses is their probability of release. VGLUT2 is expressed at synapses with a high release probability and VGLUT1 at synapses with lower probabilities of release (Fremeau et al., 2001; Weston et al., 2011). A study by Santos et al. (2014) evaluated the proteins interacting with the c-terminal tail

of VGLUT1, which differentiates it from the other VGLUT isoforms. Their results showed that VGLUT1 interacts with actin-cytoskeletal adaptor proteins, including some that have been previously linked to Arc/Arg3.1 such as endophilin and the clathrin adaptor protein 2 (AP-2) (Wall & Correa, 2018). Further research is needed to pinpoint the precise mechanisms underlying the effects of Arc/Arg3.1 specifically on VGLUT1 positive synapses.

The observed alterations in excitatory transmission in the early-cKO and the fact that inhibitory transmission also undergoes substantial maturation during the first postnatal month, motivated us to evaluate inhibitory synaptic clusters in this mouse line. The results showed no changes at P14 but a massive reduction of inhibitory clusters at P28. However, the functional evaluation of inhibitory transmission using patch-clamp recordings revealed no alterations in any of their physiological properties. A possible explanation for this discrepancy could be a threshold too permissive for the colocalization of the pre and postsynaptic markers, potentially leading to inaccurate synapse quantification. However, several factors argue against this limitation. First, the reduction in the number of clusters was observed at P28 but not at P14 indicating that the effects are age-specific. Second, the colocalization threshold was identical to the one used for the detection of excitatory clusters, which showed high consistency with the electrophysiological data. Finally, the distribution of synapses along the axodendritic axis aligns with previous reports, showing the highest density of inhibitory synapses in the perisomatic region and the LM layer (Megias et al., 2001). Taken together, these observations collectively support the reliability of our quantification.

We observed that not only the number of colocalized VGAT with gephyrin or GABAγ2 but also the total number of gephyrin and GABAγ2 clusters are significantly reduced in early-cKO mice (data not shown). A possible explanation for the discrepancy between the number of clusters and the functional results is that inhibitory synapses in early-cKO cells might still function through an alternative mechanism, independent of gephyrin or GABAγ2. Supporting this, there are reports on the existence of GABAergic synapses lacking gephyrin (Groeneweg et al., 2018; Kneussel et al., 2001; Panzanelli et al., 2011). Levi et al. (2004) showed unaltered mIPSC frequency in hippocampal neurons from gephyrin KO mice and proposed the dystrophin-glycoprotein complex as an alternative to gephyrin for clustering GABAAR at synapses. However, the role of dystrophin as a scaffolding protein remains controversial, as its levels do not always correlate with GABAergic strength (Groeneweg et al., 2018).

Yet another possibility is that the reductions in the number of inhibitory synaptic clusters correspond to the elimination of silent or non-functional synapses. Silent synapses have been

well-described in excitatory transmission, these synapses have a normal structure with functional NMDAR, but they lack function either via presynaptic mechanisms; by a failure to release neurotransmitter, or via postsynaptic mechanisms; by a lack of surface AMPA receptors (Gasparini et al., 2000; Malenka & Nicoll, 1997). In CA1, silent excitatory synapses seem to be particularly prevalent during early development (Durand et al., 1996; Gasparini et al., 2000). While there are no studies of inhibitory silent synapses in the hippocampus, one of the first reports on silent synapses described them in glycinergic synapses in the frog neuromuscular junction. In this preparation, the authors observed that up to 25 % of paired recordings yielded no postsynaptic responses, despite the observation of a normal number of synaptic contacts upon anatomical reconstructions. Furthermore, they revealed that these synapses were postsynaptically silent, as a postsynaptic injection of cAMP was capable of converting a silent synaptic connection into a functional one, presumably due to upregulation of glycine receptors (Faber et al., 1991).

Taken together, our findings in the WT animals showed developmental changes from the second to the fourth week that were very consistent with the ones reported in the literature. Regarding the effects of Arc/Arg3.1 deletion on the various stages of development, our results indicate that Arc/Arg3.1 does not play a role in the maturation of gross dendritic morphology or passive membrane properties. Intriguingly, while our previous study identified deficits in the germline KO in the adult brain, these animals did not exhibit substantial alterations during the first postnatal month. This could indicate that the alterations observed in the adult brain, although originating before P14, only manifest at later stages of development, suggesting that the impact of Arc/Arg3.1 deletion on excitatory synaptic transmission might become more pronounced as synaptic circuits mature and undergo activity-dependent synaptic remodeling. Supporting this notion, we observed that despite the complete absence of Arc/Arg3.1 in the early-cKO already at P14, the alterations in excitatory transmission were only obvious at P28.

Consistent with our previous findings in adult brains, where neither spatial navigation nor hippocampal oscillatory activity were affected, late Arc/Arg3.1 deletion did not alter any of the parameters we evaluated. This further supports the critical role of Arc/Arg3.1 expression before postnatal day 21 (in both germline and early-deletion models) in shaping hippocampal circuit development, albeit likely through distinct mechanisms in each case.

5 Concluding Remarks and Outlook

Part I of this thesis aimed to investigate the effect of Arc/Arg3.1 deletion during early development on the microarchitecture of synaptic transmission in the adult hippocampus. Our results revealed that deletion after P21 results in a phenotype comparable to that of a WT animal. In contrast, deletion before P21 permanently alters the hippocampal network, though through slightly different mechanisms between germline and early Arc/Arg3.1 deletions. Both types of deletions shared a reduced excitatory drive from CA3, reductions in the expression of PSD-95, and decreases in excitatory synaptic clusters along the axodendritic axis. The germline deletion resulted in stronger alterations in the kinetics of excitatory currents, an effect associated with lower expression of TARP γ 8 in the postsynaptic density. These findings support recent reports pinpointing an indirect interaction between PSD-95 and Arc/Arg3.1.

Moreover, we discovered that, despite the frequent association of *Arc/Arg3.1* with excitatory synapses, its germline deletion permanently alters inhibitory transmission as well. This specifically involves slowing the kinetics of inhibitory currents in a location-specific manner, preferentially targeting perisomatic synapses. We speculate that this effect might occur via an interaction of *Arc/Arg3.1* with CaMKII, which in turn modulates the phosphorylation state of GABAARs, ultimately shaping the kinetics of inhibitory currents. These results align well with previously observed alterations in oscillatory activity and spatial navigation.

Part II aimed to evaluate the efficacy of a recently developed laser ablation system for accurately dissecting specific structures in the mouse brain. The second purpose was to compare the proteomic profiles of non-stimulated hippocampi of WT and germline Arc/Arg3.1 KO mice, focusing on hippocampal subfield differences. Our results showed strong differences between the proteomes of the hippocampal subfields, which aligned well with previous reports using transcriptomics and even better with other studies using proteomics. Furthermore, the molecular profiles of the different subfields showed noticeable agreement with their functional differences. This demonstrated that laser ablation can successfully isolate different brain regions for mass spectrometry-based proteomics.

Importantly, the comparison between WT and *Arc/Arg3.1* KO mice revealed a relatively low number of *Arc/Arg3.1*-regulated proteins under baseline conditions. Given the activity-dependent nature of *Arc/Arg3.1* and its consequent low baseline expression, we anticipate that stronger differences would be observed under conditions of high synaptic activity.

Nevertheless, we observed that Arc/Arg3.1 deletion alters the hippocampal proteomic profile in a subfield-specific way. This specificity aligned well with the functional differences of the various subfields and with previous observations on the differential timelines of Arc/Arg3.1 expression in these subfields. Additionally, we identified several new, exciting molecules modulated by Arc/Arg3.1 in the different hippocampal subfields. Enrichment analysis revealed that many of these molecules participate in biological processes often associated with Arc/Arg3.1, with protein transport being the most prevalent among them.

Finally, while Parts I and II focused on the consequences of *Arc/Arg3.1* deletion during the first postnatal month for the adult brain, Part III of this thesis aimed to investigate the potential changes induced by *Arc/Arg3.1* deletion during this period that support the alterations observed in the adult brain. Our results showed that *Arc/Arg3.1* does not alter the maturation of gross dendritic morphology or the development of passive membrane properties. Moreover, we corroborated that there were no changes upon late *Arc/Arg3.1* deletion in any of the parameters we evaluated.

In contrast, we observed decreases in the duration of the action potential (AP) in germline KO neurons, possibly due to the regulation of Na+ and K+ channels. Surprisingly, we did not observe any changes in excitatory transmission in these animals at any of the time points evaluated. In striking contrast, early Arc/Arg3.1 deletion resulted in a substantial reduction in the strength and number of excitatory synapses at P28. This effect is likely the result of active elimination rather than a failure to create new synapses in this group. Furthermore, we observed clear reductions in the number of inhibitory synaptic puncta in these animals; however, these reductions were not observed at a functional level, indicating that the synapses eliminated were silent or immature. These findings highlight that despite the similar deficits observed in the adult brain in germline and early-cKO, the mechanisms differ in the two lines.

The findings of the three parts of this thesis provide valuable insight into the mechanisms by which natural upregulation of Arc/Arg3.1 during the first postnatal month modulates the wiring of hippocampal circuits, resulting in altered hippocampal rhythms and impaired spatial learning and navigation in adulthood. Several elements drawn from the different parts of the study complement each other, though some findings have opened new questions that should be addressed in future research.

For instance, in Part II, we identified IQsec3 and GABA_Aβ1 as *Arc/Arg3.1*-regulated proteins, supporting a role for *Arc/Arg3.1* in inhibitory synaptic transmission. Additionally, our proteomic profile results revealed small yet significant reductions in PSD-95 in the dorsal

hippocampus, an effect corroborated by western blot analysis. This result confirms the reductions observed in Part I, both in synaptic clusters and through western blot analysis of the entire hippocampus. This consistency was also observed for all other proteins evaluated via western blot analysis in Part I, none of which were found to be regulated by Arc/Arg3.1 in the proteomic analysis either.

Intriguingly, we did not detect changes in VGAT in our proteomic study. However, given that the alterations in cluster intensity we observed were limited to the pyramidal and LM layers, it is possible that these changes are not large enough to be detected in a global CA1 sample extracted via laser ablation.

Additionally, in Part III, we observed that early *Arc/Arg3.1* deletion preferentially affected VGLUT1-containing synapses. Consistent with this, the proteomic profiles showed downregulation of VGLUT1 in *Arc/Arg3.1* KO specifically in CA1, while VGLUT2 appeared downregulated in the DG. It remains to be tested whether *Arc/Arg3.1* alters baseline synaptic transmission in the DG. If so, it would be interesting to evaluate if it specifically targets VGLUT2 synapses there.

Collectively, our results show that late Arc/Arg3.1 deletion does not alter hippocampal wiring, neither in the adult brain nor during the first postnatal month. In contrast, germline and early deletions resulted in clear alterations, though these alterations were not the same in the juvenile and adult brains. In the adult brain, we observed an acceleration of the sEPSC kinetics in the germline KO, associated with lower PSD-95 expression and decreases in TARP γ 8 in the postsynaptic density. However, these changes were not detected during the first postnatal month. We found this surprising considering that in Part I, the lack of effect on TARP γ 8 localization in the early-cKO indicated that Arc/Arg3.1 expression during the first postnatal week is crucial for an interaction between these two proteins.

However, it is possible that the kinetics of AMPA currents are not strongly modulated by the presence of TARPγ8 in the PSD during this early period. Alternatively, a third molecule could regulate this interaction, developing at a later stage, and therefore the effects of *Arc/Arg3.1* are only observed then. A proteomic analysis of the germline and early-cKO mice at P28 could help answer these questions in future studies.

On the other hand, in the early-cKO, we observed clear reductions in sEPSC amplitude and frequency by the end of the first month, whereas in the adult, we only observed a tendency towards faster kinetics in this mouse line. This could indicate that perhaps early *Arc/Arg3.1*

deletion accelerates synapse elimination that would eventually occur in WT mice as well, leading to unaltered sEPSCs observed in the adult. Future studies evaluating a time point after P28 but before adulthood could help answer this question. Alternatively, the decreases in sEPSCs might only be detectable at P28 because baseline synaptic activity is higher and, therefore, more vulnerable to the lack of *Arc/Arg3.1*.

6 References

- Advani, R. J., Yang, B., Prekeris, R., Lee, K. C., Klumperman, J., & Scheller, R. H. (1999). VAMP-7 mediates vesicular transport from endosomes to lysosomes. *J Cell Biol*, 146(4), 765-776. https://doi.org/10.1083/jcb.146.4.765
- Altman, J., Brunner, R. L., & Bayer, S. A. (1973). The hippocampus and behavioral maturation. *Behav Biol*, *8*(5), 557-596. https://doi.org/10.1016/s0091-6773(73)80144-0
- Amaral, D., & Lavenex, P. (2006). Hippocampal Neuroanatomy. In P. Andersen, R. Morris, D. Amaral, T. Bliss, & J. O'Keefe (Eds.), *The hippocampus book* (pp. 0). Oxford University Press. https://doi.org/10.1093/acprof:oso/9780195100273.003.0003
- Andreasen, M., & Lambert, J. D. (1998). Factors determining the efficacy of distal excitatory synapses in rat hippocampal CA1 pyramidal neurones. *J Physiol*, 507 (Pt 2)(Pt 2), 441-462. https://doi.org/10.1111/j.1469-7793.1998.441bt.x
- Andrews, S. J., Freeman, J. H., Jr., Carter, C. S., & Stanton, M. E. (1995). Ontogeny of eyeblink conditioning in the rat: auditory frequency and discrimination learning effects. *Dev Psychobiol*, 28(6), 307-320. https://doi.org/10.1002/dev.420280602
- Angevine Jr, J. B. (1965). Time of neuron origin in the hippocampal region: an autoradiographic study in the mouse. *Experimental Neurology*.
- Ascher, P., & Nowak, L. (1988). The Role of Divalent-Cations in the N-Methyl-D-Aspartate Responses of Mouse Central Neurons in Culture. *Journal of Physiology-London*, 399, 247-266. <Go to ISI>://WOS:A1988N034600015
- Azevedo, R., Jacquemin, C., Villain, N., Fenaille, F., Lamari, F., & Becher, F. (2022). Mass Spectrometry for Neurobiomarker Discovery: The Relevance of Post-Translational Modifications. *Cells*, *11*(8). https://doi.org/10.3390/cells11081279
- Banks, M. I., Hardie, J. B., & Pearce, R. A. (2002). Development of GABA(A) receptor-mediated inhibitory postsynaptic currents in hippocampus. *J Neurophysiol*, 88(6), 3097-3107. https://doi.org/10.1152/jn.00026.2002
- Banks, M. I., Li, T. B., & Pearce, R. A. (1998). The synaptic basis of GABA. *Journal of Neuroscience*, 18(4), 1305-1317. <Go to ISI>://WOS:000071825800012
- Barondes, S. H., & Cohen, H. D. (1966). Puromycin effect on successive phases of memory storage. *Science*, *151*(3710), 594-595. https://doi.org/10.1126/science.151.3710.594
- Bats, C., Groc, L., & Choquet, D. (2007). The interaction between Stargazin and PSD-95 regulates AMPA receptor surface trafficking. *Neuron*, *53*(5), 719-734. https://doi.org/10.1016/j.neuron.2007.01.030
- Bayer, S. A. (1980). Development of the hippocampal region in the rat. I. Neurogenesis examined with 3H-thymidine autoradiography. *J Comp Neurol*, 190(1), 87-114. https://doi.org/10.1002/cne.901900107
- Becq, H., Jorquera, I., Ben-Ari, Y., Weiss, S., & Represa, A. (2005). Differential properties of dentate gyrus and CA1 neural precursors. *J Neurobiol*, 62(2), 243-261. https://doi.org/10.1002/neu.20089
- Beique, J. C., Na, Y., Kuhl, D., Worley, P. F., & Huganir, R. L. (2011). Arc-dependent synapse-specific homeostatic plasticity. *Proc Natl Acad Sci U S A, 108*(2), 816-821. https://doi.org/10.1073/pnas.1017914108
- Bekenstein, J. W., & Lothman, E. W. (1991). An in vivo study of the ontogeny of long-term potentiation (LTP) in the CA1 region and in the dentate gyrus of the rat hippocampal formation. *Brain Res Dev Brain Res*, 63(1-2), 245-251. https://doi.org/10.1016/0165-3806(91)90084-v
- Bellocchio, E. E., Reimer, R. J., Fremeau, R. T., Jr., & Edwards, R. H. (2000). Uptake of glutamate into synaptic vesicles by an inorganic phosphate transporter. *Science*, *289*(5481), 957-960. https://doi.org/10.1126/science.289.5481.957

- Benavides-Piccione, R., Regalado-Reyes, M., Fernaud-Espinosa, I., Kastanauskaite, A., Tapia-Gonzalez, S., Leon-Espinosa, G., Rojo, C., Insausti, R., Segev, I., & DeFelipe, J. (2020). Differential Structure of Hippocampal CA1 Pyramidal Neurons in the Human and Mouse. *Cereb Cortex*, *30*(2), 730-752. https://doi.org/10.1093/cercor/bbz122
- Berry, K. P., & Nedivi, E. (2017). Spine Dynamics: Are They All the Same? *Neuron*, *96*(1), 43-55. https://doi.org/10.1016/j.neuron.2017.08.008
- Bessieres, B., Travaglia, A., Mowery, T. M., Zhang, X., & Alberini, C. M. (2020). Early life experiences selectively mature learning and memory abilities. *Nat Commun*, *11*(1), 628. https://doi.org/10.1038/s41467-020-14461-3
- Bhatt, D. H., Zhang, S., & Gan, W. B. (2009). Dendritic spine dynamics. *Annu Rev Physiol*, 71, 261-282. https://doi.org/10.1146/annurev.physiol.010908.163140
- Bjerknes, T. L., Moser, E. I., & Moser, M. B. (2014). Representation of geometric borders in the developing rat. *Neuron*, 82(1), 71-78. https://doi.org/10.1016/j.neuron.2014.02.014
- Blankenship, A. G., & Feller, M. B. (2010). Mechanisms underlying spontaneous patterned activity in developing neural circuits. *Nat Rev Neurosci*, *11*(1), 18-29. https://doi.org/10.1038/nrn2759
- Bliss, T. V., & Collingridge, G. L. (1993). A synaptic model of memory: long-term potentiation in the hippocampus. *Nature*, *361*(6407), 31-39. https://doi.org/10.1038/361031a0
- Bliss, T. V., & Lomo, T. (1973). Long-lasting potentiation of synaptic transmission in the dentate area of the anaesthetized rabbit following stimulation of the perforant path. *J Physiol*, 232(2), 331-356. https://doi.org/10.1113/jphysiol.1973.sp010273
- Bormann, J., Hamill, O. P., & Sakmann, B. (1987). Mechanism of anion permeation through channels gated by glycine and gamma-aminobutyric acid in mouse cultured spinal neurones. *J Physiol*, 385, 243-286. https://doi.org/10.1113/jphysiol.1987.sp016493
- Boshans, R. L., Szanto, S., van Aelst, L., & D'Souza-Schorey, C. (2000). ADP-ribosylation factor 6 regulates actin cytoskeleton remodeling in coordination with Rac1 and RhoA. *Mol Cell Biol*, 20(10), 3685-3694. https://doi.org/10.1128/MCB.20.10.3685-3694.2000
- Boyce, R., Glasgow, S. D., Williams, S., & Adamantidis, A. (2016). Causal evidence for the role of REM sleep theta rhythm in contextual memory consolidation. *Science*, *352*(6287), 812-816. https://doi.org/10.1126/science.aad5252
- Boyer, C., Schikorski, T., & Stevens, C. F. (1998). Comparison of hippocampal dendritic spines in culture and in brain. *J Neurosci*, 18(14), 5294-5300. https://doi.org/10.1523/JNEUROSCI.18-14-05294.1998
- Bramham, C. R., Alme, M. N., Bittins, M., Kuipers, S. D., Nair, R. R., Pai, B., Panja, D., Schubert, M., Soule, J., Tiron, A., & Wibrand, K. (2010). The Arc of synaptic memory. *Exp Brain Res*, 200(2), 125-140. https://doi.org/10.1007/s00221-009-1959-2
- Brandt, M. D., Jessberger, S., Steiner, B., Kronenberg, G., Reuter, K., Bick-Sander, A., von der Behrens, W., & Kempermann, G. (2003). Transient calretinin expression defines early postmitotic step of neuronal differentiation in adult hippocampal neurogenesis of mice. *Mol Cell Neurosci*, 24(3), 603-613. https://doi.org/10.1016/s1044-7431(03)00207-0
- Brickley, S. G., & Mody, I. (2012). Extrasynaptic GABA
- Receptors: Their Function in the CNS and Implications for Disease. *Neuron*, 73(1), 23-34. https://doi.org/10.1016/j.neuron.2011.12.012
- Brunel, N., & Wang, X. J. (2003). What determines the frequency of fast network oscillations with irregular neural discharges? I. Synaptic dynamics and excitation-inhibition balance. *J Neurophysiol*, 90(1), 415-430. https://doi.org/10.1152/jn.01095.2002
- Brunig, I., Scotti, E., Sidler, C., & Fritschy, J. M. (2002). Intact sorting, targeting, and clustering of gamma-aminobutyric acid A receptor subtypes in hippocampal neurons in vitro. *J Comp Neurol*, 443(1), 43-55. https://doi.org/10.1002/cne.10102
- Budzinska, M. I., Villarroel-Campos, D., Golding, M., Weston, A., Collinson, L., Snijders, A. P., & Schiavo, G. (2020). PTPN23 binds the dynein adaptor BICD1 and is required for endocytic sorting of neurotrophin receptors. *J Cell Sci*, 133(6). https://doi.org/10.1242/jcs.242412

- Buhl, D. L., & Buzsaki, G. (2005). Developmental emergence of hippocampal fast-field "ripple" oscillations in the behaving rat pups. *Neuroscience*, *134*(4), 1423-1430. https://doi.org/10.1016/j.neuroscience.2005.05.030
- Burgin, K. E., Waxham, M. N., Rickling, S., Westgate, S. A., Mobley, W. C., & Kelly, P. T. (1990). In situ hybridization histochemistry of Ca2+/calmodulin-dependent protein kinase in developing rat brain. *J Neurosci*, *10*(6), 1788-1798. https://doi.org/10.1523/JNEUROSCI.10-06-01788.1990
- Bush, D., Barry, C., & Burgess, N. (2014). What do grid cells contribute to place cell firing? *Trends Neurosci*, *37*(3), 136-145. https://doi.org/10.1016/j.tins.2013.12.003
- Buzsaki, G. (1984a). Feed-forward inhibition in the hippocampal formation. *Prog Neurobiol*, 22(2), 131-153. https://doi.org/10.1016/0301-0082(84)90023-6
- Buzsaki, G. (1984b). Long-term changes of hippocampal sharp-waves following high frequency afferent activation. *Brain Res*, 300(1), 179-182. https://doi.org/10.1016/0006-8993(84)91356-8
- Buzsaki, G. (2002). Theta oscillations in the hippocampus. *Neuron*, *33*(3), 325-340. https://doi.org/10.1016/s0896-6273(02)00586-x
- Buzsaki, G. (2005). Theta rhythm of navigation: link between path integration and landmark navigation, episodic and semantic memory. *Hippocampus*, *15*(7), 827-840. https://doi.org/10.1002/hipo.20113
- Buzsaki, G. (2015). Hippocampal sharp wave-ripple: A cognitive biomarker for episodic memory and planning. *Hippocampus*, *25*(10), 1073-1188. https://doi.org/10.1002/hipo.22488
- Buzsáki, G., & Wang, X. J. (2012). Mechanisms of Gamma Oscillations. *Annual Review of Neuroscience, Vol 35*, 35, 203-225. https://doi.org/10.1146/annurev-neuro-062111-150444
- Campillos, M., Doerks, T., Shah, P. K., & Bork, P. (2006). Computational characterization of multiple Gag-like human proteins. *Trends Genet*, *22*(11), 585-589. https://doi.org/10.1016/j.tig.2006.09.006
- Cao, C., Rioult-Pedotti, M. S., Migani, P., Yu, C. J., Tiwari, R., Parang, K., Spaller, M. R., Goebel, D. J., & Marshall, J. (2013). Impairment of TrkB-PSD-95 signaling in Angelman syndrome. *PLoS Biol*, 11(2), e1001478. https://doi.org/10.1371/journal.pbio.1001478
- Carr, M. F., Jadhav, S. P., & Frank, L. M. (2011). Hippocampal replay in the awake state: a potential substrate for memory consolidation and retrieval. *Nat Neurosci*, *14*(2), 147-153. https://doi.org/10.1038/nn.2732
- Carta, M., Fièvre, S., Gorlewicz, A., & Mulle, C. (2014). Kainate receptors in the hippocampus. *European Journal of Neuroscience*, *39*(11), 1835-1844. https://doi.org/10.1111/ejn.12590
- Carulli, D., Pizzorusso, T., Kwok, J. C., Putignano, E., Poli, A., Forostyak, S., Andrews, M. R., Deepa, S. S., Glant, T. T., & Fawcett, J. W. (2010). Animals lacking link protein have attenuated perineuronal nets and persistent plasticity. *Brain*, 133(Pt 8), 2331-2347. https://doi.org/10.1093/brain/awq145
- Castro Gómez, M. S. (2016). Developmental and adult expression of Arc/Arg3. 1 in corticolimbic structures determines memory and emotional control [Ph.D. Thesis, Universität Hamburg]. Staats-und Universitätsbibliothek Hamburg Carl von Ossietzky.
- Chaerkady, R., Kerr, C. L., Marimuthu, A., Kelkar, D. S., Kashyap, M. K., Gucek, M., Gearhart, J. D., & Pandey, A. (2009). Temporal analysis of neural differentiation using quantitative proteomics. *J Proteome Res*, 8(3), 1315-1326. https://doi.org/10.1021/pr8006667
- Chan, J. N., Sanchez-Vidana, D. I., Anoopkumar-Dukie, S., Li, Y., & Benson Wui-Man, L. (2022). RNA-binding protein signaling in adult neurogenesis. *Front Cell Dev Biol*, *10*, 982549. https://doi.org/10.3389/fcell.2022.982549
- Chancey, J. H., Adlaf, E. W., Sapp, M. C., Pugh, P. C., Wadiche, J. I., & Overstreet-Wadiche, L. S. (2013). GABA depolarization is required for experience-dependent synapse unsilencing in adult-born neurons. *J Neurosci*, 33(15), 6614-6622. https://doi.org/10.1523/JNEUROSCI.0781-13.2013
- Chattopadhyaya, B., Di Cristo, G., Higashiyama, H., Knott, G. W., Kuhlman, S. J., Welker, E., & Huang, Z. J. (2004). Experience and activity-dependent maturation of perisomatic GABAergic innervation in primary visual cortex during a postnatal critical period. *J Neurosci*, *24*(43), 9598-9611. https://doi.org/10.1523/JNEUROSCI.1851-04.2004

- Chawla, M. K., Gray, D. T., Nguyen, C., Dhaliwal, H., Zempare, M., Okuno, H., Huentelman, M. J., & Barnes, C. A. (2018). Seizure-Induced Arc mRNA Expression Thresholds in Rat Hippocampus and Perirhinal Cortex. *Front Syst Neurosci*, *12*, 53. https://doi.org/10.3389/fnsys.2018.00053
- Chen, L., Chetkovich, D. M., Petralia, R. S., Sweeney, N. T., Kawasaki, Y., Wenthold, R. J., Bredt, D. S., & Nicoll, R. A. (2000). Stargazin regulates synaptic targeting of AMPA receptors by two distinct mechanisms. *Nature*, 408(6815), 936-943. https://doi.org/10.1038/35050030
- Chen, X., Jia, B., Araki, Y., Liu, B., Ye, F., Huganir, R., & Zhang, M. (2022). Arc weakens synapses by dispersing AMPA receptors from postsynaptic density via modulating PSD phase separation. *Cell Res*, 32(10), 914-930. https://doi.org/10.1038/s41422-022-00697-9
- Chen, X., Levy, J. M., Hou, A., Winters, C., Azzam, R., Sousa, A. A., Leapman, R. D., Nicoll, R. A., & Reese, T. S. (2015). PSD-95 family MAGUKs are essential for anchoring AMPA and NMDA receptor complexes at the postsynaptic density. *Proc Natl Acad Sci U S A, 112*(50), E6983-6992. https://doi.org/10.1073/pnas.1517045112
- Chinnakkaruppan, A., Wintzer, M. E., McHugh, T. J., & Rosenblum, K. (2014). Differential contribution of hippocampal subfields to components of associative taste learning. *J Neurosci*, *34*(33), 11007-11015. https://doi.org/10.1523/JNEUROSCI.0956-14.2014
- Cho, C. H., St-Gelais, F., Zhang, W., Tomita, S., & Howe, J. R. (2007). Two families of TARP isoforms that have distinct effects on the kinetic properties of AMPA receptors and synaptic currents. *Neuron*, *55*(6), 890-904. https://doi.org/10.1016/j.neuron.2007.08.024
- Chowdhury, S., Shepherd, J. D., Okuno, H., Lyford, G., Petralia, R. S., Plath, N., Kuhl, D., Huganir, R. L., & Worley, P. F. (2006). Arc/Arg3.1 interacts with the endocytic machinery to regulate AMPA receptor trafficking. *Neuron*, *52*(3), 445-459. https://doi.org/10.1016/j.neuron.2006.08.033
- Cid, E., Marquez-Galera, A., Valero, M., Gal, B., Medeiros, D. C., Navarron, C. M., Ballesteros-Esteban, L., Reig-Viader, R., Morales, A. V., Fernandez-Lamo, I., Gomez-Dominguez, D., Sato, M., Hayashi, Y., Bayes, A., Barco, A., Lopez-Atalaya, J. P., & de la Prida, L. M. (2021). Sublayer- and cell-type-specific neurodegenerative transcriptional trajectories in hippocampal sclerosis. *Cell Rep*, 35(10), 109229. https://doi.org/10.1016/j.celrep.2021.109229
- Claiborne, B. J., Amaral, D. G., & Cowan, W. M. (1986). A light and electron microscopic analysis of the mossy fibers of the rat dentate gyrus. *J Comp Neurol*, 246(4), 435-458. https://doi.org/10.1002/cne.902460403
- Clayton, D. A., Mesches, M. H., Alvarez, E., Bickford, P. C., & Browning, M. D. (2002). A hippocampal NR2B deficit can mimic age-related changes in long-term potentiation and spatial learning in the Fischer 344 rat. *J Neurosci*, 22(9), 3628-3637. https://doi.org/10.1523/JNEUROSCI.22-09-03628.2002
- Cobb, S. R., Buhl, E. H., Halasy, K., Paulsen, O., & Somogyi, P. (1995). Synchronization of neuronal activity in hippocampus by individual GABAergic interneurons. *Nature*, *378*(6552), 75-78. https://doi.org/10.1038/378075a0
- Colgin, L. L. (2016). Rhythms of the hippocampal network. *Nat Rev Neurosci*, *17*(4), 239-249. https://doi.org/10.1038/nrn.2016.21
- Colgin, L. L., Denninger, T., Fyhn, M., Hafting, T., Bonnevie, T., Jensen, O., Moser, M. B., & Moser, E. I. (2009). Frequency of gamma oscillations routes flow of information in the hippocampus. *Nature*, *462*(7271), 353-357. https://doi.org/10.1038/nature08573
- Colgin, L. L., & Moser, E. I. (2010). Gamma oscillations in the hippocampus. *Physiology (Bethesda)*, 25(5), 319-329. https://doi.org/10.1152/physiol.00021.2010
- Colucci-D'Amato, L., Speranza, L., & Volpicelli, F. (2020). Neurotrophic Factor BDNF, Physiological Functions and Therapeutic Potential in Depression, Neurodegeneration and Brain Cancer. *Int J Mol Sci*, 21(20). https://doi.org/10.3390/ijms21207777
- Cossart, R., & Khazipov, R. (2022). How development sculpts hippocampal circuits and function. *Physiol Rev*, 102(1), 343-378. https://doi.org/10.1152/physrev.00044.2020
- Costa, P. F. (1996). The kinetic parameters of sodium currents in maturing acutely isolated rat hippocampal CA1 neurones. *Brain Res Dev Brain Res*, 91(1), 29-40. https://doi.org/10.1016/0165-3806(95)00159-x

- Costa, P. F., Santos, A. I., & Ribeiro, M. A. (1994). Potassium currents in acutely isolated maturing rat hippocampal CA1 neurones. *Brain Res Dev Brain Res*, 83(2), 216-223. https://doi.org/10.1016/0165-3806(94)00140-5
- Csicsvari, J., Hirase, H., Mamiya, A., & Buzsaki, G. (2000). Ensemble patterns of hippocampal CA3-CA1 neurons during sharp wave-associated population events. *Neuron*, *28*(2), 585-594. https://doi.org/10.1016/s0896-6273(00)00135-5
- Curran, O. E., Qiu, Z., Smith, C., & Grant, S. G. N. (2021). A single-synapse resolution survey of PSD95-positive synapses in twenty human brain regions. *Eur J Neurosci*, *54*(8), 6864-6881. https://doi.org/10.1111/ejn.14846
- Cutsuridis, V., & Taxidis, J. (2013). Deciphering the role of CA1 inhibitory circuits in sharp wave-ripple complexes. *Front Syst Neurosci*, *7*, 13. https://doi.org/10.3389/fnsys.2013.00013
- Czeh, B., Varga, Z. K., Henningsen, K., Kovacs, G. L., Miseta, A., & Wiborg, O. (2015). Chronic stress reduces the number of GABAergic interneurons in the adult rat hippocampus, dorsal-ventral and region-specific differences. *Hippocampus*, *25*(3), 393-405. https://doi.org/10.1002/hipo.22382
- Danglot, L., Triller, A., & Bessis, A. (2003). Association of gephyrin with synaptic and extrasynaptic GABAA receptors varies during development in cultured hippocampal neurons. *Mol Cell Neurosci*, 23(2), 264-278. https://doi.org/10.1016/s1044-7431(03)00069-1
- Danglot, L., Triller, A., & Marty, S. (2006). The development of hippocampal interneurons in rodents. *Hippocampus*, *16*(12), 1032-1060. https://doi.org/10.1002/hipo.20225
- Davolio, C., & Greenamyre, J. T. (1995). Selective Vulnerability of the Ca1 Region of Hippocampus to the Indirect Excitotoxic Effects of Malonic-Acid. *Neuroscience Letters*, 192(1), 29-32. https://doi.org/Doi 10.1016/0304-3940(95)11600-2
- Deacon, R. M., Bannerman, D. M., Kirby, B. P., Croucher, A., & Rawlins, J. N. (2002). Effects of cytotoxic hippocampal lesions in mice on a cognitive test battery. *Behav Brain Res*, *133*(1), 57-68. https://doi.org/10.1016/s0166-4328(01)00451-x
- Deller, T., Adelmann, G., Nitsch, R., & Frotscher, M. (1996). The alvear pathway of the rat hippocampus. *Cell Tissue Res*, 286(3), 293-303. https://doi.org/10.1007/s004410050699
- Delpech, J. C., Pathak, D., Varghese, M., Kalavai, S. V., Hays, E. C., Hof, P. R., Johnson, W. E., Ikezu, S., Medalla, M., Luebke, J. I., & Ikezu, T. (2021). Wolframin-1-expressing neurons in the entorhinal cortex propagate tau to CA1 neurons and impair hippocampal memory in mice. *Sci Transl Med*, 13(611), eabe8455. https://doi.org/10.1126/scitranslmed.abe8455
- Deng, J. B., Yu, D. M., Wu, P., & Li, M. S. (2007). The tracing study of developing entorhino-hippocampal pathway. *Int J Dev Neurosci*, 25(4), 251-258. https://doi.org/10.1016/j.ijdevneu.2007.03.002
- Dolleman-Van Der Weel, M. J., & Witter, M. P. (1996). Projections from the nucleus reuniens thalami to the entorhinal cortex, hippocampal field CA1, and the subiculum in the rat arise from different populations of neurons. *J Comp Neurol*, 364(4), 637-650. https://doi.org/10.1002/(SICI)1096-9861(19960122)364:4<637::AID-CNE3>3.0.CO;2-4
- Domjan, M. (2018). Basic concepts and definitions. In *The essentials of conditioning and learning, 4th ed.* (pp. 3-14). American Psychological Association. https://doi.org/10.1037/0000057-001
- Donai, H., Sugiura, H., Ara, D., Yoshimura, Y., Yamagata, K., & Yamauchi, T. (2003). Interaction of Arc with CaM kinase II and stimulation of neurite extension by Arc in neuroblastoma cells expressing CaM kinase II. *Neurosci Res*, 47(4), 399-408. https://doi.org/10.1016/j.neures.2003.08.004
- Donato, F., Jacobsen, R. I., Moser, M. B., & Moser, E. I. (2017). Stellate cells drive maturation of the entorhinal-hippocampal circuit. *Science*, *355*(6330). https://doi.org/10.1126/science.aai8178
- Dong, H. W., Swanson, L. W., Chen, L., Fanselow, M. S., & Toga, A. W. (2009). Genomic-anatomic evidence for distinct functional domains in hippocampal field CA1. *Proc Natl Acad Sci U S A*, 106(28), 11794-11799. https://doi.org/10.1073/pnas.0812608106
- Dougherty, K. A. (2020). Differential developmental refinement of the intrinsic electrophysiological properties of CA1 pyramidal neurons from the rat dorsal and ventral hippocampus. *Hippocampus*, 30(3), 233-249. https://doi.org/10.1002/hipo.23152

- Du, F. (2019). Golgi-Cox Staining of Neuronal Dendrites and Dendritic Spines With FD Rapid GolgiStain Kit. *Curr Protoc Neurosci*, 88(1), e69. https://doi.org/10.1002/cpns.69
- Dudai, Y. (1996). Consolidation: fragility on the road to the engram. *Neuron*, *17*(3), 367-370. https://doi.org/10.1016/s0896-6273(00)80168-3
- Dudai, Y. (2004). The neurobiology of consolidations, or, how stable is the engram? *Annu Rev Psychol*, 55, 51-86. https://doi.org/10.1146/annurev.psych.55.090902.142050
- Dumas, T. C., & Foster, T. C. (1995). Developmental increase in CA3-CA1 presynaptic function in the hippocampal slice. *J Neurophysiol*, 73(5), 1821-1828. https://doi.org/10.1152/jn.1995.73.5.1821
- Durand, G. M., Kovalchuk, Y., & Konnerth, A. (1996). Long-term potentiation and functional synapse induction in developing hippocampus. *Nature*, *381*(6577), 71-75. https://doi.org/10.1038/381071a0
- Eriksen, M. S., & Bramham, C. R. (2022). Molecular physiology of Arc/Arg3.1: The oligomeric state hypothesis of synaptic plasticity. *Acta Physiol (Oxf)*, 236(3), e13886. https://doi.org/10.1111/apha.13886
- Faber, D. S., Lin, J. W., & Korn, H. (1991). Silent synaptic connections and their modifiability. *Ann N Y Acad Sci*, 627, 151-164. https://doi.org/10.1111/j.1749-6632.1991.tb25920.x
- Falcón-Moya, R., Martínez-Gallego, I., & Rodríguez-Moreno, A. (2021). Kainate receptor modulation of glutamatergic synaptic transmission in the CA2 region of the hippocampus. *Journal of Neurochemistry*, *158*(5), 1083-1093. https://doi.org/10.1111/jnc.15481
- Ferguson, K. A., & Skinner, F. K. (2022). Hippocampus, model excitatory cells. In *Encyclopedia of Computational Neuroscience* (pp. 1590-1602). Springer.
- Fernandez, E., Collins, M. O., Frank, R. A. W., Zhu, F., Kopanitsa, M. V., Nithianantharajah, J., Lempriere, S. A., Fricker, D., Elsegood, K. A., McLaughlin, C. L., Croning, M. D. R., McLean, C., Armstrong, J. D., Hill, W. D., Deary, I. J., Cencelli, G., Bagni, C., Fromer, M., Purcell, S. M., . . . Grant, S. G. N. (2017). Arc Requires PSD95 for Assembly into Postsynaptic Complexes Involved with Neural Dysfunction and Intelligence. *Cell Rep*, 21(3), 679-691. https://doi.org/10.1016/j.celrep.2017.09.045
- Fiala, J. C., Feinberg, M., Popov, V., & Harris, K. M. (1998). Synaptogenesis via dendritic filopodia in developing hippocampal area CA1. *J Neurosci*, 18(21), 8900-8911. https://doi.org/10.1523/JNEUROSCI.18-21-08900.1998
- Filippini, A., Bonini, D., La Via, L., & Barbon, A. (2017). The Good and the Bad of Glutamate Receptor RNA Editing. *Mol Neurobiol*, *54*(9), 6795-6805. https://doi.org/10.1007/s12035-016-0201-z
- Flexner, L. B., & Flexner, J. B. (1966). Effect of acetoxycycloheximide and of an acetoxycycloheximide-puromycin mixture on cerebral protein synthesis and memory in mice. *Proc Natl Acad Sci U S A*, 55(2), 369-374. https://doi.org/10.1073/pnas.55.2.369
- Fremeau, R. T., Jr., Burman, J., Qureshi, T., Tran, C. H., Proctor, J., Johnson, J., Zhang, H., Sulzer, D., Copenhagen, D. R., Storm-Mathisen, J., Reimer, R. J., Chaudhry, F. A., & Edwards, R. H. (2002). The identification of vesicular glutamate transporter 3 suggests novel modes of signaling by glutamate. *Proc Natl Acad Sci U S A*, 99(22), 14488-14493. https://doi.org/10.1073/pnas.222546799
- Fremeau, R. T., Jr., Troyer, M. D., Pahner, I., Nygaard, G. O., Tran, C. H., Reimer, R. J., Bellocchio, E. E., Fortin, D., Storm-Mathisen, J., & Edwards, R. H. (2001). The expression of vesicular glutamate transporters defines two classes of excitatory synapse. *Neuron*, *31*(2), 247-260. https://doi.org/10.1016/s0896-6273(01)00344-0
- French, P. J., O'Connor, V., Jones, M. W., Davis, S., Errington, M. L., Voss, K., Truchet, B., Wotjak, C., Stean, T., Doyere, V., Maroun, M., Laroche, S., & Bliss, T. V. (2001). Subfield-specific immediate early gene expression associated with hippocampal long-term potentiation in vivo. *Eur J Neurosci*, *13*(5), 968-976. https://doi.org/10.1046/j.0953-816x.2001.01467.x
- Freund, T. F., & Buzsaki, G. (1996). Interneurons of the hippocampus. *Hippocampus*, *6*(4), 347-470. https://doi.org/Doi 10.1002/(Sici)1098-1063(1996)6:4<347::Aid-Hipo1>3.0.Co;2-I

- Fritschy, J. M., Johnson, D. K., Mohler, H., & Rudolph, U. (1998). Independent assembly and subcellular targeting of GABA(A)-receptor subtypes demonstrated in mouse hippocampal and olfactory neurons in vivo. *Neurosci Lett*, 249(2-3), 99-102. https://doi.org/10.1016/s0304-3940(98)00397-8
- Frotscher, M., & Seress, L. (2006). Morphological Development of the Hippocampus. In P. Andersen, R. Morris, D. Amaral, T. Bliss, & J. O'Keefe (Eds.), *The hippocampus book* (pp. 0). Oxford University Press. https://doi.org/10.1093/acprof:oso/9780195100273.003.0004
- Gao, M., Sossa, K., Song, L., Errington, L., Cummings, L., Hwang, H., Kuhl, D., Worley, P., & Lee, H. K. (2010). A specific requirement of Arc/Arg3.1 for visual experience-induced homeostatic synaptic plasticity in mouse primary visual cortex. *J Neurosci*, 30(21), 7168-7178. https://doi.org/10.1523/JNEUROSCI.1067-10.2010
- Gao, X., Castro-Gomez, S., Grendel, J., Graf, S., Susens, U., Binkle, L., Mensching, D., Isbrandt, D., Kuhl, D., & Ohana, O. (2018). Arc/Arg3.1 mediates a critical period for spatial learning and hippocampal networks. *Proc Natl Acad Sci U S A*, 115(49), 12531-12536. https://doi.org/10.1073/pnas.1810125115
- Gasnier, B. (2000). The loading of neurotransmitters into synaptic vesicles. *Biochimie*, 82(4), 327-337. https://doi.org/Doi 10.1016/S0300-9084(00)00221-2
- Gasparini, S., Saviane, C., Voronin, L. L., & Cherubini, E. (2000). Silent synapses in the developing hippocampus: lack of functional AMPA receptors or low probability of glutamate release? *Proc Natl Acad Sci U S A*, *97*(17), 9741-9746. https://doi.org/10.1073/pnas.170032297
- Gerber, K. J., Dammer, E. B., Duong, D. M., Deng, Q., Dudek, S. M., Seyfried, N. T., & Hepler, J. R. (2019). Specific Proteomes of Hippocampal Regions CA2 and CA1 Reveal Proteins Linked to the Unique Physiology of Area CA2. *J Proteome Res*, 18(6), 2571-2584. https://doi.org/10.1021/acs.jproteome.9b00103
- Giglio, A. M., & Storm, J. F. (2014). Postnatal development of temporal integration, spike timing and spike threshold regulation by a dendrotoxin-sensitive K(+) current in rat CA1 hippocampal cells. *Eur J Neurosci*, 39(1), 12-23. https://doi.org/10.1111/ejn.12385
- Girardeau, G., Benchenane, K., Wiener, S. I., Buzsáki, G., & Zugaro, M. B. (2009). Selective suppression of hippocampal ripples impairs spatial memory. *Nature Neuroscience*, *12*(10), 1222-1223. https://doi.org/10.1038/nn.2384
- Glick, S. D., & Greenstein, S. (1973). Comparative learning and memory deficits following hippocampal and caudate lesions in mice. *J Comp Physiol Psychol*, 82(2), 188-194. https://doi.org/10.1037/h0033916
- Gomez-Di Cesare, C. M., Smith, K. L., Rice, F. L., & Swann, J. W. (1997). Axonal remodeling during postnatal maturation of CA3 hippocampal pyramidal neurons. *J Comp Neurol*, *384*(2), 165-180. https://www.ncbi.nlm.nih.gov/pubmed/9215716
- Gorski, J. A., Zeiler, S. R., Tamowski, S., & Jones, K. R. (2003). Brain-derived neurotrophic factor is required for the maintenance of cortical dendrites. *J Neurosci*, *23*(17), 6856-6865. https://doi.org/10.1523/JNEUROSCI.23-17-06856.2003
- Gould, E., Woolley, C. S., Frankfurt, M., & McEwen, B. S. (1990). Gonadal steroids regulate dendritic spine density in hippocampal pyramidal cells in adulthood. *J Neurosci*, *10*(4), 1286-1291. https://doi.org/10.1523/JNEUROSCI.10-04-01286.1990
- Gras, C., Herzog, E., Bellenchi, G. C., Bernard, V., Ravassard, P., Pohl, M., Gasnier, B., Giros, B., & El Mestikawy, S. (2002). A third vesicular glutamate transporter expressed by cholinergic and serotoninergic neurons. *J Neurosci*, 22(13), 5442-5451. https://doi.org/10.1523/JNEUROSCI.22-13-05442.2002
- Greenough, W. T., Juraska, J. M., & Volkmar, F. R. (1979). Maze training effects on dendritic branching in occipital cortex of adult rats. *Behav Neural Biol*, 26(3), 287-297. https://doi.org/10.1016/s0163-1047(79)91278-0
- Greer, P. L., Hanayama, R., Bloodgood, B. L., Mardinly, A. R., Lipton, D. M., Flavell, S. W., Kim, T. K., Griffith, E. C., Waldon, Z., Maehr, R., Ploegh, H. L., Chowdhury, S., Worley, P. F., Steen, J., & Greenberg, M. E. (2010). The Angelman Syndrome protein Ube3A regulates synapse

- development by ubiquitinating arc. *Cell*, *140*(5), 704-716. https://doi.org/10.1016/j.cell.2010.01.026
- Groc, L., Heine, M., Cousins, S. L., Stephenson, F. A., Lounis, B., Cognet, L., & Choquet, D. (2006). NMDA receptor surface mobility depends on NR2A-2B subunits. *Proc Natl Acad Sci U S A, 103*(49), 18769-18774. https://doi.org/10.1073/pnas.0605238103
- Groeneweg, F. L., Trattnig, C., Kuhse, J., Nawrotzki, R. A., & Kirsch, J. (2018). Gephyrin: a key regulatory protein of inhibitory synapses and beyond. *Histochem Cell Biol*, *150*(5), 489-508. https://doi.org/10.1007/s00418-018-1725-2
- Guo, A., Wang, T., Ng, E. L., Aulia, S., Chong, K. H., Teng, F. Y., Wang, Y., & Tang, B. L. (2006). Open brain gene product Rab23: expression pattern in the adult mouse brain and functional characterization. *J Neurosci Res*, *83*(6), 1118-1127. https://doi.org/10.1002/jnr.20788
- Gurden, H., Schiffmann, S. N., Lemaire, M., Bohme, G. A., Parmentier, M., & Schurmans, S. (1998). Calretinin expression as a critical component in the control of dentate gyrus long-term potentiation induction in mice. *Eur J Neurosci*, *10*(9), 3029-3033. https://doi.org/10.1111/j.1460-9568.1998.00373.x
- Guzowski, J. F., Lyford, G. L., Stevenson, G. D., Houston, F. P., McGaugh, J. L., Worley, P. F., & Barnes, C. A. (2000). Inhibition of activity-dependent arc protein expression in the rat hippocampus impairs the maintenance of long-term potentiation and the consolidation of long-term memory. *J Neurosci*, 20(11), 3993-4001. https://doi.org/10.1523/JNEUROSCI.20-11-03993.2000
- Guzowski, J. F., McNaughton, B. L., Barnes, C. A., & Worley, P. F. (1999). Environment-specific expression of the immediate-early gene Arc in hippocampal neuronal ensembles. *Nat Neurosci*, *2*(12), 1120-1124. https://doi.org/10.1038/16046
- Hainmueller, T., Cazala, A., Huang, L. W., & Bartos, M. (2024). Subfield-specific interneuron circuits govern the hippocampal response to novelty in male mice. *Nat Commun*, *15*(1), 714. https://doi.org/10.1038/s41467-024-44882-3
- Hallin, E. I., Eriksen, M. S., Baryshnikov, S., Nikolaienko, O., Grodem, S., Hosokawa, T., Hayashi, Y., Bramham, C. R., & Kursula, P. (2018). Structure of monomeric full-length ARC sheds light on molecular flexibility, protein interactions, and functional modalities. *J Neurochem*, 147(3), 323-343. https://doi.org/10.1111/jnc.14556
- Hamid, Z., Zimmerman, K. D., Guillen-Ahlers, H., Li, C., Nathanielsz, P., Cox, L. A., & Olivier, M. (2022). Assessment of label-free quantification and missing value imputation for proteomics in non-human primates. *BMC Genomics*, 23(1), 496. https://doi.org/10.1186/s12864-022-08723-1
- Han, D., Jin, J., Woo, J., Min, H., & Kim, Y. (2014). Proteomic analysis of mouse astrocytes and their secretome by a combination of FASP and StageTip-based, high pH, reversed-phase fractionation. *Proteomics*, *14*(13-14), 1604-1609. https://doi.org/10.1002/pmic.201300495
- Han, X., Aslanian, A., & Yates, J. R., 3rd. (2008). Mass spectrometry for proteomics. *Curr Opin Chem Biol*, 12(5), 483-490. https://doi.org/10.1016/j.cbpa.2008.07.024
- Harris, K. M., Jensen, F. E., & Tsao, B. (1992). Three-dimensional structure of dendritic spines and synapses in rat hippocampus (CA1) at postnatal day 15 and adult ages: implications for the maturation of synaptic physiology and long-term potentiation. *J Neurosci*, 12(7), 2685-2705. https://doi.org/10.1523/JNEUROSCI.12-07-02685.1992
- He, H., Mahnke, A. H., Doyle, S., Fan, N., Wang, C. C., Hall, B. J., Tang, Y. P., Inglis, F. M., Chen, C., & Erickson, J. D. (2012). Neurodevelopmental role for VGLUT2 in pyramidal neuron plasticity, dendritic refinement, and in spatial learning. *J Neurosci*, 32(45), 15886-15901. https://doi.org/10.1523/JNEUROSCI.4505-11.2012
- $\label{lem:hebb_def} \mbox{Hebb, D. O. (2005)}. \mbox{ $\it The organization of behavior: A neuropsychological theory. Psychology press.}$
- Hensch, T. K. (2005). Critical period plasticity in local cortical circuits. *Nat Rev Neurosci*, *6*(11), 877-888. https://doi.org/10.1038/nrn1787
- Hensch, T. K. (2018). Critical periods in cortical development. In *The neurobiology of brain and behavioral development* (pp. 133-151). Elsevier.

- Hensch, T. K., & Fagiolini, M. (2005). Excitatory-inhibitory balance and critical period plasticity in developing visual cortex. *Prog Brain Res, 147,* 115-124. https://doi.org/10.1016/S0079-6123(04)47009-5
- Henson, M. A., Larsen, R. S., Lawson, S. N., Perez-Otano, I., Nakanishi, N., Lipton, S. A., & Philpot, B. D. (2012). Genetic deletion of NR3A accelerates glutamatergic synapse maturation. *PLoS One*, 7(8), e42327. https://doi.org/10.1371/journal.pone.0042327
- Herbison, A. E., & Moenter, S. M. (2011). Depolarising and hyperpolarising actions of GABA(A) receptor activation on gonadotrophin-releasing hormone neurones: towards an emerging consensus. *J Neuroendocrinol*, 23(7), 557-569. https://doi.org/10.1111/j.1365-2826.2011.02145.x
- Hetzenauer, A., Corti, C., Herdy, S., Corsi, M., Ferraguti, F., & Singewald, N. (2008). Individual contribution of metabotropic glutamate receptor (mGlu) 2 and 3 to c-Fos expression pattern evoked by mGlu2/3 antagonism. *Psychopharmacology (Berl)*, *201*(1), 1-13. https://doi.org/10.1007/s00213-008-1236-2
- Hjorth-Simonsen, A. (1973). Some intrinsic connections of the hippocampus in the rat: An experimental analysis. *Journal of Comparative Neurology*, 147(2), 145-161. https://doi.org/10.1002/cne.901470202
- Holloway, C. M., & McIntyre, C. K. (2011). Post-training disruption of Arc protein expression in the anterior cingulate cortex impairs long-term memory for inhibitory avoidance training. *Neurobiol Learn Mem*, *95*(4), 425-432. https://doi.org/10.1016/j.nlm.2011.02.002
- Horvath, P. M., Piazza, M. K., Monteggia, L. M., & Kavalali, E. T. (2020). Spontaneous and evoked neurotransmission are partially segregated at inhibitory synapses. *Elife*, *9*. https://doi.org/10.7554/eLife.52852
- Hotulainen, P., & Hoogenraad, C. C. (2010). Actin in dendritic spines: connecting dynamics to function. *J Cell Biol*, 189(4), 619-629. https://doi.org/10.1083/jcb.201003008
- Houston, C. M., He, Q., & Smart, T. G. (2009). CaMKII phosphorylation of the GABA(A) receptor: receptor subtype- and synapse-specific modulation. *J Physiol*, *587*(Pt 10), 2115-2125. https://doi.org/10.1113/jphysiol.2009.171603
- Huang, Z. J. (2009). Activity-dependent development of inhibitory synapses and innervation pattern: role of GABA signalling and beyond. *J Physiol*, *587*(Pt 9), 1881-1888. https://doi.org/10.1113/jphysiol.2008.168211
- Hughes, C. S., Moggridge, S., Muller, T., Sorensen, P. H., Morin, G. B., & Krijgsveld, J. (2019). Single-pot, solid-phase-enhanced sample preparation for proteomics experiments. *Nat Protoc*, *14*(1), 68-85. https://doi.org/10.1038/s41596-018-0082-x
- Husi, H., Ward, M. A., Choudhary, J. S., Blackstock, W. P., & Grant, S. G. (2000). Proteomic analysis of NMDA receptor-adhesion protein signaling complexes. *Nat Neurosci*, *3*(7), 661-669. https://doi.org/10.1038/76615
- Irie, Y., Yamagata, K., Gan, Y., Miyamoto, K., Do, E., Kuo, C. H., Taira, E., & Miki, N. (2000). Molecular cloning and characterization of Amida, a novel protein which interacts with a neuron-specific immediate early gene product arc, contains novel nuclear localization signals, and causes cell death in cultured cells. *J Biol Chem*, 275(4), 2647-2653. https://doi.org/10.1074/jbc.275.4.2647
- Isaacson, J. S., & Scanziani, M. (2011). How inhibition shapes cortical activity. *Neuron*, 72(2), 231-243. https://doi.org/10.1016/j.neuron.2011.09.027
- Isagai, T., Fujimura, N., Tanaka, E., Yamamoto, S., & Higashi, H. (1999). Membrane dysfunction induced by in vitro ischemia in immature rat hippocampal CA1 neurons. *J Neurophysiol*, *81*(4), 1866-1871. https://doi.org/10.1152/jn.1999.81.4.1866
- Ishii, K., Kohno, T., Sakai, K., & Hattori, M. (2023). Reelin regulates the migration of late-born hippocampal CA1 neurons via cofilin phosphorylation. *Mol Cell Neurosci*, *124*, 103794. https://doi.org/10.1016/j.mcn.2022.103794
- Ishikawa, R. (2017). Biochemistry of Drebrin and Its Binding to Actin Filaments. *Adv Exp Med Biol*, 1006, 37-47. https://doi.org/10.1007/978-4-431-56550-5 3

- Iwano, T., Masuda, A., Kiyonari, H., Enomoto, H., & Matsuzaki, F. (2012). Prox1 postmitotically defines dentate gyrus cells by specifying granule cell identity over CA3 pyramidal cell fate in the hippocampus. *Development*, *139*(16), 3051-3062. https://doi.org/10.1242/dev.080002
- Iwata, K., Cafe-Mendes, C. C., Schmitt, A., Steiner, J., Manabe, T., Matsuzaki, H., Falkai, P., Turck, C. W., & Martins-de-Souza, D. (2013). The human oligodendrocyte proteome. *Proteomics*, *13*(23-24), 3548-3553. https://doi.org/10.1002/pmic.201300201
- Jacobi, E., & von Engelhardt, J. (2021). Modulation of information processing by AMPA receptor auxiliary subunits. *J Physiol*, 599(2), 471-483. https://doi.org/10.1113/JP276698
- Jane, D. E., Lodge, D., & Collingridge, G. L. (2009). Kainate receptors: pharmacology, function and therapeutic potential. *Neuropharmacology*, 56(1), 90-113. https://doi.org/10.1016/j.neuropharm.2008.08.023
- Jenks, K. R., Kim, T., Pastuzyn, E. D., Okuno, H., Taibi, A. V., Bito, H., Bear, M. F., & Shepherd, J. D. (2017). Arc restores juvenile plasticity in adult mouse visual cortex. *Proc Natl Acad Sci U S A*, 114(34), 9182-9187. https://doi.org/10.1073/pnas.1700866114
- Ji, J., & Maren, S. (2008). Differential roles for hippocampal areas CA1 and CA3 in the contextual encoding and retrieval of extinguished fear. *Learn Mem*, *15*(4), 244-251. https://doi.org/10.1101/lm.794808
- Ji, J. Z., & Maren, S. (2007). Hippocampal involvement in contextual modulation of fear extinction. *Hippocampus*, *17*(9), 749-758. https://doi.org/10.1002/hipo.20331
- Karlsson, K. A., Mohns, E. J., di Prisco, G. V., & Blumberg, M. S. (2006). On the co-occurrence of startles and hippocampal sharp waves in newborn rats. *Hippocampus*, *16*(11), 959-965. https://doi.org/10.1002/hipo.20224
- Kato, A. S., Gill, M. B., Ho, M. T., Yu, H., Tu, Y. A., Siuda, E. R., Wang, H., Qian, Y. W., Nisenbaum, E. S., Tomita, S., & Bredt, D. S. (2010). Hippocampal AMPA Receptor Gating Controlled by Both TARP and Cornichon Proteins. *Neuron*, *68*(6), 1082-1096. https://doi.org/10.1016/j.neuron.2010.11.026
- Katz, L. C., & Shatz, C. J. (1996). Synaptic activity and the construction of cortical circuits. *Science*, 274(5290), 1133-1138. https://doi.org/10.1126/science.274.5290.1133
- Kempermann, G. (2022). Adult Neurogenesis. In D. W. Pfaff, N. D. Volkow, & J. L. Rubenstein (Eds.), Neuroscience in the 21st Century: From Basic to Clinical (pp. 321-339). Springer International Publishing. https://doi.org/10.1007/978-3-030-88832-9_9
- Kemppainen, S., Jolkkonen, E., & Pitkanen, A. (2002). Projections from the posterior cortical nucleus of the amygdala to the hippocampal formation and parahippocampal region in rat. *Hippocampus*, 12(6), 735-755. https://doi.org/10.1002/hipo.10020
- Kerchner, G. A., & Nicoll, R. A. (2008). Silent synapses and the emergence of a postsynaptic mechanism for LTP. *Nat Rev Neurosci*, *9*(11), 813-825. https://doi.org/10.1038/nrn2501
- Kerti-Szigeti, K., & Nusser, Z. (2016). Similar GABAA receptor subunit composition in somatic and axon initial segment synapses of hippocampal pyramidal cells. *Elife*, *5*. https://doi.org/10.7554/eLife.18426
- Kim, M. S., Zhong, J., & Pandey, A. (2016). Common errors in mass spectrometry-based analysis of post-translational modifications. *Proteomics*, 16(5), 700-714. https://doi.org/10.1002/pmic.201500355
- Kim, S. W., & Cho, K. J. (2014). Activity-dependent alterations in the sensitivity to BDNF-TrkB signaling may promote excessive dendritic arborization and spinogenesis in fragile X syndrome in order to compensate for compromised postsynaptic activity. *Med Hypotheses*, *83*(4), 429-435. https://doi.org/10.1016/j.mehy.2014.07.007
- Klugbauer, N., Dai, S., Specht, V., Lacinova, L., Marais, E., Bohn, G., & Hofmann, F. (2000). A family of gamma-like calcium channel subunits. *FEBS Lett*, *470*(2), 189-197. https://doi.org/10.1016/s0014-5793(00)01306-5
- Kneussel, M., Brandstatter, J. H., Gasnier, B., Feng, G., Sanes, J. R., & Betz, H. (2001). Gephyrin-independent clustering of postsynaptic GABA(A) receptor subtypes. *Mol Cell Neurosci*, *17*(6), 973-982. https://doi.org/10.1006/mcne.2001.0983

- Koike, M., Tsukada, S., Tsuzuki, K., Kijima, H., & Ozawa, S. (2000). Regulation of kinetic properties of GluR2 AMPA receptor channels by alternative splicing. *J Neurosci*, 20(6), 2166-2174. https://doi.org/10.1523/JNEUROSCI.20-06-02166.2000
- Kolleker, A., Zhu, J. J., Schupp, B. J., Qin, Y., Mack, V., Borchardt, T., Kohr, G., Malinow, R., Seeburg, P. H., & Osten, P. (2003). Glutamatergic plasticity by synaptic delivery of GluR-B(long)-containing AMPA receptors. *Neuron*, 40(6), 1199-1212. https://doi.org/10.1016/s0896-6273(03)00722-0
- Korb, E., Wilkinson, C. L., Delgado, R. N., Lovero, K. L., & Finkbeiner, S. (2013). Arc in the nucleus regulates PML-dependent GluA1 transcription and homeostatic plasticity. *Nat Neurosci*, *16*(7), 874-883. https://doi.org/10.1038/nn.3429
- Kucera, A., Bakke, O., & Progida, C. (2016). The multiple roles of Rab9 in the endolysosomal system. *Commun Integr Biol*, 9(4), e1204498. https://doi.org/10.1080/19420889.2016.1204498
- Kuipers, S. D., Tiron, A., Soule, J., Messaoudi, E., Trentani, A., & Bramham, C. R. (2009). Selective survival and maturation of adult-born dentate granule cells expressing the immediate early gene Arc/Arg3.1. *PLoS One*, *4*(3), e4885. https://doi.org/10.1371/journal.pone.0004885
- Kullmann, D. (2006). Synaptic Function. In P. Andersen, R. Morris, D. Amaral, T. Bliss, & J. O'Keefe (Eds.), *The hippocampus book* (pp. 0). Oxford University Press. https://doi.org/10.1093/acprof:oso/9780195100273.003.0006
- Kumari, S., & Mayor, S. (2008). ARF1 is directly involved in dynamin-independent endocytosis. *Nat Cell Biol*, *10*(1), 30-41. https://doi.org/10.1038/ncb1666
- Kwon, Y. W., Jo, H. S., Bae, S., Seo, Y., Song, P., Song, M., & Yoon, J. H. (2021). Application of Proteomics in Cancer: Recent Trends and Approaches for Biomarkers Discovery. *Front Med (Lausanne)*, *8*, 747333. https://doi.org/10.3389/fmed.2021.747333
- Lai, X., Wang, L., & Witzmann, F. A. (2013). Issues and applications in label-free quantitative mass spectrometry. *Int J Proteomics*, 2013, 756039. https://doi.org/10.1155/2013/756039
- Langston, R. F., Ainge, J. A., Couey, J. J., Canto, C. B., Bjerknes, T. L., Witter, M. P., Moser, E. I., & Moser, M. B. (2010). Development of the spatial representation system in the rat. *Science*, *328*(5985), 1576-1580. https://doi.org/10.1126/science.1188210
- Laurie, D. J., & Seeburg, P. H. (1994). Ligand affinities at recombinant N-methyl-D-aspartate receptors depend on subunit composition. *Eur J Pharmacol*, 268(3), 335-345. https://doi.org/10.1016/0922-4106(94)90058-2
- Lee, A. R., Kim, J. H., Cho, E., Kim, M., & Park, M. (2017). Dorsal and Ventral Hippocampus Differentiate in Functional Pathways and Differentially Associate with Neurological Disease-Related Genes during Postnatal Development. *Front Mol Neurosci*, 10, 331. https://doi.org/10.3389/fnmol.2017.00331
- Lee, I., & Kesner, R. P. (2004). Differential contributions of dorsal hippocampal subregions to memory acquisition and retrieval in contextual fear-conditioning. *Hippocampus*, *14*(3), 301-310. https://doi.org/10.1002/hipo.10177
- Lee, M. G., Chrobak, J. J., Sik, A., Wiley, R. G., & Buzsaki, G. (1994). Hippocampal theta activity following selective lesion of the septal cholinergic system. *Neuroscience*, 62(4), 1033-1047. https://doi.org/10.1016/0306-4522(94)90341-7
- Lein, E. S., Zhao, X., & Gage, F. H. (2004). Defining a molecular atlas of the hippocampus using DNA microarrays and high-throughput in situ hybridization. *J Neurosci*, 24(15), 3879-3889. https://doi.org/10.1523/JNEUROSCI.4710-03.2004
- Leinekugel, X., Khazipov, R., Cannon, R., Hirase, H., Ben-Ari, Y., & Buzsaki, G. (2002). Correlated bursts of activity in the neonatal hippocampus in vivo. *Science*, *296*(5575), 2049-2052. https://doi.org/10.1126/science.1071111
- Leonard, A. S., Lim, I. A., Hemsworth, D. E., Horne, M. C., & Hell, J. W. (1999). Calcium/calmodulin-dependent protein kinase II is associated with the N-methyl-D-aspartate receptor. *Proc Natl Acad Sci U S A*, *96*(6), 3239-3244. https://doi.org/10.1073/pnas.96.6.3239
- Leonardo, E. D., Richardson-Jones, J. W., Sibille, E., Kottman, A., & Hen, R. (2006). Molecular heterogeneity along the dorsal-ventral axis of the murine hippocampal CA1 field: a microarray

- analysis of gene expression. *Neuroscience*, *137*(1), 177-186. https://doi.org/10.1016/j.neuroscience.2005.08.082
- Lester, R. A., Clements, J. D., Westbrook, G. L., & Jahr, C. E. (1990). Channel kinetics determine the time course of NMDA receptor-mediated synaptic currents. *Nature*, *346*(6284), 565-567. https://doi.org/10.1038/346565a0
- Leuner, B., & Shors, T. J. (2004). New spines, new memories. *Mol Neurobiol*, *29*(2), 117-130. https://doi.org/10.1385/MN:29:2:117
- Leung, H. W., Foo, G., & VanDongen, A. (2022). Arc Regulates Transcription of Genes for Plasticity, Excitability and Alzheimer's Disease. *Biomedicines*, 10(8). https://doi.org/10.3390/biomedicines10081946
- Lever, C., Burton, S., Jeewajee, A., O'Keefe, J., & Burgess, N. (2009). Boundary vector cells in the subiculum of the hippocampal formation. *J Neurosci*, 29(31), 9771-9777. https://doi.org/10.1523/JNEUROSCI.1319-09.2009
- Levi, S., Logan, S. M., Tovar, K. R., & Craig, A. M. (2004). Gephyrin is critical for glycine receptor clustering but not for the formation of functional GABAergic synapses in hippocampal neurons. *J Neurosci*, 24(1), 207-217. https://doi.org/10.1523/JNEUROSCI.1661-03.2004
- Linden, D. J., & Connor, J. A. (1995). Long-term synaptic depression. *Annu Rev Neurosci*, *18*, 319-357. https://doi.org/10.1146/annurev.ne.18.030195.001535
- Link, W., Konietzko, U., Kauselmann, G., Krug, M., Schwanke, B., Frey, U., & Kuhl, D. (1995). Somatodendritic expression of an immediate early gene is regulated by synaptic activity. *Proc Natl Acad Sci U S A*, 92(12), 5734-5738. https://doi.org/10.1073/pnas.92.12.5734
- Liu, Y., Fujise, N., & Kosaka, T. (1996). Distribution of calretinin immunoreactivity in the mouse dentate gyrus. I. General description. *Exp Brain Res*, 108(3), 389-403. https://doi.org/10.1007/BF00227262
- Loh, K. H., Stawski, P. S., Draycott, A. S., Udeshi, N. D., Lehrman, E. K., Wilton, D. K., Svinkina, T., Deerinck, T. J., Ellisman, M. H., Stevens, B., Carr, S. A., & Ting, A. Y. (2016). Proteomic Analysis of Unbounded Cellular Compartments: Synaptic Clefts. *Cell*, *166*(5), 1295-1307 e1221. https://doi.org/10.1016/j.cell.2016.07.041
- Lohmann, C., & Kessels, H. W. (2014). The developmental stages of synaptic plasticity. *J Physiol*, *592*(1), 13-31. https://doi.org/10.1113/jphysiol.2012.235119
- Ludvigsen, M., & Honoré, B. (2018). Transcriptomics and proteomics: Integration? eLS, 1-7.
- Lyford, G. L., Yamagata, K., Kaufmann, W. E., Barnes, C. A., Sanders, L. K., Copeland, N. G., Gilbert, D. J., Jenkins, N. A., Lanahan, A. A., & Worley, P. F. (1995). Arc, a growth factor and activity-regulated gene, encodes a novel cytoskeleton-associated protein that is enriched in neuronal dendrites. *Neuron*, *14*(2), 433-445. https://doi.org/10.1016/0896-6273(95)90299-6
- Lynch, M. A., & Bliss, T. V. (1986). Noradrenaline modulates the release of [14C]glutamate from dentate but not from CA1/CA3 slices of rat hippocampus. *Neuropharmacology*, 25(5), 493-498. https://doi.org/10.1016/0028-3908(86)90173-5
- Maccaferri, G., Roberts, J. D., Szucs, P., Cottingham, C. A., & Somogyi, P. (2000). Cell surface domain specific postsynaptic currents evoked by identified GABAergic neurones in rat hippocampus in vitro. *J Physiol*, *524 Pt 1*(Pt 1), 91-116. https://doi.org/10.1111/j.1469-7793.2000.t01-3-00091.x
- Machesky, L. M. (2019). Rab11FIP proteins link endocytic recycling vesicles for cytoskeletal transport and tethering. *Biosci Rep*, *39*(1). https://doi.org/10.1042/BSR20182219
- Maffei, A., Nelson, S. B., & Turrigiano, G. G. (2004). Selective reconfiguration of layer 4 visual cortical circuitry by visual deprivation. *Nat Neurosci*, *7*(12), 1353-1359. https://doi.org/10.1038/nn1351
- Maier, N., Nimmrich, V., & Draguhn, A. (2003). Cellular and network mechanisms underlying spontaneous sharp wave-ripple complexes in mouse hippocampal slices. *J Physiol*, *550*(Pt 3), 873-887. https://doi.org/10.1113/jphysiol.2003.044602
- Malenka, R. C., & Nicoll, R. A. (1997). Silent synapses speak up. *Neuron*, *19*(3), 473-476. https://doi.org/10.1016/s0896-6273(00)80362-1

- Malkki, H. A., Mertens, P. E., Lankelma, J. V., Vinck, M., van Schalkwijk, F. J., van Mourik-Donga, L. B., Battaglia, F. P., Mahlke, C., Kuhl, D., & Pennartz, C. M. (2016). Effects of Arc/Arg3.1 gene deletion on rhythmic synchronization of hippocampal CA1 neurons during locomotor activity and sleep. *Neurobiol Learn Mem*, *131*, 155-165. https://doi.org/10.1016/j.nlm.2016.03.021
- Marty, S., Wehrle, R., Alvarez-Leefmans, F. J., Gasnier, B., & Sotelo, C. (2002). Postnatal maturation of Na+, K+, 2Cl- cotransporter expression and inhibitory synaptogenesis in the rat hippocampus: an immunocytochemical analysis. *Eur J Neurosci*, 15(2), 233-245. https://doi.org/10.1046/j.0953-816x.2001.01854.x
- Masser, D. R., Bixler, G. V., Brucklacher, R. M., Yan, H., Giles, C. B., Wren, J. D., Sonntag, W. E., & Freeman, W. M. (2014). Hippocampal subregions exhibit both distinct and shared transcriptomic responses to aging and nonneurodegenerative cognitive decline. *J Gerontol A Biol Sci Med Sci*, 69(11), 1311-1324. https://doi.org/10.1093/gerona/glu091
- Mata, A., Gil, V., Perez-Clausell, J., Dasilva, M., Gonzalez-Calixto, M. C., Soriano, E., Garcia-Verdugo, J. M., Sanchez-Vives, M. V., & Del Rio, J. A. (2018). New functions of Semaphorin 3E and its receptor PlexinD1 during developing and adult hippocampal formation. *Sci Rep, 8*(1), 1381. https://doi.org/10.1038/s41598-018-19794-0
- McCurry, C. L., Shepherd, J. D., Tropea, D., Wang, K. H., Bear, M. F., & Sur, M. (2010). Loss of Arc renders the visual cortex impervious to the effects of sensory experience or deprivation. *Nat Neurosci*, 13(4), 450-457. https://doi.org/10.1038/nn.2508
- McHugh, S. B., Fillenz, M., Lowry, J. P., Rawlins, J. N., & Bannerman, D. M. (2011). Brain tissue oxygen amperometry in behaving rats demonstrates functional dissociation of dorsal and ventral hippocampus during spatial processing and anxiety. *Eur J Neurosci*, *33*(2), 322-337. https://doi.org/10.1111/j.1460-9568.2010.07497.x
- McLellan, M. A., Rosenthal, N. A., & Pinto, A. R. (2017). Cre-loxP-Mediated Recombination: General Principles and Experimental Considerations. *Curr Protoc Mouse Biol*, 7(1), 1-12. https://doi.org/10.1002/cpmo.22
- Megias, M., Emri, Z., Freund, T. F., & Gulyas, A. I. (2001). Total number and distribution of inhibitory and excitatory synapses on hippocampal CA1 pyramidal cells. *Neuroscience*, *102*(3), 527-540. https://doi.org/10.1016/s0306-4522(00)00496-6
- Menuz, K., O'Brien, J. L., Karmizadegan, S., Bredt, D. S., & Nicoll, R. A. (2008). TARP redundancy is critical for maintaining AMPA receptor function. *Journal of Neuroscience*, *28*(35), 8740-8746. https://doi.org/10.1523/Jneurosci.1319-08.2008
- Mergiya, T. F., Gundersen, J. E. T., Kanhema, T., Brighter, G., Ishizuka, Y., & Bramham, C. R. (2023). Detection of Arc/Arg3.1 oligomers in rat brain: constitutive and synaptic activity-evoked dimer expression in vivo. *Front Mol Neurosci*, *16*, 1142361. https://doi.org/10.3389/fnmol.2023.1142361
- Messaoudi, E., Kanhema, T., Soule, J., Tiron, A., Dagyte, G., da Silva, B., & Bramham, C. R. (2007). Sustained Arc/Arg3.1 synthesis controls long-term potentiation consolidation through regulation of local actin polymerization in the dentate gyrus in vivo. *J Neurosci*, *27*(39), 10445-10455. https://doi.org/10.1523/JNEUROSCI.2883-07.2007
- Mikuni, T., Uesaka, N., Okuno, H., Hirai, H., Deisseroth, K., Bito, H., & Kano, M. (2013). Arc/Arg3.1 is a postsynaptic mediator of activity-dependent synapse elimination in the developing cerebellum. *Neuron*, 78(6), 1024-1035. https://doi.org/10.1016/j.neuron.2013.04.036
- Milstein, A. D., Bloss, E. B., Apostolides, P. F., Vaidya, S. P., Dilly, G. A., Zemelman, B. V., & Magee, J. C. (2015). Inhibitory Gating of Input Comparison in the CA1 Microcircuit. *Neuron*, *87*(6), 1274-1289. https://doi.org/10.1016/j.neuron.2015.08.025
- Milstein, A. D., Zhou, W., Karimzadegan, S., Bredt, D. S., & Nicoll, R. A. (2007). TARP subtypes differentially and dose-dependently control synaptic AMPA receptor gating. *Neuron*, *55*(6), 905-918. https://doi.org/10.1016/j.neuron.2007.08.022
- Mitchell, S. J., Rawlins, J. N., Steward, O., & Olton, D. S. (1982). Medial septal area lesions disrupt theta rhythm and cholinergic staining in medial entorhinal cortex and produce impaired radial arm

- maze behavior in rats. *J Neurosci*, *2*(3), 292-302. https://doi.org/10.1523/JNEUROSCI.02-03-00292.1982
- Miyazaki, T., Fukaya, M., Shimizu, H., & Watanabe, M. (2003). Subtype switching of vesicular glutamate transporters at parallel fibre-Purkinje cell synapses in developing mouse cerebellum. *Eur J Neurosci*, *17*(12), 2563-2572. https://doi.org/10.1046/j.1460-9568.2003.02698.x
- Mohns, E. J., & Blumberg, M. S. (2008). Synchronous bursts of neuronal activity in the developing hippocampus: modulation by active sleep and association with emerging gamma and theta rhythms. *J Neurosci*, 28(40), 10134-10144. https://doi.org/10.1523/JNEUROSCI.1967-08.2008
- Monyer, H., Seeburg, P. H., & Wisden, W. (1991). Glutamate-operated channels: developmentally early and mature forms arise by alternative splicing. *Neuron*, *6*(5), 799-810. https://doi.org/10.1016/0896-6273(91)90176-z
- Morris, R. G., Davis, S., & Butcher, S. P. (1990). Hippocampal synaptic plasticity and NMDA receptors: a role in information storage? *Philos Trans R Soc Lond B Biol Sci, 329*(1253), 187-204. https://doi.org/10.1098/rstb.1990.0164
- Mosbacher, J., Schoepfer, R., Monyer, H., Burnashev, N., Seeburg, P. H., & Ruppersberg, J. P. (1994). A molecular determinant for submillisecond desensitization in glutamate receptors. *Science*, 266(5187), 1059-1062. https://doi.org/10.1126/science.7973663
- Moser, M. B., Trommald, M., & Andersen, P. (1994). An increase in dendritic spine density on hippocampal CA1 pyramidal cells following spatial learning in adult rats suggests the formation of new synapses. *Proc Natl Acad Sci U S A*, 91(26), 12673-12675. https://doi.org/10.1073/pnas.91.26.12673
- Muessig, L., Hauser, J., Wills, T. J., & Cacucci, F. (2015). A Developmental Switch in Place Cell Accuracy Coincides with Grid Cell Maturation. *Neuron*, *86*(5), 1167-1173. https://doi.org/10.1016/j.neuron.2015.05.011
- Nadasdy, Z., Hirase, H., Czurko, A., Csicsvari, J., & Buzsaki, G. (1999). Replay and time compression of recurring spike sequences in the hippocampus. *J Neurosci*, 19(21), 9497-9507. https://doi.org/10.1523/JNEUROSCI.19-21-09497.1999
- Nader, K., Schafe, G. E., & Le Doux, J. E. (2000). Fear memories require protein synthesis in the amygdala for reconsolidation after retrieval. *Nature*, 406(6797), 722-726. https://doi.org/10.1038/35021052
- Nagura, H., Ishikawa, Y., Kobayashi, K., Takao, K., Tanaka, T., Nishikawa, K., Tamura, H., Shiosaka, S., Suzuki, H., Miyakawa, T., Fujiyoshi, Y., & Doi, T. (2012). Impaired synaptic clustering of postsynaptic density proteins and altered signal transmission in hippocampal neurons, and disrupted learning behavior in PDZ1 and PDZ2 ligand binding-deficient PSD-95 knockin mice. *Mol Brain*, *5*, 43. https://doi.org/10.1186/1756-6606-5-43
- Nair, D., Hosy, E., Petersen, J. D., Constals, A., Giannone, G., Choquet, D., & Sibarita, J. B. (2013). Super-Resolution Imaging Reveals That AMPA Receptors Inside Synapses Are Dynamically Organized in Nanodomains Regulated by PSD95. *Journal of Neuroscience*, 33(32), 13204-13224. https://doi.org/10.1523/Jneurosci.2381-12.2013
- Nair, R. R., Patil, S., Tiron, A., Kanhema, T., Panja, D., Schiro, L., Parobczak, K., Wilczynski, G., & Bramham, C. R. (2017). Dynamic Arc SUMOylation and Selective Interaction with F-Actin-Binding Protein Drebrin A in LTP Consolidation In Vivo. *Front Synaptic Neurosci*, *9*, 8. https://doi.org/10.3389/fnsyn.2017.00008
- Nakamura, K., Hioki, H., Fujiyama, F., & Kaneko, T. (2005). Postnatal changes of vesicular glutamate transporter (VGluT)1 and VGluT2 immunoreactivities and their colocalization in the mouse forebrain. *J Comp Neurol*, 492(3), 263-288. https://doi.org/10.1002/cne.20705
- Nakashiba, T., Buhl, D. L., McHugh, T. J., & Tonegawa, S. (2009). Hippocampal CA3 Output Is Crucial for Ripple-Associated Reactivation and Consolidation of Memory. *Neuron*, *62*(6), 781-787. https://doi.org/10.1016/j.neuron.2009.05.013
- Nathanson, A. J., Davies, P. A., & Moss, S. J. (2019). Inhibitory Synapse Formation at the Axon Initial Segment. *Frontiers in Molecular Neuroscience*, 12. https://doi.org/ARTN 266

- Newpher, T. M., Harris, S., Pringle, J., Hamilton, C., & Soderling, S. (2018). Regulation of spine structural plasticity by Arc/Arg3.1. *Semin Cell Dev Biol*, 77, 25-32. https://doi.org/10.1016/j.semcdb.2017.09.022
- Niethammer, M., Kim, E., & Sheng, M. (1996). Interaction between the C terminus of NMDA receptor subunits and multiple members of the PSD-95 family of membrane-associated guanylate kinases. *J Neurosci*, *16*(7), 2157-2163. https://doi.org/10.1523/JNEUROSCI.16-07-02157.1996
- Nishimura, M., Gu, X., & Swann, J. W. (2011). Seizures in early life suppress hippocampal dendrite growth while impairing spatial learning. *Neurobiol Dis*, 44(2), 205-214. https://doi.org/10.1016/j.nbd.2011.07.002
- Nowak, L., Bregestovski, P., Ascher, P., Herbet, A., & Prochiantz, A. (1984). Magnesium gates glutamate-activated channels in mouse central neurones. *Nature*, *307*(5950), 462-465. https://doi.org/10.1038/307462a0
- Nusser, Z., Sieghart, W., Benke, D., Fritschy, J. M., & Somogyi, P. (1996). Differential synaptic localization of two major gamma-aminobutyric acid type A receptor alpha subunits on hippocampal pyramidal cells. *Proceedings of the National Academy of Sciences of the United States of America*, 93(21), 11939-11944. https://doi.org/DOI 10.1073/pnas.93.21.11939
- O'keefe, J., & Nadel, L. (1978). The hippocampus as a cognitive map. Oxford university press.
- O'Malley, A., O'Connell, C., Murphy, K. J., & Regan, C. M. (2000). Transient spine density increases in the mid-molecular layer of hippocampal dentate gyrus accompany consolidation of a spatial learning task in the rodent. *Neuroscience*, *99*(2), 229-232. https://doi.org/10.1016/s0306-4522(00)00182-2
- O'Keefe, J. (2006). Hippocampal Neurophysiology in the Behaving Animal. In P. Andersen, R. Morris, D. Amaral, T. Bliss, & J. O'Keefe (Eds.), *The hippocampus book* (pp. 0). Oxford University Press. https://doi.org/10.1093/acprof:oso/9780195100273.003.0011
- Oermann, E., Warskulat, U., Heller-Stilb, B., Haussinger, D., & Zilles, K. (2005). Taurine-transporter gene knockout-induced changes in GABA(A), kainate and AMPA but not NMDA receptor binding in mouse brain. *Anat Embryol (Berl)*, 210(5-6), 363-372. https://doi.org/10.1007/s00429-005-0024-6
- Ohana, O., Alberini, C. M., & Donato, F. (2022). Introduction to the special issue on the ontogeny of hippocampal functions. *Hippocampus*, 32(2), 69-72. https://doi.org/10.1002/hipo.23406
- Okamoto, K., Ishikawa, T., Abe, R., Ishikawa, D., Kobayashi, C., Mizunuma, M., Norimoto, H., Matsuki, N., & Ikegaya, Y. (2014). Ex vivo cultured neuronal networks emit in vivo-like spontaneous activity. *J Physiol Sci*, 64(6), 421-431. https://doi.org/10.1007/s12576-014-0337-4
- Okamoto, K., Narayanan, R., Lee, S. H., Murata, K., & Hayashi, Y. (2007). The role of CaMKII as an Factin-bundling protein crucial for maintenance of dendritic spine structure. *Proc Natl Acad Sci U S A*, 104(15), 6418-6423. https://doi.org/10.1073/pnas.0701656104
- Okuno, H., Akashi, K., Ishii, Y., Yagishita-Kyo, N., Suzuki, K., Nonaka, M., Kawashima, T., Fujii, H., Takemoto-Kimura, S., Abe, M., Natsume, R., Chowdhury, S., Sakimura, K., Worley, P. F., & Bito, H. (2012). Inverse synaptic tagging of inactive synapses via dynamic interaction of Arc/Arg3.1 with CaMKIIbeta. *Cell*, *149*(4), 886-898. https://doi.org/10.1016/j.cell.2012.02.062
- Oliva, A., Fernandez-Ruiz, A., Buzsaki, G., & Berenyi, A. (2016). Spatial coding and physiological properties of hippocampal neurons in the Cornu Ammonis subregions. *Hippocampus*, 26(12), 1593-1607. https://doi.org/10.1002/hipo.22659
- Olvera-Cortes, E., Cervantes, M., & Gonzalez-Burgos, I. (2002). Place-learning, but not cue-learning training, modifies the hippocampal theta rhythm in rats. *Brain Res Bull*, *58*(3), 261-270. https://doi.org/10.1016/s0361-9230(02)00769-4
- Opazo, P., Labrecque, S., Tigaret, C. M., Frouin, A., Wiseman, P. W., De Koninck, P., & Choquet, D. (2010). CaMKII triggers the diffusional trapping of surface AMPARs through phosphorylation of stargazin. *Neuron*, *67*(2), 239-252. https://doi.org/10.1016/j.neuron.2010.06.007
- Osten, P., Wisden, W., & Sprengel, R. (2006). Molecular Mechanisms of Synaptic Function in the Hippocampus: Neurotransmitter Exocytosis and Glutamatergic, GABAergic, and Cholinergic Transmission. In P. Andersen, R. Morris, D. Amaral, T. Bliss, & J. O'Keefe (Eds.), *The*

- hippocampus book (pp. 0). Oxford University Press. https://doi.org/10.1093/acprof:oso/9780195100273.003.0007
- Pandya, N. J., Koopmans, F., Slotman, J. A., Paliukhovich, I., Houtsmuller, A. B., Smit, A. B., & Li, K. W. (2017). Correlation profiling of brain sub-cellular proteomes reveals co-assembly of synaptic proteins and subcellular distribution. *Sci Rep*, 7(1), 12107. https://doi.org/10.1038/s41598-017-11690-3
- Panzanelli, P., Gunn, B. G., Schlatter, M. C., Benke, D., Tyagarajan, S. K., Scheiffele, P., Belelli, D., Lambert, J. J., Rudolph, U., & Fritschy, J. M. (2011). Distinct mechanisms regulate GABAA receptor and gephyrin clustering at perisomatic and axo-axonic synapses on CA1 pyramidal cells. *J Physiol*, *589*(Pt 20), 4959-4980. https://doi.org/10.1113/jphysiol.2011.216028
- Papp, E., Leinekugel, X., Henze, D. A., Lee, J., & Buzsáki, G. (2001). The apical shaft of CA1 pyramidal cells is under GABAergic interneuronal control. *Neuroscience*, 102(4), 715-721. https://doi.org/Doi 10.1016/S0306-4522(00)00584-4
- Parra, A. S., & Johnston, C. A. (2022). Emerging Roles of RNA-Binding Proteins in Neurodevelopment. *J Dev Biol*, 10(2). https://doi.org/10.3390/jdb10020023
- Pastuzyn, E. D., Day, C. E., Kearns, R. B., Kyrke-Smith, M., Taibi, A. V., McCormick, J., Yoder, N., Belnap, D. M., Erlendsson, S., Morado, D. R., Briggs, J. A. G., Feschotte, C., & Shepherd, J. D. (2018). The Neuronal Gene Arc Encodes a Repurposed Retrotransposon Gag Protein that Mediates Intercellular RNA Transfer. *Cell*, 173(1), 275. https://doi.org/10.1016/j.cell.2018.03.024
- Pelkey, K. A., Chittajallu, R., Craig, M. T., Tricoire, L., Wester, J. C., & McBain, C. J. (2017). Hippocampal GABAergic Inhibitory Interneurons. *Physiol Rev*, *97*(4), 1619-1747. https://doi.org/10.1152/physrev.00007.2017
- Penttonen, M., Kamondi, A., Sik, A., Acsady, L., & Buzsaki, G. (1997). Feed-forward and feed-back activation of the dentate gyrus in vivo during dentate spikes and sharp wave bursts. *Hippocampus*, 7(4), 437-450. https://doi.org/10.1002/(SICI)1098-1063(1997)7:4<437::AID-HIPO9>3.0.CO;2-F
- Pickard, L., Noel, J., Henley, J. M., Collingridge, G. L., & Molnar, E. (2000). Developmental changes in synaptic AMPA and NMDA receptor distribution and AMPA receptor subunit composition in living hippocampal neurons. *J Neurosci*, 20(21), 7922-7931. https://doi.org/10.1523/JNEUROSCI.20-21-07922.2000
- Pignatelli, M., & Rockland, K. S. (2020). Organization and development of hippocampal circuits. In *Neural Circuit and Cognitive Development* (pp. 201-219). https://doi.org/10.1016/b978-0-12-814411-4.00009-3
- Pires, G., Ueberheide, B., Wisniewski, T., & Drummond, E. (2023). Use of Affinity Purification-Mass Spectrometry to Identify Phosphorylated Tau Interactors in Alzheimer's Disease. *Methods Mol Biol*, 2561, 263-277. https://doi.org/10.1007/978-1-0716-2655-9 14
- Plath, N., Ohana, O., Dammermann, B., Errington, M. L., Schmitz, D., Gross, C., Mao, X. S., Engelsberg, A., Mahlke, C., Welzl, H., Kobaz, U., Stawrakakis, A., Fernandez, E., Waltereit, R., Bick-Sander, A., Therstappen, E., Cooke, S. F., Blanquet, V., Wurst, W., . . . Kuhl, D. (2006). Arc/Arg3.1 is essential for the consolidation of synaptic plasticity and memories. *Neuron*, *52*(3), 437-444. https://doi.org/10.1016/j.neuron.2006.08.024
- Ploski, J. E., Pierre, V. J., Smucny, J., Park, K., Monsey, M. S., Overeem, K. A., & Schafe, G. E. (2008). The activity-regulated cytoskeletal-associated protein (Arc/Arg3.1) is required for memory consolidation of pavlovian fear conditioning in the lateral amygdala. *J Neurosci*, 28(47), 12383-12395. https://doi.org/10.1523/JNEUROSCI.1662-08.2008
- Pokorny, J., & Yamamoto, T. (1981). Postnatal ontogenesis of hippocampal CA1 area in rats. I. Development of dendritic arborisation in pyramidal neurons. *Brain Res Bull, 7*(2), 113-120. https://doi.org/10.1016/0361-9230(81)90075-7
- Pressey, J. C., & Woodin, M. A. (2021). Kainate receptor regulation of synaptic inhibition in the hippocampus. *Journal of Physiology-London*, 599(2), 485-492. https://doi.org/10.1113/Jp279645

- Pugh, C. R., & Rudy, J. W. (1996). A developmental analysis of contextual fear conditioning. *Dev Psychobiol*, 29(2), 87-100. https://doi.org/10.1002/(SICI)1098-2302(199603)29:2<87::AID-DEV1>3.0.CO;2-H
- Purves, D., Cabeza, R., Huettel, S. A., Platt, M. L., LaBar, K. S., & Woldorff, M. G. (2013). *Principles of cognitive neuroscience* (Vol. 83). Sinauer Associates Sunderland, MA.
- Ramirez-Amaya, V., Angulo-Perkins, A., Chawla, M. K., Barnes, C. A., & Rosi, S. (2013). Sustained transcription of the immediate early gene Arc in the dentate gyrus after spatial exploration. *J Neurosci*, 33(4), 1631-1639. https://doi.org/10.1523/JNEUROSCI.2916-12.2013
- Rampon, C., Tang, Y. P., Goodhouse, J., Shimizu, E., Kyin, M., & Tsien, J. Z. (2000). Enrichment induces structural changes and recovery from nonspatial memory deficits in CA1 NMDAR1-knockout mice. *Nat Neurosci*, *3*(3), 238-244. https://doi.org/10.1038/72945
- Rauskolb, S., Zagrebelsky, M., Dreznjak, A., Deogracias, R., Matsumoto, T., Wiese, S., Erne, B., Sendtner, M., Schaeren-Wiemers, N., Korte, M., & Barde, Y. A. (2010). Global deprivation of brain-derived neurotrophic factor in the CNS reveals an area-specific requirement for dendritic growth. *J Neurosci*, 30(5), 1739-1749. https://doi.org/10.1523/JNEUROSCI.5100-09.2010
- Ray, S., & Brecht, M. (2016). Structural development and dorsoventral maturation of the medial entorhinal cortex. *Elife*, *5*, e13343. https://doi.org/10.7554/eLife.13343
- Rial Verde, E. M., Lee-Osbourne, J., Worley, P. F., Malinow, R., & Cline, H. T. (2006). Increased expression of the immediate-early gene arc/arg3.1 reduces AMPA receptor-mediated synaptic transmission. *Neuron*, *52*(3), 461-474. https://doi.org/10.1016/j.neuron.2006.09.031
- Riccio, D. C., & Schulenburg, C. J. (1969). Age-related deficits in acquisition of a passive aviodance response. *Can J Psychol*, 23(6), 429-437. https://doi.org/10.1037/h0082828
- Rivera, C., Voipio, J., Payne, J. A., Ruusuvuori, E., Lahtinen, H., Lamsa, K., Pirvola, U., Saarma, M., & Kaila, K. (1999). The K+/Cl- co-transporter KCC2 renders GABA hyperpolarizing during neuronal maturation. *Nature*, *397*(6716), 251-255. https://doi.org/10.1038/16697
- Rouach, N., Byrd, K., Petralia, R. S., Elias, G. M., Adesnik, H., Tomita, S., Karimzadegan, S., Kealey, C., Bredt, D. S., & Nicoll, R. A. (2005). TARP gamma-8 controls hippocampal AMPA receptor number, distribution and synaptic plasticity. *Nat Neurosci*, 8(11), 1525-1533. https://doi.org/10.1038/nn1551
- Roumis, D. K., & Frank, L. M. (2015). Hippocampal sharp-wave ripples in waking and sleeping states. *Current Opinion in Neurobiology*, 35, 6-12. https://doi.org/10.1016/j.conb.2015.05.001
- Rudolph, U., & Knoflach, F. (2011). Beyond classical benzodiazepines: novel therapeutic potential of GABAA receptor subtypes. *Nat Rev Drug Discov*, 10(9), 685-697. https://doi.org/10.1038/nrd3502
- Rudy, J. W., & Morledge, P. (1994). Ontogeny of contextual fear conditioning in rats: implications for consolidation, infantile amnesia, and hippocampal system function. *Behav Neurosci*, 108(2), 227-234. https://doi.org/10.1037//0735-7044.108.2.227
- Rudy, J. W., Stadler-Morris, S., & Albert, P. (1987). Ontogeny of spatial navigation behaviors in the rat: dissociation of "proximal"- and "distal"-cue-based behaviors. *Behav Neurosci*, 101(1), 62-73. https://doi.org/10.1037//0735-7044.101.1.62
- Runge, K., Cardoso, C., & de Chevigny, A. (2020). Dendritic Spine Plasticity: Function and Mechanisms. Front Synaptic Neurosci, 12, 36. https://doi.org/10.3389/fnsyn.2020.00036
- Sakimoto, Y., Shintani, A., Yoshiura, D., Goshima, M., Kida, H., & Mitsushima, D. (2022). A critical period for learning and plastic changes at hippocampal CA1 synapses. *Sci Rep*, *12*(1), 7199. https://doi.org/10.1038/s41598-022-10453-z
- Sala, C., Roussignol, G., Meldolesi, J., & Fagni, L. (2005). Key role of the postsynaptic density scaffold proteins Shank and Homer in the functional architecture of Ca2+ homeostasis at dendritic spines in hippocampal neurons. *J Neurosci*, 25(18), 4587-4592. https://doi.org/10.1523/JNEUROSCI.4822-04.2005
- Sallard, E., Letourneur, D., & Legendre, P. (2021). Electrophysiology of ionotropic GABA receptors. *Cell Mol Life Sci*, 78(13), 5341-5370. https://doi.org/10.1007/s00018-021-03846-2

- Sanchez-Aguilera, A., Monedero, G., Colino, A., & Vicente-Torres, M. A. (2020). Development of Action Potential Waveform in Hippocampal CA1 Pyramidal Neurons. *Neuroscience*, *442*, 151-167. https://doi.org/10.1016/j.neuroscience.2020.06.042
- Sanchez-Alonso, J. L., Munoz-Cuevas, J., Vicente-Torres, M. A., & Colino, A. (2010). Role of low-voltage-activated calcium current on the firing pattern alterations induced by hypothyroidism in the rat hippocampus. *Neuroscience*, 171(4), 993-1005. https://doi.org/10.1016/j.neuroscience.2010.10.003
- Sans, N., Petralia, R. S., Wang, Y. X., Blahos, J., 2nd, Hell, J. W., & Wenthold, R. J. (2000). A developmental change in NMDA receptor-associated proteins at hippocampal synapses. *J Neurosci*, 20(3), 1260-1271. https://doi.org/10.1523/JNEUROSCI.20-03-01260.2000
- Santos, M. S., Foss, S. M., Park, C. K., & Voglmaier, S. M. (2014). Protein interactions of the vesicular glutamate transporter VGLUT1. *PLoS One*, *9*(10), e109824. https://doi.org/10.1371/journal.pone.0109824
- Schachtele, S. J., Losh, J., Dailey, M. E., & Green, S. H. (2011). Spine formation and maturation in the developing rat auditory cortex. *J Comp Neurol*, 519(16), 3327-3345. https://doi.org/10.1002/cne.22728
- Schindelin, J., Arganda-Carreras, I., Frise, E., Kaynig, V., Longair, M., Pietzsch, T., Preibisch, S., Rueden, C., Saalfeld, S., Schmid, B., Tinevez, J. Y., White, D. J., Hartenstein, V., Eliceiri, K., Tomancak, P., & Cardona, A. (2012). Fiji: an open-source platform for biological-image analysis. *Nat Methods*, 9(7), 676-682. https://doi.org/10.1038/nmeth.2019
- Schlingloff, D., Kali, S., Freund, T. F., Hajos, N., & Gulyas, A. I. (2014). Mechanisms of sharp wave initiation and ripple generation. *J Neurosci*, *34*(34), 11385-11398. https://doi.org/10.1523/JNEUROSCI.0867-14.2014
- Schmitz, L. J. M., Klaassen, R. V., Ruiperez-Alonso, M., Zamri, A. E., Stroeder, J., Rao-Ruiz, P., Lodder, J. C., van der Loo, R. J., Mansvelder, H. D., Smit, A. B., & Spijker, S. (2017). The AMPA receptor-associated protein Shisa7 regulates hippocampal synaptic function and contextual memory. *Elife*, 6. https://doi.org/10.7554/eLife.24192
- Schonberger, J., Draguhn, A., & Both, M. (2014). Lamina-specific contribution of glutamatergic and GABAergic potentials to hippocampal sharp wave-ripple complexes. *Front Neural Circuits*, *8*, 103. https://doi.org/10.3389/fncir.2014.00103
- Scoville, W. B., & Milner, B. (1957). Loss of recent memory after bilateral hippocampal lesions. *J Neurol Neurosurg Psychiatry*, 20(1), 11-21. https://doi.org/10.1136/jnnp.20.1.11
- Seeburg, P. H., Single, F., Kuner, T., Higuchi, M., & Sprengel, R. (2001). Genetic manipulation of key determinants of ion flow in glutamate receptor channels in the mouse. *Brain Res*, 907(1-2), 233-243. https://doi.org/10.1016/s0006-8993(01)02445-3
- Sengar, A. S., Wang, W., Bishay, J., Cohen, S., & Egan, S. E. (1999). The EH and SH3 domain Ese proteins regulate endocytosis by linking to dynamin and Eps15. *EMBO J*, 18(5), 1159-1171. https://doi.org/10.1093/emboj/18.5.1159
- Seress, L., & Ribak, C. E. (1988). The development of GABAergic neurons in the rat hippocampal formation. An immunocytochemical study. *Brain Res Dev Brain Res*, 44(2), 197-209. https://doi.org/10.1016/0165-3806(88)90218-0
- Sfakianos, M. K., Eisman, A., Gourley, S. L., Bradley, W. D., Scheetz, A. J., Settleman, J., Taylor, J. R., Greer, C. A., Williamson, A., & Koleske, A. J. (2007). Inhibition of Rho via Arg and p190RhoGAP in the postnatal mouse hippocampus regulates dendritic spine maturation, synapse and dendrite stability, and behavior. *J Neurosci*, 27(41), 10982-10992. https://doi.org/10.1523/JNEUROSCI.0793-07.2007
- Sharma, K., Schmitt, S., Bergner, C. G., Tyanova, S., Kannaiyan, N., Manrique-Hoyos, N., Kongi, K., Cantuti, L., Hanisch, U. K., Philips, M. A., Rossner, M. J., Mann, M., & Simons, M. (2015). Cell type- and brain region-resolved mouse brain proteome. *Nat Neurosci*, *18*(12), 1819-1831. https://doi.org/10.1038/nn.4160

- Shepherd, J. D., Rumbaugh, G., Wu, J., Chowdhury, S., Plath, N., Kuhl, D., Huganir, R. L., & Worley, P. F. (2006). Arc/Arg3.1 mediates homeostatic synaptic scaling of AMPA receptors. *Neuron*, *52*(3), 475-484. https://doi.org/10.1016/j.neuron.2006.08.034
- Shevchenko, A., Tomas, H., Havlis, J., Olsen, J. V., & Mann, M. (2006). In-gel digestion for mass spectrometric characterization of proteins and proteomes. *Nat Protoc*, 1(6), 2856-2860. https://doi.org/10.1038/nprot.2006.468
- Simon, J., Wakimoto, H., Fujita, N., Lalande, M., & Barnard, E. A. (2004). Analysis of the set of GABA(A) receptor genes in the human genome. *J Biol Chem*, 279(40), 41422-41435. https://doi.org/10.1074/jbc.M401354200
- Sivaguru, M., Khaw, Y. M., & Inoue, M. (2019). A Confocal Reflection Super-Resolution Technique to Image Golgi-Cox Stained Neurons. *J Microsc*, 275(2), 115-130. https://doi.org/10.1111/jmi.12821
- Smith, G., Rani, A., Kumar, A., Barter, J., & Foster, T. C. (2020). Hippocampal Subregion Transcriptomic Profiles Reflect Strategy Selection during Cognitive Aging. *J Neurosci*, 40(25), 4888-4899. https://doi.org/10.1523/JNEUROSCI.2944-19.2020
- Solstad, T., Boccara, C. N., Kropff, E., Moser, M. B., & Moser, E. I. (2008). Representation of geometric borders in the entorhinal cortex. *Science*, *322*(5909), 1865-1868. https://doi.org/10.1126/science.1166466
- Sommer, B., Keinanen, K., Verdoorn, T. A., Wisden, W., Burnashev, N., Herb, A., Kohler, M., Takagi, T., Sakmann, B., & Seeburg, P. H. (1990). Flip and flop: a cell-specific functional switch in glutamate-operated channels of the CNS. *Science*, *249*(4976), 1580-1585. https://doi.org/10.1126/science.1699275
- Somogyi, P. (1977). A specific 'axo-axonal' interneuron in the visual cortex of the rat. *Brain Res*, *136*(2), 345-350. https://doi.org/10.1016/0006-8993(77)90808-3
- Spigelman, I., Zhang, L., & Carlen, P. L. (1992). Patch-clamp study of postnatal development of CA1 neurons in rat hippocampal slices: membrane excitability and K+ currents. *J Neurophysiol*, 68(1), 55-69. https://doi.org/10.1152/jn.1992.68.1.55
- Sprengel, R. (2006). Role of AMPA receptors in synaptic plasticity. *Cell Tissue Res*, *326*(2), 447-455. https://doi.org/10.1007/s00441-006-0275-4
- Spruston, N., Jaffe, D. B., & Johnston, D. (1994). Dendritic attenuation of synaptic potentials and currents: the role of passive membrane properties. *Trends Neurosci*, *17*(4), 161-166. https://doi.org/10.1016/0166-2236(94)90094-9
- Spruston, N., & Johnston, D. (1992). Perforated patch-clamp analysis of the passive membrane properties of three classes of hippocampal neurons. *J Neurophysiol*, *67*(3), 508-529. https://doi.org/10.1152/jn.1992.67.3.508
- Spruston, N., & McBain, C. (2006). Structural and Functional Properties of Hippocampal Neurons. In P. Andersen, R. Morris, D. Amaral, T. Bliss, & J. O'Keefe (Eds.), *The hippocampus book* (pp. 0). Oxford University Press. https://doi.org/10.1093/acprof:oso/9780195100273.003.0005
- Squire, L. R. (2009). Memory and brain systems: 1969-2009. *J Neurosci*, 29(41), 12711-12716. https://doi.org/10.1523/JNEUROSCI.3575-09.2009
- Stanke, C. (2022). Investigating dendrite development in the
- hippocampus of Arc/Arg3.1 deficient mice [Master's Thesis, Universitât Rostock].
- Stanton, M. E. (2000). Multiple memory systems, development and conditioning. *Behav Brain Res*, 110(1-2), 25-37. https://doi.org/10.1016/s0166-4328(99)00182-5
- Stanton, M. E., Ivkovich Claflin, D., & Herbert, J. (2009). Ontogeny of Multiple Memory Systems: Eyeblink Conditioning in Rodents and Humans. In M. S. Blumberg, J. H. Freeman, & S. R. Robinson (Eds.), Oxford Handbook of Developmental Behavioral Neuroscience (pp. 0). Oxford University Press. https://doi.org/10.1093/oxfordhb/9780195314731.013.0025
- Steward, O., & Falk, P. M. (1991). Selective localization of polyribosomes beneath developing synapses: a quantitative analysis of the relationships between polyribosomes and developing synapses in the hippocampus and dentate gyrus. *J Comp Neurol*, 314(3), 545-557. https://doi.org/10.1002/cne.903140311

- Steward, O., Wallace, C. S., Lyford, G. L., & Worley, P. F. (1998). Synaptic activation causes the mRNA for the IEG Arc to localize selectively near activated postsynaptic sites on dendrites. *Neuron*, 21(4), 741-751. https://doi.org/10.1016/s0896-6273(00)80591-7
- Steward, O., & Worley, P. F. (2001). Selective targeting of newly synthesized Arc mRNA to active synapses requires NMDA receptor activation. *Neuron*, *30*(1), 227-240. https://doi.org/10.1016/s0896-6273(01)00275-6
- Stortz, J. F., Del Rosario, M., Singer, M., Wilkes, J. M., Meissner, M., & Das, S. (2019). Formin-2 drives polymerisation of actin filaments enabling segregation of apicoplasts and cytokinesis in Plasmodium falciparum. *Elife*, *8*. https://doi.org/10.7554/eLife.49030
- Stubblefield, E. A., & Benke, T. A. (2010). Distinct AMPA-type glutamatergic synapses in developing rat CA1 hippocampus. *J Neurophysiol*, 104(4), 1899-1912. https://doi.org/10.1152/jn.00099.2010
- Super, H., & Soriano, E. (1994). The organization of the embryonic and early postnatal murine hippocampus. II. Development of entorhinal, commissural, and septal connections studied with the lipophilic tracer Dil. *J Comp Neurol*, 344(1), 101-120. https://doi.org/10.1002/cne.903440108
- Sur, C., Fresu, L., Howell, O., McKernan, R. M., & Atack, J. R. (1999). Autoradiographic localization of alpha5 subunit-containing GABAA receptors in rat brain. *Brain Res*, *822*(1-2), 265-270. https://doi.org/10.1016/s0006-8993(99)01152-x
- Szczot, M., Wojtowicz, T., & Mozrzymas, J. W. (2010). GABAergic and glutamatergic currents in hippocampal slices and neuronal cultures show profound differences: a clue to a potent homeostatic modulation. *J Physiol Pharmacol*, 61(4), 501-506. https://www.ncbi.nlm.nih.gov/pubmed/20814079
- Takesian, A. E., & Hensch, T. K. (2013). Balancing plasticity/stability across brain development. *Prog Brain Res*, 207, 3-34. https://doi.org/10.1016/B978-0-444-63327-9.00001-1
- Takesian, A. E., Kotak, V. C., Sharma, N., & Sanes, D. H. (2013). Hearing loss differentially affects thalamic drive to two cortical interneuron subtypes. *J Neurophysiol*, *110*(4), 999-1008. https://doi.org/10.1152/jn.00182.2013
- Tan, H. M., Bassett, J. P., O'Keefe, J., Cacucci, F., & Wills, T. J. (2015). The development of the head direction system before eye opening in the rat. *Curr Biol*, *25*(4), 479-483. https://doi.org/10.1016/j.cub.2014.12.030
- Tan, H. M., Wills, T. J., & Cacucci, F. (2017). The development of spatial and memory circuits in the rat. *Wiley Interdiscip Rev Cogn Sci*, 8(3). https://doi.org/10.1002/wcs.1424
- Taube, J. S. (2007). The head direction signal: origins and sensory-motor integration. *Annu Rev Neurosci*, 30, 181-207. https://doi.org/10.1146/annurev.neuro.29.051605.112854
- Taube, J. S., Muller, R. U., & Ranck, J. B., Jr. (1990). Head-direction cells recorded from the postsubiculum in freely moving rats. I. Description and quantitative analysis. *J Neurosci*, *10*(2), 420-435. https://doi.org/10.1523/JNEUROSCI.10-02-00420.1990
- Tomita, S., Chen, L., Kawasaki, Y., Petralia, R. S., Wenthold, R. J., Nicoll, R. A., & Bredt, D. S. (2003). Functional studies and distribution define a family of transmembrane AMPA receptor regulatory proteins. *J Cell Biol*, *161*(4), 805-816. https://doi.org/10.1083/jcb.200212116
- Travaglia, A., Bisaz, R., Sweet, E. S., Blitzer, R. D., & Alberini, C. M. (2016). Infantile amnesia reflects a developmental critical period for hippocampal learning. *Nat Neurosci*, *19*(9), 1225-1233. https://doi.org/10.1038/nn.4348
- Tsai, C. F., Zhang, P., Scholten, D., Martin, K., Wang, Y. T., Zhao, R., Chrisler, W. B., Patel, D. B., Dou, M., Jia, Y., Reduzzi, C., Liu, X., Moore, R. J., Burnum-Johnson, K. E., Lin, M. H., Hsu, C. C., Jacobs, J. M., Kagan, J., Srivastava, S., . . . Shi, T. (2021). Surfactant-assisted one-pot sample preparation for label-free single-cell proteomics. *Commun Biol*, *4*(1), 265. https://doi.org/10.1038/s42003-021-01797-9
- Turner, D. A. (1988). Waveform and amplitude characteristics of evoked responses to dendritic stimulation of CA1 guinea-pig pyramidal cells. *J Physiol*, *395*, 419-439. https://doi.org/10.1113/jphysiol.1988.sp016927

- Turrigiano, G. G., & Nelson, S. B. (2004). Homeostatic plasticity in the developing nervous system. *Nat Rev Neurosci*, 5(2), 97-107. https://doi.org/10.1038/nrn1327
- Tyagarajan, S. K., & Fritschy, J. M. (2014). Gephyrin: a master regulator of neuronal function? *Nat Rev Neurosci*, *15*(3), 141-156. https://doi.org/10.1038/nrn3670
- Tyanova, S., Temu, T., Sinitcyn, P., Carlson, A., Hein, M. Y., Geiger, T., Mann, M., & Cox, J. (2016). The Perseus computational platform for comprehensive analysis of (prote)omics data. *Nat Methods*, *13*(9), 731-740. https://doi.org/10.1038/nmeth.3901
- Uchizono, K. (1965). Characteristics of excitatory and inhibitory synapses in the central nervous system of the cat. *Nature*, *207*(997), 642-643. https://doi.org/10.1038/207642a0
- Urbanska, M., Blazejczyk, M., & Jaworski, J. (2008). Molecular basis of dendritic arborization. *Acta Neurobiol Exp (Wars)*, *68*(2), 264-288. https://doi.org/10.55782/ane-2008-1695
- van der Spek, S. J. F., Pandya, N. J., Koopmans, F., Paliukhovich, I., van der Schors, R. C., Otten, M., Smit, A. B., & Li, K. W. (2022). Expression and Interaction Proteomics of GluA1- and GluA3-Subunit-Containing AMPARs Reveal Distinct Protein Composition. *Cells*, 11(22). https://doi.org/10.3390/cells11223648
- Vazdarjanova, A., Ramirez-Amaya, V., Insel, N., Plummer, T. K., Rosi, S., Chowdhury, S., Mikhael, D., Worley, P. F., Guzowski, J. F., & Barnes, C. A. (2006). Spatial exploration induces ARC, a plasticity-related immediate-early gene, only in calcium/calmodulin-dependent protein kinase II-positive principal excitatory and inhibitory neurons of the rat forebrain. *J Comp Neurol*, 498(3), 317-329. https://doi.org/10.1002/cne.21003
- Vicini, S., Wang, J. F., Li, J. H., Zhu, W. J., Wang, Y. H., Luo, J. H., Wolfe, B. B., & Grayson, D. R. (1998). Functional and pharmacological differences between recombinant N-methyl-D-aspartate receptors. *J Neurophysiol*, *79*(2), 555-566. https://doi.org/10.1152/jn.1998.79.2.555
- von Ziegler, L. M., Selevsek, N., Tweedie-Cullen, R. Y., Kremer, E., & Mansuy, I. M. (2018). Subregion-Specific Proteomic Signature in the Hippocampus for Recognition Processes in Adult Mice. *Cell Rep*, 22(12), 3362-3374. https://doi.org/10.1016/j.celrep.2018.02.079
- Voss, H., Moritz, M., Pelczar, P., Gagliani, N., Huber, S., Nippert, V., Schluter, H., & Hahn, J. (2022). Tissue Sampling and Homogenization with NIRL Enables Spatially Resolved Cell Layer Specific Proteomic Analysis of the Murine Intestine. *Int J Mol Sci*, 23(11). https://doi.org/10.3390/ijms23116132
- Wall, M. J., & Correa, S. A. L. (2018). The mechanistic link between Arc/Arg3.1 expression and AMPA receptor endocytosis. *Semin Cell Dev Biol*, 77, 17-24. https://doi.org/10.1016/j.semcdb.2017.09.005
- Walton, N. M., Zhou, Y., Kogan, J. H., Shin, R., Webster, M., Gross, A. K., Heusner, C. L., Chen, Q., Miyake, S., Tajinda, K., Tamura, K., Miyakawa, T., & Matsumoto, M. (2012). Detection of an immature dentate gyrus feature in human schizophrenia/bipolar patients. *Transl Psychiatry*, 2(7), e135. https://doi.org/10.1038/tp.2012.56
- Wang, F., Flanagan, J., Su, N., Wang, L. C., Bui, S., Nielson, A., Wu, X., Vo, H. T., Ma, X. J., & Luo, Y. (2012). RNAscope: a novel in situ RNA analysis platform for formalin-fixed, paraffin-embedded tissues. *J Mol Diagn*, 14(1), 22-29. https://doi.org/10.1016/j.jmoldx.2011.08.002
- Waung, M. W., Pfeiffer, B. E., Nosyreva, E. D., Ronesi, J. A., & Huber, K. M. (2008). Rapid translation of Arc/Arg3.1 selectively mediates mGluR-dependent LTD through persistent increases in AMPAR endocytosis rate. *Neuron*, *59*(1), 84-97. https://doi.org/10.1016/j.neuron.2008.05.014
- Wenthold, R. J., Petralia, R. S., Blahos, J., II, & Niedzielski, A. S. (1996). Evidence for multiple AMPA receptor complexes in hippocampal CA1/CA2 neurons. *J Neurosci*, 16(6), 1982-1989. https://doi.org/10.1523/JNEUROSCI.16-06-01982.1996
- Weston, M. C., Nehring, R. B., Wojcik, S. M., & Rosenmund, C. (2011). Interplay between VGLUT isoforms and endophilin A1 regulates neurotransmitter release and short-term plasticity. *Neuron*, 69(6), 1147-1159. https://doi.org/10.1016/j.neuron.2011.02.002
- Wigstrom, H., & Gustafsson, B. (1986). Postsynaptic control of hippocampal long-term potentiation. *J Physiol (Paris)*, 81(4), 228-236. https://www.ncbi.nlm.nih.gov/pubmed/2883309

- Wilkins, M. R., Pasquali, C., Appel, R. D., Ou, K., Golaz, O., Sanchez, J. C., Yan, J. X., Gooley, A. A., Hughes, G., Humphery-Smith, I., Williams, K. L., & Hochstrasser, D. F. (1996). From proteins to proteomes: large scale protein identification by two-dimensional electrophoresis and amino acid analysis. *Biotechnology (N Y)*, 14(1), 61-65. https://doi.org/10.1038/nbt0196-61
- Wilkins, M. R., Sanchez, J. C., Gooley, A. A., Appel, R. D., Humphery-Smith, I., Hochstrasser, D. F., & Williams, K. L. (1996). Progress with proteome projects: why all proteins expressed by a genome should be identified and how to do it. *Biotechnol Genet Eng Rev, 13,* 19-50. https://doi.org/10.1080/02648725.1996.10647923
- Wills, T. J., Cacucci, F., Burgess, N., & O'Keefe, J. (2010). Development of the hippocampal cognitive map in preweanling rats. *Science*, *328*(5985), 1573-1576. https://doi.org/10.1126/science.1188224
- Witter, M. P. (1986). A survey of the anatomy of the hippocampal formation, with emphasis on the septotemporal organization of its intrinsic and extrinsic connections. *Adv Exp Med Biol*, 203, 67-82. https://doi.org/10.1007/978-1-4684-7971-3_5
- Wu, Y. K., Fujishima, K., & Kengaku, M. (2015). Differentiation of apical and basal dendrites in pyramidal cells and granule cells in dissociated hippocampal cultures. *PLoS One*, *10*(2), e0118482. https://doi.org/10.1371/journal.pone.0118482
- Yamamoto, J., Suh, J., Takeuchi, D., & Tonegawa, S. (2014). Successful Execution of Working Memory Linked to Synchronized High-Frequency Gamma Oscillations. *Cell*, 157(4), 845-857. https://doi.org/10.1016/j.cell.2014.04.009
- Yin, Y., Edelman, G. M., & Vanderklish, P. W. (2002). The brain-derived neurotrophic factor enhances synthesis of Arc in synaptoneurosomes. *Proc Natl Acad Sci U S A*, 99(4), 2368-2373. https://doi.org/10.1073/pnas.042693699
- Ylinen, A., Bragin, A., Nadasdy, Z., Jando, G., Szabo, I., Sik, A., & Buzsaki, G. (1995). Sharp wave-associated high-frequency oscillation (200 Hz) in the intact hippocampus: network and intracellular mechanisms. *J Neurosci*, 15(1 Pt 1), 30-46. https://doi.org/10.1523/JNEUROSCI.15-01-00030.1995
- Zeng, M., Diaz-Alonso, J., Ye, F., Chen, X., Xu, J., Ji, Z., Nicoll, R. A., & Zhang, M. (2019). Phase Separation-Mediated TARP/MAGUK Complex Condensation and AMPA Receptor Synaptic Transmission. *Neuron*, *104*(3), 529-543 e526. https://doi.org/10.1016/j.neuron.2019.08.001
- Zhang, H., & Bramham, C. R. (2021). Arc/Arg3.1 function in long-term synaptic plasticity: Emerging mechanisms and unresolved issues. *Eur J Neurosci*, *54*(8), 6696-6712. https://doi.org/10.1111/ejn.14958
- Zhang, W., Wu, J., Ward, M. D., Yang, S., Chuang, Y. A., Xiao, M., Li, R., Leahy, D. J., & Worley, P. F. (2015). Structural basis of arc binding to synaptic proteins: implications for cognitive disease. *Neuron*, 86(2), 490-500. https://doi.org/10.1016/j.neuron.2015.03.030
- Zhou, Y., Lai, C. S. W., Bai, Y., Li, W., Zhao, R., Yang, G., Frank, M. G., & Gan, W. B. (2020). REM sleep promotes experience-dependent dendritic spine elimination in the mouse cortex. *Nat Commun*, *11*(1), 4819. https://doi.org/10.1038/s41467-020-18592-5
- Zhu, J. J., Esteban, J. A., Hayashi, Y., & Malinow, R. (2000). Postnatal synaptic potentiation: delivery of GluR4-containing AMPA receptors by spontaneous activity. *Nat Neurosci*, *3*(11), 1098-1106. https://doi.org/10.1038/80614
- Zhu, Y. H., Stornetta, R. L., & Zhu, J. J. (2004). Chandelier cells control excessive cortical excitation: Characteristics of whisker-evoked synaptic responses of layer 2/3 nonpyramidal and pyramidal neurons. *Journal of Neuroscience*, 24(22), 5101-5108. https://doi.org/10.1523/Jneurosci.0544-04.2004

7 Statement of contributions

The conception and funding of these projects were provided by Dr. Ora Ohana and Prof. Dietmar Kuhl (Institute for Molecular and Cellular Cognition, UKE).

Part I: Fig. 2.1: fEPSP recordings were performed by Lilianna Stanislawa Kucharczyk and Francesca Xompero. Figs. 2.2 recordings were performed by Alexa Nicole Sliby. Dr. Ora Ohana herself conducted the experiments in Fig. 2.4. Ute Süsens handled all western blots. Analysis and statistical testing of the experiments in 2.1 and 2.2 were performed by Daniela Ballesteros. Daniela Ballesteros designed all other experiments and performed and analyzed them. Ute Süsens assisted with western blotting.

Part II: Dr. Ora Ohana, Prof. Dietmar Kuhl, and Daniela Ballesteros designed the mass spectrometry experiments. Daniela Ballesteros dissected mouse brains and prepared sections for NIRL and brain samples for WB. Mass spectrometry was performed at the Core Facility Mass Spectrometric Proteomics of the UKE, by Thomas Mair and Bente Siebels. Thomas Mair performed the initial analysis of protein detection. Enrichment analysis and statistics were conducted by Daniela Ballesteros.

Part III: Fig. 4.1: Daniela Ballesteros performed all patch clamp experiments, filled live cells with Biocytin, and fixed and stained the cells with DAB. Performed all analyses of physiological properties and conducted all the statistical tests. Dendritic reconstructions in Fig. 4.1. and Golgi experiments were conducted by Christina Stanke, Sara Obeso, and Tobias Gellrich.

8 Acknowledgments

First of all, I would like to thank my family; my mom and sisters, who have always believed in me and supported every project I have embarked on. None of my achievements would have been possible without their love, help, and sacrifice.

I would also like to thank Dr. Ora Ohana not only for her invaluable supervision and contributions to this work but also for her trust, encouragement, and support. Especially during moments of uncertainty and confusion. Also, for the lessons and patience throughout this slow learning process.

I express my sincere gratitude to the entire Institute of Molecular and Cellular Cognition and the Center of Molecular Neurobiology, especially to Prof. Dietmar Kuhl, for offering me the opportunity to join his Institute and for trusting me to represent it.

My appreciation also extends to Prof. Stefan Kindler and Prof. Hans-Jürgen Kreienkamp for agreeing to be part of my thesis committee, for their helpful comments, and for taking time out of their busy schedules to review this thesis.

To my fellow Ph.D. students, Abdu, Marcel, and Xiaoyu, I am grateful for the good moments we shared, their patience, and their advice during tough times. Thank you for all the helpful discussions, the beers, wine, cookies, dumplings, and ice cream, and simply for being there. A special thanks to Abdu for his constant support in the analysis of the data presented here and almost every other aspect; an adult-like life in Germany would not have been possible without him.

I would also like to acknowledge the master's and bachelor's students and interns: Cristina, Sara, Iris, Tobias, Noa, Frederic, and Yeji. Thank you not only for your contributions to this work but mainly for the good moments we spent together and for how much I learned from you by teaching and simply sharing.

Thank you to Xiaoyan Gao and Tiemo Marquarding for their advice, and patience, and for teaching me techniques that made this work possible.

To Daks, thank you for helping me start a new life on a new continent, for the free German lessons, the bureaucratic assistance, the colors, the flowers, and most importantly, for the constant good vibes.

Ute, thank you for your immense contribution to this thesis, for the technical advice, and patience in always answering my questions. But above all, for making the lab a lively place.

I am grateful to my former lab members, friends, and second family. The experiences we shared motivated me to pursue this academic path, making this incredible journey worthwhile despite its ups and downs.

Last but not least, I would like to thank Andrés for crossing the Atlantic to keep me warm and supporting every step of this adventure.

9 Curriculum Vitae

PERSONAL INFORMATION

Surnames / First Names: Ballesteros Cadena / Daniela Carolina Address: Noldering 33, 22309, Hamburg, Germany

E-mail: danicaro94@gmail.com

Nationality: Colombian

Date and place of birth: 15.01.1994 in Bogotá, Colombia

EDUCATION

Ph.D. Non-medical Ph.D. Program, Medical Faculty of the University

2020-2024 Center Hamburg-Eppendorf (UKE), Hamburg

M.Sc. Neuroscience, Universidad Nacional de Colombia, Bogotá,

2016-2019 Colombia. (Prof. Marisol Lamprea)

B.Sc. Psychology, Universidad Nacional de Colombia, Bogotá,

2011-2016 Colombia. (Prof. Marisol Lamprea)

Complementary training

Lab Animal Training FELASA B, Federation of Laboratory Animal Science

Feb 2020 Associations, Berlin.

Research Internship Laboratory of Learning and Memory. Institute of Neurobiology Aug-Oct 2018 (INB) Universidad Nacional Autónoma de México (UNAM).

(INB) Universidad Nacional Autónoma de México (UNAM). Juriquilla, QRO, Mexico. (Prof. Gina Quirarte & Prof. Roberto

Prado-Alcalá)

WORK EXPERIENCE

Associate researcher Institute for Molecular & Cellular Cognition (IMCC). Center

for Molecular Neurobiology Hamburg (ZMNH), University

Medical Center Hamburg-Eppendorf (UKE). (Prof. Dietmar

Kuhl)

Young researcher

01.12.2019-present

2018-2019

Colciencias, Universidad Nacional de Colombia

Lecturer Psychology Department, Universidad Nacional de Colombia, 2018-2019 Bogotá, Colombia. Course: Motivation (35 students per term)

Academic Honors

Meritorious Thesis Award, Universidad Nacional de Colombia

January 2019

1st Place Best Master's Colegio Colombiano de Neurociencias COLNE

Thesis Award, June 2019

10 Eidesstattliche Versicherung

Ich versichere ausdrücklich, dass ich die Arbeit selbständig und ohne fremde Hilfe verfasst, andere als die von mir angegebenen Quellen und Hilfsmittel nicht benutzt und die aus den benutzten Werken wörtlich oder inhaltlich entnommenen Stellen einzeln nach Ausgabe (Auflage und Jahr des Erscheinens), Band und Seite des benutzten Werkes kenntlich gemacht habe.

Ferner versichere ich, dass ich die Dissertation bisher nicht einem Fachvertreter an einer anderen Hochschule zur Überprüfung vorgelegt oder mich anderweitig um Zulassung zur Promotion beworben habe.

Ich erkläre mich einverstanden, dass meine Dissertation vom Dekanat der Medizinischen Fakultät mit einer gängigen Software zur Erkennung von Plagiaten überprüft werden kann.